Université d'Ottawa · University of Ottawa

Dedicated to the loving memories of

my father Gerard Berinstain

and

my grandmother Rosette Modiano.

They will have the best seats in the house at my graduation ceremony.

Abstract

The work presented in this thesis demonstrates how laser flash photolysis techniques can be employed in the application of the study of biomolecules and in cellular environments. The development of a new laser flash photolysis system is described, and a user-oriented, integrated hardware and software solution is presented.

The combination of hardware and software used in this approach makes use of the concept of virtual instrumentation through the LabVIEW programming environment. This graphical approach to programming is optimized for data acquisition and instrument control, and for creating a user-friendly environment for the experimenter.

Laser techniques have been used to study the biomolecule lignin and some of its model compounds in order to address the issue of light-induced colour reversion of pulp and paper products. High-yield pulps which contain lignin could have new and different industrial uses if the colour could be stabilized. Our work in this field has helped to elucidate the mechanism of yellowing of lignin mainly through the use of lignin model compounds such as α-guaiacoxyacetoveratrone (α-GAV) and related compounds. Our studies show that the formation of radicals from the excited singlet state is much more important than what is expected from aromatic ketones, and under certain conditions, the singlet pathway is the only degradative one.

The results obtained in studies of crystalline α-GAV show that efficient excited state deactivation pathways can be created by intermolecular interactions, leading to very good photostability of the molecule. Excited state transients detectable in solution are not present in the crystalline

form. In contrast, α-(*p*-methoxyphenoxy)-*p*-methoxy acetophenone (**VII**), does produce triplet state absorption on sufficiently long time scale to be detected. This difference is attributed to a different packing structure of crystalline **VII** which does not allow for efficient excited state deactivation as in the case of α-GAV.

Pulse radiolysis studies were carried out on **VII**, giving us insight into the fragmentation of the ketyl radical derived from this molecule. These results demonstrate that this ketyl radical is extremely short-lived and any strategy involving trapping of these types of radicals in the paper environment will most probably prove to be unsuccessful.

The properties of the *p*-methoxyphenacyl radical (**IX**) were studied and show some interesting aspects of reactivity (acting as a carbon-centred radical), whereas the spectroscopic properties show a long-wavelength absorption which shows some oxygen-centred radical characteristics. These are supported by molecular modeling calculations.

Laser techniques have also been used to probe biologically-relevant environments such as liposomes, bacterial and mammalian cell suspensions, and cultured skin models. These exploratory studies show that issues such as photodynamic therapy mechanisms and the biological effects of magnetic fields have the potential to be studied directly in living cells by laser flash photolysis.

Much of the work presented in this part of the thesis involves the development of techniques for incorporating probes of interest into the biological environment. Many of the incorporation techniques attempted are presented.

This thesis presents the first use of diffuse reflectance laser flash photolysis to directly monitor photochemically generated transients in living cell suspensions. This includes the study of the photochemistry some porphyrins, benzophenones, anthraquinones, and thioxanthones in biologically-relevant environments. 5-Aminolevulinic acid can be used in the growth medium of bacteria to increase the natural concentration of porphyrins in cells, and the laser flash photolysis studies on these systems are presented.

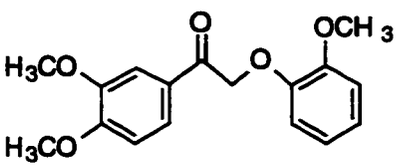

α-GAV

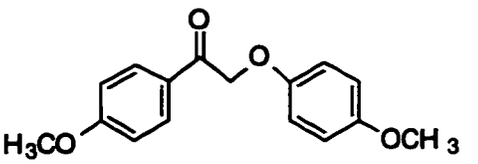

VII

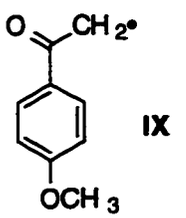

IX

Acknowledgements

Many people have made the successful completion of my graduate studies possible and I am grateful to them. J. C. (Tito) Scaiano, my PhD supervisor, has been an incredible source of inspiration and knowledge for me to learn from. Tito has given me an extraordinary amount of freedom to follow my scientific interests and personal interests during the time I have been working with him; and he acted not only as my professor and my mentor, but also as my friend.

I would like to thank all the past and present members of the Scaiano group; it has been a pleasure to work and study with them. I would especially like to thank the many people I have collaborated with: André Simard and Fran Cozens in the laser system setup; Mike Whittlesey, Corinne Bensimon, Robert Schuler (Notre Dame Radiation Laboratory), John Schmidt and Cyril Heitner (Pulp and Paper Research Institute of Canada) in the lignin photochemistry work; and Nadereh Mohtat, Cornelia Bohne, Jack McLean (Health Canada), and Dennis Sprott (National Research Council of Canada) in the work in biological environments. Thanks also go to Patrick Malenfant and Jocelyn Renaud who I supervised when they were undergraduates and for their continued friendship. Dean Weldon and Terry Connolly have helped to make this experience so enriching, as have all the other friends I have made during my graduate studies.

I would also like to thank the Natural Sciences and Engineering Research Council, Eco-Research, the Pulp and Paper Research Institute of Canada, DuPont, Stentor, and the Chemical Institute of Canada for financial support during my PhD studies.

During my educational career, I have met a few scientists who have made a positive influence; I would like to thank Nabil Kozman at Lindsay Place High School, Gordon Hambly at John Abbott College, Raymond Zienius and Ann English at Concordia University, and Dan Wayner at the National Research Council of Canada.

During the writing phase of this thesis, Rosie O'Donnell helped to put a smile on my face every morning through her television show so I could be productive and successful at putting together this document.

The most heart-felt thanks and expressions of love go to my mother Stella, to my sisters Brigitte and Roselyne and to my partner in life Mónica. Their never-ending support was my strength during this time and the sacrifices they have made for me to be able to successfully complete this PhD will always be remembered.

Table of Contents

List of Figures

CHAPTER 1

CHAPTER 2

CHAPTER 3

List of Schemes

List of Tables

List of Abbreviations

α-GAV	α-guaiacoxyacetoveratrone
AC	alternating current
ACP	acetophenone
ACV	acetoveratrone
AET	2-aminoethanethiol
ALA	5-aminolevulinic acid
AQS	anthraquinone-1,5-disulfonate
αT	α-terthienyl
ATS	Advanced Tissue Sciences™
BAEE	4-benzoyl benzoic acid ethyl ester
BCU	baseline compensation unit
CIDEP	chemically induced dynamic electron polarization
CIDNP	chemically induced dynamic nuclear polarization
CIE	Commission Internationale de l'Eclairage
CTMP	chemithermomechanical pulp
DAQ	data acquisition
DMSO	dimethyl sulfoxide
DNA	deoxyribonucleic acid
DODAC	dioctadecyldimethylammonium chloride
DPPC	dipalmitoylphosphatidylcholine
EPR	electron paramagnetic resonance
ESR	electron spin resonance
GC	gas chromatograph
GPIB	general purpose interface bus
GUOH	guaiacol
HALS	hindered amine light stabilizers
HEPES	N-2-hydroxyethylpiperazine-N'-ethanesulfonic acid
HOMO	highest occupied molecular orbital
ITX	isopropylthioxanthone
KPF	ketoprofen
LFP	laser flash photolysis
LSE	Living Skin Equivalent™
LUMO	lowest unoccupied molecular orbital
MEL	mouse erythroleukemia cells
MPIX	mesoporphyrin IX
MV	methyl viologen
NMR	nuclear magnetic resonance
NSAID	non-steroidal anti-inflammatory drug
OD	optical density
PAPRICAN	Pulp and Paper Research Institute of Canada
PMB	protoplast maintenance buffer
PMT	photomutliplier tube
PPIX	protoporphyrin IX
RAM	random access memory
SDS	sodium dodecyl sulfate
TMP	thermomechanical pulp
TPP	time per point
TTL	transistor-transistor linked
VI	virtual instrument
YAG	yttrium:aluminum:germanium
ZPTS	zinc phthalocyanine tetrasulfonate

I met a stranger in the night
Whose lamp had ceased to shine.
I paused to let him light
His lamp from mine.
A tempest sprang up later on
And shook the world about,
And when the wind was gone
My lamp was out.
But back to me the stranger came-
His lamp was glowing fine.
He held the precious flame
And lighted mine.

-LON WOODRUM

Your attitude may determine your altitude.

-UNKNOWN AUTHOR

1.Nanosecond Laser Flash Photolysis

The earliest publications describing laser flash photolysis date from 1965 by Kosonocky and coworkers[1] and 1966 by Lindqvist.[2] Although Kosonocky was the first to report using a laser as the excitation source, Lindqvist was the first to take advantage of the time resolution that a laser offers by developing a system with ~100 ns resolution. Porter described a laser flash photolysis system at the Nobel symposium in 1967,[3] followed by his first detailed report in 1970.[4] From 1967 to 1970, it was clear that several groups were developing similar but original systems,[5-11] but it is interesting to note that even today's systems are very similar in architecture to that first reported by Lindqvist in 1966.

This chapter describes the nanosecond laser flash photolysis facilities at the University of Ottawa. The author of this thesis was fortunate enough to have participated in the setting up of the new facilities and to have lead the programming efforts for the system.

First, a general overview of laser flash photolysis will be presented, followed by a detailed description of the software written for the data acquisition and instrument control of the system. To fully appreciate how the system works, a top-level description of the hardware components and

how they are interfaced to each other and to the computers will be presented. Although the author did not design and build the custom electronics used in the system (most of the credit should go to André Simard for that work), the author was a major player in the team that did the top-level design of the system, and this is the information presented in the latter part of this chapter.

This chapter describes a novel design of a nanosecond laser flash photolysis system, and the first one to use the Macintosh platform in combination with the LabVIEW programming environment.

1.1.Overview of a Nanosecond Laser Flash Photolysis Experiment

Laser flash photolysis uses a pulsed laser to generate an excited state or other transient from an appropriate precursor and a monitoring light source to analyze the transient's absorption. The laser must have a pulse duration shorter than the processes under investigation and have a high enough intensity that an appreciable amount of transient (typically 10-50 μM) is generated for detection purposes. After the laser hits the sample, there is a change in absorptivity of the sample solution which alters the intensity of a monitoring beam as it passes through the solution. This intensity change is measured by a photomultiplier tube (PMT) detector as a function of time in order to extract spectral and kinetic information. In general, the system can be viewed as a very fast spectrophotometer with a laser as the excitation source.

There are a variety of lasers available in the laser lab at the University of Ottawa which can effectively cover wavelengths of excitation from 248 nm to 1064 nm. The lasers used primarily in these studies are the 308 nm EX 530 Lumonics excimer laser, a 337 nm Molectron UV-24 nitrogen laser and

a 266, 355, or 532 nm Surelite Nd:YAG laser with pulse durations typically under 10 ns and energies of <100, 5, 10, 30, and 60 mJ, respectively. The laser pulses were directed towards and concentrated (but not focused) on the samples at right angles with respect to the monitoring beam by a series of prisms and lenses. The experimental setup is shown in Figure 1.1. The lasers are usually operated at 1 Hz and shutters controlled exposure of the sample to either the monitoring or laser light sources. The energy of the lasers can be effectively attenuated with the use of calibrated neutral density filters.

Samples are prepared at concentrations that do not exceed an optical density of 0.4 at the laser wavelength to avoid shock waves or a concentration gradient of the transient species. The sample solutions are contained in cells made of 7 x 7 mm^2 Suprasil square quartz tubing or can be flowed through specially constructed sample cells if a net chemical reaction occurs upon irradiation. To avoid product buildup or sample depletion in static samples, the solutions can be shaken after every laser shot. Altering the gas content of the solution is achieved through bubbling with the desired gas for 15-30 min depending on the sample volume.

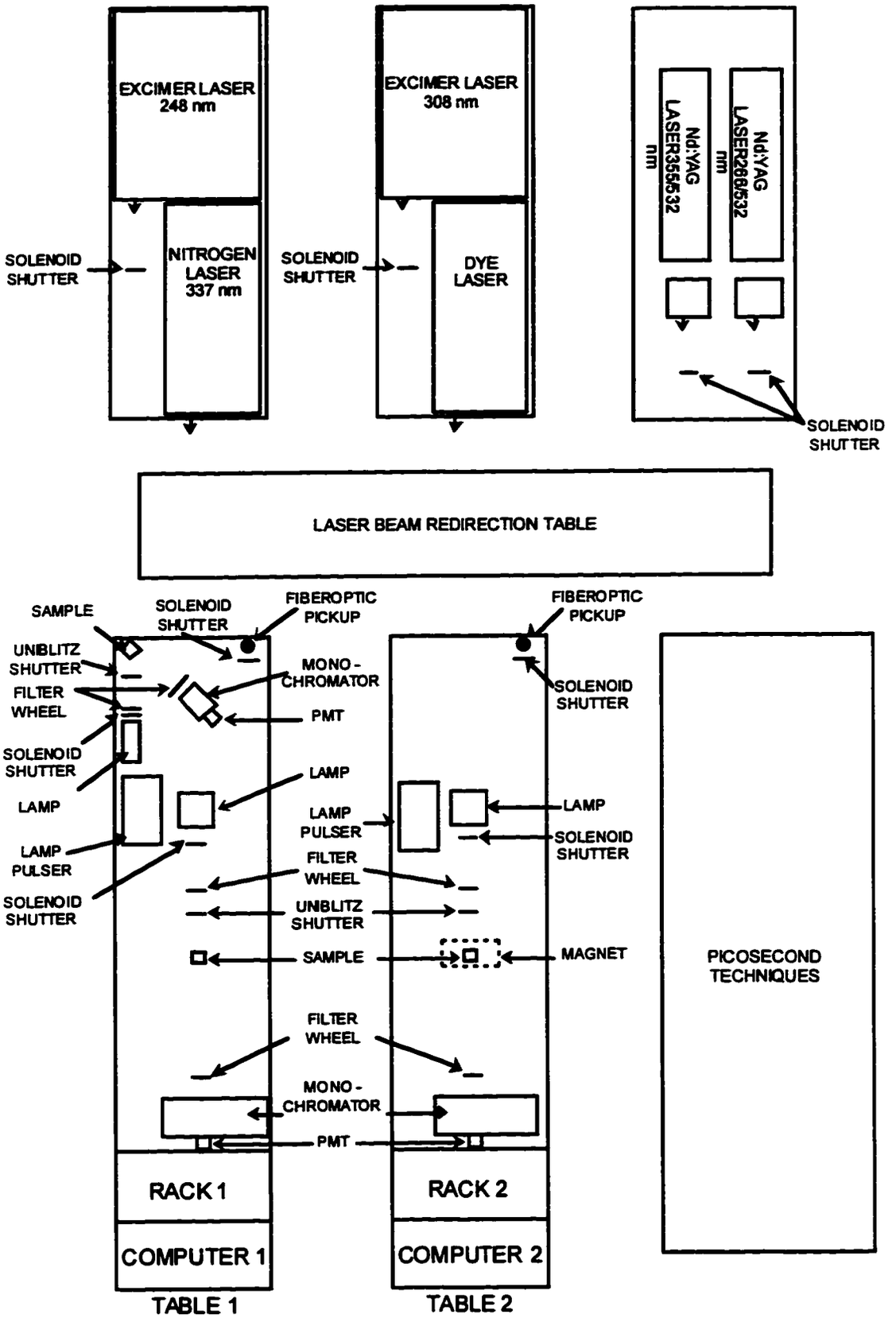

Figure 1.1 Layout of the laser lab at the University of Ottawa.

The monitoring/detection system consists of a pulsed 150 Watt xenon lamp (75 W for diffuse reflectance detection mode), a high intensity monochromator and a photomultiplier tube detector operating on six dynodes. The monitoring lamp is pulsed so that the intensity of the beam is increased by a factor of 5 - 20 during a few ms. This enhances the signal-to-noise ratio which is especially important for small or short-lived (<100 ns) signals. The monitoring beam is focused through the sample and into a monochromator which selects the wavelength of light to be monitored. The selected wavelengths of light are detected by the PMT detector which yields a current terminated into an appropriate load resistor (typically 93 Ohms) giving a voltage signal. The voltage signal changed with time and is captured by a Tektronix 2440 digital storage oscilloscope equipped with pre-trigger capabilities which is interfaced with Macintosh computers controlled by LabVIEW software. A line synchronizer coordinates the various components of the LFP system including the lasers, lamp pulser and shutters through a series of transistor-transistor linked (TTL) pulses that originates at the same point on a 60 Hz AC sine wave so that proper time sequences of events are maintained.

Figure 1.2 shows a plot of PMT output versus time for a period from one second before to one second after a particular laser pulse. At the beginning of the experiment, light from the monitoring beam is recorded before it is pulsed which causes a sharp increase in the PMT output. The laser then fires and subsequently strikes a fiber optic cable which triggers the transient digitizer to start saving data points. The signal that results is shown in the small box in the figure. The intensity of the monitoring beam, I_o, is measured on a second channel and represents the baseline from which changes in PMT voltage (sample absorption) are measured.

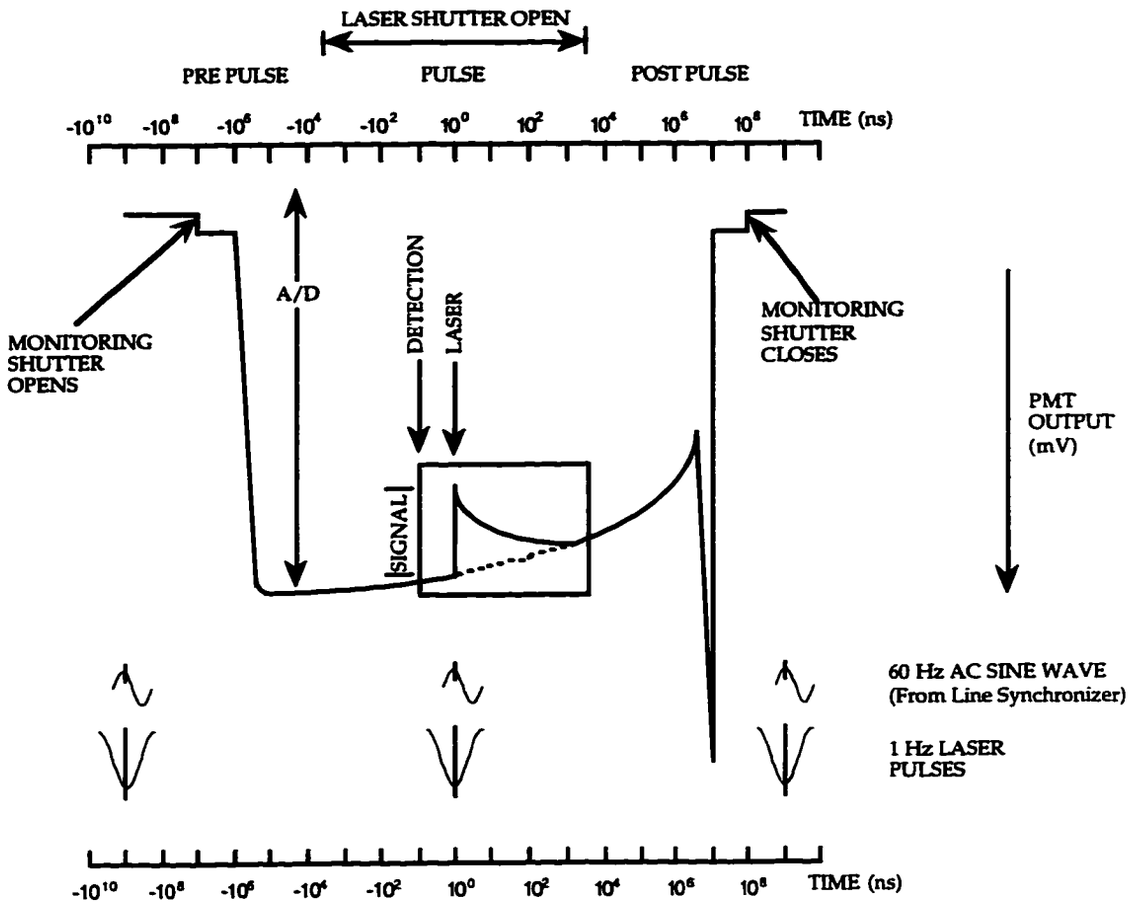

Figure 1.2 Sequence of timed events in a laser flash photolysis experiment.

1.2.The LabVIEW programming environment

All the software written at the University of Ottawa for data acquisition and instrument control have been written in the LabVIEW programming environment. LabVIEW is a product of National Instruments Corporation of Austin, Texas and has been revolutionizing the world of data acquisition and instrument control for scientists and engineers since its original release in the mid-1980s.

LabVIEW is a graphical programming environment, full-featured and general purpose, with a set of function libraries that make data acquisition

and instrument control applications easier, faster, and more pleasurable to build than conventional text-based environments. It contains an integral compiler and debugger, and an application builder for stand-alone applications. Since LabVIEW version 3 (1993), it has been available on the Macintosh, Windows, and SunOS platforms. Programs written on one platform are easily portable to another.

National Instruments, with their LabVIEW product, introduced the concept of a Virtual Instrument, or VI. This concept allows for the programmer to build a single user interface which represents the capabilities and functions of any number of real instruments in a laboratory environment. A simple voltmeter can be converted into a software chart recorder, for example.

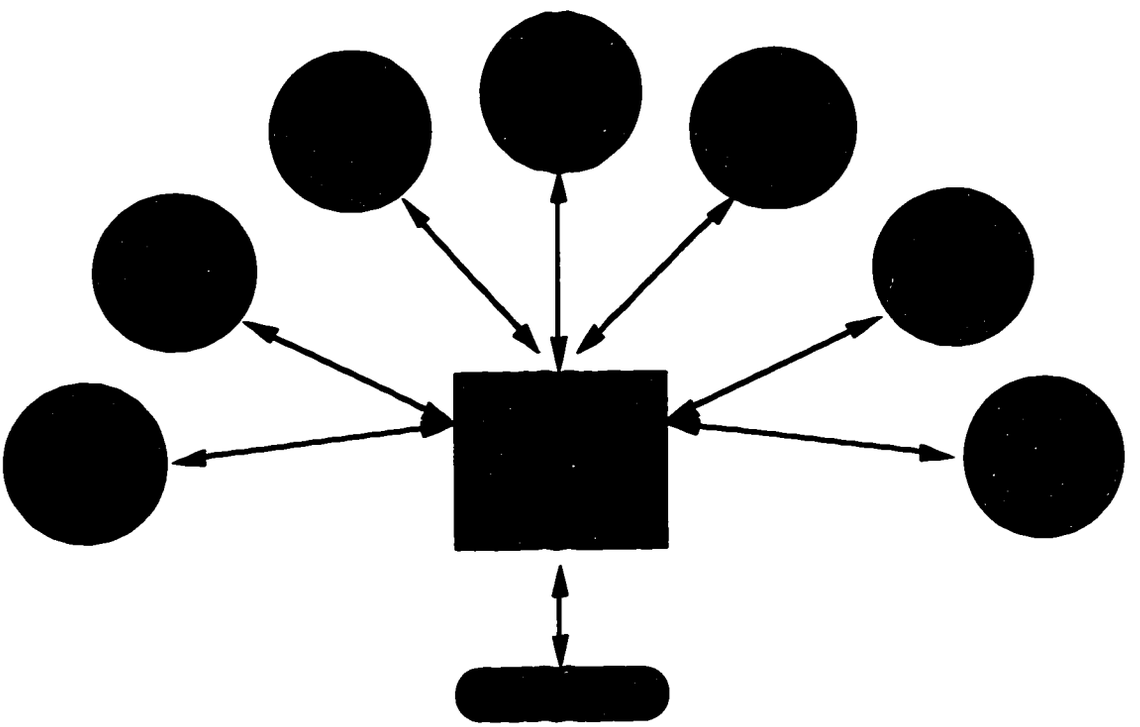

Figure 1.3 Virtual Instrumentation and Laser Flash Photolysis.

Figure 1.3 illustrates the concept of virtual instrumentation in the laser flash photolysis application. The user interfaces with single instrument on the computer screen, with buttons, displays, and switches, as with a real instrument; however this instrument represents a number of real devices which exist in the laboratory. All data acquisition and instrument control is centralized making the experiment not only computerized but highly automated, increasing the productivity of the experimenter.

The unique programming interface is another feature of LabVIEW. All programming is done via a block diagram, consisting of icons and wires, which is directly compiled into executable code; there is no underlying procedural language or menu-driven system.[12]

A virtual instrument, or VI is made up of components called subVIs, all connected and communicating with each other via wires on a block diagram. The user interacts with the program via a front panel. The programs written for the purposes of this thesis work contain over 200 VIs and subVIs; presenting them all in this thesis is not practical and probably not useful. A sample of a block diagram is shown in Figure 1.4 as an illustration and a full, detailed description of the use and capabilities of the programs from the users point of view will be presented instead.

Figure 1.4 shows the code for part of the flash photolysis program. In this part of the program, the laser has already fired; the data is read from the scope, the I_0 channel is separated from the signal channel, the I_0 is calculated, the signal points are grouped, a running average of the signal and I_0 are calculated, and if it is the right time, the trace and I_0 will be output to the front panel.

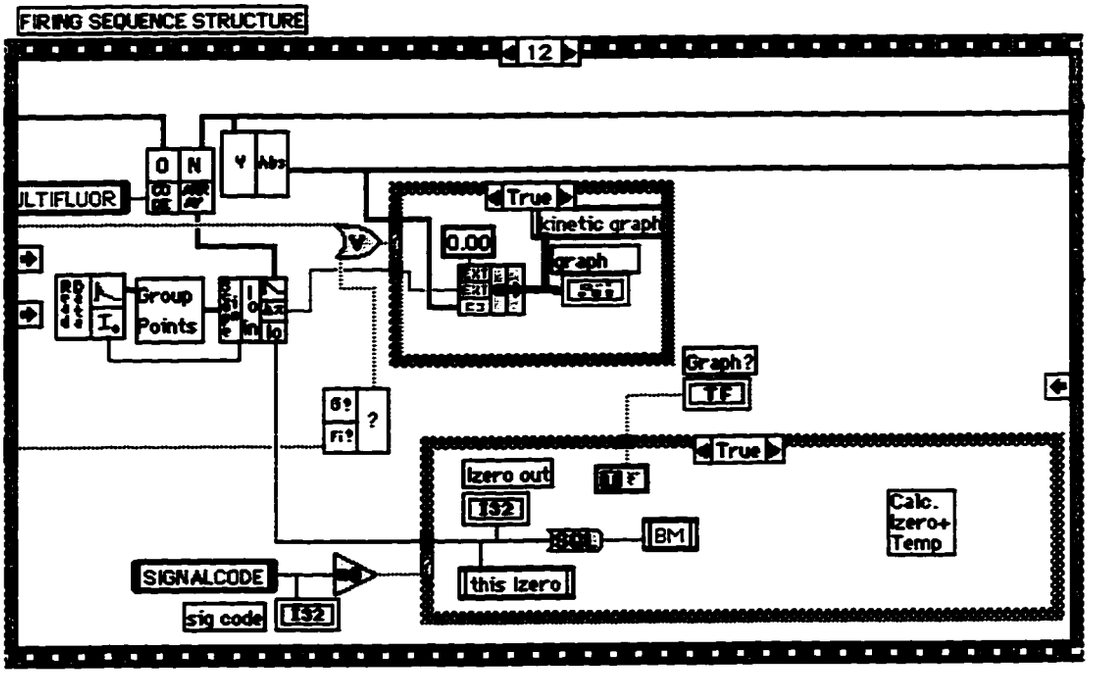

Figure 1.4 Sample block diagram in the LabVIEW programming environment.

It should be noted that the flow of the main kinetics and spectrum programs and their main capabilities and features were modeled after the FORTRAN program authored by J. C. Scaiano for the system at the National Research Council in the early 1980s.

The main steps involved in acquiring a kinetic trace are shown in Figure 1.5. Although this is the core of the program, it turns out to be a small part of the overall code written, since a total solution which takes into account full automation, not just computerization, and creates a friendly user interface becomes a large programming project.

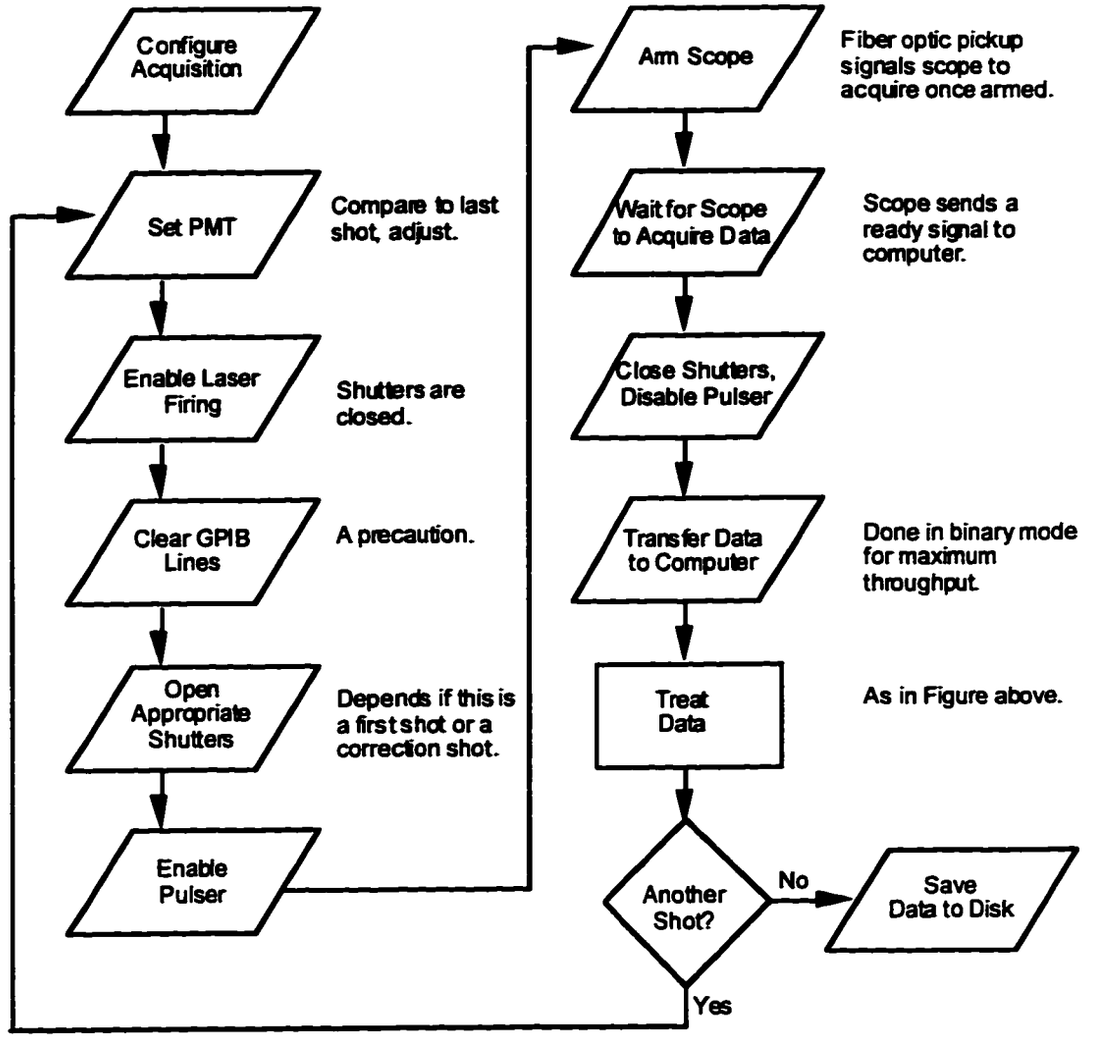

Figure 1.5 Flow chart for firing sequence in LFP program.

1.3.Programs written as part of this thesis work

The suite of programs written and described in this thesis offer the users of the nanosecond laser flash photolysis system at the University of Ottawa tools for automated data acquisition and instrument control during experiments, as well as a set of data analysis programs. The main programs are:

- Flash 5.0
- Kinetic Fit
- SuperSpec

The Flash 5.0 program is a top-level program which is split into two parts (or subVIs), the Kinetics program (called LFP) and the Spectrum program (called L3) , and controls the initiation of each of the sub-programs. Starting the Flash 5.0 program automatically initiates the Kinetics program.

The Kinetics program allows the user to run experiments and acquire kinetic traces at single wavelengths. This includes experiments measuring transient absorbance and luminescence in transmission detection mode or diffuse reflectance detection mode, as well as singlet oxygen detection and conductivity. The Spectrum program automates the acquisition of kinetic traces at a predefined set of wavelengths and calculates the average absorbance at user-defined time intervals, allowing the user to build a point-by-point transient absorption spectrum.

The Kinetic Fit program provides a hard-copy output of a kinetic trace including the results of a first-order decay fit, a first-order growth fit, or a second-order decay fit, depending on which option the user selects. The

hard-copy output contains most relevant experimental conditions and can be used as a primary record of the experiment. A representative output will be shown in the section describing the Kinetic Fit program, section 1.7, page 41.

The SuperSpec program allows re-analysis of the results obtained during a session of running the Spectrum program. It provides a tool for generating transient absorption spectra at any delay, printing them out, and saving them to file.

1.4.The Kinetics Program (LFP VI)

1.4.1.Initialization

The first step of the LFP VI is to initialize the system. The user is presented with a window notifying him/her that initialization is occurring, and to please wait.

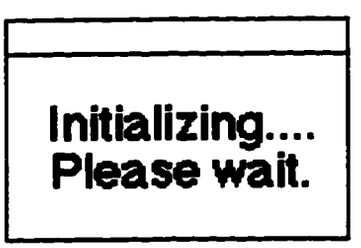

During this time, several steps are being executed:

- Serial port initialization
- Table information obtained
- Data acquisition board initialization
- GPIB board initialization

- Cutoff filter wheel initialization
- Program variables set at defaults
- Oscilloscope initialization
- Monochromator initialization
- Thermocouple monitor initialization

The modem port on the Macintosh (LabVIEW port 0) is configured for use with the diffuse reflectance monochromator (CVI Laser Corp. Digikrom 120). Default values for serial port configuration are used (9600 baud, 8 data bits, 1 stop bit, no parity). The monochromator's manufacturer recommends using the following flow control settings: Data Terminal Ready (DTR) handshaking on, software handshaking off, Request to Send (RTS) off, Clear to Send (CTS) handshaking on, and Data Set Ready (DSR) handshaking off.

The table information is obtained by running the LFP Preferences subVI which checks for a "LFP Prefs" file in the Preferences folder in the System Folder. This file contains an array of numbers containing the slot number of the Lab-NB Board in the Macintosh, Laser Table Number, and some calibration factors for PMT power on Table 1. If no Prefs file is found, it asks the user for the info and creates the file.

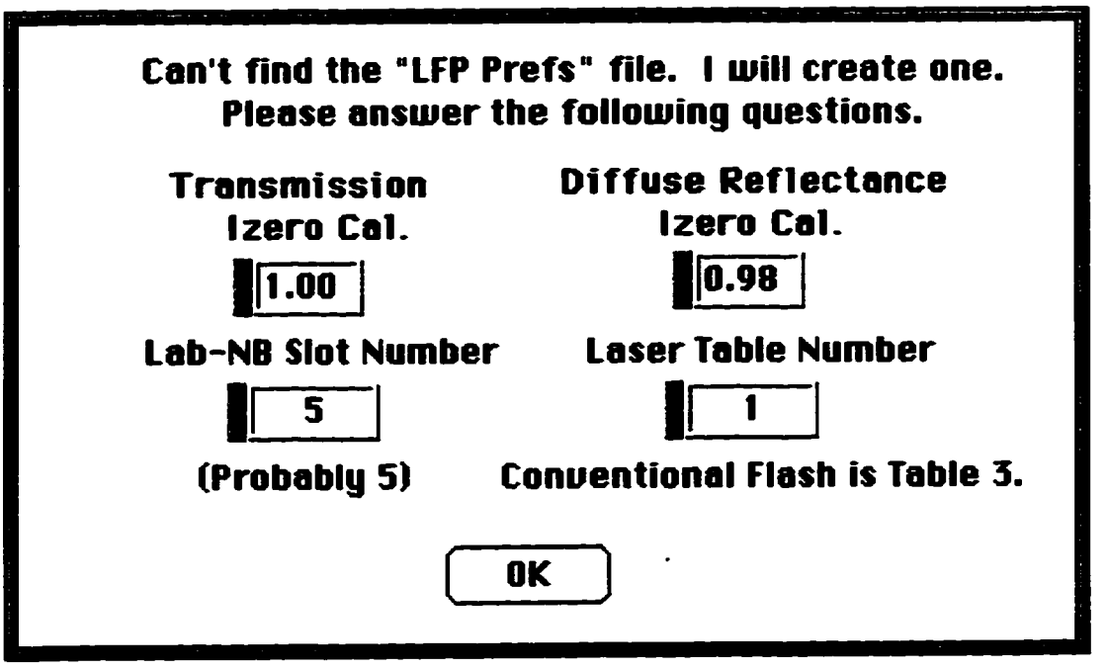

Having this information saved in a separate file on the host computer allows the use of a single version of the Flash program on all three systems (Table 1, Table 2, and conventional flash, which is considered as Table 3). If a computer is changed location or if for some reason the Lab-NB board is moved from one slot to another, the LFP Prefs file should be deleted and the program run. The user will then be prompted for new information (since the program will not find the file in the preferences folder) and a new LFP Prefs file will be created. The calibration factors are empirical values that reflect the fact that diffuse reflectance detection usually requires less PMT power to obtain an appropriate light level.

The system at the University of Ottawa uses a general data acquisition board called Lab-NB from National Instruments (see section 1.8.3, page 52 for a description of the board). At this point in the program, the board is initialized with digital ports 0 and 1 as outputs (8 channels each) and digital port 2 as input (8 channels).

The default settings for program variables are set to run the 308 nm standard sample (methylnaphthalene) using transmission detection, since this is the most common setup. If there is a problem with the initialization of the cutoff filter wheels, the user is warned.

1.4.2.Front Panel

The front panel of the LFP VI presents the user with status information and experiment control functions. The main navigation tool is the array of buttons found at the top of the front panel.

Clicking the **Go** button (also accessible by pushing the F1 key) initiates data acquisition, according to the parameters set in the New Settings screen. A running average of the acquired data will be continuously updated on the screen.

The **New Settings** button (F2) brings up the New Settings screen, setting the experiment parameters. See section 1.4.3 for an explanation of the options available on the New Settings screen.

The **Stop Early** button (F3) will stop the acquisition at the next appropriate opportunity, and continue on by asking for a line of information and a filename. This is useful if a certain number of shots to average was requested but during the experiment the user realizes that less shots will be sufficient.

The **Diagnostics** button (F4) brings up the Diagnostics panel, which gives the user direct access to open and close shutters, fire lasers, set a voltage on a PMT, etc. This is useful when aligning the system or troubleshooting.

The **Test Shots** button (F5) is similar to the **Go** button, but every shot displayed is independent of any previous shots, no running average is displayed. This is useful when optimizing the alignment of the system. When the number of shots requested is reached, the user is not prompted for a file name.

The **Pause** button (F6), when pushed, will suspend an experiment and prompt the user for permission to continue. This can be used when a sample needs to be changed or shaken between shots.

The **Abort** button (escape key) will terminate an experiment and the user will not be prompted to save the file.

The **Get L4** button (F8) calls up the Kinetic Fit program.

A line of information is shown which is updated between shots. The I_0 level is displayed for each shot and the number of shots acquired and the number of shots requested are displayed.

The high voltage provided by the programmable power supply is normally computer-controlled and adjusted. The value used during a specific laser shot is shown in the **Power** field. 1 milliVolt from the Lab-NB analog out port is translated to 1 Volt applied to the photomultiplier tube. However, the user can override the computer control by switching the **PMT Manual** button to the up position. When this is done, the value in the **PMT Voltage** field is used and can be adjusted between shots. The **PMT Manual** switch can be turned on and off during the middle of an experiment and the program will switch accordingly.

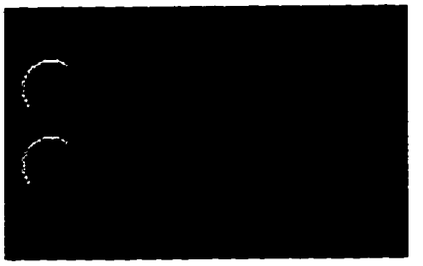

Table 2 is equipped with a Tektronix SCD-1000 oscilloscope which can be used instead of the usual Tektronix 2440 if very fast timescales are needed. The SCD-1000 is an analog oscilloscope and the intensity of the trace on the screen must be adjusted and differs under different timescale and vertical amplitude settings. The program will select a default setting for the intensity which may need to be adjusted slightly up or down. It is recommended that test shots be run and the intensity be adjusted in order to get the maximum percent channels (close to 100%) at the lowest intensity possible.

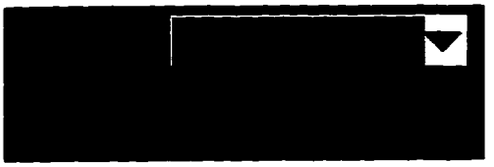

Although vertical amplitude and number of shots are set in the **New Settings** panel, these can be changed in the middle of an experiment by using these controls and the program will adjust accordingly. The number of shots requested will be updated at the top of the screen and the vertical amplitude on the oscilloscope will be updated between shots.

The bottom right of the LFP panel shows these buttons. At the end of an experiment, the program prompts the user for a line of information and a filename. It is possible at this point to cancel the operation and not save a file. In case an error was made, the results of the last experiment run can be saved by clicking the **Re-save last trace** button. Clicking the **Switch to spectrum program** button will change from the Kinetics program to the Spectrum program.

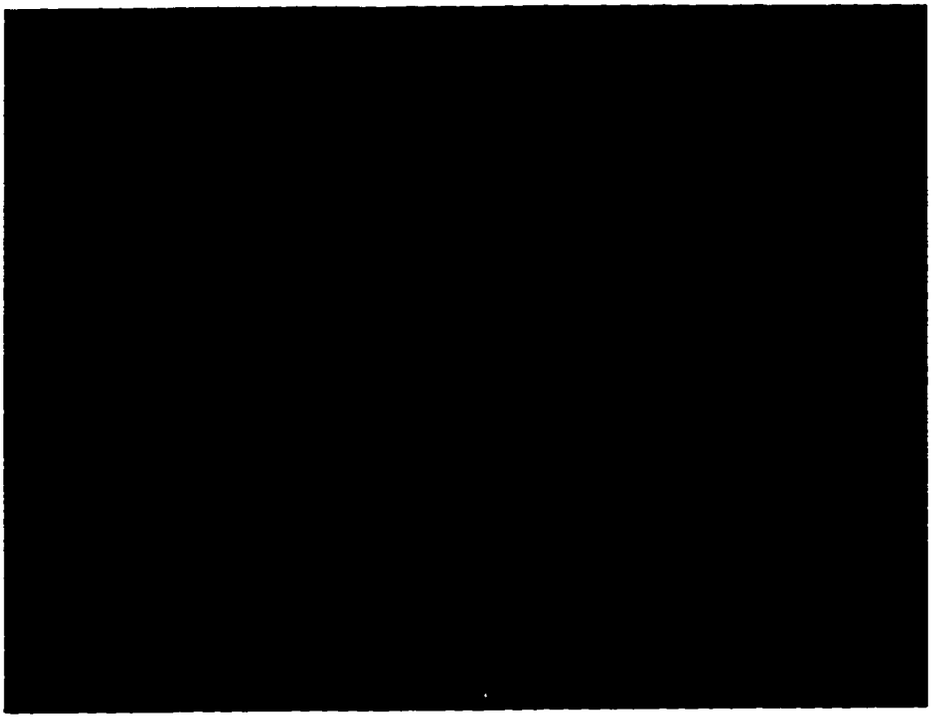

This settings status panel displays the experiment parameters in effect. The detection mode in use (transmission, diffuse reflectance, etc.) is displayed, as are the monitoring wavelength, timescale, vertical amplitude, number of shots requested, etc. See section 1.4.3 for a description of the New Settings panel and the options for each of the experiment parameters.

1.4.3.New Settings Panel

Clicking the **New Settings** button (F2) brings up a panel which allows the user to set the experiment parameters.

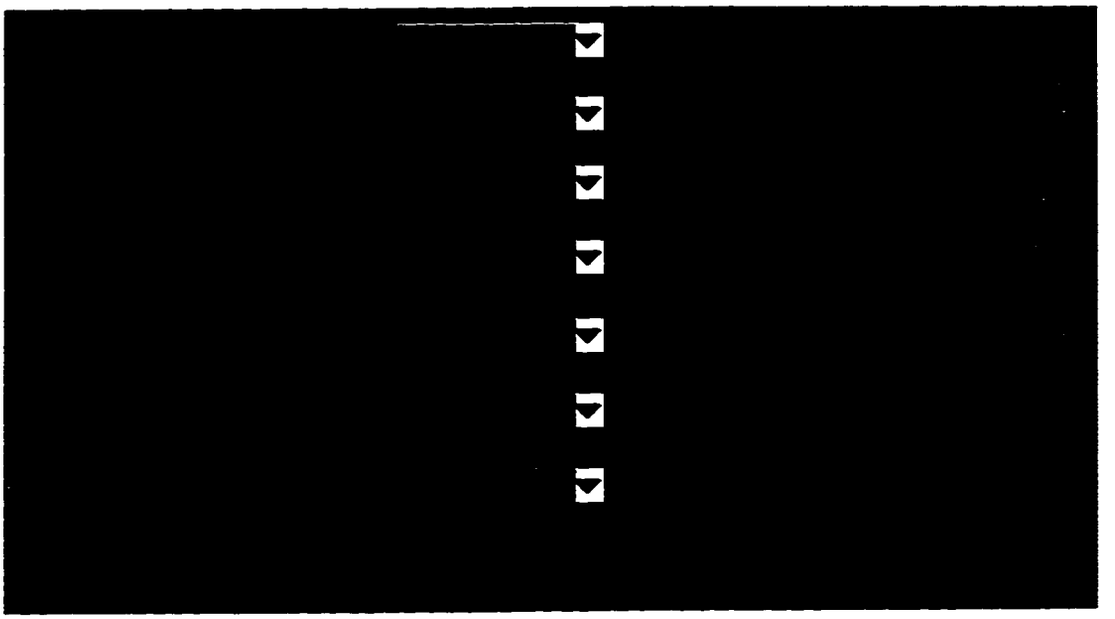

NDF allows the user to select a neutral density filter from a wheel in front of the laser. This option is not used at this time.

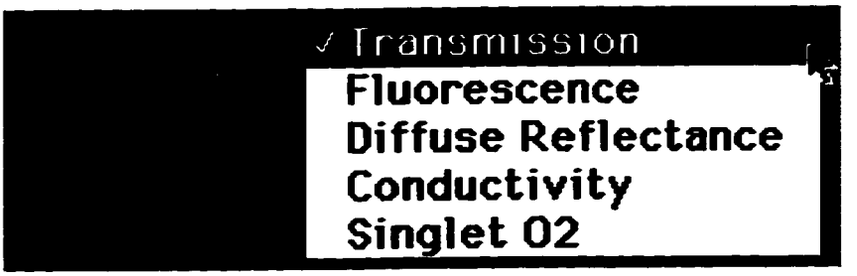

The **Measurement Type** list is used for selecting the type of detection mode being used for a particular experiment. By changing the measurement type, the program not only changes which components are controlled (shutters, filter wheels, etc.), but the data is dealt with in different ways for different modes of detection.

In the case of transmission detection, the voltage signal is transformed into absorbance by using Equation 1.

$$\Delta OD = -\log(1 - \frac{signal}{I_0}) \qquad \textbf{Equation 1}$$

Where I_0 is the pre-laser flash voltage level and signal is the voltage measured, over time, containing the transient information. Note that this treatment for the transmission data assumes that the signal being recorded has been corrected for baseline light level externally to the input of the recording oscilloscope. See the section on baseline compensation for more details.

Fluorescence values are measured in arbitrary units, and the direct voltage off the oscilloscope is used. Since the monitoring beam is not used in fluorescence measurements, there is no consideration of I_0. The only treatment of data in this case is inversion of the voltage values since an increase in light level on our system is measured as a negative voltage. When fluorescence is selected, the PMT is set to manual control at 500 Volts. Also, the user must specify if the measurements are being done on the transmission optical bench or on the diffuse reflectance optical bench in order for the correct shutters, filters, and monochromators to be controlled.

For strongly scattering (or opaque) samples, absorbance is calculated using the Kubelka-Munk[13] treatment for strongly scattering samples, Equation 2;

$$F(R) = \frac{K}{S} = \frac{(1-R)^2}{2R} \qquad \textbf{Equation 2}$$

where $K = 2\varepsilon C$, ε is the extinction coefficient, R and S are the reflectivity and scattering coefficients respectively, and C is the concentration. However, in the case of diffuse reflectance detection mode for small and

moderate reflectance changes as in the work done in our laboratory, this function is linear with concentration. Therefore, Equation 2 simplifies to transient concentration being proportional to $\Delta J/J_0$ (where ΔJ is the signal and J_0 is the pre-laser flash voltage level), and this is used to calculate the change in reflectance values used for diffuse reflectance work.

Conductivity and singlet oxygen detection modes are similar to fluorescence in the way that the voltage values are used as arbitrary units. Like fluorescence, the conductivity values need to be inverted but the singlet oxygen values of voltage are used as read from the digitizer (with appropriate averaging of shots, as in all cases).

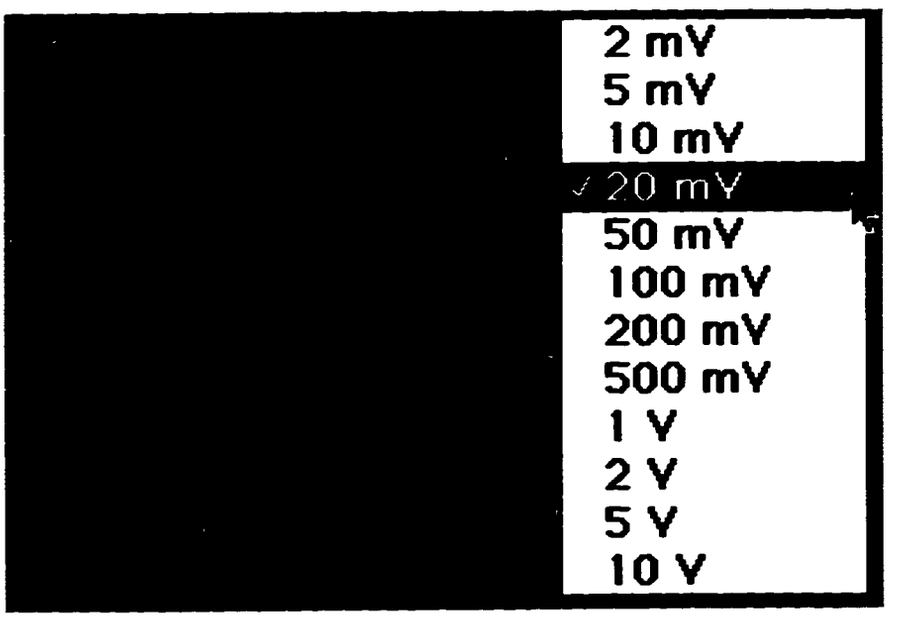

The vertical amplitude is set by choosing the **Voltage per Division** from a list of choices which correspond to valid values on the oscilloscope. Note that if the SCD-1000 is being used, the vertical amplitude selected here corresponds to the total voltage range, and valid values are 100 mV to 10 V.

The timescale to which the digitizer is set is controlled with a similar menu. Again, if the SCD-1000 is in use, the timescale selected is the total time window, not the time per division. Valid values for the SCD-1000 are 5 ns to 100 μs. If a value outside this range is requested, the program will automatically default to the closest legal value.

It is important to note here that there is a limit to the timescale one should select to do an experiment using the Tektronix 2440 oscilloscope. The maximum sampling rate for the 2440 is 500 x 10^6 samples/second. According to the manufacturer of the scope, both input signals are acquired simultaneously at all times. Although the total sampling rate for the scope is 500 MS/s, the fact that it acquires two channels at the same time and that it uses some bandwidth for operations during acquisition, the maximum useable bandwidth is 200 MHz. No matter what timescale the scope is set at, 1024 points will be collected in 20 time divisions, corresponding to approximately 51 points per division.

$$\left(\frac{51.2\,points}{division}\right)\left(\frac{1second}{500x10^6\,points}\right)=\frac{102ns}{division} \qquad \textbf{Equation 3}$$

Equation 3 demonstrates that the Tektronix 2440 digitizing oscilloscope, used under the conditions on our laser system, has a timescale limit of 100 ns/division. However, the scope allows the user to select timescales as fast as 2 ns/division, and it will continue to give 1024 points in 20 divisions in single sequence mode. Care must be taken when working at fast timescales. In the mode that we use the oscilloscope (with the REPET function off), at timescale settings faster than 100 ns/division, the scope will use random sampling and digital interpolation to create the trace and not all of the data obtained will be real. It is not recommended to use

timescale settings faster than 100 ns/division. See the description of using Chop Mode for working at fast timescales.

Also, the scope has an additional bandwidth setting feature which must be set to match the timescale selected and the lifetime (growth or decay) of the transient being measured.

This bandwidth setting (in conjunction with the maximum sampling rate) controls the vertical sampling resolution and will affect the effective rise time of a signal that can be measured. Although the user can set the bandwidth at any time and override computer control, the program will set the bandwidth at Full bandwidth (200 MHz) at 100 ns/division or faster, at 100 MHz bandwidth if the user selects 200 ns/division or 500 ns/division, and at 20 MHz if the user selects 1 μs/division or slower.

According to the manufacturer, the minimum useable rise time is the greater of:

- 0.35 divided by the selected bandwidth, or
- 1.6 times the sample interval

Table 1.1 shows the performance of the Tektronix 2440 oscilloscope. The bandwidth settings labeled with an asterisk show which setting is automatically selected by the program.

Table 1.1 Performance of the Tektronix 2440 Digitizing Oscilloscope

Timescale (/div)	*Bandwidth (MHz)*	*Sample Interval (ns/point)*	*Minimum Rise Time (ns)*
100 ns	Full*	2	3.2
	100		3.5
	20		17.5
200 ns	Full	4	6.4
	100*		6.4
	20		17.5
500 ns	Full	10	16
	100*		16
	20		17.5
1 µs	Full	20	32
	100		32
	20*		32
2 µs	Full	40	64
	100		64
	20*		64
5 µs	Full	100	160
	100		160
	20*		160
10 µs	Full	200	320
	100		320
	20*		320

*Automatically selected by the program.

The important information to be retained by the experimenter is that the lifetime being measured must always be greater than the minimum rise time for the scope at that timescale and bandwidth setting. Therefore, if the user sets the timescale to 100 ns/division and knows that the lifetime being measured is significantly greater than 17.5 ns (growth or decay), the user can override the program's bandwidth setting to 20 MHz. The effect of this may be to increase the signal to noise ratio since any fast-frequency noise may be smoothed by the 20 MHz bandwidth setting. This can also be used on fast timescales when fluorescence interferes with the signal, since most fluorescence signals are short-lived and setting a 20 MHz bandwidth can effectively help in filtering out these fast signals. The program is set, however, to always get the maximum digitizing performance from the system.

As mentioned above, the scope will always digitize and transfer 1024 points per trace, no matter what the timescale is set at. For our purposes, using 1024 points per trace and storing all this data is usually not necessary. Accurate kinetic fits can be made with 10 to 50 points in the area of the trace being fit.

In order to reduce the number of points from 1024 to 128 (the default setting), every 8 points in the trace are averaged and replaced by that average value. When 256 points are selected, every 4 points are averaged and when 512 points are selected every 2 points are averaged.

More points are usually necessary when the growth or decay being monitored is fast on the timescale selected, and occurs at the beginning of the trace. If every 8 points are averaged, not many points are saved and not much information is kept for fitting the trace. **Chop** mode is most useful in these situations.

In **Chop** mode, no grouping occurs (the full 1024-point-per-trace resolution is conserved), but the user can select a window in time to display and save as useable data, using the controls for number of points in chop mode and start point.

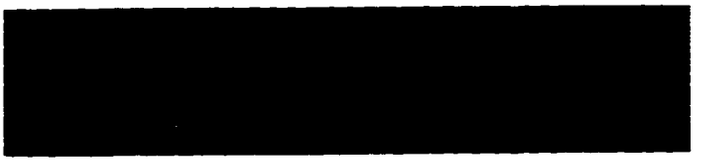

The pre-trigger on the Tektronix 2440 is set to one-eighth of the timebase so the laser pulse usually occurs approximately at point number 125. Selecting a starting point of 70 to 80 allows to see part of the pre-flash baseline (this is necessary). The user can then select how many points of the trace to select, at the full time resolution. With this option, the user can fit fast growths or decays at fast timescales without being forced to work with very large files.

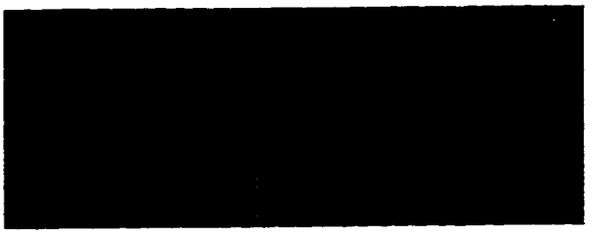

The light level measured preceding the laser flash (I_0) is a function of the monochromator throughput, the monitoring lamp profile, the sensitivity of the PMT, and the level of high voltage applied to the PMT. Using 93 Ω termination between the PMT and the digitizer, it has empirically been found that a light level of approximately 280 mV is in the linear range of response of the PMT.

The PMT gets its power from a programmable power supply which is interfaced to the controlling computer. The computer stores a calibration function which estimates the voltage necessary to apply in order to obtain a 280 mV response. After every shot, the computer then adjusts the power applied in order to stay as close to the 280 mV as possible.

This value of 280 mV is user-configurable and may be changed, for example, if something other than 93 Ω termination is used. Also, the computer will not consider data that has an I_0 value associated with it which is out of a specified range, as configured in the I_0 lower limit and upper limit controls. If a bad shot (I_0 out of range) occurs, the computer beeps, the event is noted and saved in a "badshots" counter, and the requested number of shots is incremented by 1, keeping the total number of shots considered in the average the same as the original number of shots requested.

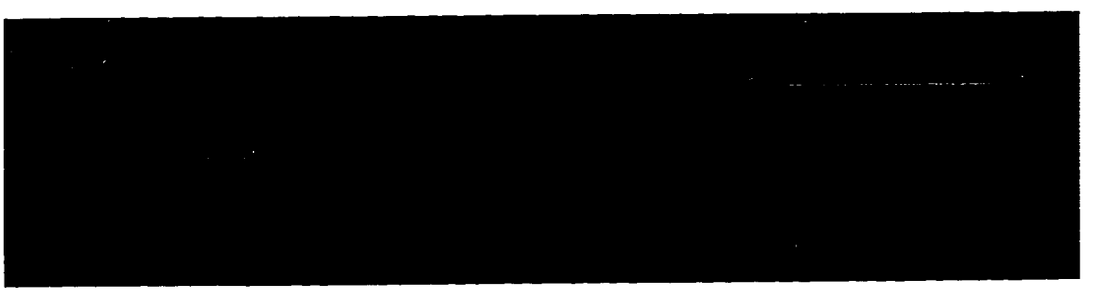

Some samples fluoresce at the wavelength one attempts to monitor a transient absorption, and it is possible to correct for this by using the **Fluorescence correction** feature. If **Fluorescence correction** is selected, each trace will take two laser shots to acquire. The first will use the laser pulse and the monitoring beam to record both the transient absorption and the fluorescence. The second shot will not use the monitoring beam and will record only the fluorescence signal at the same PMT setting. The results of the second shot are then subtracted from the results of the first shot to give the absorption-only signal. We have found, however, that the PMT is often more sensitive to the fluorescence in the laser-only second shot than it is in the first shot when the monitoring beam is used. This sometimes causes an over-correction. We have dealt with this in two ways. The first method is to use the **Fluorescence + lamp** correction, which keeps the

monitoring beam on (but does not pulse the lamp). The second method is to use a fluorescence correction factor, which is used to subtract a percentage of the fluorescence correction signal, decreasing the over-correction. The most appropriate fluorescence correction factor to use must be determined by trial and error by the experimenter.

Baseline correction is used at longer timescales when the monitoring beam intensity profile changes with time, due to instability in the pulsing of the lamp. In a baseline correction shot, the laser does not hit the sample but the lamp is pulsed, giving a monitoring-only profile to be subtracted from the first shot, correcting for any drift in the baseline.

If necessary, both a baseline correction and a fluorescence correction can be done, meaning that every cycle will take three shots; the first being laser and monitoring beam, the second being laser only and the third monitoring only. However, any uncorrelated noise will be subtracted twice, increasing the overall noise. Clicking the **Average Corrections** button will first average the two correction shots before subtracting them from the first shot. Doing both a baseline correction and a fluorescence correction is not often necessary.

Since the Tektronix 2440 is almost always the scope used when doing an experiment, the program assumes this is the one used. However, the program contains the interface code to communicate with two other models of oscilloscopes, the Tektronix 2432 and the Tektronix SCD-1000. Clicking on the **Other Digitizer** button will allow the user to select another scope model if necessary.

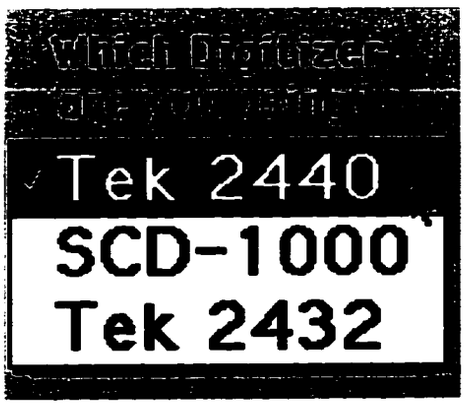

The continue button on the New Settings panel will return the user to the main front panel of the LFP program, save the parameters selected to the appropriate program variables, and communicate with the appropriate devices to set monochromator wavelength, scope settings, filter wheel selection, etc.

1.4.4.Diagnostics Panel

Clicking the **Diagnostics** button on the main front panel of the LFP program brings up the Diagnostics Panel.

This part of the program allows the user to have individual control of some key components in the laser system. These features are most useful when aligning the laser system or troubleshooting.

The terms "Little Shutter" and "Big Shutter" refer to the uniblitz-type shutters and the solenoid-type shutters, respectively. The shutters controlling the monitoring beam can be individually controlled, as can the shutters controlling the laser beam reaching the sample. The laser can be triggered and the lamp pulser can be triggered with the controls on this panel.

In addition, the sample temperature can be monitored, the PMT voltage can be set, the cutoff filter wheels can be re-initialized, and the magnetic field can be set if using the magnet. The magnet on Table 2 is controlled with its own programmable power supply.

No matter what state the controls are in at the time, clicking on the Return to Main Program button will set all controls to their off position and any programmable power supplies will be set to zero.

1.4.5.Saving a kinetics file

Upon completion of an experiment (after completing the requested number of shots or after clicking the Stop Early button), the user will be asked if more shots are needed. If the user responds yes, a prompt will appear asking the new total shots requested, a default value of the present total + 5 will be suggested. If the user responds no, a dialog box asking for a line of information will be presented. Suggested information to enter in this line includes the system being studied, whether the solution is being flowed or not, laser power, etc. Any of the parameters set in the program (in the New Settings panel), the date and time, and other relevant information will be recorded in the file and output in the printout (see the section describing the output of the fitting program for a full description). Only a single line of information is permitted; the program removes any carriage returns and any information following a carriage return.

1.4.6.Kinetics file format

The regular kinetics file format is one which saves all relevant experimental information. This file is readable by the kinetic fit program. It is a text file in ASCII format and is described as follows:

```
<CR>
MONI,LASER,PULSE,I0CONS,EXTRA1,EXTRA2,NSHTOTAL,EXTRA3,EXTRA4,EXTRA5<CR>
EXPOS,EXTRA6,EXTRA7,EXTRA8,EXTRA9,EXPT,NPTS,EXTRA10,EXTRA11,EXTRA12<CR>
LINE OF INFO.<CR>
MONLAMBDA,TPP,IZERO,AMPLITUDE,RELENERGY,EXTRA15,EXTRA16,EXTRA17,EXTRA18,EXTRA19<CR>
CHAN,HV,TEMP,NDF,GAUSS,SLITIN,SLITOUT,EXTRA20,EXTRA21,EXTRA22<CR>
ABSORBANCE DATA<CR>
.<CR>
.<CR>
.<CR>
.<CR>
.<CR>
END OF ABSORBANCE DATA<CR>
VERTICAL AMPLITUDE        TIMESCALE<CR>
DATE<CR>
TIME<CR>
LASER WAVELENGTH<CR>
TYPE OF DETECTION<CR>
DIGITIZER USED<CR>
TABLE NUMBER<CR>
```

The file starts with a carriage return (<CR>). The next two lines are integers, followed by the line of information. The next two lines are in exponential notation, formatted to 5 places after the decimal. The absorbance data then follows with 10 points per line. This data is in exponential notation, formatted to 4 places after the decimal. The total number of lines of data is variable, depending on the number of points acquired (according to the NPTS variable). The rest of the file consists of lines of strings; note that the vertical amplitude and timescale share a single line. TPP is the time-per-point variable which is used to rebuild the time array in the kinetic fit program. This compact file format saves on disk space. Note that, when saving a file, the user is always given the option to also save the "Kaleidagraph" format (X-Y data file), but the original kinetic file format is always saved.

1.5.The Spectrum Program (L3 VI)

A transient absorption spectrum can be obtained by acquiring kinetic traces at a series of wavelengths and recording the ΔOD at specified times after the laser pulse. The Spectrum program automates this process.

Some of the front panel controls are identical to those found on the Kinetic program's front panel. Being able to change the vertical amplitude in the middle of an acquisition is particularly useful while running a spectrum. The PMT can be set to manual, the number of shots requested adjusted, and the intensity on the SCD-1000 can be adjusted as well. All of these settings, as in the Kinetics program, can be adjusted "on the fly". There are some controls on the Spectrum program front panel which are particular to that program.

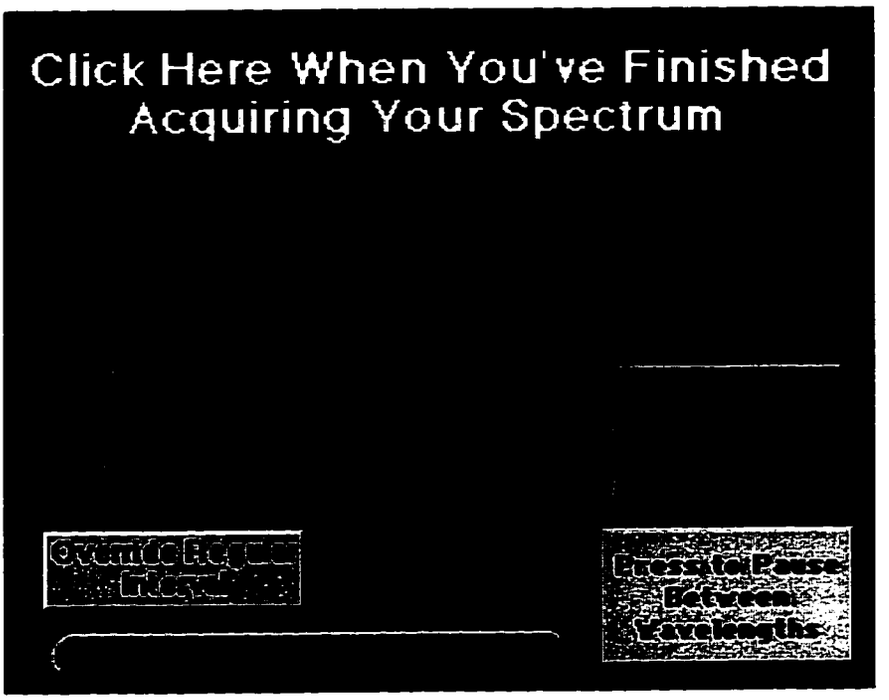

Test shots can be acquired by clicking on the corresponding button. The New Settings panel will be presented to the user to set the appropriate acquisition parameters.

When the experimenter is ready to start acquiring a new spectrum, the **Start Spectrum** button should be clicked. The user will be prompted for a filename. The first step will be initialization, then a sample trace must be obtained in order to set the time windows to be averaged. The New Settings panel will appear (identical to the one in the Kinetics program; it is the same subVI) and the experimental conditions should be entered. The number of shots requested and the monitoring wavelength will only apply to the sample trace. A panel very similar to the front panel of the Kinetics program will appear and the acquisition of the sample trace will execute.

The sample trace serves two main purposes. First, the experimenter can be assured that a signal can be obtained at a specified wavelength, timescale, correction factors, etc. Timescale cannot be changed during a spectrum

acquisition, so confirming that the correct timescale has been selected at this point is important. After acquiring a sample trace, the user will be asked if the current settings are satisfactory. If the user replies that they are not, the New Settings panel will be presented again and a new sample trace will be obtained.

The second main purpose for acquiring a sample trace is to select time windows for building the spectrum. After acquiring the sample trace and confirmation that it is satisfactory, the sample trace will be presented with a set of cursors overlayed on top of it. There are 4 pairs of cursors, alternating green and red, and a ninth yellow cursor to be used to set the zero time. The yellow cursor should be positioned at the approximate point on the trace at which the laser pulse occurred. As the Spectrum program slews through wavelengths, ΔOD values will be extracted at the times specified by the 4 pairs of cursors. The positions of the cursors correspond to point numbers on the trace. If, for example, the first pair of cursors is set at point number 25 and point number 35, the average of the ΔOD values corresponding to those found between points 25 and 35 will be extracted for each wavelength acquired. This is the same for the other 3 pairs of cursors.

It is important to note that the sample trace serves only these two purposes. The data (the actual ΔOD information) in the sample trace is not conserved and will not be used in creating the spectrum. For this reason, if the experimenter is working in a system where the number of laser shots hitting the sample must be minimized, a "perfect" trace is not necessary to obtain. The sample trace is useful to visualize the decay process over time, helping to select the time windows, but this can often be obtained by just a few shots to give an idea of the decay kinetics.

It is also important to note that the time windows selected at the beginning of the program are not final. The SuperSpec program can be used to generate new time windows and therefore new transient absorption spectra from the data saved during the execution of the Spectrum program. See the section describing the SuperSpec program.

Once a sample trace has been obtained and the time windows selected, the main front panel of the Spectrum program will return and wait for one of three buttons to be clicked by the user: **Regular Interval, One Wavelength,** and **Irregular Interval.** When Regular Interval is selected, the user will be prompted for a starting wavelength for the spectrum, an ending wavelength, a sampling interval (i.e. every 10 nm), and the number of shots requested to average at each wavelength. After confirmation, the program will start acquiring data at the starting wavelength. After the first trace has been acquired, the user will be prompted for a line of information.

Note that the user can specify if the wavelength scan will go from high wavelength to low wavelength or vice versa. If the starting wavelength is lower than the end wavelength, the program will scan in increasing increments, and the opposite is true.

It is possible that during an acquisition the user may desire to change the wavelength interval (to larger increments if there is no spectral feature or to smaller increments if an interesting spectral feature appears during acquisition). The **Override Regular Interval** feature is useful in these situations. When this button is activated (it turns black), the wavelength increment in the box next to it will be used instead of the one specified at the beginning of the program. Another click of the button will deactivate it and the program will return to the originally specified wavelength

interval. This feature can be used repeatedly during an acquisition and the override value can be changed. Note that entering a negative value in this box will reverse the direction of the acquisition until the button is deactivated when the original course and interval will be resumed.

At any time during acquisition the **Stop Early** button can be used to suspend acquisition and the program will be returned to a wait state expecting one of the three acquisition buttons to be clicked or to end spectrum acquisition altogether. As in the Kinetics program, the **Pause** button can be used at any time to temporarily suspend execution of the program, allowing for shaking of a sample or other adjustments. The **Pause Between Wavelengths** feature will suspend the program only between wavelengths as long as the button is activated. Its state can be changed at any time during acquisition.

If the ΔOD values at a single wavelength is needed, the **One Wavelength** feature can be used. The user will be prompted for the wavelength and number of shots. It should be noted that wavelengths can be repeated, all data will be conserved (SuperSpec is useful for removing unwanted data).

If the characteristics of a spectrum are well known, the **Irregular Interval** feature can be used for variable wavelength intervals. The user will be prompted for a ΔOD value below which a certain wavelength interval will apply and above which another wavelength interval will be used.

All data acquisitions are cumulative until the **Click Here When You've Finished Acquiring Your Spectrum** button is activated. Wavelengths can be repeated, new sets of regular intervals can be added, and single wavelengths can be added, in any order. All data will be saved and will be retrievable by the SuperSpec program. When the **Click Here...** button is activated, the user will be asked if the data should be printed and the

program will return to a wait state, expecting the the **Start Spectrum** button to be clicked or the **Switch to Kinetics Program** button to be clicked.

The Spectrum program saves two files. The first file, with the name given by the user, contains the ΔOD information for each of the traces acquired, along with the number of shots, the temperature, and the average I_0 for that trace. This can be a large file, depending on the number of traces acquired. The second file has the same filename with ".aux" appended to the filename. This is a summary file, with relevant experimental information including the average ΔOD for each of the time windows selected. Both of these files are needed for the SuperSpec program to function.

1.6.The SuperSpec Program

The SuperSpec program is a tool for analysis of data acquired during execution of the Spectrum program. When a spectrum is acquired, every kinetic trace is saved to file, and the SuperSpec program gives the user access to this data and allows for:

- Creation of new time windows to be averaged
- Kinetic traces to be extracted and saved into separate files readable by the Kinetic Fit program
- "Bad" traces to be removed from the data set on a temporary basis
- Newly calculated spectra can be printed and saved to new ASCII files.

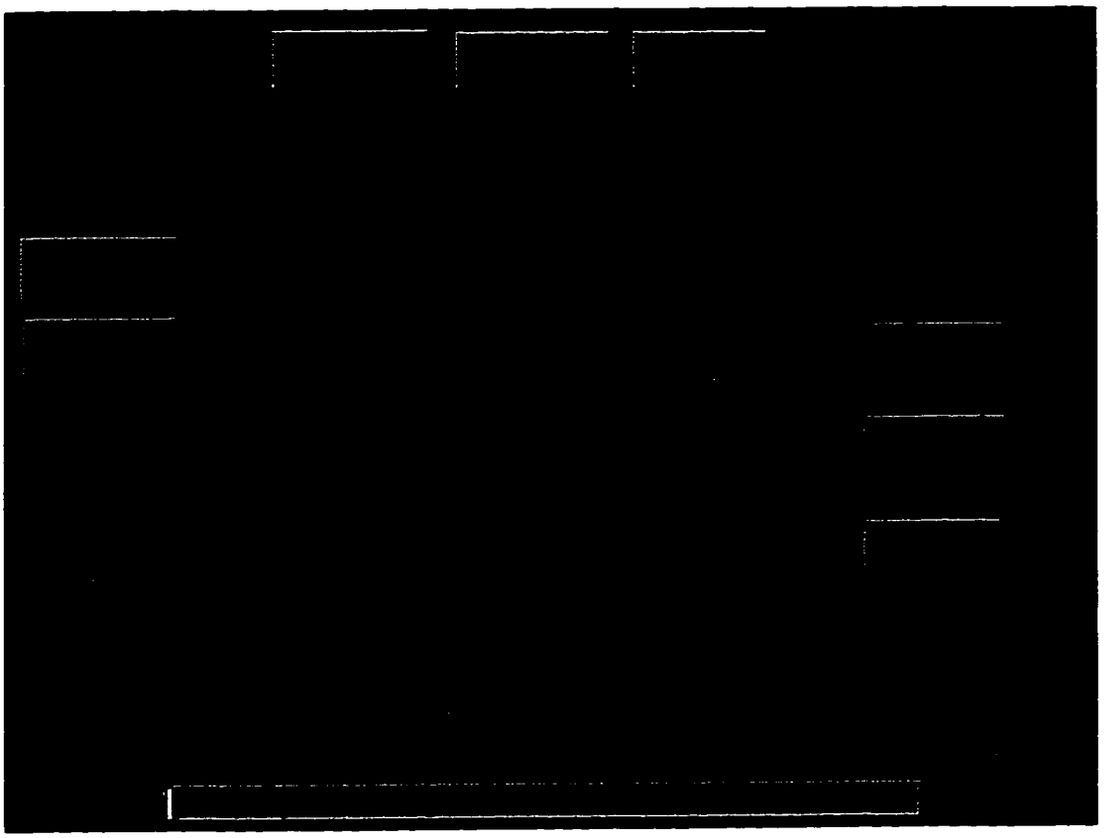

When the program is first run, a dialog box appears and the user must find one of the spectrum files (either the original file or the .aux file). They both must be found in the same directory. The traces will then be sorted since it is possible to not have run the spectrum in any specific order.

The top window will display the active trace, given a number between 0 and the number of points in the spectrum. To the right of the trace window is the corresponding **Wavelength** and $\mathbf{I_0}$ for that trace. The **Trace Number** control can be used to display a different trace number. The x-axis of the trace window can be either labeled with time in microseconds or with point number, depending on which position the **X-axis** control is in.

The first step in using the program to its fullest extent is to set the zero time. The green marker (a vertical green line overlayed on top of the trace) should be positioned over the point at which the laser pulse occurs on the trace (usually point 17 in a 128-point trace). The green marker

position is controlled with the **Time Index 1** control. Once the green marker is in position, the **Set Zero Time** button should be clicked. If the x-axis of the trace window is in time mode, the axis will shift to mark time zero at the laser pulse. This step is necessary for correct spectrum times to be calculated (displayed in the **Average Time (1)** and **Average Time (2)** windows).

The Kinetic Fit-compatible file of the active trace can be saved by clicking the **Save Kinetic File** button. A dialog box asking for a filename will appear. The Kinetic Fit program is embedded in the SuperSpec program, as it is in the Kinetics program and can be called up by clicking on the **Get Kinetic Fit** button. These two steps can be done in one step by clicking on the **Save & Get Kinetic Fit** button. Quitting the Kinetic Fit program when called up from the SuperSpec program will return the user to the SuperSpec program.

The **Time Index 1** control in conjunction with the **Width 1** control will form a time window from which a spectrum will be calculated and output in the lower window in green. Its corresponding average time after the laser pulse will be displayed in the **Average Time (1)** display, hence the importance of setting the zero time properly. The units of time index and width are in number of points. The points used to calculate the spectrum for window 1 will be highlighted in green in the upper trace window and the calculated spectrum will appear in green in the lower window. In the spectrum window, the point of the spectrum corresponding to the trace displayed in the trace window will be highlighted in black.

All that applies to the controls for the first spectrum applies to a second spectrum, controlled with **Time Index 2** and **Width 2**. The data for the second spectrum is labeled in red instead of green.

Occasionally, a "bad" trace is acquired during an experiment, giving a spectrum which contains a bad point at a particular wavelength. A bad trace (or any individual trace) can be removed and not used in the calculation of the spectrum. The trace to be removed must be active in the upper trace window and then the **Remove This Trace** button must be pushed. This does not remove the trace from the original files and only temporarily suppresses the data from that trace for the purposes of the SuperSpec program.

Once satisfactory spectra have been generated in the lower window, the user can save the data to an ASCII file by clicking on the **Save Spectra** button and the results can be printed by clicking on the **Print Spectra** button.

Any repeated wavelengths will be treated individually and labeled separately in the **Wavelength** window by an increment in the third decimal place, i.e. 460.000 and 460.001.

1.7.The Kinetic Fit Program (L4 VI)

The Kinetic Fit program is embedded in the Kinetics program and in the SuperSpec program, but it can also be run as a stand-alone utility. Its main purpose is to allow the experimenter to do initial kinetic analysis on the data obtained in a kinetics experiment. Also, it provides the primary hard-copy output for records of experiments by outputting the main experimental parameters relevant to the experiment, as well as the line of information entered by the user.

When the program is executed, a dialog box appears requesting the kinetics file to be analyzed. A window will then appear with the trace on a black background and 3 cursors which can be positioned by dragging them with

the mouse to the desired position. Two vertical markers must be positioned, one at the first point to be fit and the other over the last point to be fit. The third cursor is a horizontal cursor which is used to define an infinity level. This level will be non-zero if, for example, a long-lived signal persists at the timescale of the experiment, or if there is net bleaching of the sample below baseline at the timescale of the experiment.

Once the cursors are positioned, one of 4 choices can be selected for the type of data fit to be carried out.

The three fit options transform the data to a linear plot and do a best linear fit to the data. For a first-order decay the function plotted against time is:

$$Y = \ln(data - inf) \qquad \textbf{Equation 4}$$

where *inf* is the infinity value corresponding to the horizontal cursor position.

For a first-order growth the function is:

$$Y = \ln\left(\frac{inf}{inf - data}\right) \qquad \textbf{Equation 5}$$

For a second-order decay the function is:

$$Y = \frac{1}{data - inf}$$ **Equation 6**

The **No Fit** option is used for those instances when a fit is either unnecessary or impossible, but a hard-copy record of the experiment is desired.

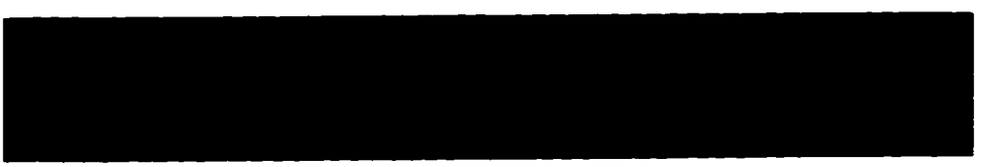

Once the cursors have been positioned, clicking **Try This Fit** will cause a fit to the data using the cursor setting selected. A fit correlation will be displayed and the program will use the fit results to overlay a data trace corresponding to the fit results on top of the real data. The user can then re-adjust the cursor positions if necessary and keep doing this until a satisfactory fit is obtained, at which point the user will click on **Click Here to Continue**. The **Reset End Pos.** and **Reset Infinity** buttons are used in case the markers go off scale, which is sometimes possible if two consecutively-fit traces have very different timescales or vertical amplitudes.

Once **Click Here to Continue** has been selected, a dialog box appears:

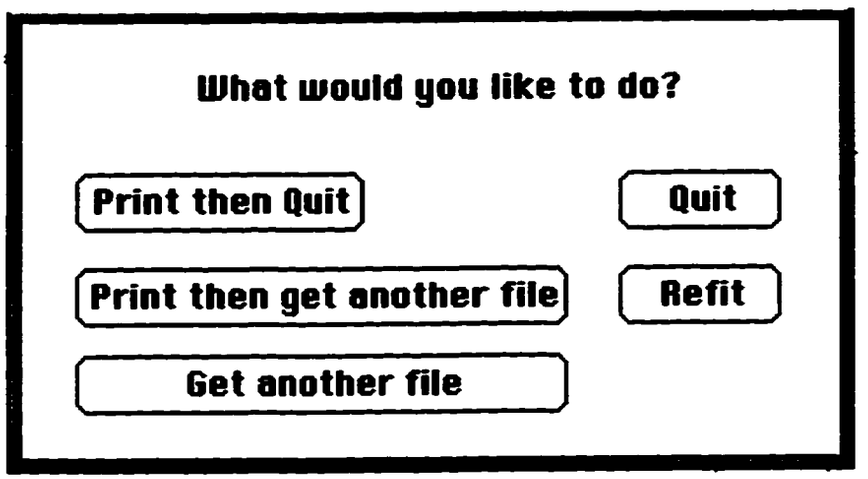

Print then Quit will do just that. **Print then get another file** will print the results then restart the program with a dialog box requesting the next file containing the trace to be fit. **Get another file** restarts the program without printing the results. **Quit** does just that. **Refit** will return the user to the panel allowing for re-positioning of the cursors and fitting parameters.

Figure 1.6 shows a typical printout of an experiment.

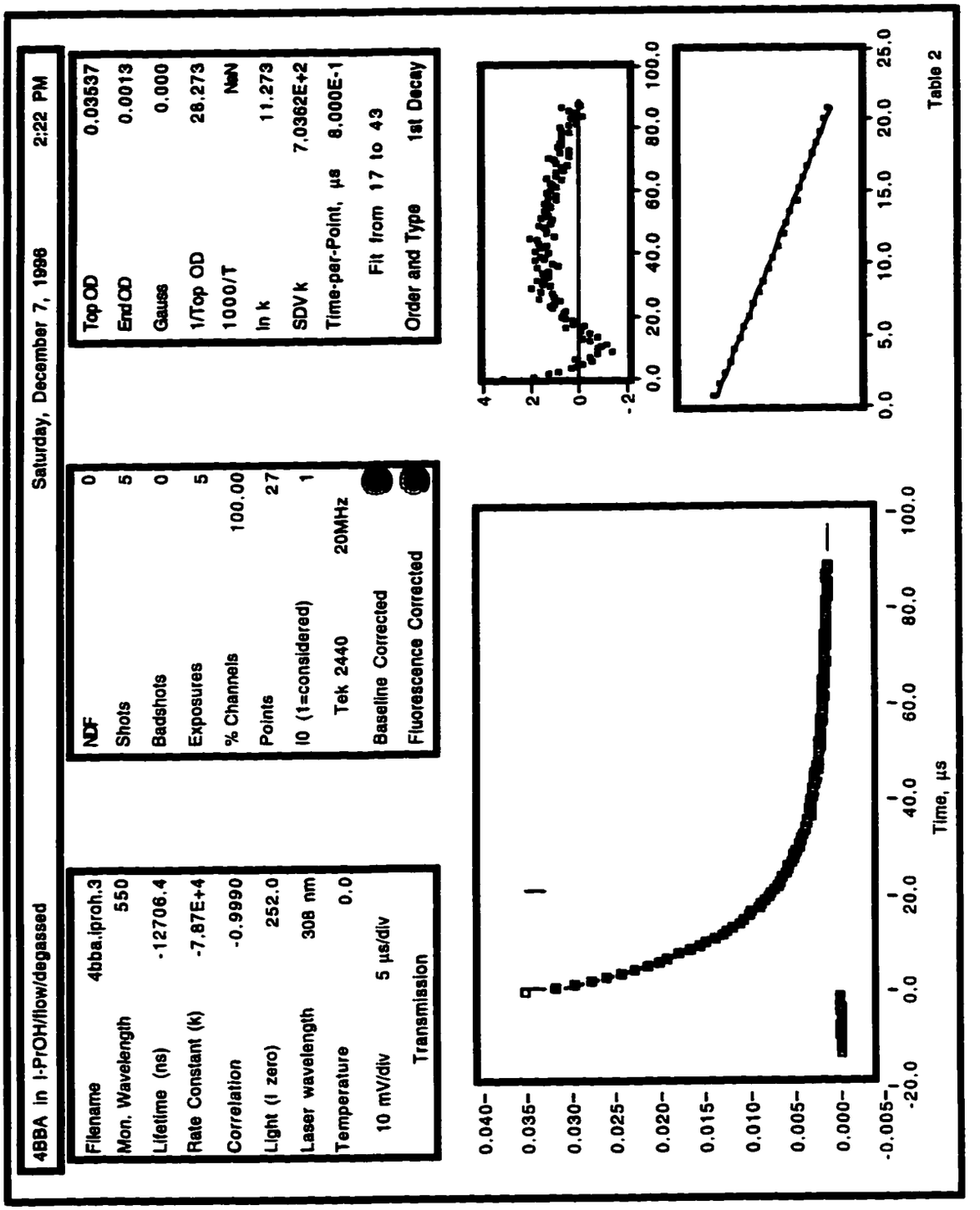

Figure 1.6 Typical Kinetic Fit program printout.

1.8.Hardware

In this section, an overview of the system architecture will be given with a general description of each of the major components and its functions. Figure 1.1, page 4, shows a schematic of the layout of the laboratory. All of the major components are shown in that schematic except for lenses and mirrors.

Experiment Table 1 contains both a transmission detection system and a diffuse reflectance detection system. The configuration of Rack 1 is shown in Figure 1.7 and that of rack 2 in Figure 1.8.

Figure 1.7 Configuration of Rack 1.

Rack 2 also contains a computer but this has been omitted in Figure 1.8.

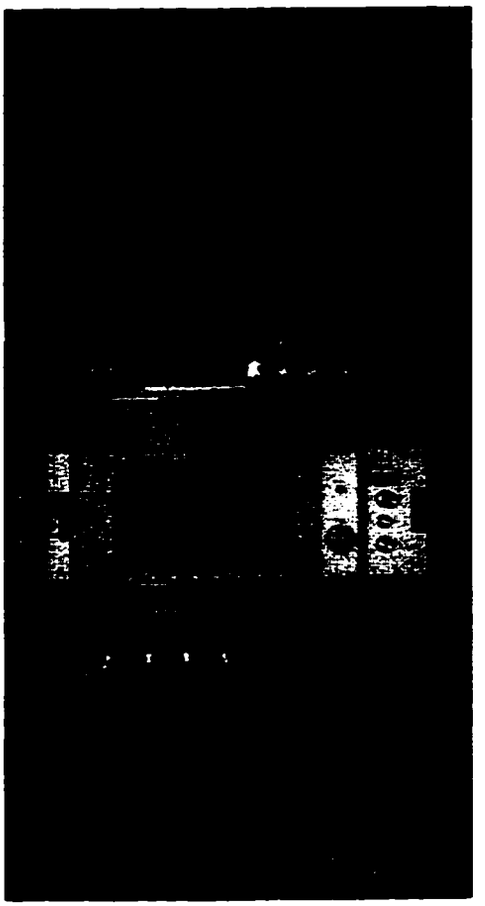

Figure 1.8 Configuration of Rack 2.

The main components, common to both racks are:

- Line synchronizer
- Digitizing oscilloscope
- Lab-NB breakout box
- Programmable PMT power supply
- Filter wheel driver (not shown in Figure 1.8).

- Computer, plug-in boards (GPIB and DAQ), external storage device, and monitor

Rack 2 contains a few additional components:

- Second oscilloscope
- Signal interface unit
- Programmable magnet power supply (not shown)
- Baseline compensation unit (mobile; can be moved to Rack 1)

1.8.1.The Line Synchronizer

The heart of the system is the Line Synchronizer. This unit acts as a multi-function pulse generator with precise, variable delays between the output control pulses. In its present configuration, it uses the 60 Hz line frequency as a reference pulse train. There are two delay banks, each with a pulse divider and pre-delay and delayed outputs. The first delay bank (delay 1) has the pulse divider set at a factor of 6, resulting in a 10 Hz pulse train generated at the outputs from delay 1. The delay 1 pre-delay pulse train used to trigger delay 2 and the delay 1 delayed pulse (set at 1360 μs) triggers the flashlamps of the YAG lasers, which must be triggered at 10 Hz for laser operation.

Delay 2 is then set to divide the pulse train from delay 1 by a factor of 35, resulting in a new pulse train of approximately 0.3 Hz. The delay 2 pre-delayed pulse triggers the lamp pulser and the delayed pulse (set at 1510 μs) triggers either the excimer laser or the Q-switch of the YAG lasers, depending on which laser is being used.

Setting delay 1 to 1360 μs and delay 2 at 1510 μs creates a time separation of 150 μs (1510-1360) between the YAG laser flashlamp signal and the Q-switch signal. This fixed time difference between the pulses is necessary for peak performance of the YAG laser. When the excimer lasers are used, the 10 Hz delayed pulse train is ignored. This is illustrated in Figure 1.9.

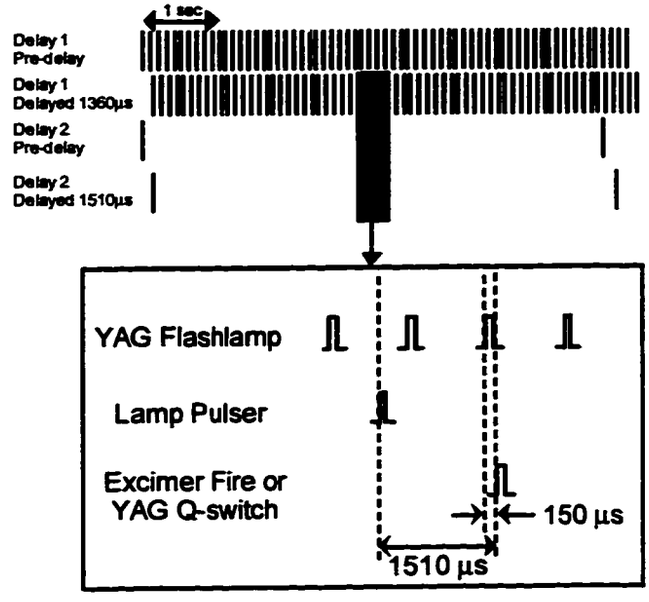

Figure 1.9 Line synchronizer pulse generation.

These bursts of pulses are continuously generated by the line synchronizer; the computer (and its associated DAQ card) is used for gating these signals, allowing signals to go to their destination or not, depending on the conditions.

Two-laser, two-colour experiments are sometimes performed. The line synchronizer does not contain a third delay bank so an external delay generator must be used. We use the Stanford Research Systems Inc. Model DG535 4 channel digital delay/pulse generator.

The most common combination of lasers is an excimer/YAG combination. This can be achieved by connecting the delay 2 delayed signal to the Stanford trigger input. The setting on line sychronizer delay 2 should be decreased by 20 μs (it will be added by the Stanford box). The Stanford box allows variable delays to be entered. Delay A should be set to 20 μs, delay B to 30 μs, delay C to 11 μs, and delay D to 30 μs. Connecting the YAG Q-switch trigger to the A-B stretched output of the Stanford box and the excimer laser trigger to the C-D stretched output will provide each laser with a 30 μs pulse, and the laser light will exit each laser at approximately the same time. Delay C sets the actual delay between the lasers. Setting delay C to less than 11 μs will cause the excimer to fire before the YAG and setting delay C to greater than 11 μs will cause the opposite to happen. 11 μs is the approximate internal delay difference between the YAG and excimer laser, where the internal delay is the time between the laser receiving the trigger and actually emitting the laser pulse. The Stanford box must be configured to trigger on the positive slope of the trigger signal and to output TTL non-inverted signals on the output channels being used.

The most important feature of the design of the line synchronizer is that all pulse trains are referenced to the same point on the 60 Hz cycle on the line. This has two main advantages. Some power sources are created from a mixture of feeds from 2 or 3 power plants. In some cases, this can cause voltage spikes at regular intervals. Second, when monitoring at very long timescales (>500 μs), it is possible to start to observe a fluctuation in the intensity of the monitoring beam corresponding to the 60 Hz cycle on the line. If all pulses are synchronized to the same point on the 60 Hz cycle, both of these effects can be corrected for.

However, these effects seldom interfere with measurements, and the line synchronizer is a complex, custom-built unit. It has recently been shown that plug-in timing boards such as the National Instruments NB-TIO-10 board can be programmed (via LabVIEW) to be used for the same purpose as the line synchronizer.[14] These pulses are not synchronized to the line, however. These boards are relatively easy to program and can in fact be more flexible than an external line synchronizer, making 2-laser experiments more simple to configure.

1.8.2. The Digitizing Oscilloscope

The digitizing oscilloscope is a key component in any laser flash photolysis system. All communication between the scope and the computer is via GPIB. Under normal operating conditions, the experimenter never needs to touch the front panel of the scope, all functions are controlled remotely by the computer. One of the most useful features of a scope such as the Tektronix 2440 is the pre-trigger capability. Pre-trigger can be set to a proportion of the total timescale and records information which occurs before the trigger signal. Using an optical pickup to determine when the laser pulse arrives at the sample, any jitter in the laser triggering becomes irrelevant, and precise timing of any pre-trigger signal is not necessary. The simplification this affords the system is tremendous.

The SCD-1000 is not a digital oscilloscope, and lacks this pre-trigger feature. When fast-timescale makes it necessary to use this scope, a pre-trigger signal must be generated. For this purpose, we again make use of the Stanford delay box in combination with an optical pickup and a long length of coaxial cable. The Stanford delay box is programmable via GPIB and the LFP program will set appropriate delays according to the timescale chosen. At timescales of 5 ns to 200 ns (total timebase), the Stanford box is

triggered by an optical pickup placed at the sample and the PMT output is forced through a 50-foot length of coaxial cable to delay its arrival at the scope by approximately 50 ns. At longer timescales than 200 ns total timebase, the signal from the delay 2 (pre-delay) is used to trigger the Stanford box and the PMT output need not go through any additional length of cable. However, these timescales are accessible by the Tektronix 2440 and these experiments can be run in the normal configuration of the system.

1.8.3.Lab-NB Data Acquisition (DAQ) Board

The Lab-NB breakout box is the interface for the National Instruments plug-in Lab-NB board. This board has 3 digital ports (8 channels each), one analog output port (2 channels) and one analog input port (8 channels). It is also equipped with two counters. The breakout box is connected to the board with a 50-pin ribbon cable and basically provides a BNC connector for each of the pins on the board's connector. The digital output ports control devices such as the shutters and gates. The digital input port is used for carrying the signal for position detection for the filter wheels. The analog output port is used to control the programmable PMT power supply. The analog input port has been used to connect a thermocouple for temperature detection, however this has been recently replaced by a GPIB-interfaced unit. The counters and timers are used to produce pulse trains for control of the filter wheels. Figure 1.10 shows a full system block diagram.

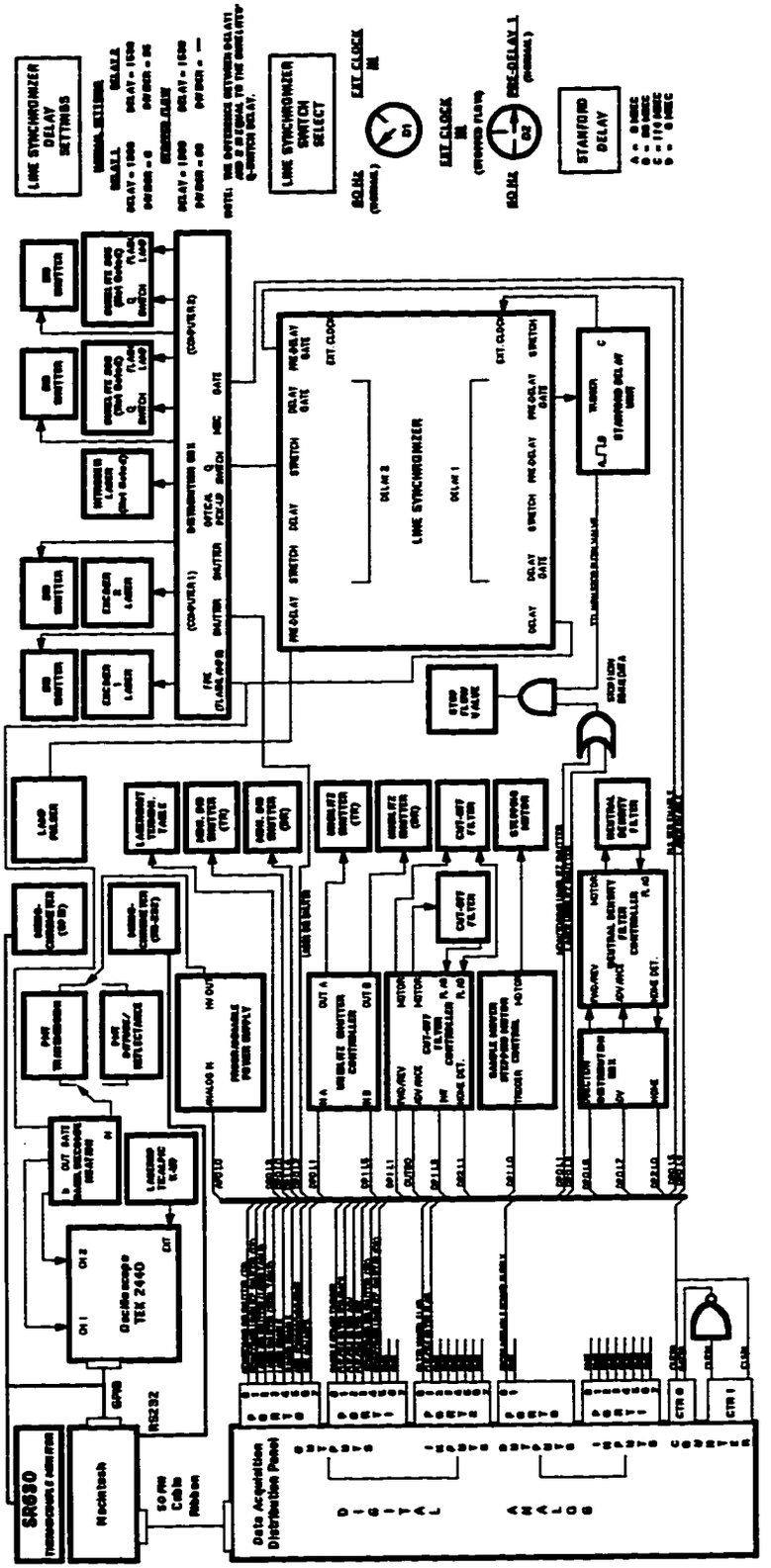

Figure 1.10 System block diagram.

1.8.4.Baseline Compensation

Figure 1.2 (page 6) shows schematically that, when measuring a transient signal, the change in voltage measured is usually small compared to the large change in voltage caused by the lamp pulsing. A typical change in signal for a transient can be on the order of 10 to 50 mV superimposed on a large voltage change of 280 mV due to the lamp pulse. In order to get the maximum resolution of the digitizer, we use one of two methods for separating the transient signal from the baseline level.

The first method uses a high-pass filter at the input of the digitizer. The pre-flash baseline acts as a low-frequency signal (which is filtered out) and the transient signal is the only signal allowed to pass through the filter and this is input into the scope. This pre-flash baseline of the transient signal appears at ground so we are able to use a small vertical amplitude in order to get maximum digitizing resolution of the trace. In order to obtain the actual pre-flash baseline which is necessary to calculate the change in absorbance, the untreated PMT signal is fed into the second channel of the digitizer (at a different and appropriate vertical amplitude) and acquired simultaneously. The limiting factor in using the high-pass filter is the cutoff frequency (determined by the capacitor used). At present, the practical upper limit for signals to be measured using this baseline compensation system is lifetimes of 20 to 30 μs.

An alternate method to achieve the same result is to use the Baseline Compensation Unit (BCU). The BCU uses a trigger pulse (provided by the delayed signal from delay bank 1 of the line sychronizer) to sample the pre-flash voltage. From that point on, the input signal from the PMT is offset that amount and the BCU outputs two channels, the I_0 and the signal, which are input to the digitizer. At present, the BCU is designed to hold and offset the I_0 for 50 ms, allowing measurements of up to 2 ms/division.

It is important to note that the lamp pulser pulses the monitoring beam for approximately 5 ms, therefore when performing any long timescale work the pulser must be disabled which affects the size of signals that can be detected.

1.8.5.The Signal Interface Unit

The Signal Interface Unit, found on Rack 2, gives full flexibility to use any laser on either Table 1 or Table 2. There are a total of 5 lasers to choose from: 2 excimer lasers, a nitrogen laser, and two Nd:YAG lasers (the dye laser is pumped by the excimer laser) and each laser has a solenoid shutter in front of it. The signals that control laser firing from the line synchronizer and the signal controlling the shutter must get to one of the five lasers. Also, the gate signal from the computer goes to this unit. There are two controlling stations. The signal interface units takes these two sets of signals and routes them to the appropriate laser and shutter, depending on what is selected on the front panel of the unit with a simple switch. There are two switches, one for control from Rack 1 and one for control from Rack 2.

The YAG lasers and the nitrogen laser benefit from greater beam stability when the laser firing is not interrupted. Therefore, the laser enable gate signal is ignored if these lasers are selected on the switches. The signal interface unit was built with additional, unused lines which can be used in the future for other purposes such as neutral density filter wheels.

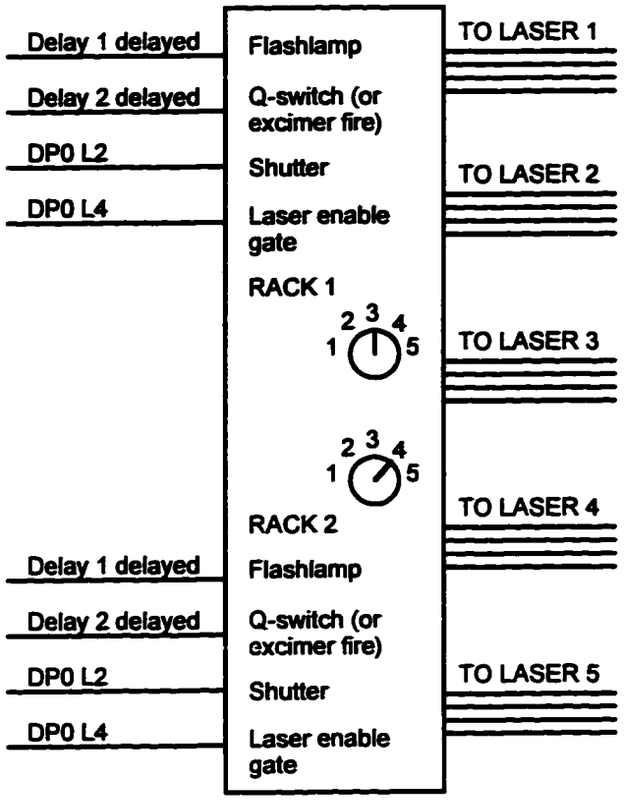

Figure 1.11 Schematic of Signal Interface Unit.

1.8.6.Other Hardware

The programmable PMT power supply provides high voltage to the PMT. 1 mV supplied from the analog output port of the Lab-NB board corresponds to 1 Volt output to the PMT. The programmable magnet power supply (Rack 2) is controlled via GPIB. The filter wheel drivers are a custom-built unit which control 5 V stepping motors equipped with a home position detection system. These drivers use pulse trains generated by the Lab-NB board, as well as initialization digital signals and a position detection system. An optical pickup placed on the laser table (refer to Figure 1.1, page 4) changes the optical laser pulse to an electrical trigger for the digitizer. The transmission detection systems on both tables use a CVI Laser Corp. Digikrom 240 monochromator (GPIB control) and the diffuse

reflectance system on Table 1 uses a CVI Laser Corp. Digikrom 120 monochromator (RS-232 control).

The computers used on the system at the University of Ottawa are Power Macintosh 7100/66 systems equipped with 24 MB of RAM, a 500 MB hard drive, and a 17" monitor. Data storage is performed on an external 44 MB Syquest drive; each user is assigned a removable cartridge and this provides a convenient multi-user system.

1.9.References

[1] W. F. Kosonocky, S. E. Harrison, and R. Stander, "Observations of the Triplet State in Phthalocyanines," *J. Chem. Phys.*, **43** (3) , 831, **1965.**

[2] L. Lindqvist, "Utilisation d'un Laser à Emission Ultraviolette Pulsé en Photolyse-Eclairs: Etude de l'Etat Triplet de l'Acridine," *Hebd. Seances Acad. Sci., Ser. C*, **263** (October 10) , 852, **1966.**

[3] G. Porter, "Flash Photolysis and Primary Processes in the Excited State," in *Fast Reactions and Primary Processes in Chemical Kinetics*, S. Claesson, Ed. Stockholm: Almqvist and Wiksell, **1967**, pp. 141.

[4] G. Porter and M. R. Topp, "Nanosecond Flash Photolysis," *Proc. Roy. Soc. Lond. A.*, **315** , 163, **1970.**

[5] R. M. Danziger, K. H. Bar-Eli, and K. Weiss, "The Laser Photolysis of Methylene Blue," *J. Phys. Chem.*, **71** (8) , 2633, **1967.**

[6] J. R. Novak and M. W. Windsor, "Laser Photolysis and Spectroscopy in the Nanosecond Time Range: Excited Singlet State Absorption in Coronene," *J. Chem. Phys.*, **47** , 3075, **1967.**

[7] R. Bonneau, J. Faure, and J. Joussot-Dubien, "Singlet-Singlet Absorption and Intersystem Crossing from the $^1B_{3u}$- State of Naphthalene," *Chem. Phys. Lett.*, **2** (2) , 65, **1968.**

[8] A. Müller and E. Pflüger, "Laser-Flashspectroscopy of Cryptocyanine," *Chem. Phys. Lett.*, **2** (3) , 155, **1968.**

[9] D. S. Kliger and A. C. Albrecht, "Nanosecond Excited-State Polarized Absorption Spectroscopy of Anthracene in the Visible Region," *J. Chem. Phys.*, **50** , 4109, **1969.**

[10] C. R. Goldschmidt and M. Ottolenghi, "Excited Singlet-Singlet Spectra of Anthracene, N,N-Diethylaniline and their CT Complex," *Chem. Phys. Lett.*, **4** (9) , 570, **1970.**

[11] J. T. Richards, G. West, and J. K. Thomas, "Formation of Ions and Excited States in the Laser Photolysis of Solutions of Pyrene," *J. Phys. Chem.*, **74** (23) , 4137, **1970.**

[12] G. W. Johnson, *LabVIEW Graphical Programming: Practical Applications in Instrumentation and Control.* New York: McGraw-Hill, Inc., **1994.**

[13] P. Kubelka, "New Contributions to the Optics of Intensely Light-Scattering Materials. Part 1.," *J. Opt. Soc. Am.*, **38** (5) , 448, **1948.**

[14] M. Barra, personal communication, **1996.**

2.Photochemistry of Lignin Model Compounds

2.1.Background

Since the invention of the printing press, techniques for mass production of paper made from wood pulps have been developed. Modern procedures for the preparation of these pulps enable production of paper grades with remarkable physical properties, but their aging is very much a modern day problem.

There are presently two main types of bleached pulps produced: chemical pulps and high-yield pulps.

Chemical pulps are obtained by delignification of the wood after selective chemical treatment, in acidic medium (bisulfite treatment: HSO_3^-/H_2SO_3) or in basic medium ("Kraft" treatment: $NaOH/Na_2S$). The pulp at this point contains about 5% residual lignin, and it is then put through a multistage bleaching process, to get virtually total delignification of the material. Bleached chemical pulps, made up of mainly cellulose and hemicellulose, have the advantages of being strong, having a high brightness level, and being relatively stable to sunlight. Important

disadvantages associated with these pulps are their low yield of productivity (about 50%) and the pollution produced in order to obtain these pulps.

High-yield pulps (yield>90%) are made directly from mechanical defribrification of wood chips. They therefore conserve all the initial constituents of wood (i.e. cellulose, hemicellulose, and lignin). They are then bleached by either oxidation (peroxide/OH^-) or reduction ($Na_2S_2O_4$) of the lignin chromophores. More elaborate mechanical treatment technologies have recently been developed, where the defibrification is done at high temperature (thermomechanical pulp or TMP), or chemical treatment of the wood chips is done by Na_2SO_3 before the thermal treatment (chemithermomechanical pulp or CTMP). Apart from being less resistant and bearing a lower brightness level than chemical pulps, TMP also has the disadvantage of yellowing very quickly in sunlight. These pulps are used for bulk newsprint and they have a limited conservation lifetime, due to their loss of desirable colour properties.

With increasing demand for paper products and depleting forest reserves, the paper industry is attempting more and more to improve and use high-yield pulps instead of chemical pulps. As photostability is one of the major drawbacks to using TMP, much discussion, effort, and research has developed in this field.

To understand the chemistry of lignin, it is important to understand its characteristics and its role in wood, in pulp, and in paper. As a tree grows, the cells divide, and each of the new cells encloses itself in a thin primary cell wall which is mostly made of cellulose, hemicellulose, pectin, and protein. At these early stages the cell is considered a "living" cell, carrying out vital biochemical functions for the tree and carrying water and

nutrients to different parts of the tree and leaves. In the following phase, the cell differentiates, it expands to its full size, and it starts to form a thick secondary cell wall. This wall consists of cellulose and hemicellulose. As the secondary wall is being formed, lignification begins.[1]

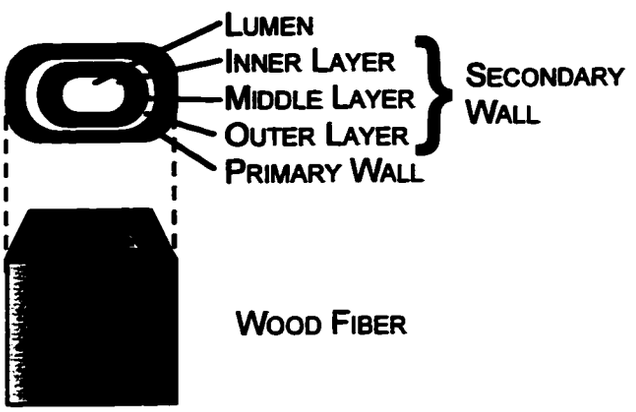

Figure 2.1 Structure of the mature wood cell.

The "living" cells in wood are cemented together by an intercellular substance (true middle lamella) which is mostly comprised of lignin. As the cell matures the primary cell wall becomes heavily lignified. At maturity, the secondary cell wall contains possibly 25% of the total lignin content in wood.[2]

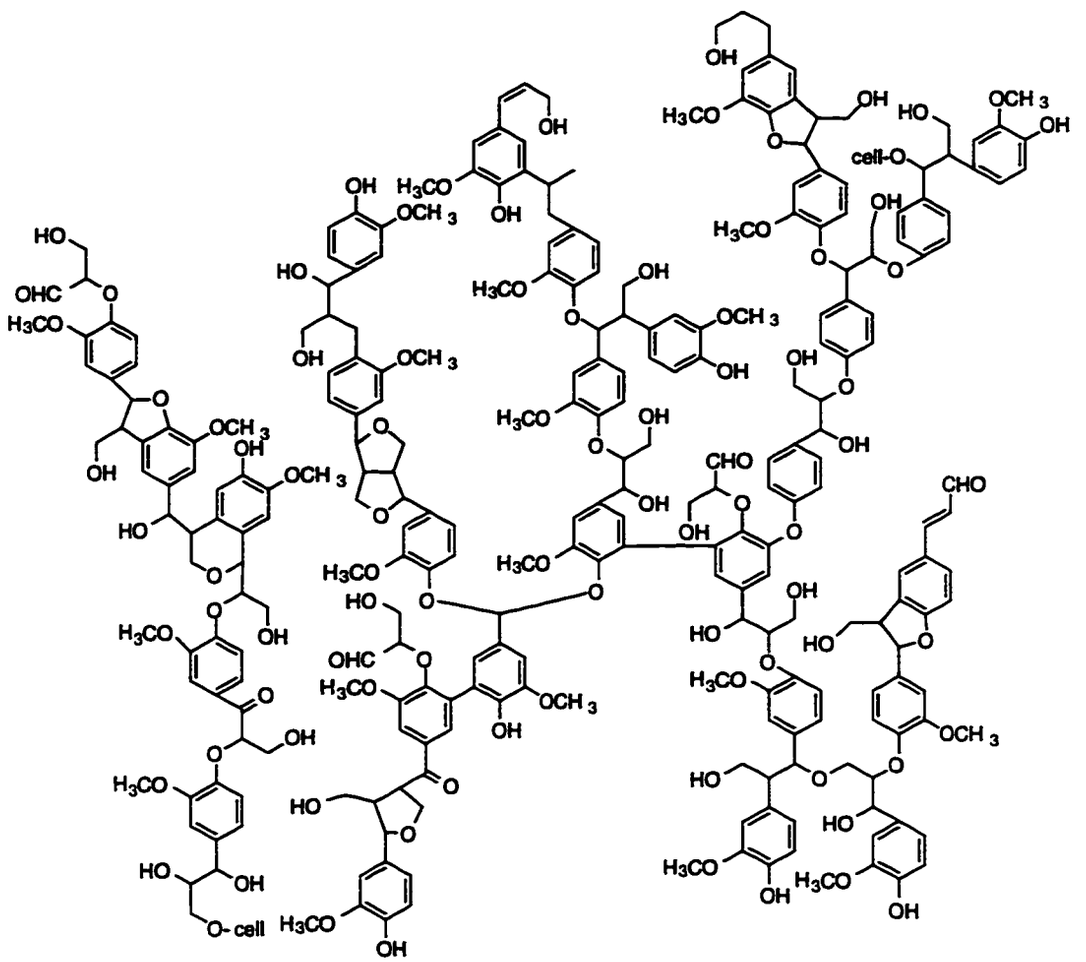

Figure 2.2 A proposed structure for lignin[3]

2.1.1.Colour Measurement

In order to measure and evaluate the changes in colour of a sample of paper, standard methods of measurement have been developed. In 1931 the CIE (Commission Internationale de l'Eclairage) established the "Standard Observer" experiment in which monochromatic light of individual wavelengths is produced by a prism system and projected onto a white screen. Three controllable coloured light sources, red, green and blue are also projected onto the white screen superimposed upon each other.

At the beginning of the experiment a single wavelength of 400 nm is projected onto the screen and the observer then adjusts the three coloured light sources until the colour produced matches the individual 400 nm wavelength. The observer then records the relative output of the three coloured light sources. This is then repeated for 410 nm, 420 nm, etc., until the entire visible spectrum of 400 nm to 700 nm has been reproduced by the three coloured light sources. This experiment is then repeated by many observers to obtain a good sampling.

Thus , the CIE tristimulus functions X(red), Y(green), and Z(blue) were developed. Although X, Y, and Z are the basic fundamental measurements on which most colour scales are based, very few people in industry use X, Y, and Z directly for colour control or specifications. A transformation of the CIE colour space into what is described as the L, a, b space was developed to simplify the reporting of the colour of paper. This space is more visually uniform and more easily understood (see Figure 2.3).

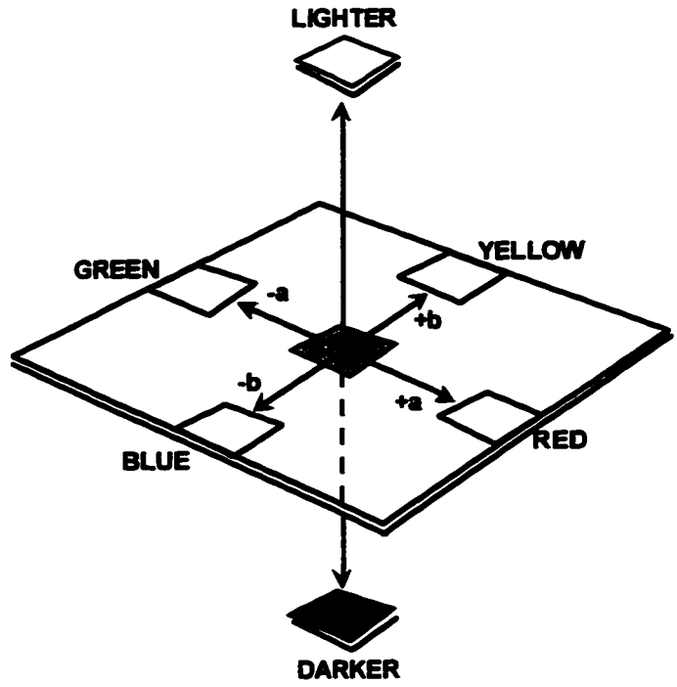

Figure 2.3 L, a, b, Colour space

L is the measure of lightness and varies from 100 for a perfect white to 0 for absolute black. +a indicates redness and -a greenness. +b indicates yellowness and -b blueness. Further improvements in the calculation of these colour parameters have produced the more recent L*, a*, and b* parameters. Industrial colourimeters like the Technidyne colourimeter, an industry standard, convert instrument response to L*, a*, and b* values using the equations that follow:

$$L^* = 116\,(Y/100)^{1/3} - 16 \qquad \textbf{Equation 7}$$

$$a^* = 500\,[(X/98.04)^{1/3} - (Y/100)^{1/3}] \qquad \textbf{Equation 8}$$

$$b^* = 200\,[(Y/100)^{1/3} - (Z/118.1)^{1/3}] \qquad \textbf{Equation 9}$$

where X, Y, and Z are the percent reflectance values at 634 nm, 556 nm, and 436 nm, respectively.

Absolute brightness (ISO Brightness) is defined as the reflectance of blue light with a specified spectral distribution peaking at 457 nm compared to that of a perfectly reflecting, diffusing surface.[4] Bleaching agents strongly influence the reflectance of pulp in this portion of the spectrum.

2.1.2.Sources of Colour Reversion

It has been proposed that phenylcoumarans are transformed into stilbenes via a mechanochemical process which takes place during the milling of wood and refining of chips.[5] Further processing can lead to the formation of α-carbonyl compounds which are also highly photoreactive (see below).[6]

trans-Stilbenes can go through photoreactions to form coloured compounds, through a stilbene-to-phenanthrene mechanism, and oxidation thereafter[7] (Scheme 2.1).

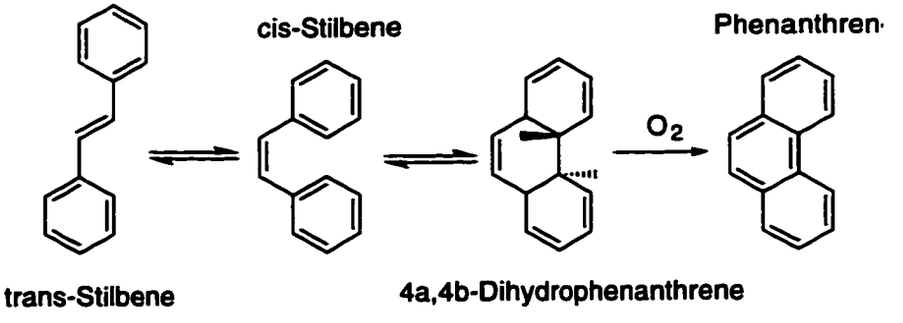

Scheme 2.1 Formation of phenanthrenes from stilbenes in lignin-rich systems.

The interconversions of *trans*-stilbene, *cis*-stilbene, and dihydrophenanthrene are photochemically reversible, while oxidation of dihydrophenanthrene to phenanthrene is essentially irreversible.

Other routes to phenanthrenes (from *o*-vinyl diaryl ethers, which are found in lignin) have been reported in the literature.[8] These are found to

photoconvert to *o*-hydroxystilbenes, and eventually to phenanthrenes, as shown in Scheme 2.2. The phenanthrenes can be formed directly, depending on the conditions.

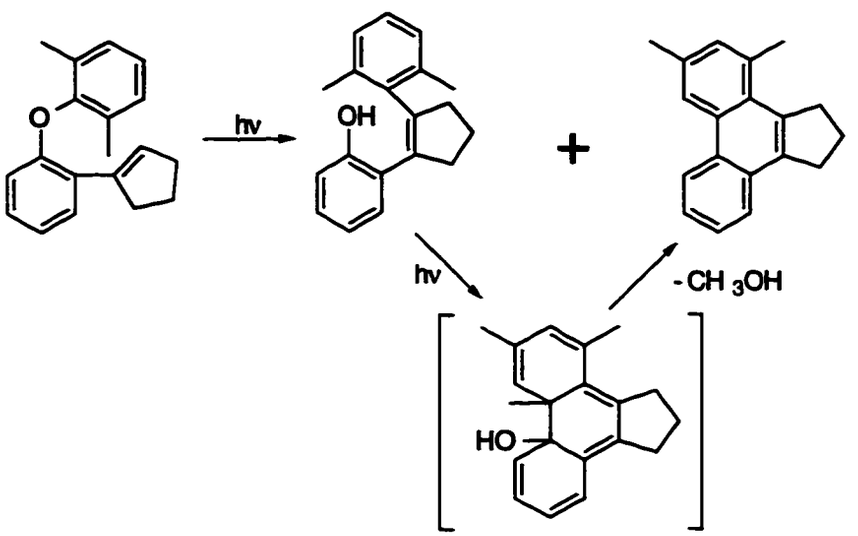

Scheme 2.2 The route to phenanthrenes from *o*-vinyl diaryl ethers.

It is believed that yellowing occurs predominantly through oxidation of phenoxy radicals supplied by the phenolic hydroxy groups of lignin, although yellowing still occurs to a certain extent with a fully alkylated lignin molecule.[9, 10] Hence there must be another source of yellowing in addition to the phenolic hydroxy groups in the natural product. It has been shown that upon irradiation, phenacyl aryl ether moieties in the lignin molecule are also an efficient source of phenoxy radicals.[11] Studies by Castellan and coworkers have suggested that α-guaiacoxyacetoveratrone (α-GAV) represents a suitable compound with which to model these phenacyl aryl ether moieties of lignin.[6, 12, 13] While this model compound does not have all the features of lignin, it does contain a carbonyl group, is heavily substituted with methoxy groups, and it contains a guaiacoxy moiety, which upon photodegradation, will produce the corresponding phenoxy radical.

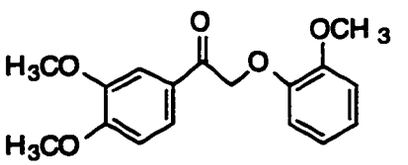

Figure 2.4 α-GAV, a Lignin Model Compound.

Grier and Lin[10] first reported a mechanism of degradation of this model compound in solution. Vanucci and coworkers[6] have further continued this work to include transient experiments using laser flash photolysis. Upon absorption of light, the molecule was thought to go through a triplet intermediate which further cleaves homolytically to form its corresponding free radicals.

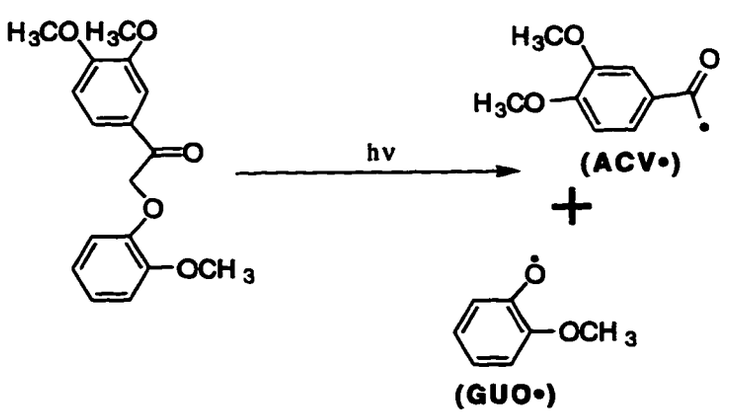

Scheme 2.3 Free Radical Formation from α-GAV.

2.1.3. The Effect of β-Phenyl Rings on Acetophenone-Type Molecules

α-GAV not only contains the same chromophore as the one in acetoveratrone (ACV, Figure 2.5), but it also contains an aromatic ring in the beta position. β-Phenyl rings are known to greatly affect the photochemistry of these compounds. For example, acetophenone has a triplet lifetime of ~2μs in benzene solution; the triplet lifetime is determined by the interactions of the solvent.

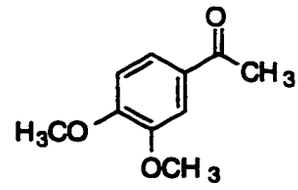

Figure 2.5 Acetoveratrone (ACV).

β-Phenylpropiophenone which now incorporates a β-phenyl ring, has a triplet lifetime 3 orders of magnitude shorter[14] (see Figure 2.6). Much work has been done on β-phenylpropiophenones and what is known is that a charge-transfer interaction will occur between the β-phenyl ring and the carbonyl group, and the β position for the phenyl ring is critical.[14, 15] If the ring is in the alpha position the molecules undergo fragmentation, while in the gamma position, the phenyl ring is too far away to induce intramolecular quenching, and this structure leads to a Norrish Type II reaction.[16]

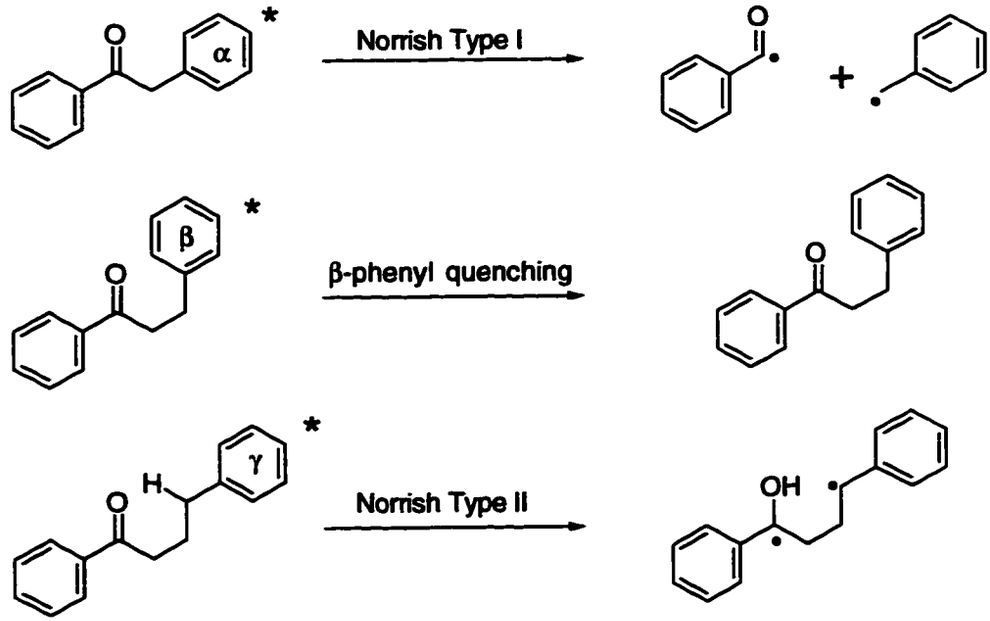

Scheme 2.4 The Effect of having a phenyl ring in the α, β, and γ positions.

Adding a methoxy group to acetophenone (ACP) to form *p*-methoxyacetophenone (II) lengthens the triplet lifetime with respect to acetophenone since the methoxy group changes the character of the lowest lying triplet state from n-π^* to a less reactive π-π^* state. Adding a β-phenyl ring to give *p*-methoxy-β-phenylpropiophenone (III) again shortens the lifetime of the triplet (see Figure 2.6) although it is enhanced with respect to the β-phenylpropiophenone (I) with no methoxy substituent.[15] This is so because the mechanism of quenching by the β-phenyl is believed to be mediated by the thermally populated triplet n-π^* state.[14, 17]

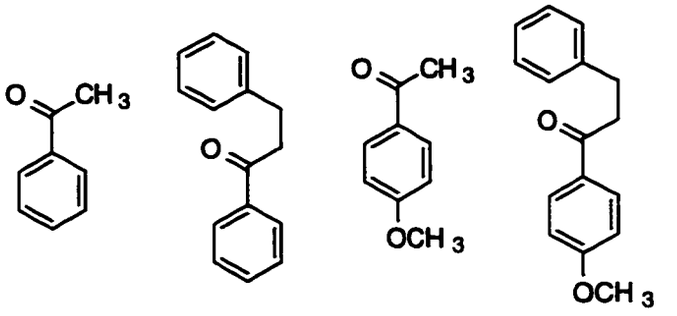

Figure 2.6 Effect of β-phenyl rings and methoxy substituents on triplet lifetimes of β-phenylpropiophenones.

2.1.4.The Presence of an Oxygen Atom in the β Position

The molecular conformation involved in β-phenyl quenching in β-phenylpropiophenones requires eclipsing the methylene hydrogens on the alpha and beta carbons which is energetically unfavourable (see Figure 2.7). When the beta carbon is replaced with an oxygen atom, these methylene hydrogens are no longer present and the quenching conformation lies at a lower energy. The consequence of this is that the α-

phenoxyacetophenones have shorter triplet lifetimes than their β-phenylpropiophenone analogs.[18]

The quantum yield of decomposition (Φ_r) for the β-phenyl-propiophenone (I) is essentially zero, but α-phenoxyacetophenone (IV) shows Φ_r, ~0.01.[18] The quantum yield is low but the chemical yield is high. The molecule reacts via β-cleavage to produce the corresponding phenoxy radical[18] in good chemical yields, similar to the reaction shown in Scheme 2.3.

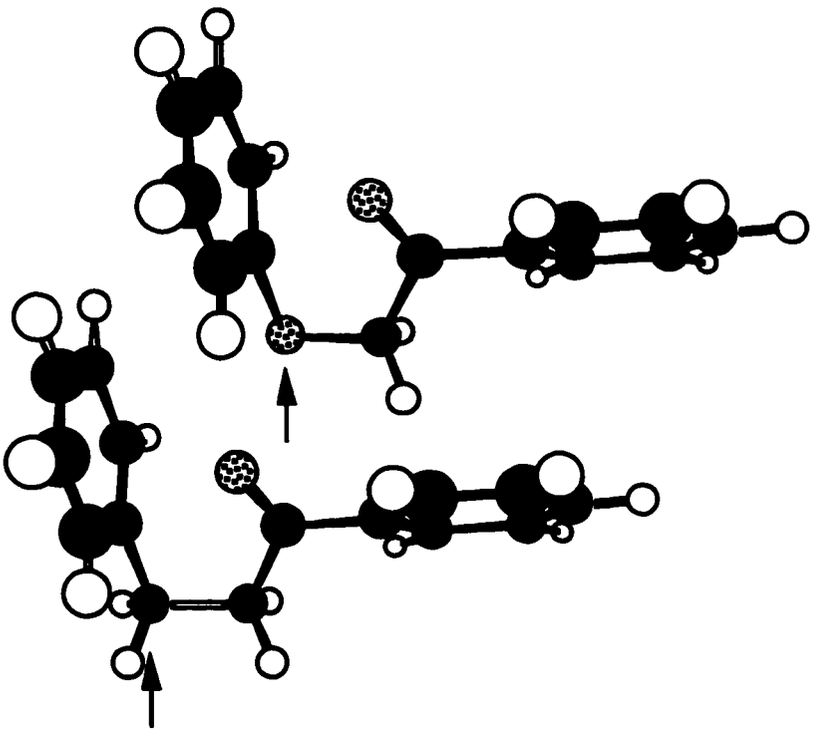

Figure 2.7 Molecular conformation of α-phenoxyacetophenone (top) and β-phenyl-propiophenone (bottom) leading to triplet deactivation via β-phenyl quenching. Arrows mark the site where the atom is different.

As in the case in Figure 2.8, adding a methoxy group increases the triplet lifetime since the molecule changes from an n-π* state to a π-π* state. Φ_r also increases slightly which perhaps suggests that the inhibiting effect of π-π* states on the fragmentation reaction is less severe than on

intramolecular quenching. Phenoxy radicals are stabilized by methoxy substitution.[19] Comparing (IV) and (VI) in Figure 2.8 shows that the triplet lifetime is not greatly affected, but Φ_r quadruples. In this case, we now produce a more stabilized phenoxy radical. Therefore it can be concluded that the presence of an oxygen atom in the β position induces fragmentation.

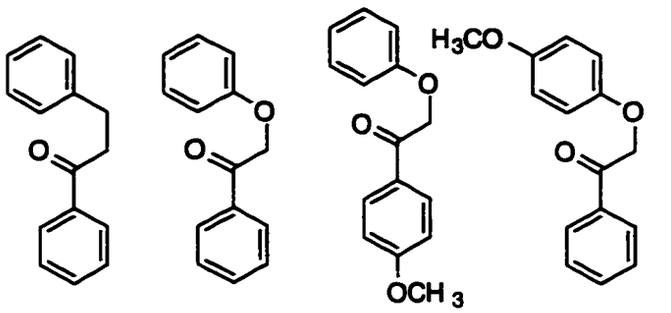

Figure 2.8 Effect of oxygen in the beta position and methoxy substituents on triplet lifetimes and degradation quantum yields.

2.1.5.Excited States of α-GAV and acetoveratrone (ACV)

For most carbonyl compounds, we expect to have two near-lying excited states in the triplet manifold, which are either n-π* or π-π* in character. The n-π* states frequently show radical-like behaviour.[20] Benzophenone is an example of such a molecule which has an n-π* triplet state for which hydrogen abstraction reactions and very efficient intersystem crossing are characteristic. When the lowest state is the π-π* state, largely centered on the aromatic part of the molecule, as in the case of *p*-methoxyacetophenone, the reactivity decreases significantly.[21, 22] Considering the nature of lignin and the nature of the model we have

chosen, we are mostly interested in molecules which have this type of behaviour.

The low temperature phosphorescence spectrum of benzophenone (see Figure 2.9) has a well-resolved structure, in which the splitting corresponds to the carbonyl vibrational frequencies. From this structure, one can determine that the triplet energy of benzophenone is approximately 69 kcal/mol.[23]

By comparison, for triplet states which are π-π^* in nature, this type of structural resolution is absent from the phosphorescence spectra (Figure 2.9). Hence for the types of molecules in this study, the exact triplet energy becomes more difficult to determine. With multiple methoxy substitution, the spectra of these molecules are often shifted to longer wavelengths and the triplet energy can be estimated at about 60 kcal/mol.

Upon absorption of light by the compounds used in this study, an excited singlet state is formed. Rapid intersystem crossing then takes place into the π-π^* triplet manifold, at about 60-63 kcal/mol. Usually carbonyl compounds will go through chemistry strictly from the triplet state, although in the case of molecules such as α-GAV, reaction is also observed from the excited singlet state.[24] In any case, the reactions involve free radicals and we expect that the products formed from the triplet reaction will arise from random encounters by the free radicals. In the case of the singlet, random radical-radical reactions can occur between radicals that have escaped the primary solvent cage, but geminate processes arising from radical pair reactions within the solvent cage are also expected since they are formed with the appropriate electronic spin to directly lead to products.

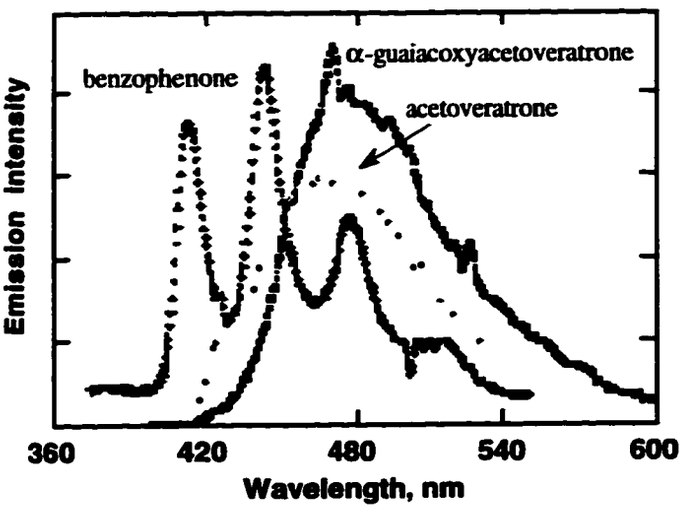

Figure 2.9 Phosphorescence spectra of benzophenone, α-guaiacoxy-acetoveratrone (α-GAV), and acetoveratrone (ACV) in ethanol glass at 77K.

2.1.6.Cleavage of Ketyl Radicals

In addition to excited state cleavage, the ketyl radicals derived from these ketones may undergo their own cleavage reaction, as in Scheme 2.5.

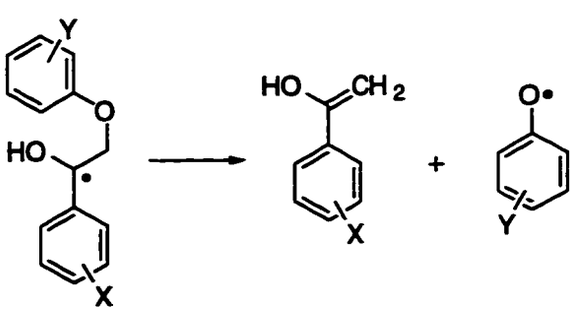

Scheme 2.5 Fragmentation of Ketyl Radicals.

This is then normally followed by the subsequent reketonization of the enol, Scheme 2.6

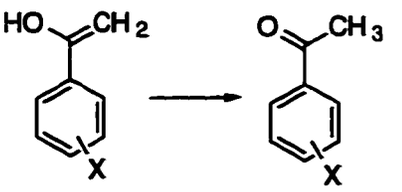

Scheme 2.6 Reketonization of the enol.

It has been shown that in simple systems (e.g., X=Y=H) the reaction in Scheme 2.5 occurs with a rate constant of 2×10^6 s^{-1}.[25] This was determined employing a technique (shown in Scheme 2.7) to generate the radicals by reaction of photo-generated tert-butoxy radicals with the corresponding alcohol.

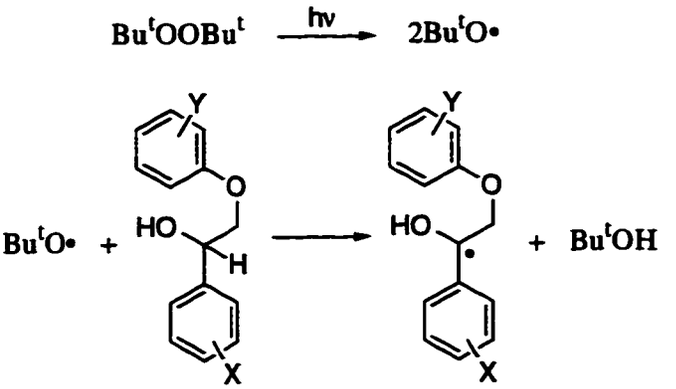

Scheme 2.7 Formation of Ketyl Radicals.

Unfortunately, the time resolution that can be achieved using this approach is limited by the rate of the hydrogen abstraction. The rate constant for this reaction and the concentration of the precursor employed limits the time resolution to approximately 0.5 μs. Further, the process can be complicated in some systems by lack of specificity of the tert-butoxy radicals abstracting hydrogen atoms from other locations in the molecule.

2.1.7.Previous Studies Conducted with α-GAV

Some preliminary work (transient and product studies) on α-GAV and other related compounds was done by Vanucci, Castellan and coworkers.[6] These results provided initial triplet lifetimes and product studies in a few different solvents. The authors attributed the yellow colour to an uncharacterized oligomeric material. The authors also reported a dependence of the transient kinetics on the irradiation wavelength in the laser flash photolysis experiments.

In a collaborative effort between the Pulp and Paper Research Institute of Canada (PAPRICAN) and the University of Ottawa,[24] a detailed study of α-GAV was published. These studies produced a series of triplet lifetimes in different solvents as well as degradation quantum yields under different conditions. The results are summarized in Table 2.1.

This work established the fact that the triplet lifetime is very solvent dependent. In general, longer triplet lifetimes are observed in protic solvents compared to aprotic solvents. When water is added to an aprotic solvent the triplet lifetime increases and when water is added to an already protic solvent, the triplet lifetime decreases. A similar behaviour is seen with the values for the degradation quantum yields.

Table 2.1. Triplet lifetimes and disappearance quantum yields for α-GAV in deaerated solvents, unless otherwise noted.[24]

Solvent	Quantum Yield	Triplet Lifetime (ns)
Dioxane	0.06 ± 0.01	183
w 40% water	0.29 ± 0.02	400
1,2-Dimethoxyethane	0.071 ± 0.002	200
w 40% water	0.49 ± 0.17	390
Ethanol	0.32 ± 0.08	550
w 40% water	0.16 ± 0.04	233
Methanol	0.45 ± 0.02	300
w 40% water	0.28 ± 0.03	175
Isopropanol	0.52 ± 0.12	590
w 40% water	0.3 ± 0.03	310
2-Ethoxyethanol	0.34 ± 0.09	600
w 40% water	0.19 ± 0.03	355
Acetonitrile	0.10 ± 0.01	230
w 40% water	0.47 ± 0.12	288
+ 0.01 M thiophenol*	0.30 ± 0.07	
oxygen (air)*	0.12 ± 0.01	
oxygen + 0.01 M thiophenol*	0.14 ± 0.08	

* In the absence of added water.

Acetophenones are usually expected to have intersystem crossing quantum yields very close to unity.[26] It has been shown, however, that under conditions where 99% of the triplets are quenched by energy transfer with a quencher like 1,3-cyclohexadiene, the degradation quantum yields remain unchanged in aprotic solvents such as acetonitrile and dioxane but decrease to 0.1 from 0.3 in a protic solvent like ethanol.[24] These results show that at least a portion of the photodecomposition must occur through a route other than through the triplet state fragmentation. It was concluded that fragmentation occurs solely from the singlet state in aprotic solvents and from both the triplet and the singlet states in protic solvents. Around the same time another group concluded that methoxy

substitution of the benzoyl chromophore appears to favour singlet state processes.[27, 28]

The triplet state is formed and detected in all solvents, but the triplet only yields products in protic solvents. This behaviour was attributed to the change in the competition between β-phenyl quenching and cleavage. Protic solvents may associate themselves, through hydrogen bonding, to the carbonyl moiety and interfere with β-phenyl quenching. This decrease in the rate of intramolecular quenching may allow for cleavage to occur.

2.1.8.Other approaches to studying the colour reversion problem.

Argyropoulos and coworkers have developed methods of detecting ortho-quinones in pulp samples and paper samples, in order to study the formation of these species. The method involves reacting the samples with trimethylphosphite (see Scheme 2.8).[29, 30] With these methods, the evolution of *ortho*-quinones can be followed over time during irradiation studies using ^{31}P NMR techniques. This sensitive technique can also differentiate between the environments of the phosphorous atom in the species shown in Scheme 2.8, according to their chemical shift in the ^{31}P NMR spectrum.

Kónya and Scaiano[31] have used this method to selectively derivatize *o*-quinone moieties produced by irradiation of lignin-rich pulp and paper with pyrene moieties following the reaction with P(III) compounds. The results of spectroscopic and time-resolved emission studies indicate that the tendency for quinone formation upon UV irradiation is enhanced by bleaching processes. The time-resolved work can differentiate between native pulp fluorescence and pyrene-derivative fluorescence, since pulp fluorescence is very short-lived (≤ 2ns). By probing for pyrene excimer emission, this method can also detect areas of larger quinone

concentration, which also implies that these areas may be more permeable

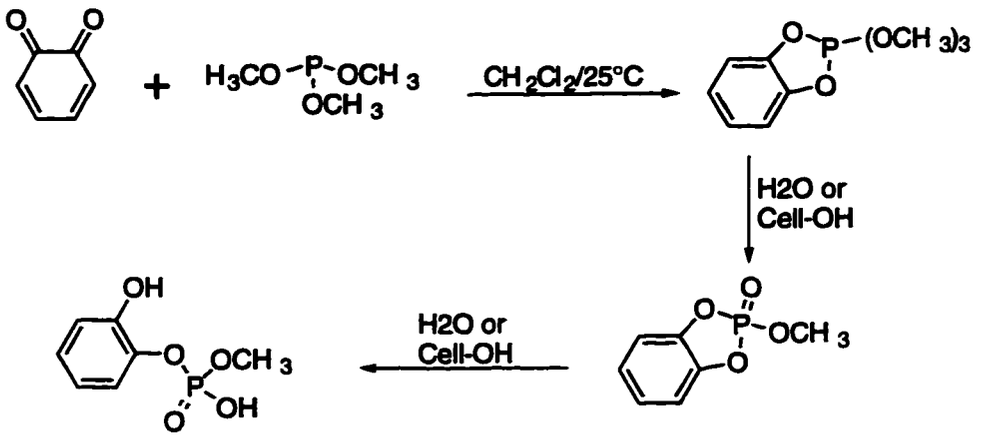

Scheme 2.8 Reaction of trimethylphosphite with *o*-quinone groups in pulp.

to oxygen. Fluorescence microscopy can be used to image the irradiated fibers.

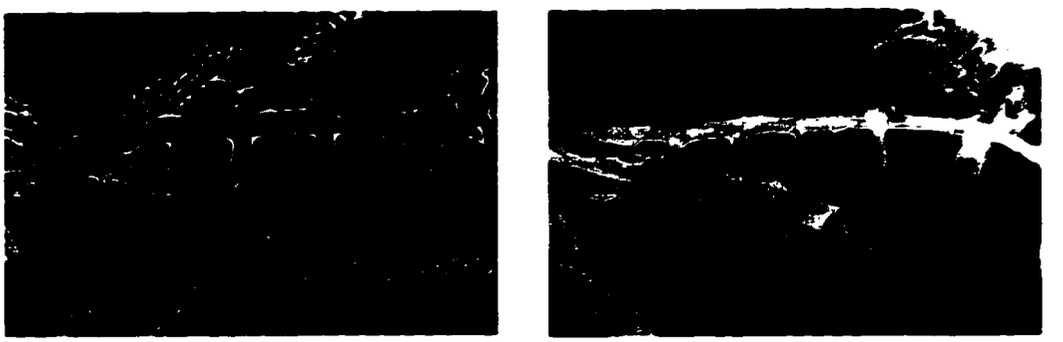

Figure 2.10 Microscope images of irradiated pulp derivatized with pyrene-containing P(III) compounds.[31] Left: phase contrast image; right: fluorescence image.

Gray and coworkers have used fluorescence techniques to characterize paper, lignin, their environment, and their photophysics.[32-35] In this work, a method has been developed to measure fluorescence quantum yields on solid supports such as paper and cellulose. They have found that the support itself, ie. the cellulose, is responsible for most of the fluorescence, since delignification of the paper results in no change in

fluorescence, or a slight increase. Adding lignin to delignified pulp actually decreases the fluorescence. It is postulated that the lignin may actually absorb the emitted light from the cellulose. This work has been contested, however.[5, 36, 37]

ESR and flash-CIDEP studies of paper made from TMP and of α-GAV on filter paper supports give some insight into radical processes in these systems.[38] Both bleached and unbleached paper made from TMP were found to contain small amounts of radicals, even before exposure to light. The signals obtained are consistent with the presence of very long-lived phenoxy radicals in the native paper environment, and these signals increase dramatically upon photolysis. These techniques allow the experimenter to probe the multiplicity of the precursors of the radicals in a photolysis event. In native paper made from TMP, signals were detected showing radical formation from triplet processes. However, this study concluded that the phenoxy radicals formed from photolysis of α-GAV deposited on filter paper were not formed directly from the cleavage of the triplet α-GAV, but possibly from the cleavage of reduced α-GAV, its ketyl radical. The fact that phenoxy radicals live so long on a paper matrix also implies that photolysis of radicals may also be a significant factor in the photoyellowing of paper.

2.1.9.Strategies for stabilizing the colour of TMP

Finding a solution to the colour reversion problem is the ultimate goal of studying the mechanism of yellowing of TMP. Not only must the commercially successful strategy slow down or stop the yellowing of TMP, this strategy must be relatively cheap, non-toxic, and it must not compromise the physical strength of the paper. Many classes of additives have been studied, however relatively little has been published due to the

potential proprietary nature and/or patentability of the process or additive used. Scheme 2.9 shows an overview of the different strategies that can be used to approach the colour reversion problem.

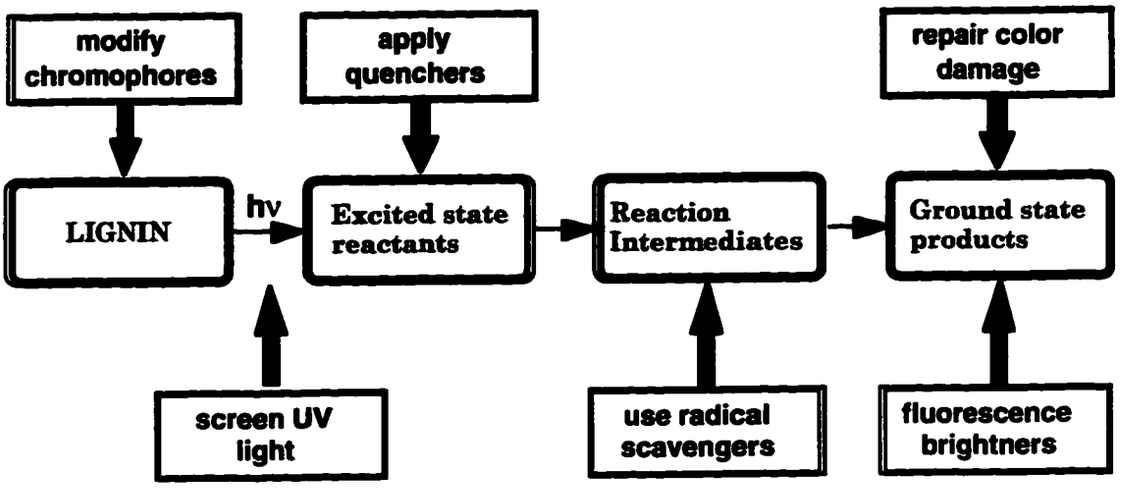

Scheme 2.9 Strategies for addressing the colour reversion problem.

Commercial UV absorbers have been studied as potential additives to TMP systems. Hydroxybenzophenones and benzotriazoles are the most widely used in polymer stabilization.[39] These have a limitation in that loading on the paper must be very high in order to preferentially absorb the incident light. Phenolic antioxidants (such as *para*-substituted-2,6-di-*t*-butyl phenols) and hindered amine light stabilizers (HALS, such as substituted 2,2,6,6'-tetramethyl piperidinyl derivatives) are widely used as additives to protect synthetic polymers against oxidation. They are believed to act as chain oxidation breakers and hydroperoxide decomposers.[39] Their efficacy in TMP systems was found to be poor. Sulfur and phosphorous additives have been widely studied, due to their strong reducing properties and general action as antioxidants; some thiols can even act as bleaching agents in mechanical pulps.[39-41] Unfortunately, the major drawback to this class of compounds is their bad smell. Ascorbic

acid, a well-known antioxidant has been shown to be a good stabilizer for paper, although the paper tends to turn brown upon storage.[39]

The work presented in this thesis as well as the work done by our partners in the Canadian Government's Network of Centres of Excellence in Mechanical Pulps attempts to elucidate some of the mechanisms involved in the yellowing of mechanical pulps . With this knowledge, we believe the scientific and industrial community comes a step closer to designing a rational inhibition strategy appropriate for this problem.

2.2.Results

2.2.1.Triplet quenching studies

Laser excitation of deaerated solutions of α-GAV leads to the detection of a reaction intermediate that can be characterized as the ketone triplet state. The triplet state was identified through its characteristic behaviour toward various quenchers.[6, 24]

In particular, conjugated dienes are well-established quenchers of triplet states.[26, 42, 43] For example, sorbic acid was used to help identify the triplet state; quenching is expected to involve energy transfer. It is a very versatile quencher since it has good solubility in a wide range of solvents including alcohols and water.

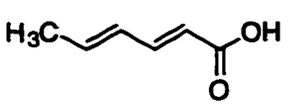

Figure 2.11 Structure of sorbic acid.

The triplet state of α-GAV has a lifetime of 550 ns in ethanol, and was quenched by sorbic acid with a rate constant of 2.8 x 10^9 M^{-1} s^{-1} at room temperature. This rate constant is derived from a plot of the first-order rate constant for triplet decay as a function of the quencher concentration, i.e.,

$$k_{decay} = \tau^{-1} + k_q[quencher] \qquad \textbf{Equation 10}$$

where τ is the triplet lifetime in the absence of quencher and the y-intercept of the quenching plot. Figure 2.12 shows a quenching plot for sorbic acid quenching of α-GAV in acetonitrile and methanol.

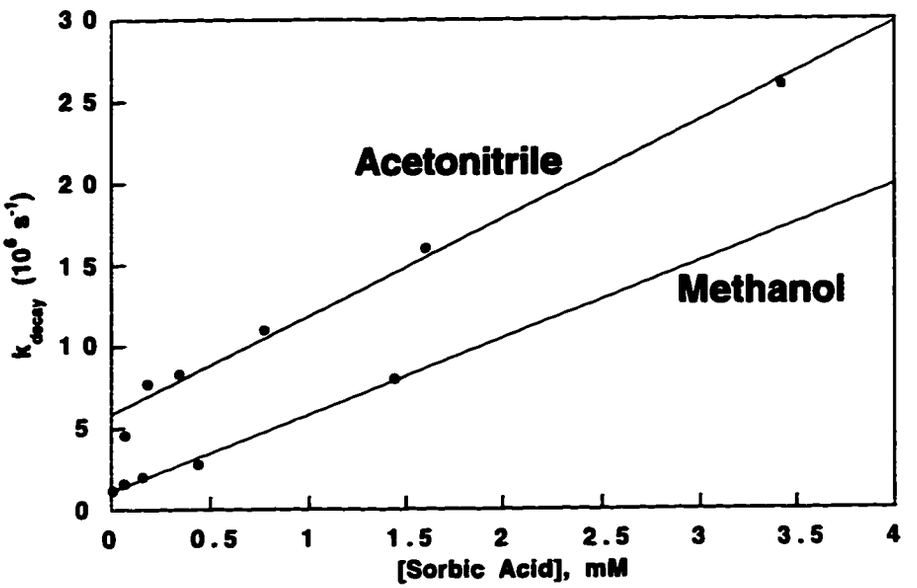

Figure 2.12 Sorbic acid quenching of α-GAV triplet in acetonitrile and methanol.

The quenching rate constant quoted above is a bit slower than most triplet-diene quenching constants; this may reflect the fact that the donor triplet has an unusually low triplet energy for a carbonyl compound (see section 2.1.5, page 72).

In the absence of quencher, the guaiacoxy group reduces the lifetime of the triplet state from > 15 μs in acetoveratrone to ~500 ns in the case of α-guaiacoxyacetoveratrone; thus, at least 97% of the triplets must decay by processes (deactivation or cleavage) that involve the guaiacoxy group.

In the presence of 0.016 M sorbic acid, and given the rate of quenching (2.8 x 10^9 M^{-1} s^{-1}), and lifetimes measured in the absence of quencher (550 ns in ethanol), it can be calculated using Equation 10 that this concentration of diene will quench 96% of the triplets. That is to say that the calculated k_{decay} at this quencher concentration is 4.7 x 10^7 s^{-1}. τ^{-1}, the rate of decay in the absence of quencher, is 1.82 x 10^6 s^{-1}, which is 4% of the value with 0.016M sorbic acid, therefore 96% of the triplets have been quenched. This

implies that the decay of the triplet occurs almost exclusively through energy transfer. (See Figure 2.13)

The surprising result is that in the presence of this large concentration of sorbic acid, the transient absorption spectrum of the guaiacoxy radical with its characteristic band in the red part of the spectrum is observed. This demonstrates that the guaiacoxy radical must be produced from the singlet state, since virtually all the triplets have been quenched by the diene.

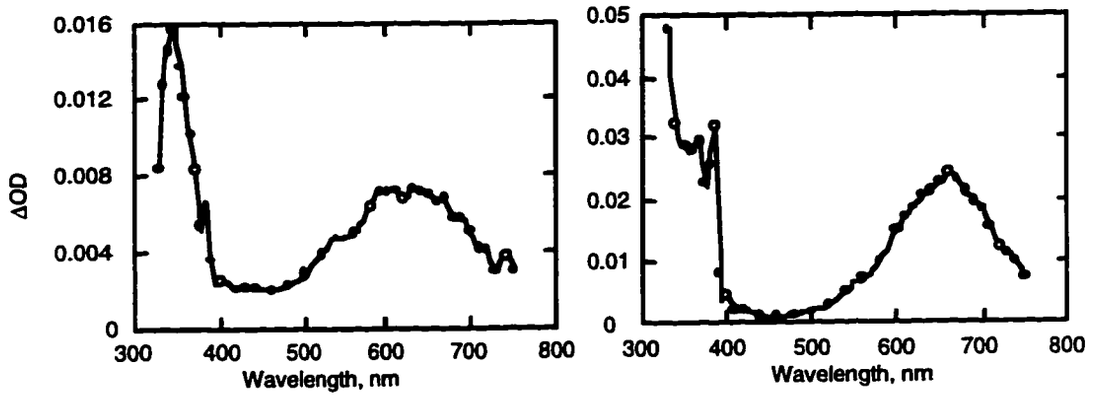

Figure 2.13 Transient absorption spectra; left: α-GAV in ethanol in the presence of 0.016M sorbic acid 0.2 μs after 337 nm excitation; right: reaction of *tert*-butoxy radicals generated by 308 nm excitation, with guaiacol in acetonitrile leading to guaiacoxy radical (GUO•, Scheme 2.3); recorded 450 ns after laser excitation.

In the presence of moderate amounts of sorbic acid (e.g., 0.0015 M), the triplet lifetime of α-GAV is shortened but can be readily time-resolved. Under these conditions we find that the characteristic guaiacoxy radical long-wavelength band is present immediately following the laser pulse as opposed to growing in as the triplet decays.

In order to confirm the identity of the guaiacoxy radical, we also generated this species by reaction of *tert*-butoxy radicals with the phenol, as indicated above (see Figure 2.13). The transient spectrum of the phenoxy radical can

be readily generated by reaction of phenol with *tert*-butoxy radicals, formed by the photodecomposition of di-*tert*-butyl peroxide. This is a very efficient reaction which takes place with a quantum yield of approximately 0.7-0.9.[44, 45]

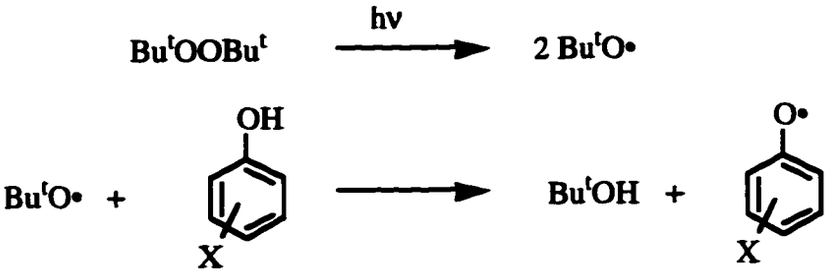

Scheme 2.10 Generation of *t*-butoxy radicals and their reaction with phenols.

These experiments also yield a band in the 600 nm region, therefore supporting the formation of guaiacoxy radicals via a singlet process from α-GAV. Small differences between the two spectra of Figure 2.13 are presumably due to the presence of other carbon centered radicals produced in the cleavage of α-GAV and to differences in the solvent employed.

2.2.2. α-GAV product studies

α-GAV was irradiated in a photoreactor with 350 nm lamps in order to study the product distribution following photodegradation. Scheme 2.11 shows the well-accepted photodecomposition pathways for α-GAV.[24]

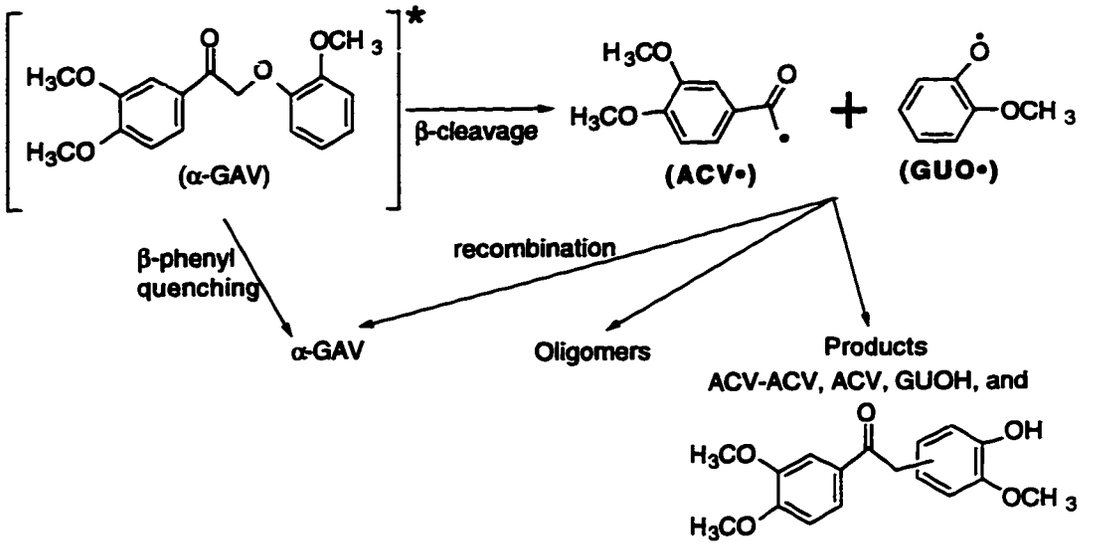

Scheme 2.11 Photodecomposition pathways for α-GAV.

Table 2.2 summarizes the results of the product studies. Sorbic acid was used as a triplet quencher to study the product distribution under singlet-only chemistry. Under these conditions, some radicals are trapped by the diene, and these are also reflected in the product distribution.

Table 2.2 Product distributions for photodegradation of α-GAV.

System	*Guaiacol (GUOH)*	*ACV*	*Coupling Products*	*ACV-ACV*	*Diene-trapped*
EtOH	44	56			
EtOH/diene	28	4	48		20
ACN	24	6	46	23	
ACN/diene	10		52	20	18

The degradation quantum yield results of previous work has been reproduced. That is, adding a triplet quencher like sorbic acid to α-GAV in methanol, enough to quench 99% of the triplets, decreases the degradation quantum yield significantly, but not totally. This supports the initial findings that some cleavage and degradation is occurring from the triplet state.

Naphthalene quenches α-GAV triplet at a rate of 4.8×10^9 M^{-1} s^{-1}. Figure 2.14 shows a naphthalene quenching plot of the α-GAV triplet in methanol. The triplet decay was monitored at 460 nm, to avoid any interference from the naphthalene triplet which is formed as a consequence of triplet quenching. Due to the overlap of the transient spectra, it was not possible to observe the growth of the naphthalene triplet. However, a 2 mM solution of naphthalene in methanol gives no appreciable ground state absorption at 337 nm, and 337 nm laser excitation gives no transient signal.

With enough naphthalene added to quench 99% of the triplets, its presence also decreases the degradation quantum yield, but not nearly as much as the sorbic acid does. Relative degradation quantum yields in side-by-side reactions with enough quencher to quench 99% of the triplets for no quencher:naphthalene:sorbic acid are 1:0.5:0.1.

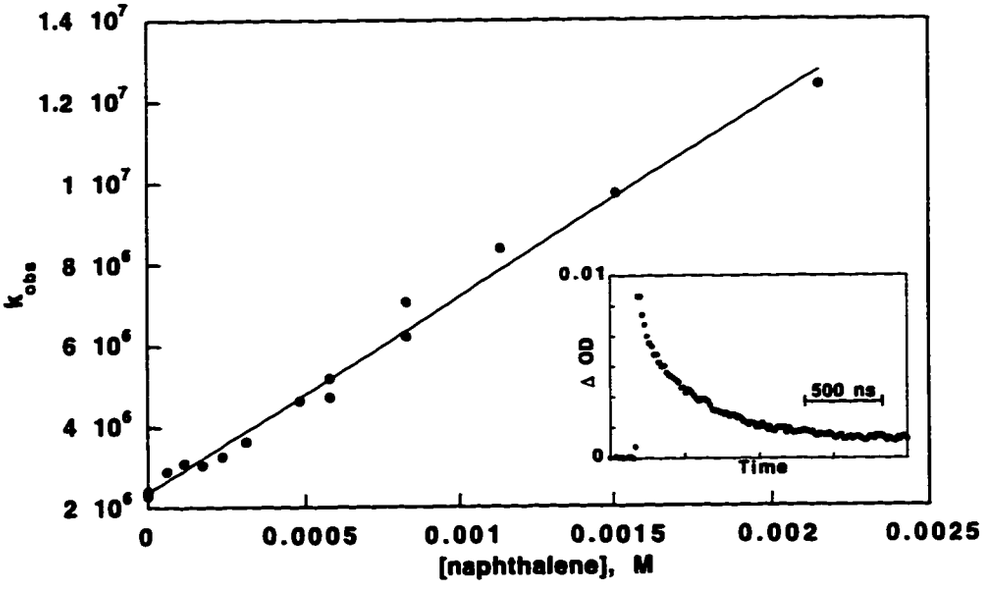

Figure 2.14 Effect of the presence of naphthalene on the rate of triplet decay of α-GAV in methanol, according to Equation 10. Inset: Representative decay trace monitored at 460 nm, 337 nm laser excitation, in the absence of naphthalene.

2.2.3. Power and wavelength effects

When α-GAV is studied under laser flash photolysis conditions, its transient behaviour, at first glance, appears to be wavelength dependent. These observations were first reported by another group[6] and were left unexplained.

We have been able to reproduce the results obtained; however we have seen that when one changes irradiation wavelength, one often changes other parameters such as stock concentration (to adjust absorbance at the laser wavelength) and laser energy (due to the nature of the different wavelengths used). In fact, at lower wavelengths (266 and 308 nm), we observe complicated kinetics which appear to be multiphotonic. At higher wavelengths (337 and 355 nm), the kinetics are clean first-order triplet-decay kinetics which match the triplet lifetime values reported earlier,[6, 24] provided that the concentration of α-GAV is kept constant. We have found that if the conditions are carefully controlled (low laser energy and constant concentration of α-GAV), these results can also be reproduced using 266 and 308 nm laser excitation. These signals are quenchable by oxygen, as reported previously by both groups.

The apparent multiphotonic chemistry of α-GAV was studied in detail. A 0.1 mM solution of α-GAV in ethanol was irradiated with a 308 nm laser in ethanol and its transient kinetics were measured at 400 nm, where the triplet is known to absorb. The laser power was varied using neutral density filters and the power was measured at the sample. Figure 2.15 shows the very different kinetics that appear at different laser powers.

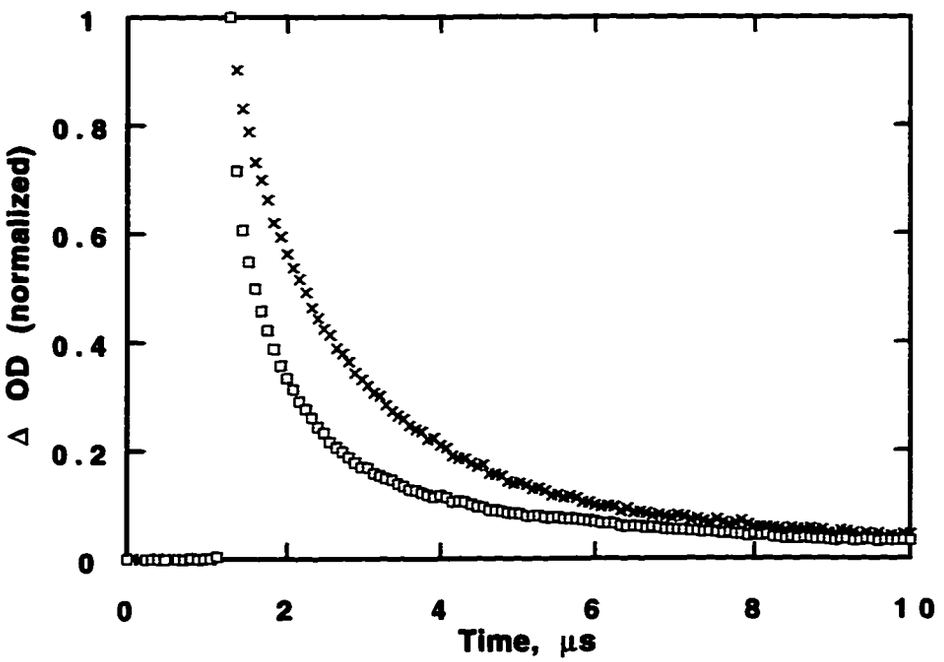

Figure 2.15 Normalized decay traces for α-GAV, monitored at 400 nm in ethanol. 308 nm laser excitation. (×) 3 mJ laser power. (□) 20 mJ laser power.

All the decay traces were fit to the sum of two first-order decays:

$$\Delta OD = ae^{k_1}t + be^{k_2}t \qquad \textbf{Equation 11}$$

From the pre-exponential terms, the calculated initial ΔOD for each of the two transients can be obtained. The two rate constants give the rates of decay for the two species, and the reciprocal of these values gives the lifetimes for each of the species. The results are shown in Table 2.3.

Table 2.3 Results of fitting of decays at various 308 nm laser powers.

Power (mJ)	*Top OD (1)*	*Top OD (2)*	*Rate (1), x10^6*	*Rate (2), x10^5*
1	0.00242	0.00113	3.02	3.32
2.5	0.00632	0.00338	2.20	2.25
4.5	0.0169	0.00903	2.41	2.44
6	0.0215	0.0122	2.37	2.37
8	0.0304	0.0174	2.39	2.40
8.5	0.0269	0.0201	2.31	2.31
12	0.0418	0.0252	2.44	2.54
14	0.0437	0.0334	2.33	2.44
15	0.0451	0.0316	2.36	2.47
18	0.0563	0.0420	2.26	2.39
19	0.0512	0.0470	2.16	2.27

The results of the calculations clearly show that the calculated lifetimes show 2 constant values, one at approximately 400 ns, and the other at approximately 4 μs. The possible reasons for this behaviour will be discussed in section 2.3.2.

2.2.4. Studies on α-(p-methoxyphenoxy)-p-methoxyacetophenone: Laser Flash photolysis

Although most of the work described in this thesis covers studies on α-GAV, some research was carried out on some α-phenoxyacetophenones with different methoxy group substitution. α-(*p*-Methoxyphenoxy)-*p*-methoxyacetophenone (**VII**) is an example of this; some laser flash photolysis studies and some pulse radiolysis studies were carried out on this compound, as well as on α-phenoxyacetophenone (**I**).

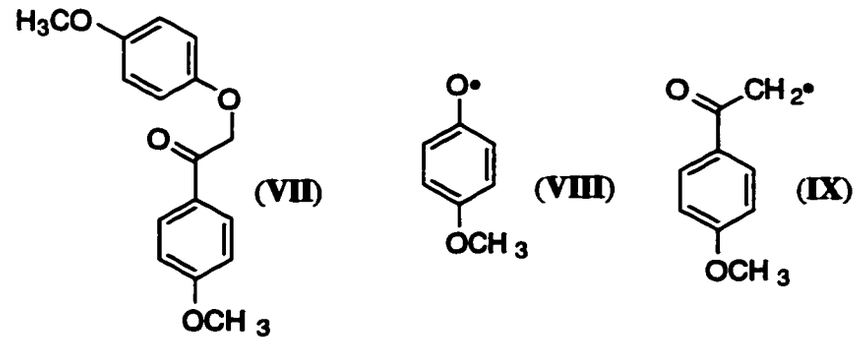

Figure 2.16 **α-(*p*-methoxyphenoxy)-*p*-methoxyacetophenone (VII), the *p*-methoxyphenoxy radical (VIII), and the *p*-methoxyphenacyl radical (IX).**

Pulsed laser excitation (308 nm) of **VII** (2.3×10^{-4}M) in methanol leads to the transient spectra shown in Figure 2.17. The spectra at different times clearly reveal the presence of at least two species, one absorbing predominantly at 410 nm and the other at ~540 nm. The latter disappears more rapidly. Further, it is evident that the 540 nm species must also absorb at wavelengths around 400 nm or shorter; this is indicated by the time-dependent shift to longer wavelengths of the minimum observed between 350 and 400 nm. A similar transient spectrum appears in acetonitrile solution, although the visible band is somewhat blue shifted (λ_{max} ~ 500 nm). Similar results were obtained upon changing the excitation wavelength from 308 to 337 nm.

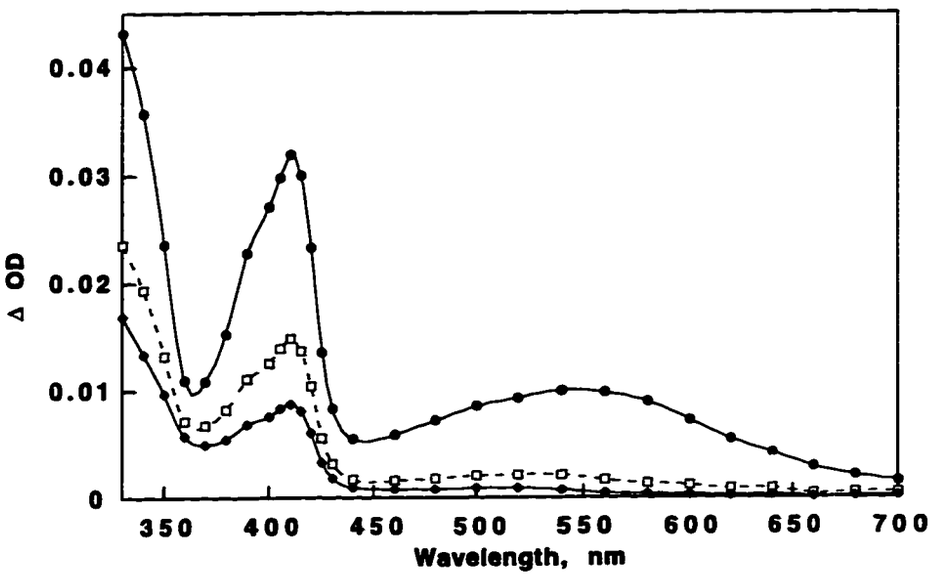

Figure 2.17 Transient spectra recorded 1.1, 11, and 21 μs following 308 nm laser excitation of VII in methanol.

The band at 410 nm can be assigned to the phenoxy radical **VIII** on the basis of experiments where the radical was generated independently by the reaction of *tert*-butoxy radicals (generated by 337 nm photolysis of a 50% solution of *tert*-butyl peroxide in acetonitrile) with *p*-methoxyphenol. An extinction coefficient of 7030 M^{-1} cm^{-1} at 417 nm has been reported for the radical upon pulse radiolysis of *p*-methoxyphenol in aqueous solution.[46] It is interesting to note that while the guaiacoxy radical (GUO•, the ortho isomer of **VIII**) shows a weak but detectable band at 660 nm (see Figure 2.13, page 28), this band appears to be absent (or to be much weaker) in the case of **VIII**. The work of Johnston and coworkers[47] supports these observations.

The complex decay behaviour of **VIII** appears to approach second-order kinetics; however, concentration studies in which the laser dose was attenuated with neutral density filters suggest a more complex behaviour, probably involving reaction with various other radicals present in the

system, as well as some overlap with decay signals associated with the short-wavelength absorption of the 540 nm transient.

The transient at 540 nm decays with dominant first-order kinetics and a lifetime of ~7 μs in methanol and ~15 μs in acetonitrile. This species is readily scavenged by oxygen, while the band at 410 nm is not affected by oxygen in the timescale of our experiments. We assign the 540 nm transient to the carbon-centered radical (**IX**) produced simultaneously with **VIII** in the β-cleavage of **VII**.

We found it to be rather surprising that **IX** would show such a long-wavelength absorption; however, the observation is not unprecedented.[48] We will show later that not only is this assignment fully consistent with our results, but in addition the spectra can be rationalized on the basis of molecular modeling calculations.

It should be noted that the 410 nm band of Figure 2.17 is not unlike typical triplet-triplet absorption from *p*-methoxybenzoyl chromophores.[23, 49] However, we feel confident that the transient derived from **VII** is not due to the triplet and the assignment of this band to **VIII** is correct. Note, for example, that the band persists in the presence of oxygen, contrary to what one would expect for a triplet state. Similarly, experiments with 2,5-dimethyl-2,4-hexadiene showed that this typical triplet quencher had no effect on the transient lifetime at 410 nm, and any changes in signal intensity were well below 10% for diene concentrations up to 1.12 M (in acetonitrile). This suggests that if the precursor of **VIII** is the triplet state, its lifetime should be <1 ns. More likely, as will be discussed below, a short triplet lifetime and contributions from singlet-state β-cleavage are responsible for the failure of diene quenching experiments. The 540 nm band was quenched by diene with a rate constant of 1.8×10^5 M^{-1} s^{-1}, a value

that is in line with radical addition rate constants to conjugated systems.[50] **IX** is also believed to abstract hydrogen from 2-propanol,[51] and we measured the reaction to occur at a rate of ~4 x 10^3 M^{-1} s^{-1}.

To obtain an estimate for the triplet lifetime of **VII**, we have employed a Stern-Volmer type of approach using 1-methylnaphthalene as a triplet quencher. This technique, which has been previously used in our laboratory in the study of short-lived triplet states,[14] makes use of Equation 12, where

$$A^{-1}_{420} = \alpha + \frac{\alpha}{k_q \tau_T [MN]} \qquad \textbf{Equation 12}$$

A_{420} is the transient absorption of methylnaphthalene triplet upon quenching of triplet **VII** at 420 nm, τ_T is the methyl naphthalene triplet lifetime, k_q is the quenching rate constant, and α is an experimental constant. In this case, complications arise due to the absorption at 420 n m of the *p*-methoxy-phenoxy radical itself formed upon direct excitation of ketone **VII**. The absorption due to the triplet state of 1-methylnaphthalene was therefore corrected by subtracting the contribution due to the singlet-derived radical. The experiment yields a value for $k_q\tau_T$ of 2.4 M^{-1}; using a quenching rate constant of 5 x 10^9 M^{-1} s^{-1} as generally accepted for this type of energy transfer,[52] a triplet lifetime of ~500 ps is calculated.

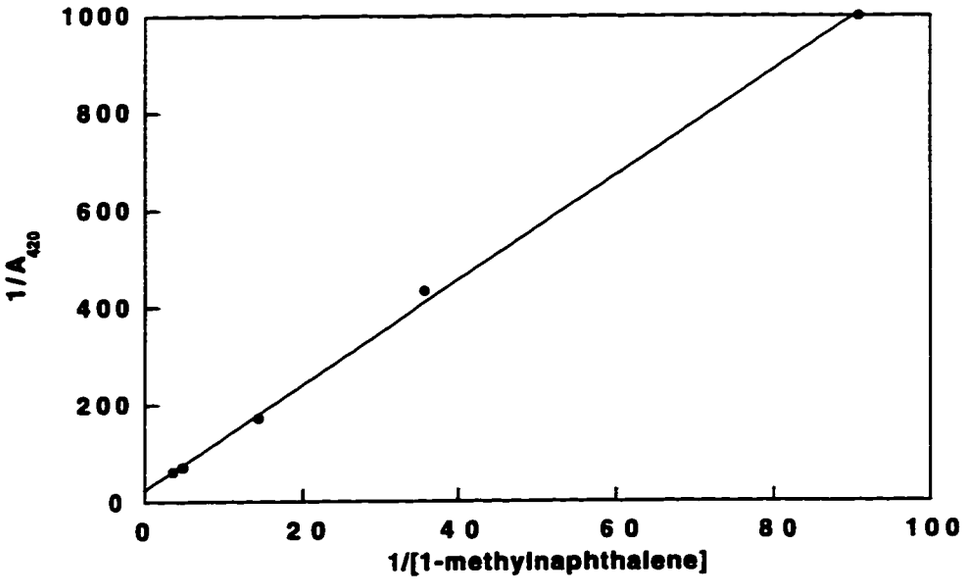

Figure 2.18 Triplet quenching of VII by 1-methylnaphthalene, according to Equation 12.

Experiments with **VII** in sodium dodecyl sulfate (SDS) micelles [**VII** = 2 x 10^{-4} M, SDS = 0.1 M] yield a transient spectrum with a strong absorption at ~700 nm and a band at ~410 nm. The long wavelength band, which is fully quenched with nitrous oxide,[53] is assigned to the solvated electron;[54] further details of this chemistry has been reported by Boch, Whittlesey, and Scaiano.[55] Nitrous oxide has no effect on the band at 410 nm, although the quenching of the absorption at 700 nm confirms that there is no significant band present in the 550 nm region. Application of moderate magnetic fields (≤1200 Gauss) had no effect on the decay kinetics at 410 nm on short time scales (≤2 μs). Significant effects could be anticipated if the cleavage generated a triplet radical pair.[56-59] The absence of magnetic field effects on this time scale is consistent with the dominance of singlet cleavage pathways.

2.2.5. Studies on α-(p-methoxyphenoxy)-p-methoxyacetophenone: Pulse Radiolysis

The reactions of solvated electrons with **VII** and **IV** were examined using pulse radiolysis techniques employing the facility at the Notre Dame Radiation Laboratory. Experiments were performed in methanol-water mixtures (70:30 v/v) which offer suitable properties in terms of ketone solubility and allow the pH of the solution to be adjusted.

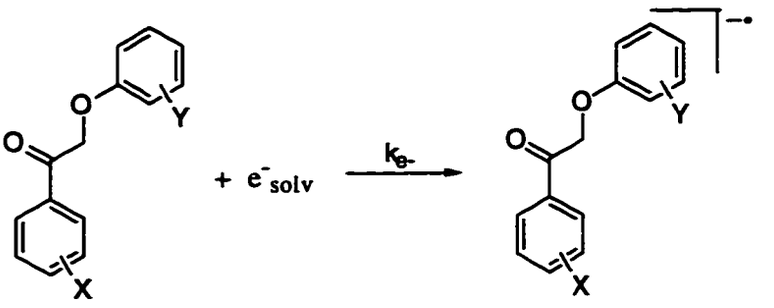

Scheme 2.12 Reduction of ketone by solvated electron.

Under pulse radiolysis conditions in methanol/water mixtures, the ketone can be reduced to the radical anion by reaction with solvated electrons (see Scheme 2.12). The anion can in turn be protonated by the solvent to form the ketyl radical according to Scheme 2.13.

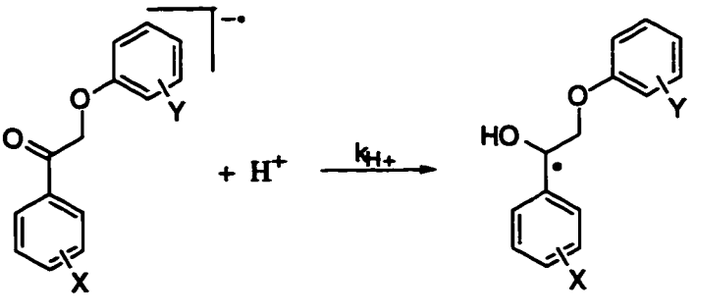

Scheme 2.13 Protonation of reduced ketone to form ketyl radical.

In experiments of this type the solvated electron can be readily monitored since it has a strong absorption in the red region (>600 nm). In our case it was possible to determine a rate constant for reaction of e^-_{solv} with **VII** by monitoring the electron decay at 550 nm using 1 mM ketone.

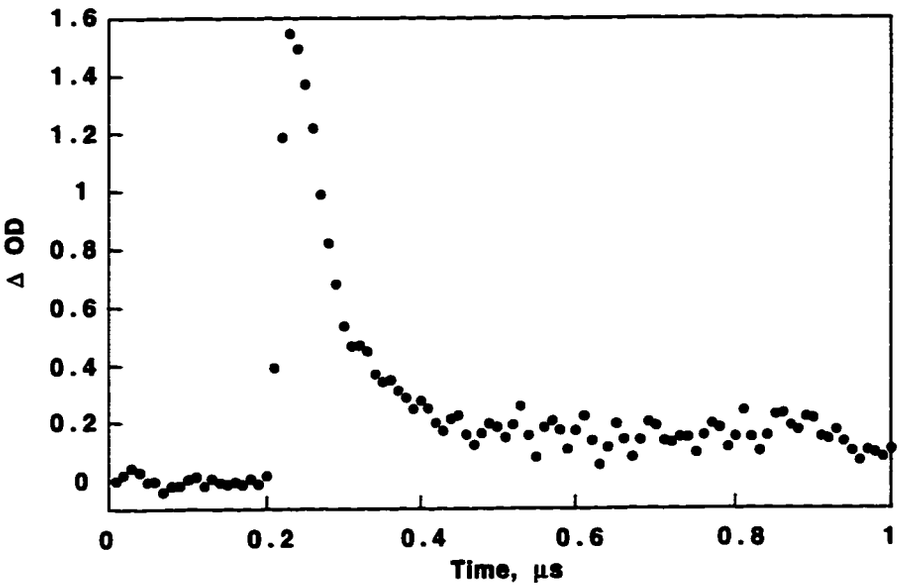

Figure 2.19 Decay of the solvated electron, monitored at 550 nm, in 70:30 methanol:water, following a pulse of electrons.

These experiments led to $k_{e^-} = 1.9 \times 10^{10}$ M^{-1} s^{-1}, a value that is in line with reported rate constants for electron scavenging by ketones.[54] For example, acetophenone scavenges hydrated electrons with a rate constant of 2.8×10^{10} M^{-1} s^{-1}.[54]

In the experiments described below the concentration of **VII** was fixed at 10 mM, which ensures the prompt formation of the anion, which under these conditions should occur with a lifetime ~6 ns.

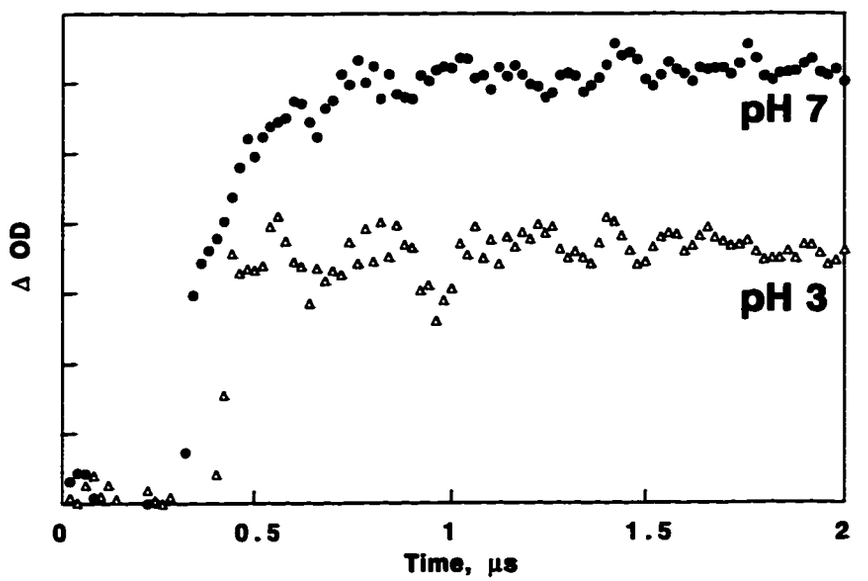

Figure 2.20 Pulse radiolysis traces showing the formation of VIII from VII at pH 7 and pH 3, monitored at 415 nm.

The protonation of the anion can be the rate determining step for the formation of the phenoxy radical. This is illustrated in Figure 2.20 which shows traces at 415 nm following pulse radiolysis of **VII** in alcohol-water at pH 7 and pH 3. The trace at pH 7 shows an initial jump due to the absorption of the anion, followed by a growth with a lifetime of ~ 100 ns. We had hoped that as the pH was lowered and the protonation became formally "instantaneous", we would be able to monitor the lifetime of the ketyl radical either through its direct detection, or by studying the growth kinetics for the p-methoxyphenoxy radical (**VIII**). While the phenoxy radical was indeed readily detectable (see Figure 2.21), we were unable to study the time dependence of Scheme 2.13, which under our experimental conditions must occur with $k_{H+} > 5 \times 10^7\ s^{-1}$. Note for example that the trace at pH 3 in Figure 2.20 represents an instantaneous growth in the time scale of the experiments.

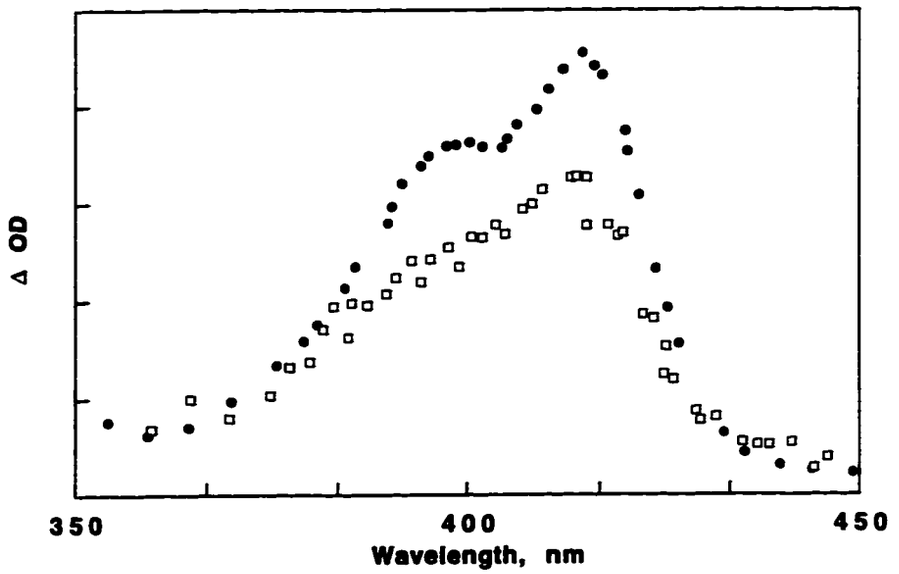

Figure 2.21 Transient spectra for VIII generated by (□) pulse radiolysis of VI and (•) control experiment where VIII was generated independently from the reaction corresponding of *tert*-butoxy radicals with the phenol.

Experiments with **IV** yielded less definitive results. Irradiation of **IV** in 70:30 methanol:water v/v ([**IV**] = 10 mM) produced a transient spectrum with λ_{max} at ~ 440 nm. The growth of this species appeared to be instantaneous and it decayed with pseudo first order kinetics (k_{obs} = 1.15 x 10^6 s^{-1}) to leave a residual absorption which has no clear maximum in this region of the spectrum. Monitoring the decay of the electron at 550 nm with a 1 mM solution of **IV** yielded a similar scavenging rate constant as for **VII** (k_{e^-} = 1.3 x 10^{10} M^{-1} s^{-1}). Lowering the pH to 3 resulted in the disappearance of the decay at 440 nm and the instantaneous formation of the residual.

2.2.6.Solid state studies

A good entry into the understanding of the photochemistry of lignin model compounds in organized and microheterogeneous systems would be to study compounds like α-GAV and **VII** in the crystalline state, where

the conformations and packing are readily determined by X-ray crystallography and solid-state NMR.

Studies on crystalline α-GAV

The fluorescence spectrum from solid crystalline α-GAV is shown in Figure 2.22, along with that recorded in methanol solution. While quantitative measurement of emission yields are difficult with the solid, the signals are intense and readily detectable and suggest an efficient process. Single photon counting studies of the decay of the fluorescence from α-GAV reveal a predominantly (>98%) monoexponential decay with a lifetime of ~ 5.0 ns. This is much longer than the emission in solution which proved to be within the time resolution of our instrument. The rise time for the emission was within the time resolution ($\leq$ 0.5 ns) of our instrument.

Laser flash photolysis experiments were performed using the time-resolved diffuse reflectance technique, since the samples are opaque. No evidence for the triplet state could be obtained, indicating that either the triplet is not populated, or its lifetime is less than 200 ns. We note that the time resolution of the technique (usually better than 50 ns) is limited in this case by interference from the fluorescence.

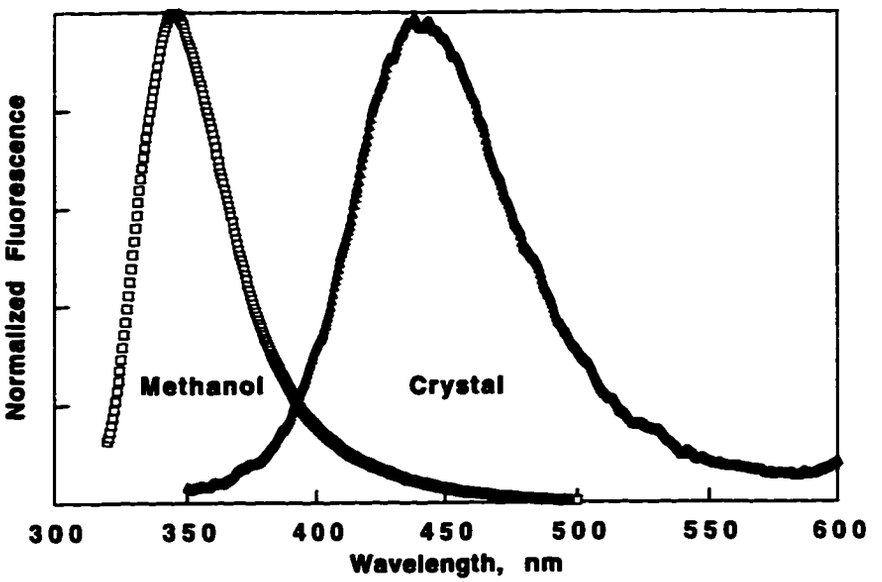

Figure 2.22 Normalized fluorescence spectra for α-GAV in methanol and in the solid state. Excitation wavelength 310 nm.

We were concerned as to whether our failure to detect the triplet state could be due to instrumental problems and/or unusual scattering properties of the solid samples of α-GAV. In order to test this, we prepared a 1:3 intimate mechanical mixture of α-GAV and **V**. The triplet state of **V** has been detected in the solid state in other work from our laboratory and the solution spectra of triplets α-GAV and **V** are very similar. Under these conditions triplet **V** was readily detectable. This experiment makes us confident that the failure to detect triplet α-GAV is not due to experimental difficulties.

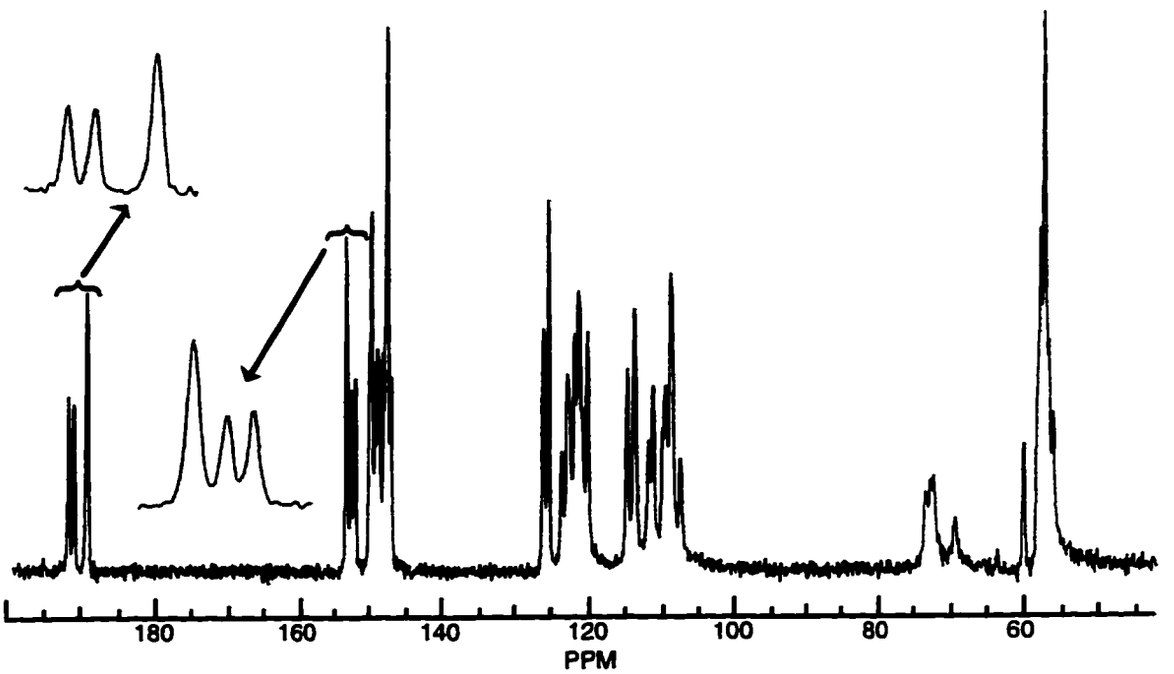

Figure 2.23 CP MAS NMR ^{13}C spectrum of crystalline α-GAV.

^{13}C-CPMAS-NMR studies on crystalline α-GAV reveal the presence of three different carbonyl resonances present in approximately a 2:1:1 ratio. Figure 2.23 shows the relevant part of the ^{13}C spectrum. The chemical shifts for the carbonyl signals are 189.69 (2), 191.35 (1) and 192.08 (1) ppm. This unexpected observation suggests the presence of two identical or very similar carbonyl groups, plus two other distinct carbonyl groups. Other positions in the molecule (e.g. C_1 in the phenoxy moiety) reveal a similar distribution. In comparison, the ^{13}C NMR spectrum of α-GAV in solution ($CDCl_3$, 500 MH_z) shows only a single carbonyl resonance at δ 193.0. These results are consistent with the crystallographic data for α-GAV, see below.

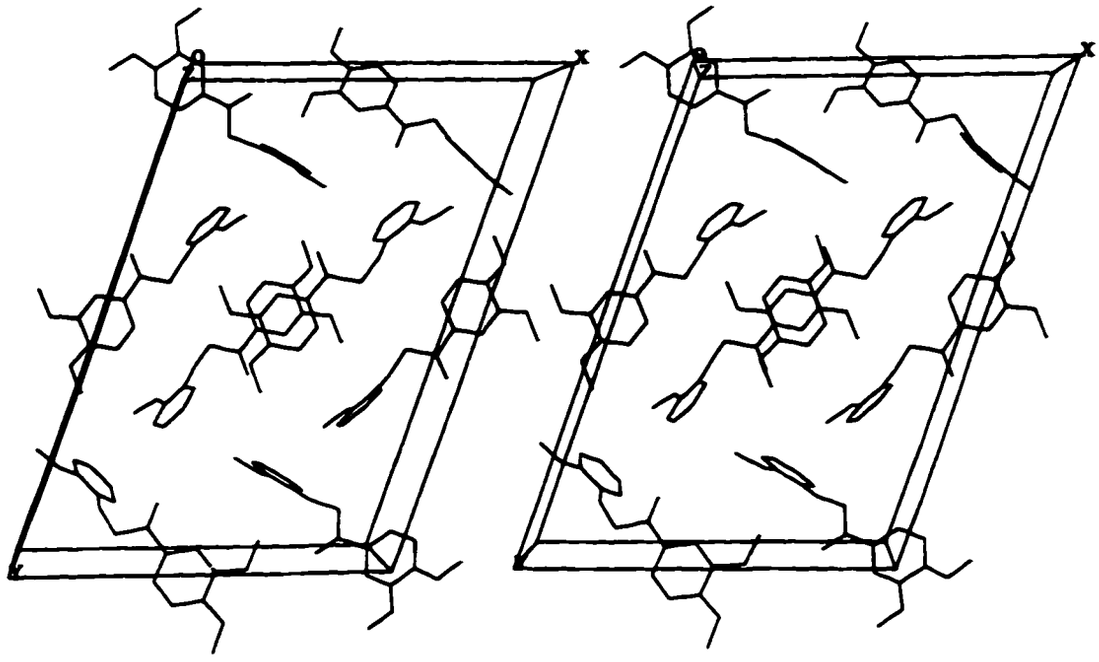

Figure 2.24 Stereo view of the unit cell in α-GAV.

α-GAV crystallizes in the triclinic system: the space group is P1. The unit cell (17.314 Å x 25.127 Å x 7.2515 Å) contains four molecules per asymmetric unit, with a Z = 2. A stereo view of the unit cell is illustrated in Figure 2.24. Figure 2.25 shows an ORTEP plot of a set of four molecules illustrating the four basic conformations within an asymmetric unit in the crystal. There are two of these asymmetric units per unit cell.

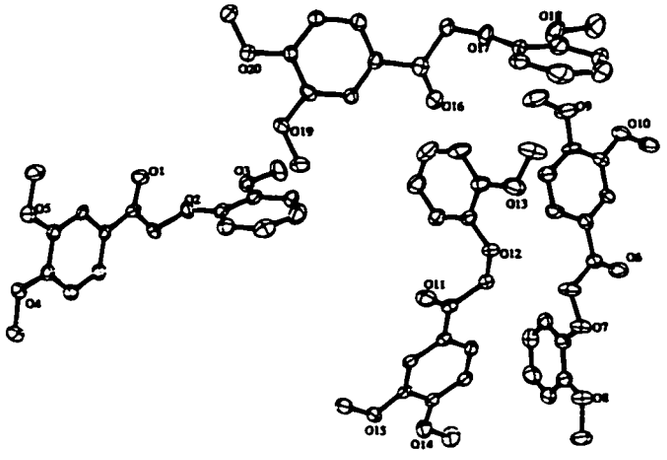

Figure 2.25 ORTEP diagram showing the four different molecules of α-GAV in an asymmetric unit of the unit cell.

Of particular interest in connection with possible triplet deactivation is the conformation of the O=C–C–O–Ar linkage between the two aromatic rings. While all molecules of α-GAV are in a cisoid conformation which appears suitable for β-aryl quenching, the distances between the carbonyl oxygen and C_1 in the β-aryl rings range from 3.16 to 3.25 Å. This may be close enough to induce β-aryl quenching, but is very unlikely to reduce the triplet lifetime beyond our detection limit. Further, the unusually red-shifted and relatively long lived fluorescence suggests that an alternate explanation, involving processes in the excited singlet surface should be considered. Another noticeable characteristic of the crystal packing is the presence of pairs of molecules (see center of unit cell in Figure 2.24) with the 3,4-dimethoxybenzoyl group almost perfectly stacked in a head-to-tail arrangement. The distance between the two rings for the example in Figure 2.24 is approximately 3.43 Å. We note however, that a similar arrangement is achieved by the molecules of α-GAV at the edges of the unit cell, by interaction with molecules at the edge of the neighbouring unit cells located at comparable distances, although in some cases the stacking of these molecules leads to a zig-zag arrangement. Such arrangement may not be as favorable as that for the pair of molecules in the center of the unit cell; these pairs are in turn aligned with those in neighbouring unit cells leading to long range stacking of the molecules.

Studies on crystalline VII

Lamp irradiation of a sample of **VII** (0.2 g) with 9 RPR-300 lamps for 7 days under nitrogen followed by dissolution in methanol and chromatographic analysis did not lead to any significant yields of new products, although the sample was significantly yellow after the photolysis. Thus, under these irradiation conditions **VII** is essentially photostable, just as α-GAV has been demonstrated to be in earlier work.

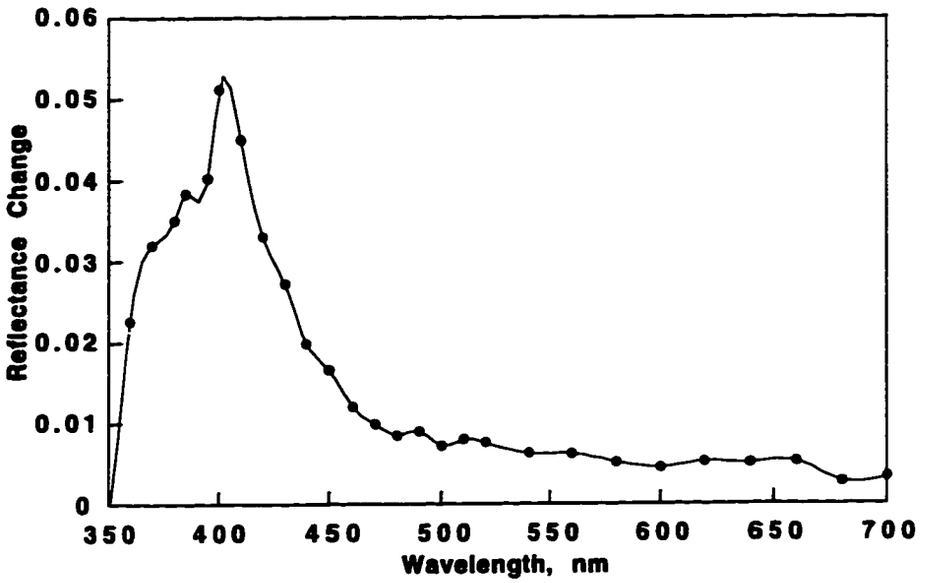

Figure 2.26 Solid-state spectrum from crystalline VII, obtained by 308 nm laser excitation and using time-resolved diffuse reflectance to monitor the signals. Spectrum recorded 500 ns after the laser pulse.

In contrast with the negative results of product studies, 308 nm laser excitation of crystals of **VII** gives a transient spectrum (monitored using diffuse reflectance detection) with λ_{max} 390 nm (Figure 2.26). At this wavelength, the transient decays with perfect second order kinetics, as illustrated in Figure 2.27, which shows both the second order fit and (inset) a representative decay trace. As is frequently the case with diffuse reflectance studies, the signal intensity did not increase linearly with laser power, although the decay of the transient followed clean second order kinetics at all powers.

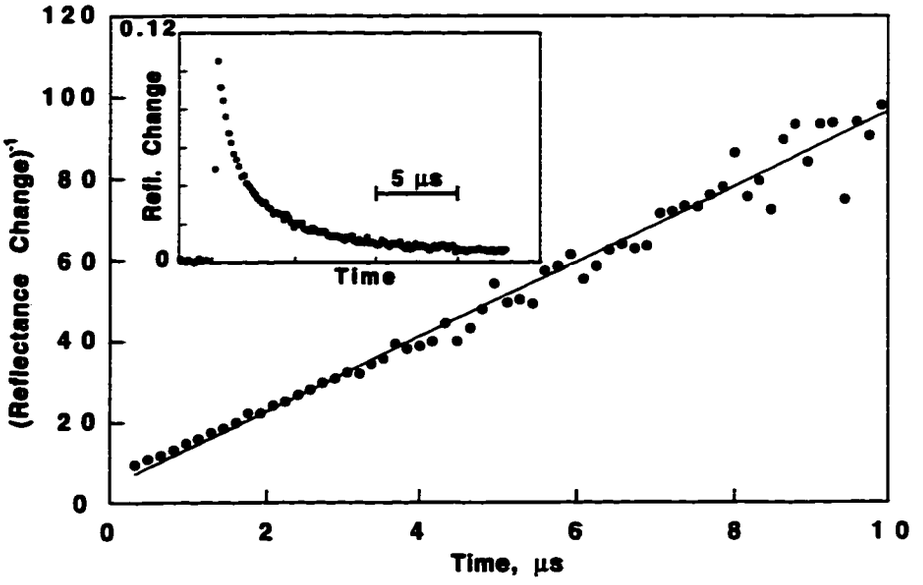

Figure 2.27 Inset: a diffuse reflectance decay trace recorded at 400 nm following 308 nm excitation of crystalline VII. A second-order kinetic fit to the data.

The transient of Figure 2.26 and Figure 2.27 is assigned to the triplet state of **VII**. The reasons which support this assignment (as opposed to free radicals) will be reviewed in detail in the discussion, section 2.3.6. No difference in the signals (spectrum or kinetics) was detected regardless of whether the crystals were irradiated under oxygen or under nitrogen.

The ^{13}C NMR spectrum of **VII** in $CDCl_3$ solution shows a single carbonyl resonance at δ 193.3 ppm. Solid-state ^{13}C CP-MAS NMR revealed a single carbonyl signal at δ 188.9 ppm.

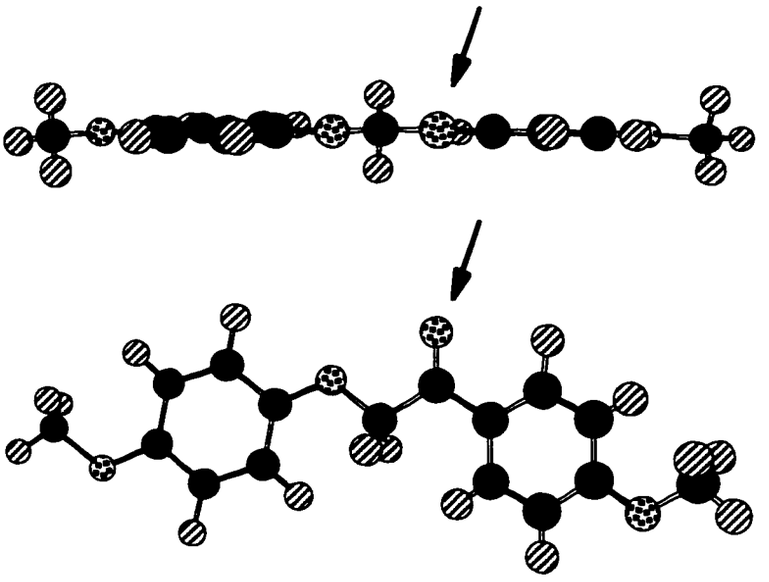

Figure 2.28 Two views of the structure of VII as determined by X-ray Crystallography. In the top view the carbonyl group (note arrow) has been aligned with the Z-axis, and in the bottom view with the Y-axis. Note that VII is essentially planar.

Crystallographic studies on **VII** indicate monoclinic crystals with a unit cell (10.68 Å x 9.27 Å x 13.53 Å) containing four molecules of **VII**, but all in identical conformations, as illustrated in Figure 2.28. This stretched conformation is totally unsuitable for β-phenyl quenching, a common form of decay for ketones of this type.[14, 18, 60] Figure 2.29 shows a stereodiagram of the unit cell illustrating the relative positioning of molecules of **VII** in the crystal. The planes of the aromatic rings in the crystal are located at distances ranging from 3.4 to 3.6 Å, but the *p*-methoxybenzyl rings are somewhat shifted relative to each other. While in the case of α-GAV we found that intermolecular interactions led to efficient singlet interaction and deactivation, this seems not to be the case for **VII** which succeeds in populating the triplet manifold.

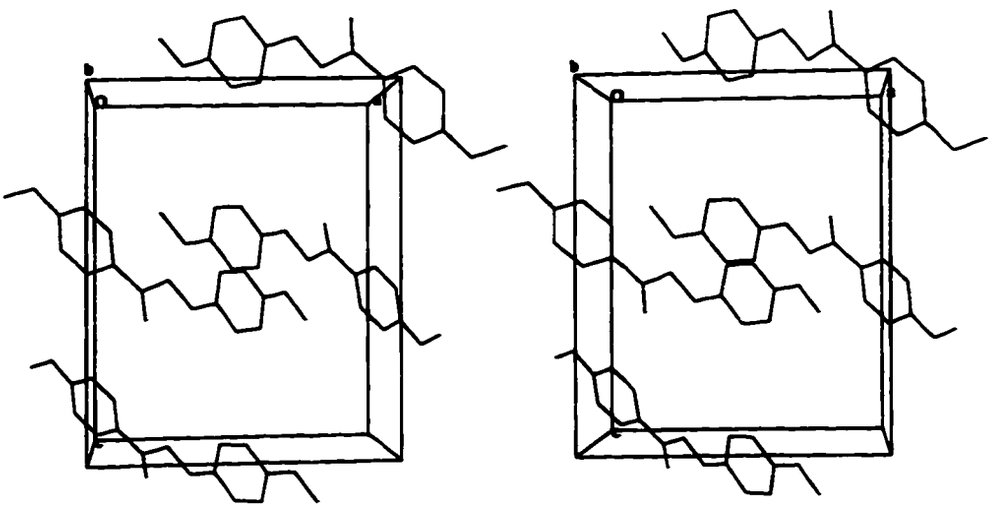

Figure 2.29 Stereodiagram of the unit cell for VII based on the X-ray crystallographic studies.

2.2.7.Studies on the p-methoxyphenacyl radical

In order to study and characterize the *p*-methoxyphenacyl radical (IX), another precursor to the radical was selected. α-Bromo-*p*-methoxyacetophenone (X), when photolysed, generates IX and bromine radical, the latter being spectroscopically invisible under the laser flash photolysis conditions used.

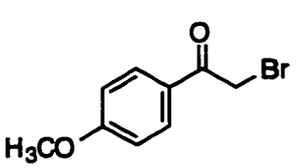

Figure 2.30 α-Bromo-*p*-methoxyacetophenone (X).

Photolysis of X in ethanol leads to the transient absorption spectrum shown in Figure 2.31. The lifetime of radical IX was measured in methanol, ethanol, isopropanol, and acetonitrile. The lifetimes were similar in all cases, approximately 10 μs.

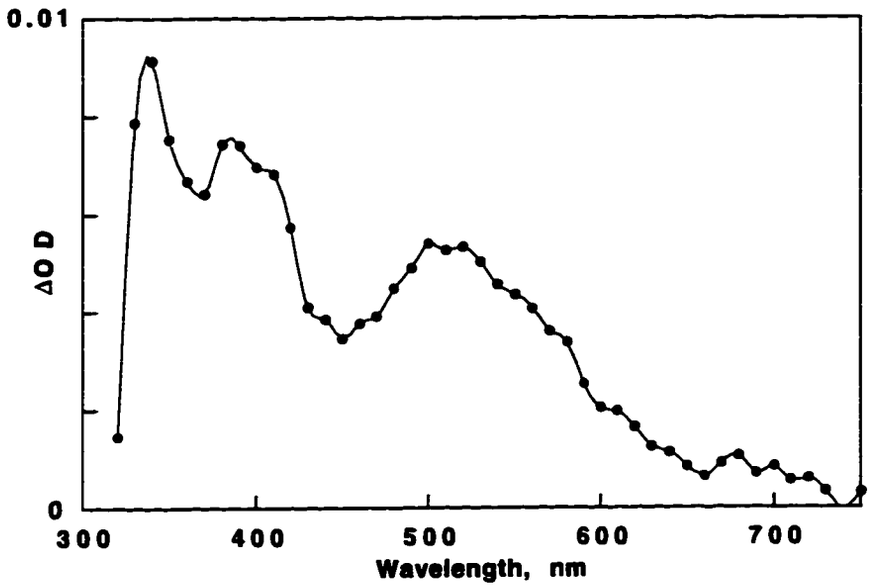

Figure 2.31 Transient absorption spectrum of radical IX, after photolysis of X in ethanol with 308 nm excitation.

To study the reactivity of phenacyl to oxygen, a series of measurements were carried out at various oxygen concentrations; these were adjusted by bubbling the samples with oxygen-nitrogen mixtures of known composition. The pseudo-first-order rate constant for radical decay follows Equation 13.

$$k_{decay} = k_o + k_{ox}[O_2] \qquad \textbf{Equation 13}$$

Figure 2.32 shows a plot of k_{decay} against oxygen concentration for the reaction of **IX**, the radical from **X**, in acetonitrile. From the slope we obtain $k_{ox} = 2.4 \times 10^9\ M^{-1}\ s^{-1}$; and essentially the same number was obtained in methanol. The value is in line with typical reactivities of stabilized carbon-centred free radicals toward oxygen.[61]

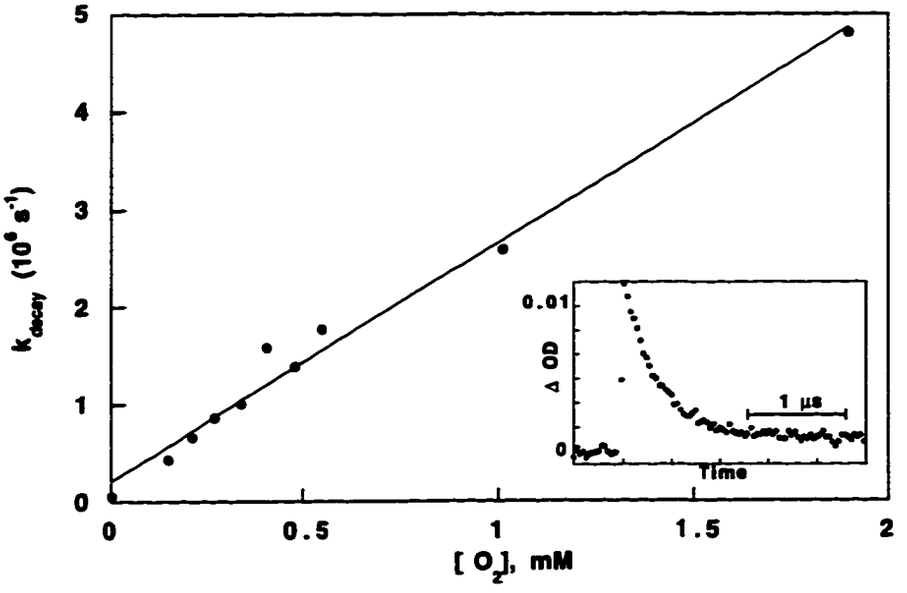

Figure 2.32 Plot of k_{decay} vs O_2 concentration for radical IX in acetonitrile. 308 nm laser. Inset: Representative trace at 520 nm.

1,1-Diphenylethylene is a well-established free radical scavenger.[62] Radical addition (Scheme 2.14) leads to a resonance-stabilized and readily detectable radical, with a characteristic intense absorption in the 330 nm region.

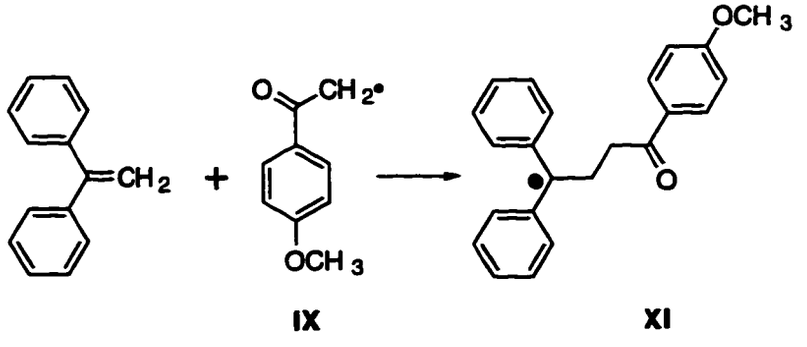

Scheme 2.14 Reaction of radical IX with 1,1-diphenylethylene to form radical XI.

The reaction shown in Scheme 2.14 can be studied by monitoring the decay of the phenacyl radical IX at 520 nm, or the formation of the product radical XI at or around 330 nm. Figure 2.33 shows a plot of k_{decay} against the

concentration of 1,1-diphenylethylene and a representative trace (inset). Monitoring of the reaction by following the phenacyl radical (rather than XI) is preferred since it should not be subject to interference by possible addition of Br• to 1,1-diphenylethylene.

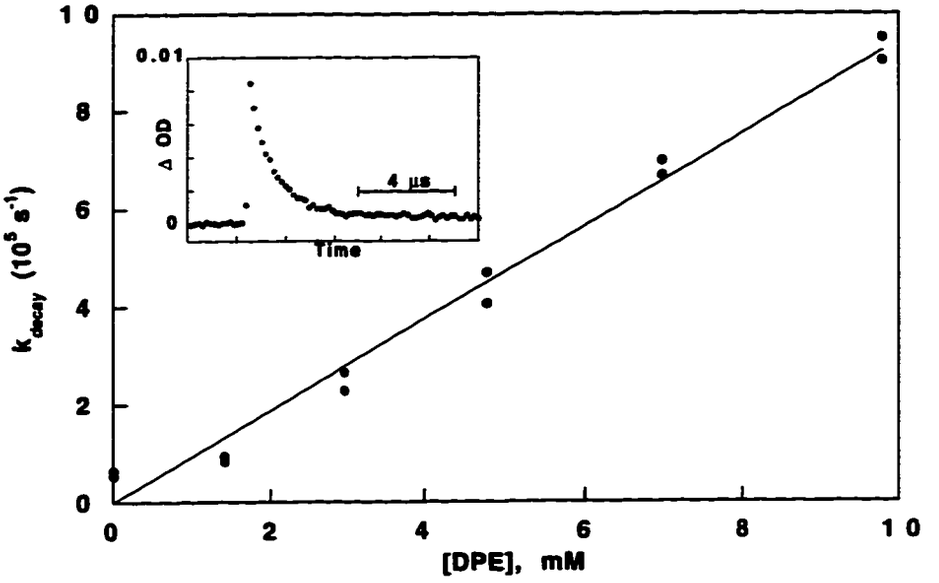

Figure 2.33 Plot of k_{decay} vs 1,1-diphenylethylene concentration for radical IX in acetonitrile. 308 nm laser. Inset: Representative trace at 520 nm.

The spectrum of the product radical XI is shown in Figure 2.34, and is typical for a diphenylmethyl radical absorption.[63] Figure 2.33 shows a plot leading to a surprisingly high rate constant of 9.4 x 10^7 M^{-1} s^{-1} for the reaction from radical IX in acetonitrile. For comparison, *n*-nonyl radicals add with a rate constant of ~3.0 x 10^5 M^{-1} s^{-1} at 20 °C.[62]

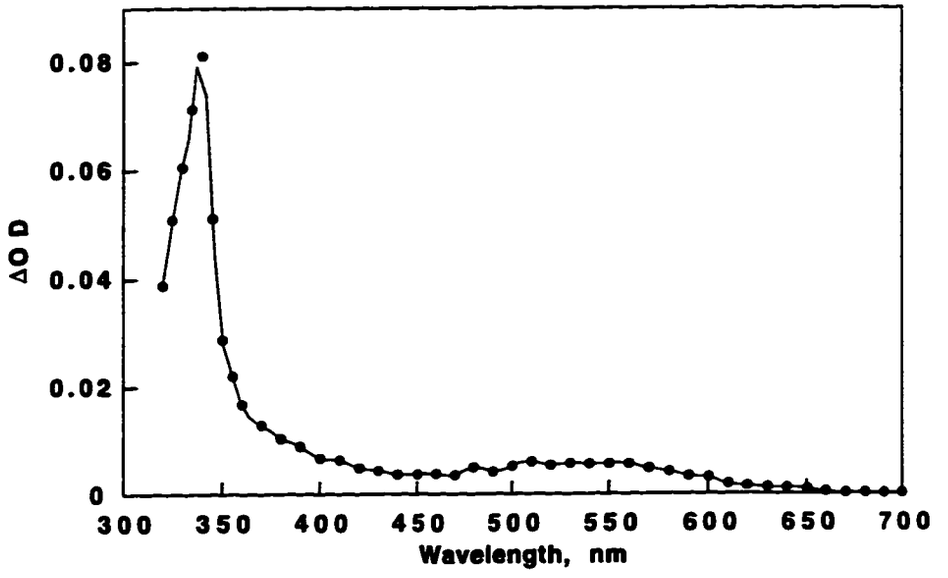

Figure 2.34 Spectrum of the product radical XI from the reaction in Scheme 2.14 in acetonitrile, 308 nm laser, 480 ns after laser pulse.

Molecular modeling

We were concerned and surprised at the long wavelength absorption of **IX**, leading us to carry out calculations on **IX**. These indicate the presence of a band in the 500 nm region and suggest considerable delocalization in the radical.

Minimized structures for **IX** were calculated using the PM3 semi-empirical SCF-MO method as implemented in a version of the MOPAC program.[64, 65] Semiempirical calculations (AM1) on the structure of **IX** suggest a significant contribution from the canonical form of the radical in which the unpaired electron is centered on the oxygen atom (see inset, Figure 2.36).

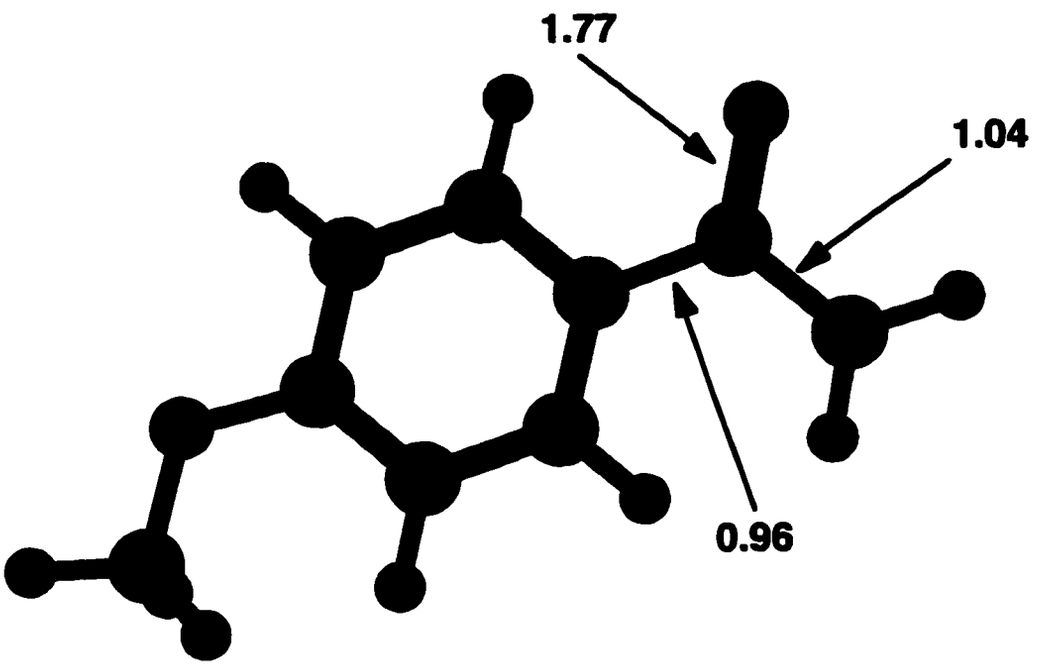

Figure 2.35 Calculated bond orders for radical IX. Results from AM1 calculations.

Figure 2.35 shows the key bond orders; these are consistent with ESR data on these types of radicals.[66] Calculated spin densities at the oxygen center are about 0.3; surprisingly this arises largely at the expense of spin density elsewhere on the ring, since the spin density at the carbon radical site remains close to one. Calculations on the ketones that would result from the hydrogen abstraction show that the enol tautomer lies generally ~10 kcal/mol above the ketone form. Thus, we expect reactions at the oxygen center to be thermodynamically less favorable than those at the carbon center.

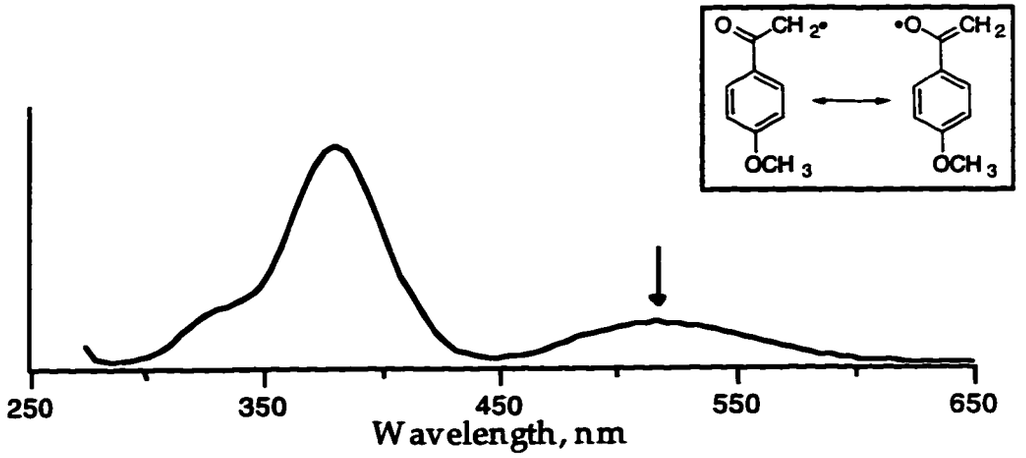

Figure 2.36 Calculated electronic absorption spectrum for *p*-methoxyphenacyl radical with long-wavelength absorption. Inset: canonical forms of the phenacyl radical.

The corresponding electronic absorption spectrum was calculated by the CI/ZINDO method. The predicted spectra each showed a weak feature at ~520 nm along with a stronger band at ~400 nm (Figure 2.36). The transition largely responsible for the 520 nm band in the *p*-methoxybenzoylmethyl radical is from (HOMO-1) to LUMO, involving delocalization of electron density out over the carbonyl moiety. The orbitals involved in these transitions and the corresponding electron densities are shown graphically in Figure 2.37.

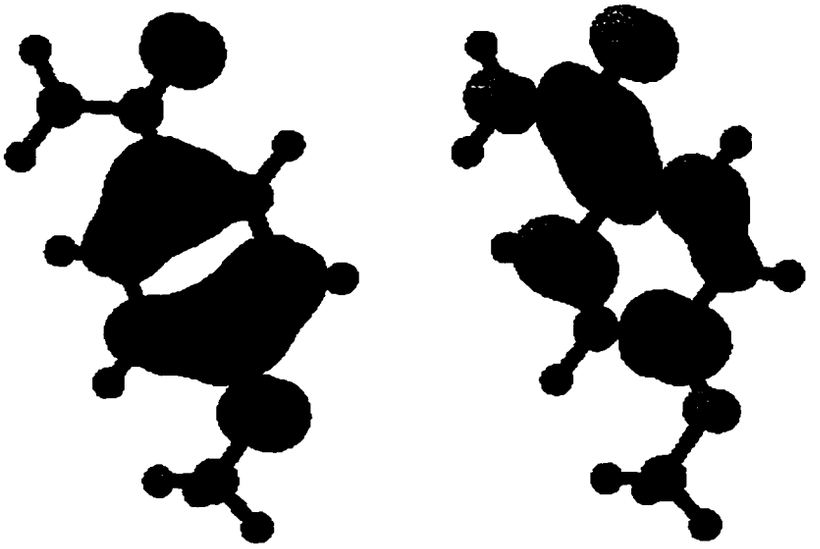

Figure 2.37 Calculated electron densities for the *p*-methoxyphenacyl radical for the two molecular orbitals responsible for the long-wavelength absorption. Left: HOMO-1; right: LUMO.

2.2.8. Studies of potential yellowing inhibitors on paper made from thermomechanical pulp (TMP).

With the knowledge acquired during this work and that from the literature, it is clear that free radicals play an important role in the light-induced yellowing process of mechanical pulps. An initial qualitative screening was carried out using a series of compounds with antioxidant properties. Tabs of TMP handsheets were soaked in aqueous solutions of the compounds shown in Scheme 2.15 and allowed to dry. Controls were also run to compare the yellowing evolution against a tab that was soaked in water.

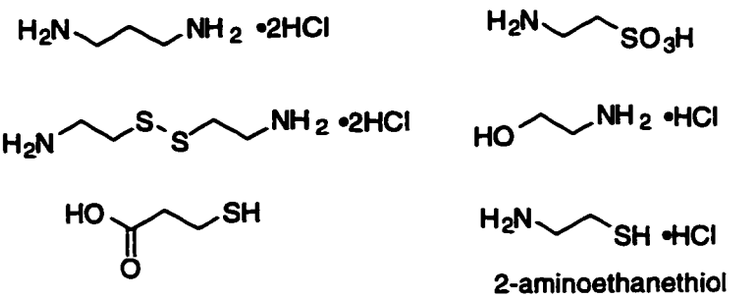

Scheme 2.15 Compounds screened for inhibition properties.

Only one of these compounds, 2-aminoethanethiol (AET), showed any significant stabilizing effect, although slight. This compound was therefore selected to do a detailed study on its effects on the light-induced yellowing of TMP handsheets.

Eight samples were studied, as described in Table 2.4. Since AET HCl lowers the pH of water when it is dissolved, TMP handsheet tabs were soaked both in AET in distilled water and in AET in 0.1 M pH7 phosphate buffer. Controls were run where the untreated samples were soaked in distilled water. Two of the eight samples were irradiated under 300 nm lamps.

Table 2.4 TMP handsheet samples irradiated.

Sample	*Lamps*	*TMP Type*	*Treatment*
A	350 nm	Unbleached	Untreated
B	350 nm	Unbleached	AET in H_2O
C	350 nm	Unbleached	AET in buffer
D	350 nm	Bleached	Untreated
E	350 nm	Bleached	AET in H_2O
F	350 nm	Bleached	AET in buffer
G	300 nm	Bleached	Untreated
H	300 nm	Bleached	AET in H_2O

Absolute reflectance spectra were measured for each sample, before irradiation and at time intervals during the irradiation period. From these reflectance spectra difference spectra were calculated in order to get an idea of the total spectral changes in the samples. This simply involves subtracting the absolute reflectance spectrum after irradiation from that before irradiation. A positive value in the difference spectrum (more reflectance after irradiation) depicts a bleaching, whereas a negative value in the difference spectrum (less reflectance after irradiation) depicts the formation of light-absorbing species at those wavelengths. As an example,

Figure 2.38 and Figure 2.39 show the results obtained for the irradiation of sample A.

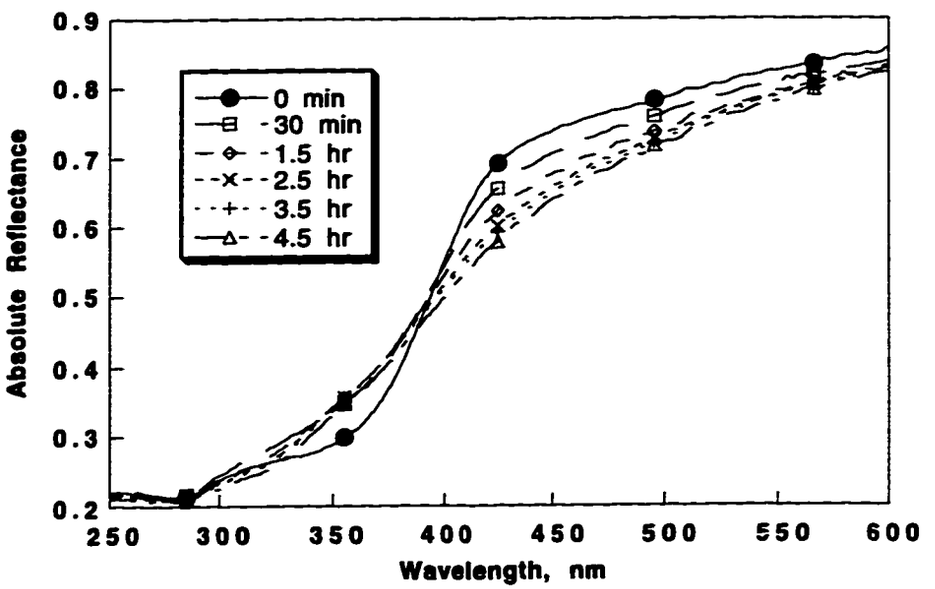

Figure 2.38 Absolute reflectance spectra for sample A (untreated, unbleached TMP) before and during irradiation with 350 nm lamps.

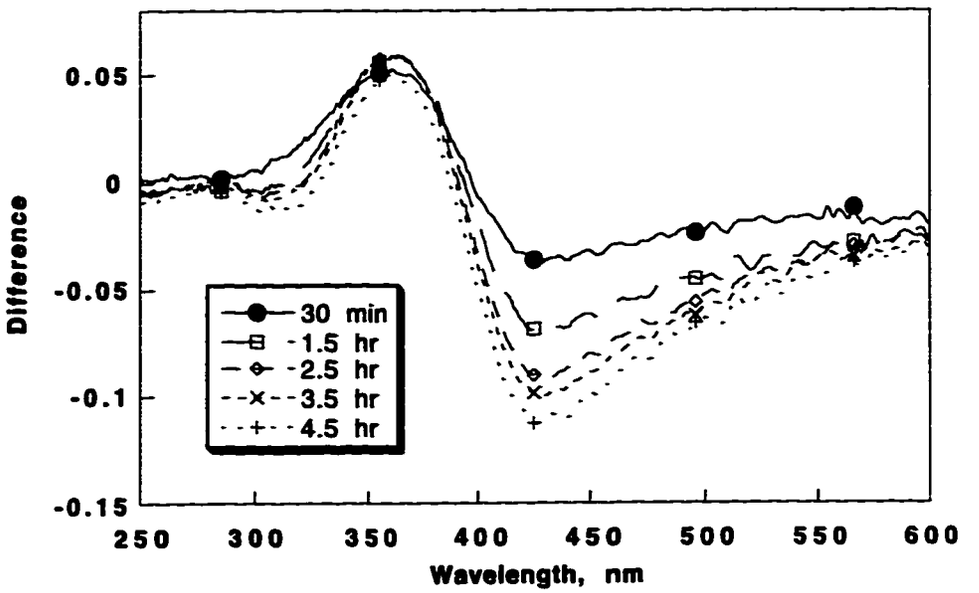

Figure 2.39 Difference spectra for sample A (untreated, unbleached TMP). Irradiation with 350 nm lamps.

These results show that there is a fast bleaching effect in the 350 nm region when unbleached , untreated TMP is irradiated with 350 nm lamps, and there is also the formation of absorbing material in the 400 to 500 nm range.

In addition, the reflectance data was converted to nominal values of ISO brightness, L*, and b* values in order to follow brightness and yellowness qualities of the samples during irradiation (see page 65 for an explanation of calculations). Note that to obtain "real" ISO brightness values, one must use certified equipment, with a certain lamp distribution and a specific spectral width at the wavelengths of interest. In our method, we use a standard spectrophotometer and use a very narrow spectral width (a single wavelength value) at the wavelengths of interest. Higher values of ISO brightness and L* and lower values of b* are desirable. Representative curves are shown in Figure 2.40, Figure 2.41, and Figure 2.42.

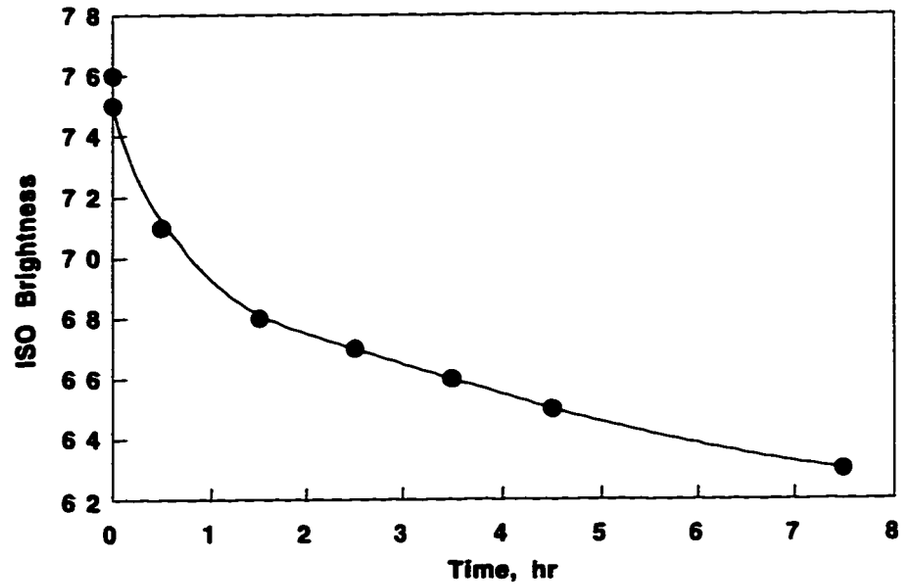

Figure 2.40 ISO brightness evolution over time for sample A.

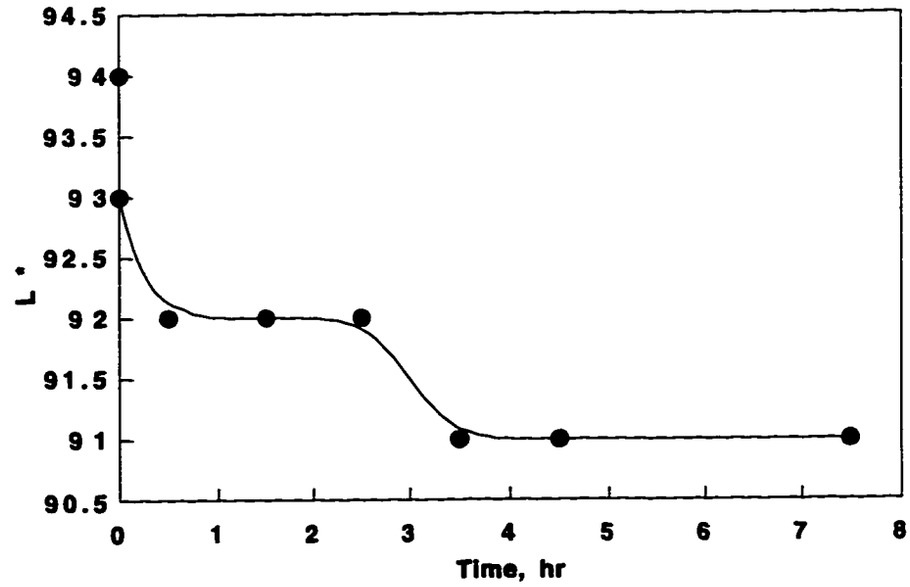

Figure 2.41 L* evolution over time for sample A.

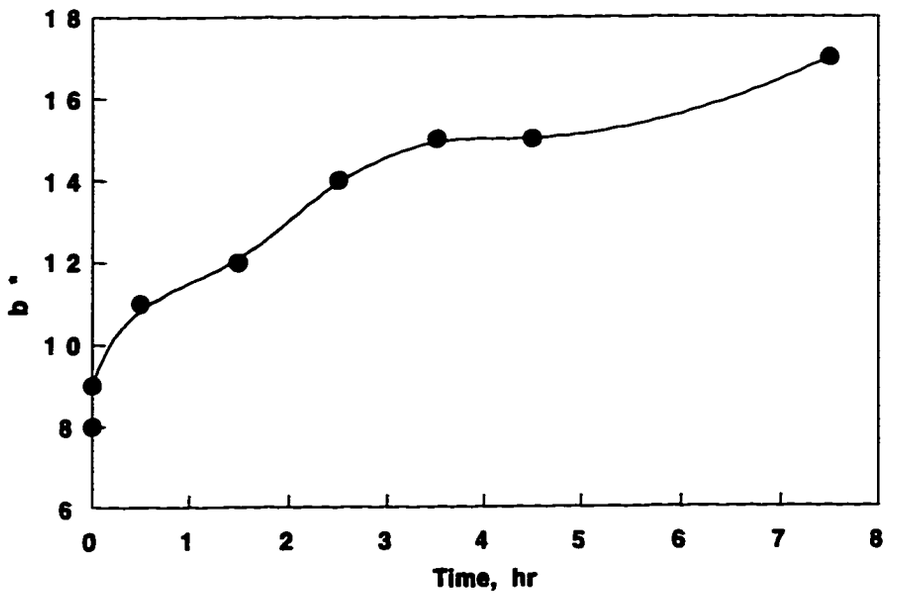

Figure 2.42 b* evolution over time for sample A.

It is interesting to note that sample D does not show the initial bleaching in the 350 nm range observed with sample A(see Figure 2.43). The peak growing in at about 430 nm does seem common in both cases. The only difference in the two samples is that sample A is unbleached TMP and sample D is bleached TMP. Both are untreated with AET.

Samples A, B, and C are all unbleached TMP handsheets, treated with no AET, AET in H_2O, and AET in buffer, respectively. Figure 2.44 shows the initial bleaching action of AET treatment, even before irradiation. As mentioned in section 2.1.9, this bleaching effect of some thiols has already been reported.[39-41]

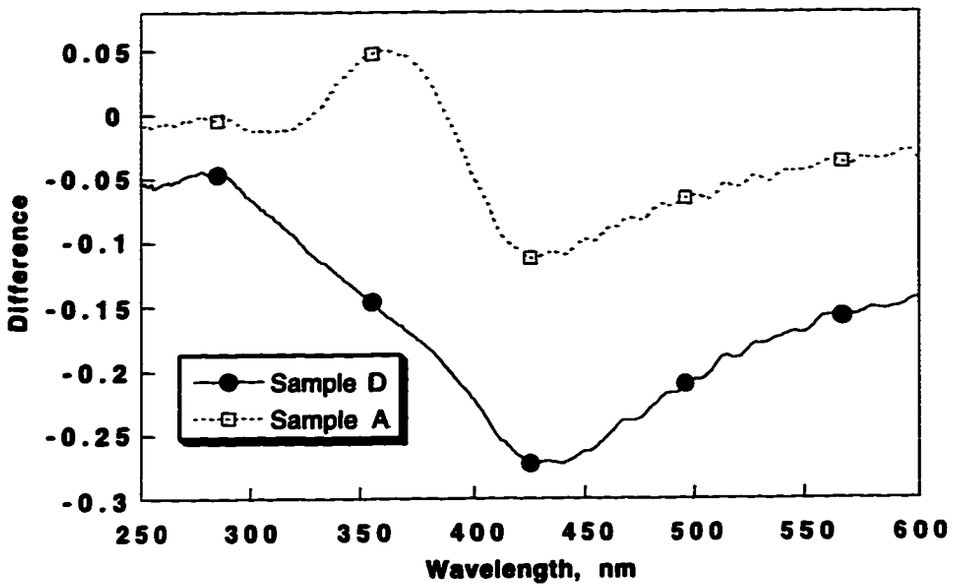

Figure 2.43 Overlay of difference spectra of samples A and D after 4.5 hours of irradiation with 350 nm lamps.

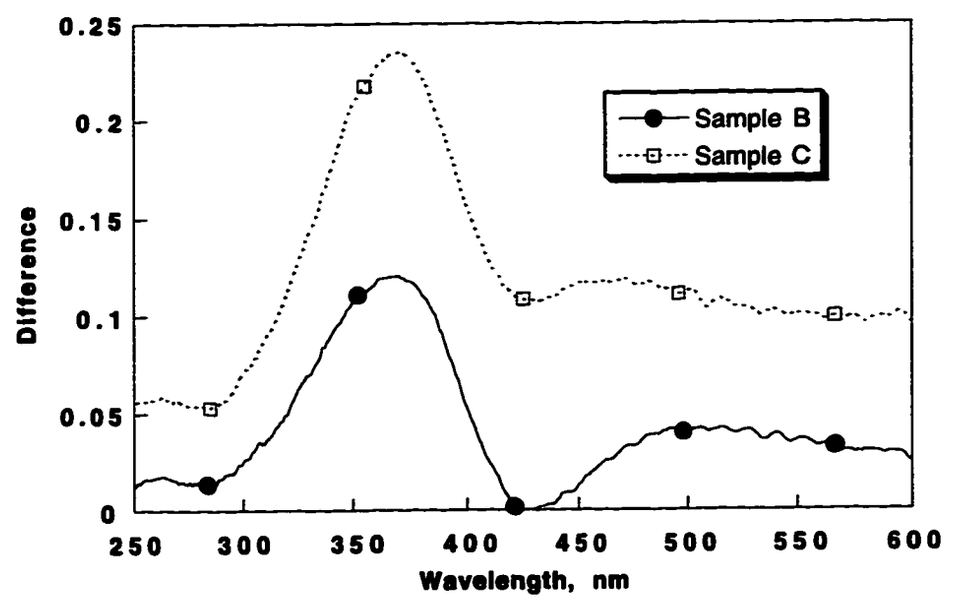

Figure 2.44 Effect of treatment of unbleached TMP with AET; sample B: from H2O; sample C: from buffer. Difference is calculated from the untreated sample A.

Presumably due to this initial bleaching effect, samples B and C do not show the same light-induced bleaching effect as sample A does in the 350

nm region. However, the longer-wavelength chromophore formation still occurs (Figure 2.45). It is clear, however, that AET stabilizes the ISO brightness, L*, and b* values. (See Figure 2.46, Figure 2.47, and Figure 2.48).

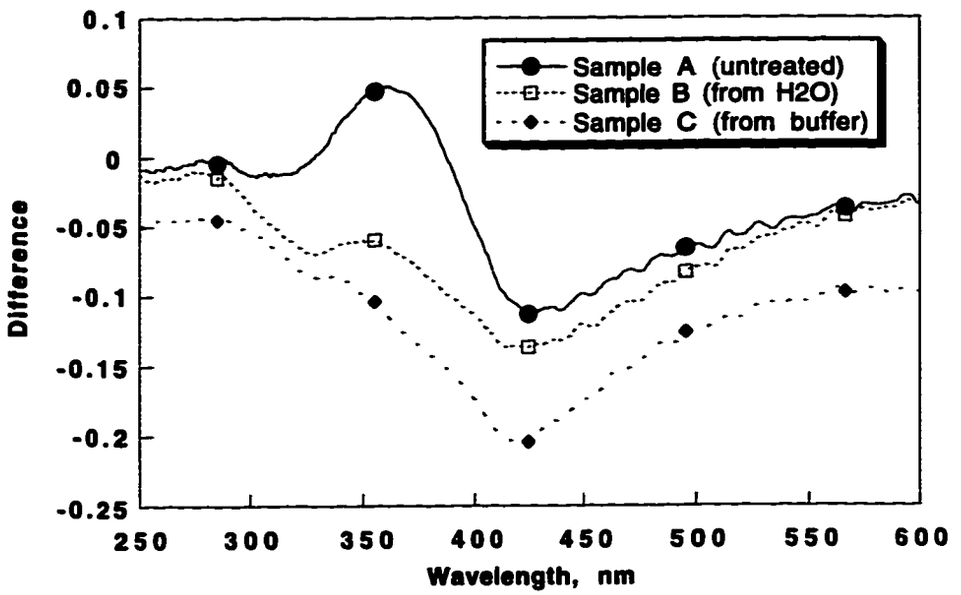

Figure 2.45 Comparison of difference spectra for unbleached samples A, B, and C after 4.5 hours of irradiation with 350 nm lamps.

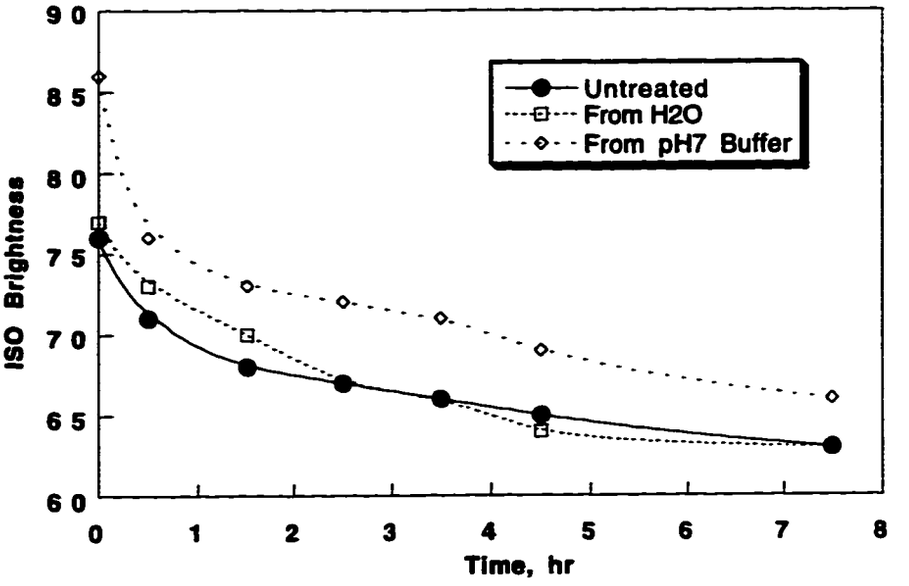

Figure 2.46 ISO Brightness evolution over time for unbleached TMP samples A, B, and C.

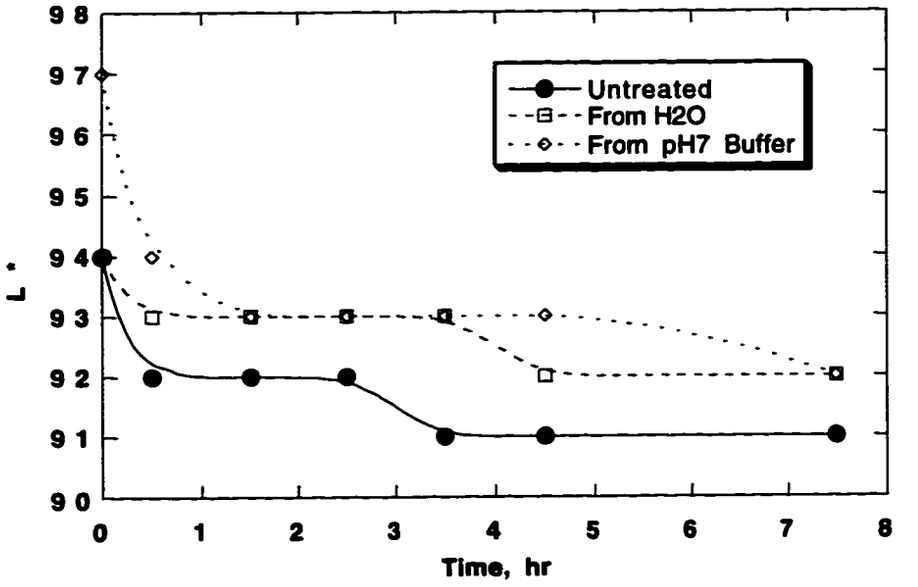

Figure 2.47 L* evolution over time for unbleached TMP samples A, B, and C.

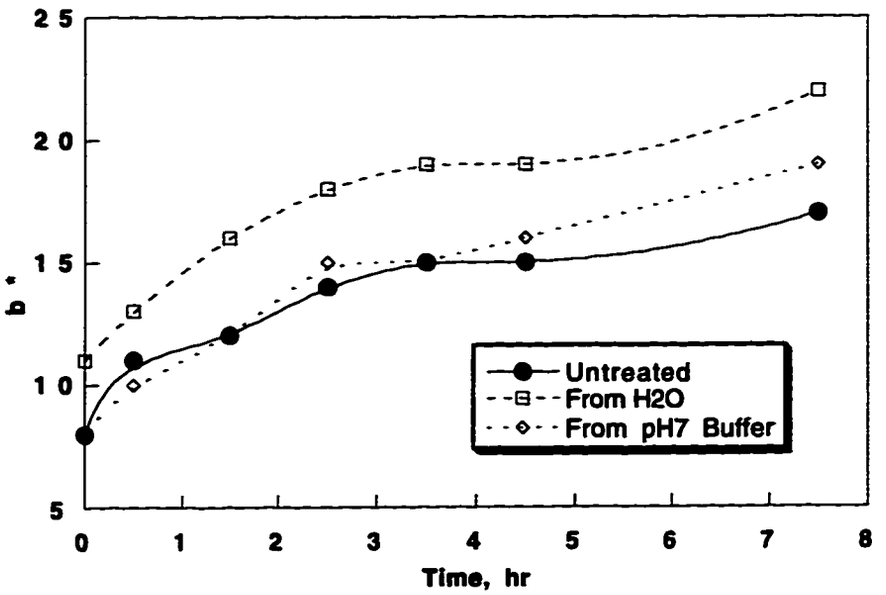

Figure 2.48 B* evolution over time for unbleached TMP samples A, B, and C.

A similar set of experiments was carried out on a set of bleached TMP handsheets (samples D, E, and F). The results are shown in Figure 2.49 through Figure 2.52.

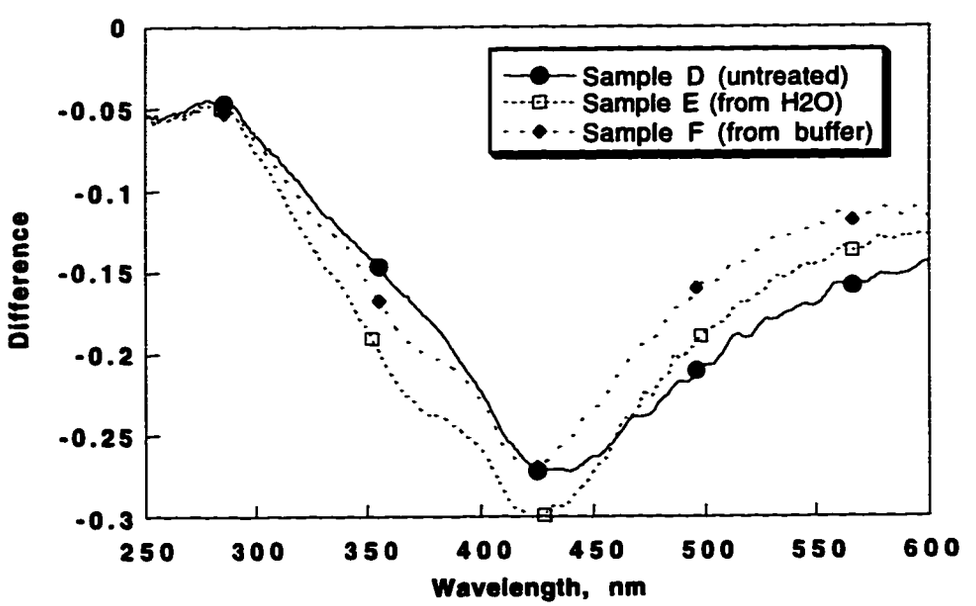

Figure 2.49 Comparison of difference spectra for bleached samples D, E, and F after 4.5 hours of irradiation with 350 nm lamps.

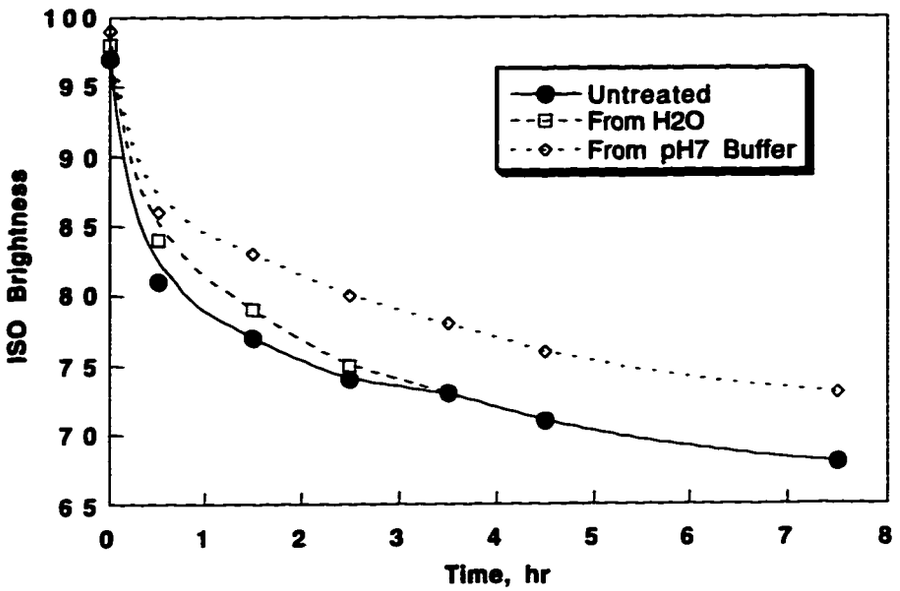

Figure 2.50 ISO Brightness evolution over time for bleached TMP samples D, E, and F.

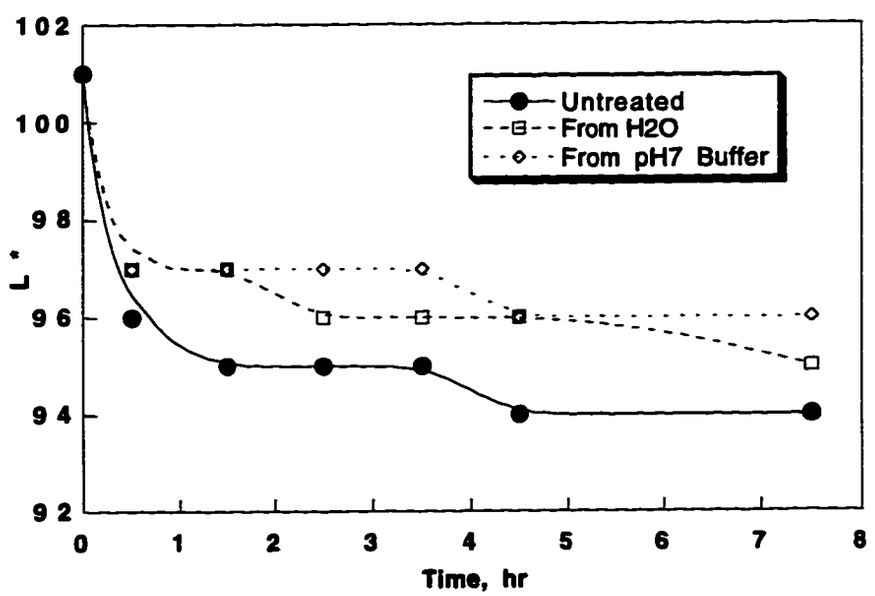

Figure 2.51 L* evolution over time for bleached TMP samples D, E, and F.

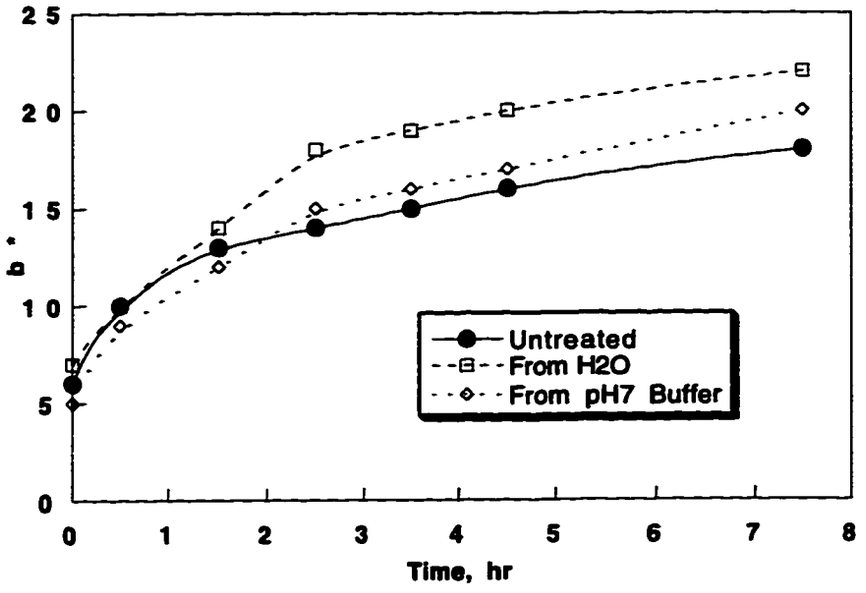

Figure 2.52 B* evolution over time for bleached TMP samples D, E, and F.

Samples G and H are analogous to samples D and E (refer to Table 2.4), except that G and H were irradiated under 300 nm lamps. Similar results were found as with the 350 nm irradiations, however the ISO brightness measurements show an even lesser degree of stabilization by AET treatment than with the 350 nm irradiations. L* and b*, however, do seem to be stabilized by AET treatment from H_2O. Figure 2.53 to Figure 2.56 summarize the results.

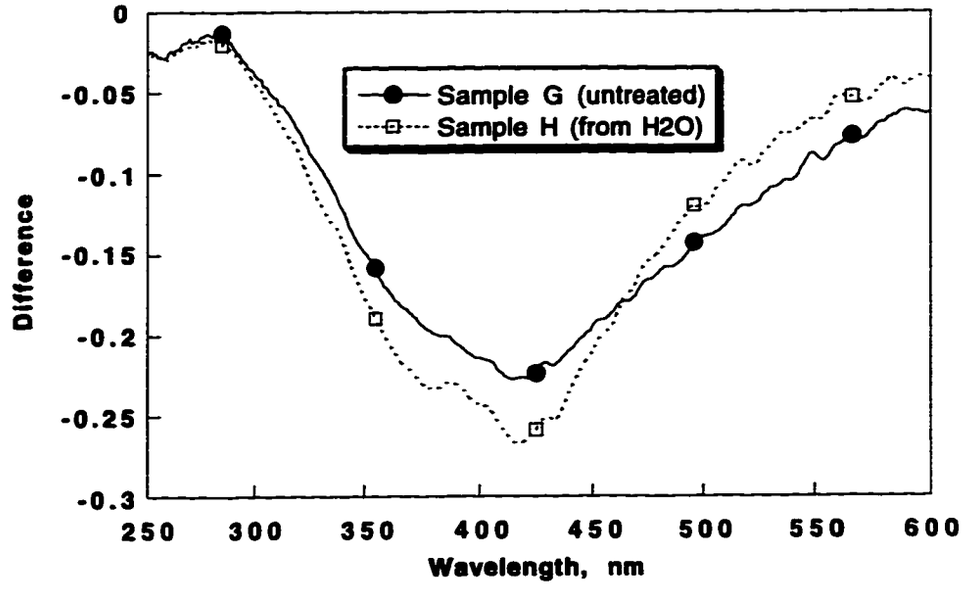

Figure 2.53 Comparison of difference spectra for bleached samples G and H after 21 hours of irradiation with 300 nm lamps.

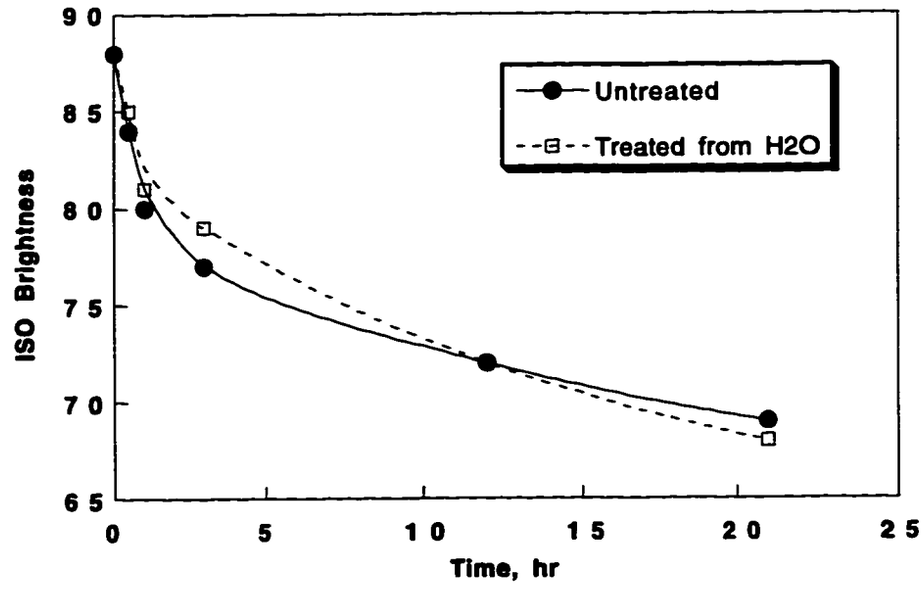

Figure 2.54 ISO Brightness evolution over time for bleached TMP samples G and H.

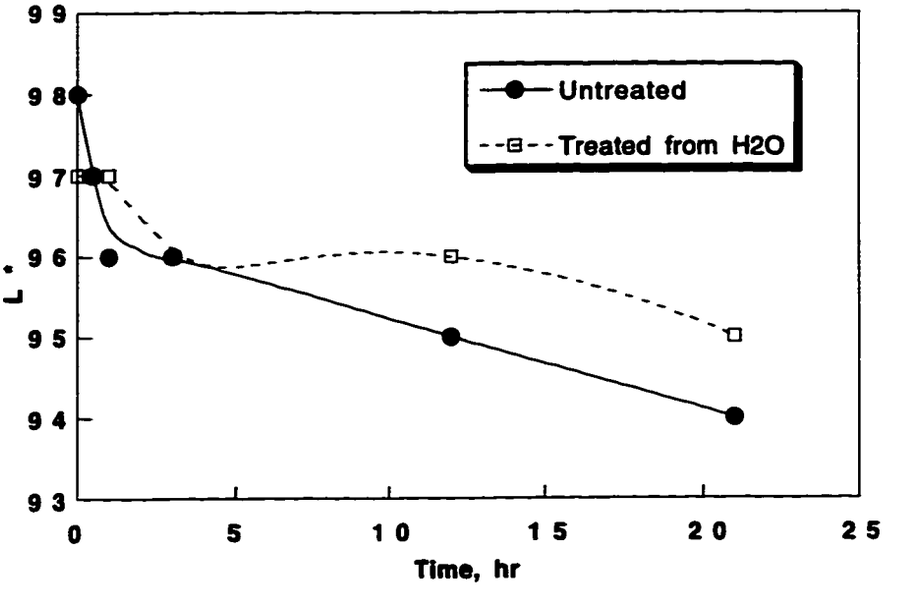

Figure 2.55 L* evolution over time for bleached TMP samples G and H.

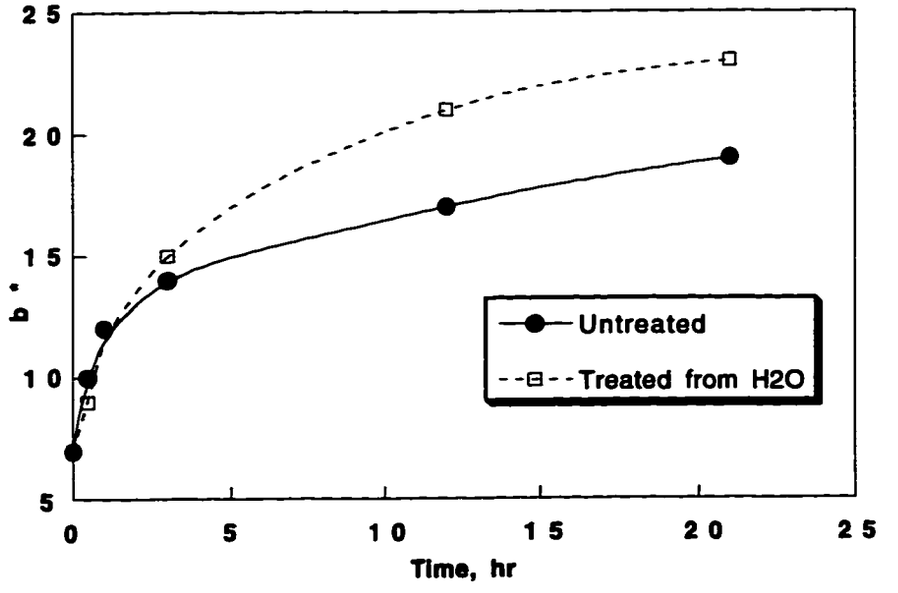

Figure 2.56 B* evolution over time for bleached TMP samples G and H.

2.3.Discussion

2.3.1.α-GAV photodecomposition: Singlet, triplet, or both?

As mentioned in the introduction to this chapter, the photodegradation of α-GAV in protic solvents is increased in comparison to aprotic solvents, as measured by the degradation quantum yields.[24] This and later work[67] suggests that protic solvents induce reactivity from the triplet state of the α-GAV by hydrogen-bonding to the triplet, thereby decreasing β-phenyl quenching, increasing the triplet lifetime, and allowing the cleavage reaction from the triplet to become competitive.

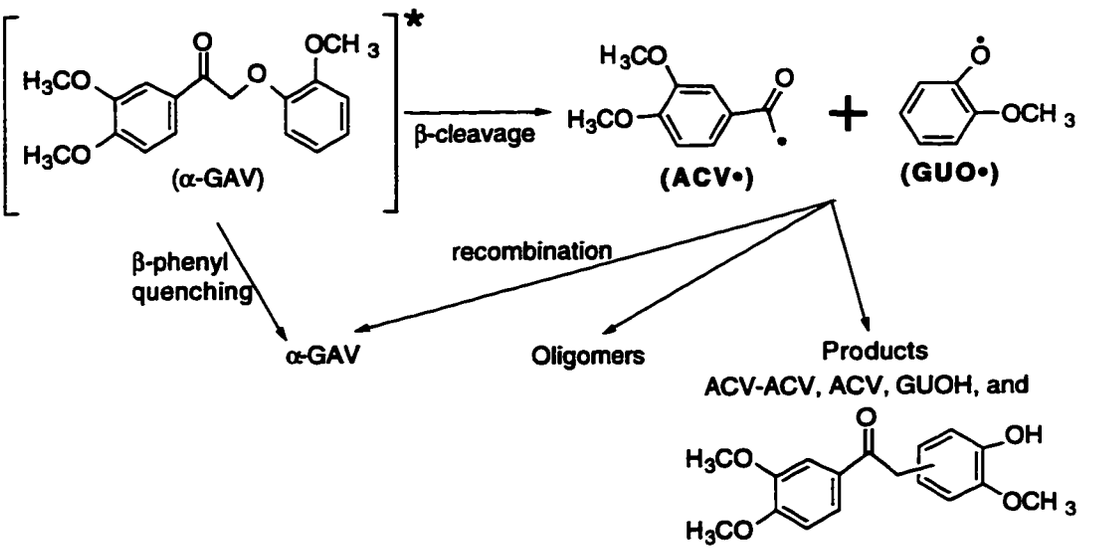

Scheme 2.16 Photodecomposition pathways for α-GAV.

This provides an explanation for both an increase in triplet lifetime in a protic environment *and* increased cleavage from the triplet, which intuitively sounds contradictory at first analysis. It is clear that the excited singlet state of α-GAV plays an important role in the mechanism of photodecomposition. However, recent publications from this research group may shed new ideas on the photodegradation of α-GAV, and

possibly on the whole family of α-phenoxyacetophenones.[68, 69] It has been found that methoxy-substituted phenacyl radicals, derived from the photodecomposition of the corresponding α-bromoacetophenone, participate in a chain reaction mechanism. A competition exists between a bromine atom mechanism, involving hydrogen transfer, and a phenacyl radical mechanism, involving electron transfer.

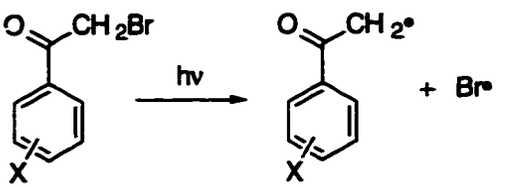

Scheme 2.17 Photolysis of α-bromoacetophenones.

$$Br^{\bullet} + CH_3OH \longrightarrow HBr + {}^{\bullet}CH_2OH$$

$$^{\bullet}CH_2OH + ArCOCH_2Br \longrightarrow ArC^{\bullet}(OH)CH_2Br + CH_2O$$

$$ArC^{\bullet}(OH)CH_2Br \longrightarrow ArC(OH)CH_2 + Br^{\bullet}$$

$$ArC(OH)CH_2 \longrightarrow ArCOCH_3$$

Scheme 2.18 Bromine atom mechanism (hydrogen transfer).

$$ArCOCH_2^{\bullet} + CH_3OH \longrightarrow ArCOCH_3 + {}^{\bullet}CH_2OH$$

$$^{\bullet}CH_2OH + ArCOCH_2Br \longrightarrow CH_2O + H^{+} + [ArCOCH_2Br]^{\bullet -}$$

$$[ArCOCH_2Br]^{\bullet -} \longrightarrow ArCOCH_2^{\bullet} + Br^{-}$$

Scheme 2.19 Phenacyl radical mechanism (electron transfer).

The photocleavage of α-GAV, shown in Scheme 2.3, can be considered analogous to the photocleavage of the α-bromoacetophenone. Analogous chains could be depicted for α-GAV as those shown in Scheme 2.18 and Scheme 2.19, with cleavage occurring from the singlet state. It should be noted that hydrogen atom transfer vs. electron transfer is not applicable in this case, since electron transfer would result in a proton and a radical anion being produced. It has been shown that the radical anion reacts quickly with protons (see section 2.2.5), and an overall hydrogen atom transfer will therefore always occur.

Since phenoxy radicals are not likely to react with alcohols such as those used in this study, the chain cannot propagate. However, an increase in the amount of α-GAV decomposing per photon absorption event can be depicted.

Wan and coworkers[70] have shown with EPR studies that α-GAV degrades by a photoreduction pathway in the presence of alcohols or water, through the intermediacy of the corresponding ketyl radical.

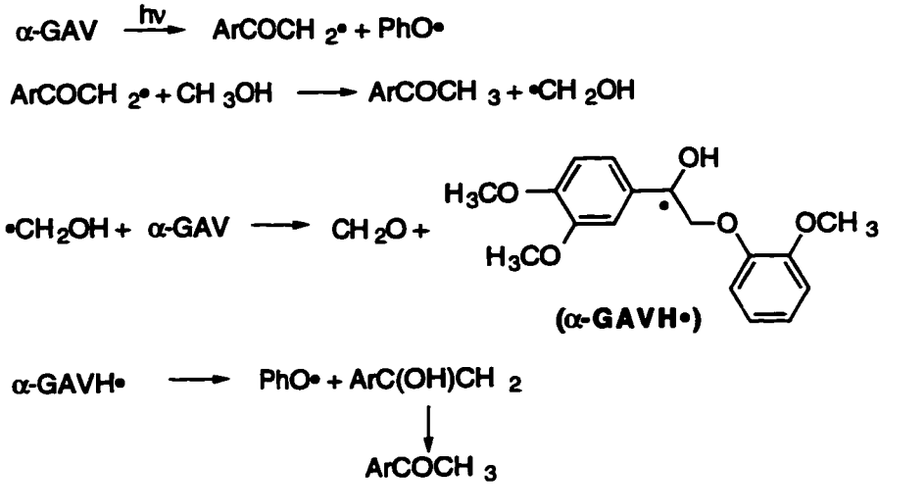

Scheme 2.20 Proposed reaction for α-GAV in protic solvents.

Although the phenoxy radical does not react with the protic solvent significantly, it is greatly stabilized in a hydrogen-bonding environment. This stabilization could decrease the amount of radical recombination, both geminate in-cage recombination and bulk solution recombination, again having the effect of increasing the overall degradation quantum yield in protic solvent environments. If the phenoxy radicals were to react as in Scheme 2.21, although very slowly, a chain reaction could be created.

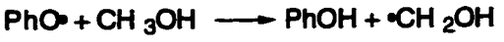

Scheme 2.21 Possible slow reaction of phenoxy radical with protic solvent.

In fact, when guaiacoxy radicals (GUO•) are generated by reaction of *t*-butoxy radicals with guaiacol, the decay kinetics of the GUO• radicals are different in methanol and in acetonitrile. In acetonitrile, the radicals decay by second-order kinetics, as can be expected for radical-radical reactions. However, in methanol, the decay kinetics fit better to a first-order decay, possibly showing that the GUO• radicals are reacting with the solvent in a pseudo-first order process. It has been shown by Bowry and Stocker that phenoxy radicals, on long timescales, can in fact abstract hydrogens from hydrogen-rich environments.[71]

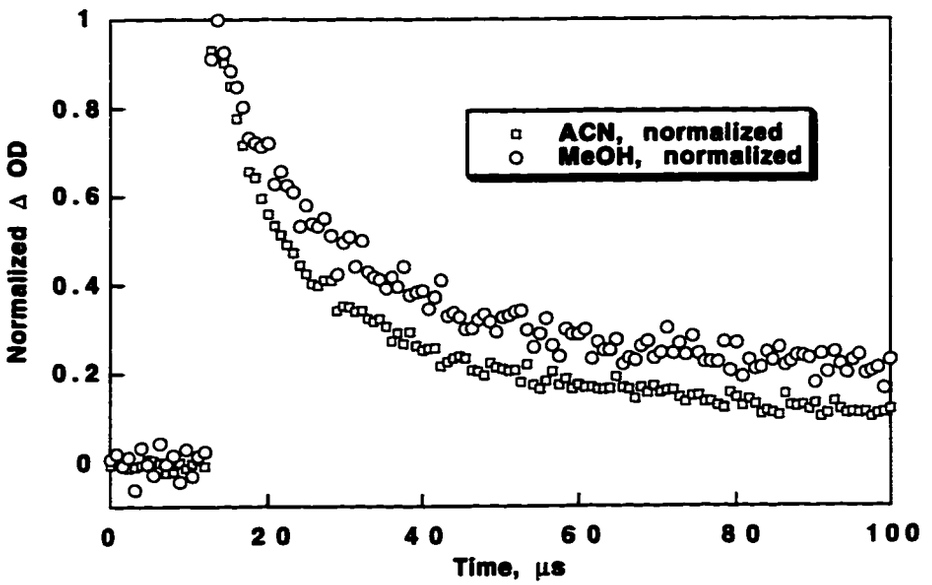

Figure 2.57 Decay of guaiacoxy radicals in (□) acetonitrile and in (○) methanol.

Product studies (section 2.2.2) show that the major products in aprotic solvents result from in-cage coupling reactions and the degradation quantum yield is relatively low. However, in alcohol, the degradation quantum yield increases (see Table 2.1, page 77). If the reactions in Scheme 2.20 occur for a few radicals escaping from the cage, this could explain the increase in degradation quantum yield, *without invoking any triplet reactivity*. The original explanation for the changes in triplet lifetime still stands, with protic solvents interacting with the triplet, decreasing the rate of β-phenyl quenching, and increasing the triplet lifetime.

Johnston and coworkers[72] have reported that when α-GAV is irradiated on solid supports, only in-cage recombination products are obtained, and the amounts of product are unaffected by the presence of triplet quenchers such as trans, trans-2,4-hexadienol, which is consistent with our results.

When triplet quenchers are added to the system in protic solvents, the quantum yield decreases to the non-protic solvent level. These triplet quenchers, in addition to acting to quench the triplets, may be simply

stopping any further reaction before it starts by reacting, for example, with the phenacyl radical (refer to Scheme 2.20). This is supported somewhat by the relative degradation quantum yields with different triplet quenchers (refer to section 2.2.2). The fact that naphthalene does not stop the degradation to the same extent as sorbic acid may mean that for the case of α-GAV, the triplet may play a much smaller role in product formation than originally thought. If α-GAV successfully models some of the photochemistry of lignin, it is clear that triplet quenchers like naphthalene may not be useful, however sorbic acid should be much more efficient.

2.3.2.Power dependence studies on α-GAV

There have been reports in the literature that the lignin model, α-GAV, shows wavelength dependent photochemistry.[6] However, we have found that these observations arise from the fact that as one changes laser wavelength, one normally changes other experimental parameters. For example, the laser power, laser pulse duration, and substrate concentration are normally changed. Changes in concentration are required to maintain a reasonable absorption at the excitation wavelength. While we reproduced without difficulty the reported wavelength effects, we find that when ground state concentrations and laser energy are kept constant in the different experiments, the rate of decay of the signal due to the transient is independent of the laser wavelength. Using 100% of our laser power at 308 nm (~ 20mJ/pulse) appears to induce multiphoton chemistry, as we observe some as yet unidentified transients which are very long lived and very easy to misinterpret as triplets of the model compound. This is not believed to be relevant to the lignin modeling system, since it is unlikely that we are dealing with multiphoton processes in the photoreversion of paper.

It is clear from the results presented in this thesis and in other work that the singlet degradation pathway plays an important role in the photochemistry of α-GAV. We propose that the complicated kinetics at lower irradiation wavelengths and higher powers are due to the absorption of a second photon, within the same laser pulse, by coupling products that are formed within the solvent cage. Since the radicals have the correct singlet spin orientation, the barrier to their reaction should be minimal. Scheme 2.22 depicts the proposed mechanism of formation of the extra transient.

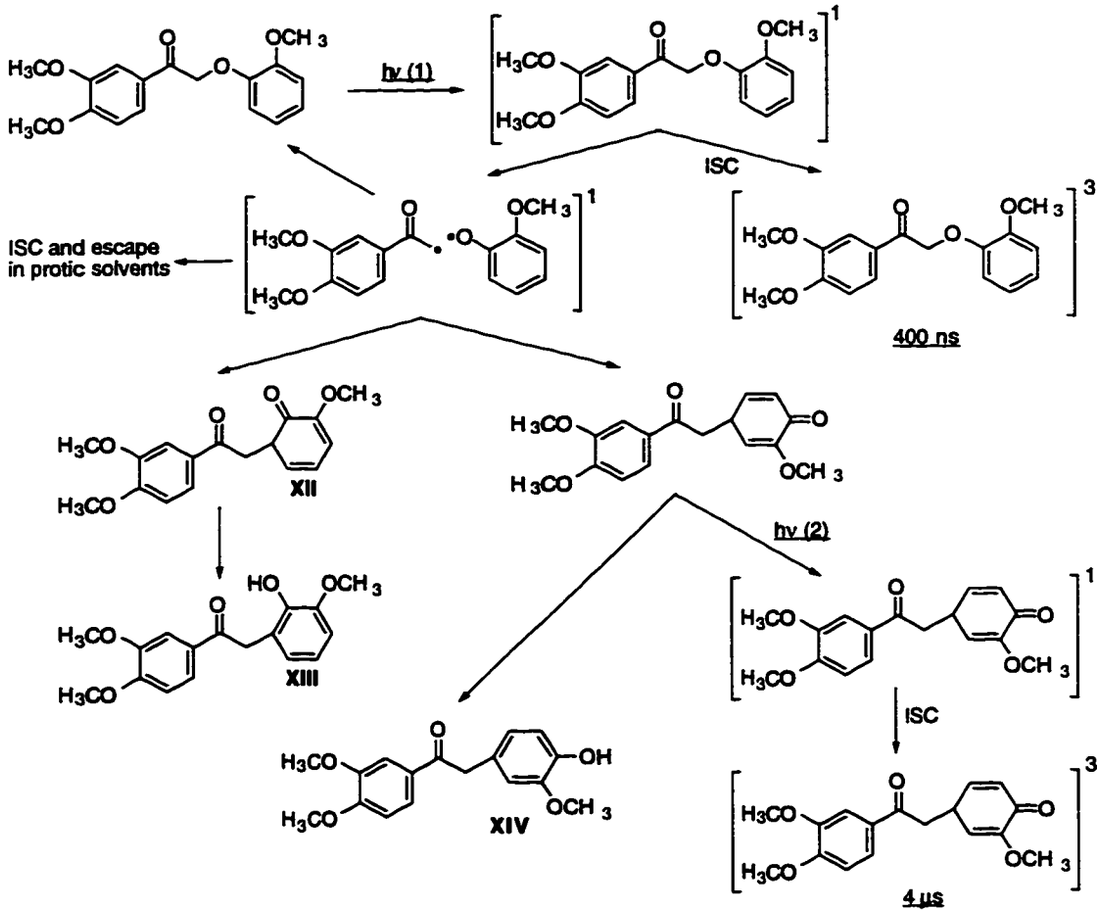

Scheme 2.22 Proposed formation of extra triplet signal at lower laser wavelengths. For simplicity, this scheme shows only the para-coupling product absorbing a second photon, however, the ortho-coupling product could also undergo the analogous reaction.

This proposed mechanism suggests that the *ortho*- and *para*-coupling products which absorb the second photon may not absorb significantly at 337 and 355 nm, which explains why cleaner kinetics are observed at those wavelengths.

In addition, this proposed mechanism is consistent with previously-reported photo-Fries reactions[73-75] and Claisen rearrangements.[76]

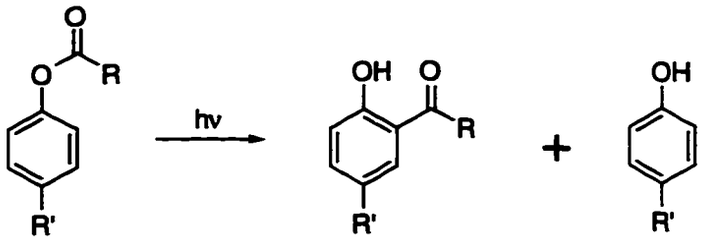

Figure 2.58 Photo-Fries reaction.[74]

Similar to the photodegradation of α-GAV, it was found that the rearrangement products were favoured in aprotic solvents, and the phenol production increased in protic solvents.[74] Rearrangement products are said to be the result of "in-cage" processes, making them less susceptible to usual quenchers like oxygen.

Work by Shizuka and coworkers[77] shows that the *ortho*- and *para*-coupling products resulting from in-cage rearrangements in photo-Fries reactions of phenyl acetate do in fact absorb appreciably in the 270 nm to 330 nm range. The extra aromatic ring and multiple methoxy substitution in α-GAV will only help to increase the extinction coefficients in this range.

2.3.3. Photochemistry of α-(p-methoxyphenoxy)-p-methoxyacetophenone (VII) in solution

Our studies confirm that at least in the case of methoxy substituted systems, such as **VII**, excited state fragmentation (β-cleavage of **VII** to give **VIII** and **IX**) occurs extensively from the singlet state. The same conclusion was recently reported by Palm and coworkers for a series of phenoxyacetophenones (including α-GAV, **VII** and **IV**) employing CIDNP techniques.[27, 28] In the case of **VII** this process is probably assisted by the gain in stability of the *p*-methoxy substituted phenoxy radical, in addition to the effect of methoxy substitution on the benzoyl chromophore. Similar arguments apply to α-GAV which fragments from both singlet and triplet states. In the case of **VII**, quantitative identification of the triplet component is difficult because the short triplet lifetime makes distinction between singlet and triplet processes hard to achieve. However, magnetic field studies in SDS micelles appear to confirm the predominance of singlet processes. Again, in the context of lignin degradation in lignin-rich products, it is hard to see that singlet precursors will be quenched by additives before fragmentation occurs. The radical products from the cleavage of **VII** should however be susceptible to trapping.

Solution studies on **VII** suggest relatively clean transient phenomena, with only two transients formed. Given the short lifetimes of the excited states of **VII** it seems reasonable to assume that the signals are due to free radical products. The *p*-methoxyphenoxy radical can be readily characterized. Firstly, an absorption maximum has been reported in the literature[46] and we have recorded the spectrum in our own pulse radiolysis experiments. Further, we generated it under our laser photolysis conditions by reaction of photogenerated *tert*-butoxy radicals with the corresponding phenol. This led to λ_{max} at 405 nm in acetonitrile.

We were particularly interested in establishing if this radical had a long wavelength band, since these are present in some substituted phenoxy radicals, but seldom reported. In the case of **VIII** we did not observe any long wavelength (> 450 nm) band, suggesting that such a band, if present must be very weak. This is consistent with work done by Johnston and coworkers.[47] This means naturally that the 540 nm absorption must be attributed to another species. This is consistent with the different decay kinetics observed at 410 nm and 540 nm. We attribute the latter to **IX**, along with shorter wavelength absorption that overlap the phenoxy band, as will be discussed later. Interestingly, several radicals of the same family are predicted by the CI/ZINDO calculations to have absorption in that region. A visible absorption band for the benzoylmethyl radical was first reported by Shida and co-workers in a low temperature glass.[78]

2.3.4. The p*-methoxyphenacyl radical (IX)*

The *p*-methoxyphenacyl (**IX**) radical shows interesting results both in its absorption characteristics and in its reactivity. As for the long-wavelength absorption characteristics of **IX**, a comparison here can be drawn to the results of Ingold and coworkers who have reported bands in the visible region for the cumyloxy radical (485 nm) and *p*-methoxycumyloxy radical (590 nm) in acetonitrile solution.[79] One canonical form of the benzoylmethyl radical involves an oxygen centered radical, not too dissimilar to the radicals reported by Ingold.

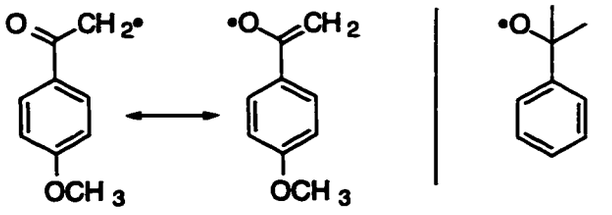

Scheme 2.23 Comparison of canonical forms of IX to the cumyloxy radical.

ESR studies have confirmed the partial C=C double bond character in both the benzoylmethyl radical[80] and related 2-alkanonyl radicals.[81]

Phenacyl radicals have an electron distribution leading to some radical character at the oxygen center, but mostly at the carbon site. This leads to the calculated bond orders of Figure 2.35. The visible absorption band of these radicals is believed to reflect their "oxy" (or n,π^*) characteristic that makes this particular resonance structure similar to that of cumyloxy radicals; as mentioned above, these have been recently shown to have also an absorption band in the visible region.

The spectroscopy and reactivity of phenacyl radicals is consistent with their ESR parameters.[66] Thus, the α-hydrogen coupling constants for $C_6H_5COCH_2\bullet$ are approximately 19.6 gauss, compared with 22.3 gauss for the ethyl radical.

While the presence of unpaired electron density at the oxygen center influences the ESR parameters and absorption spectroscopy of the radicals, their reactivity is clearly a reflection of their carbon-centered properties, as reported by our results and in recent work by Russell and Kulkarui[82, 83] who showed that phenacyl addition to alkenes occurs with C-C bond formation.

2.3.5.Fragmentation of ketyl radicals

The pulse radiolysis results from **VII** show that perhaps the most important observation in relation to lignin processes is that its ketyl radical undergoes the fragmentation reaction very rapidly; in fact the reaction in Scheme 2.5 is even faster than suggested by previous work, with a rate constant in excess of 5×10^7 s^{-1} in the case of **VII** (X = Y = *p*-CH_3O). The implication for lignin photochemistry is that ketyl radicals of this type, if formed, will cleave to produce phenoxy radicals fast, efficiently, and with little probability of scavenging them before cleavage. Thus, if radicals are to be intercepted as a way of preventing yellowing of lignin-rich products, the ketyl radicals should not be the preferred targets for such scavenging.

Although the results of the pulse radiolysis experiments support earlier work done by Scaiano and coworkers,[84] a recent paper from Wayner and coworkers seems contradictory.[85] In this latter publication, the authors show that decomposition of the unsubstituted ketyl radical from **I** (Figure 2.6, page 70; or X=Y=H in Scheme 2.5, page 74), is a much slower process than previously reported and is much slower than the decomposition of **VII** in the pulse radiolysis results. They report an upper limit of the decomposition of the radical from **I** to be only 1 s^{-1}.

The heavy methoxy substitution on **VII** greatly stabilizes the radicals formed, both through resonance and with interaction with the solvent. The pulse radiolysis experiments were carried out in methanol/water mixtures. These factors may contribute to the dramatic differences reported in the rates of cleavage of the ketyl radicals.

2.3.6.Solid state studies

Some of the understanding of the photochemical behaviour of α-GAV and **VII** must be contained in the details of its solid state structure. The fact that no transients were detected in the laser flash photolysis of crystalline samples implies that triplet states and/or free radicals are either not formed in any significant yields, or are remarkably short lived. We note that since solution results show that most of the radicals are formed from the singlet state, a short triplet lifetime would not necessarily explain the failure to detect free radicals.

We thought initially that as all the molecules in the unit cell show a cisoid conformation of the O=C–C–O– moiety, there could be an efficient excited state deactivation pathway through β-aryl quenching, such as occurs in β-phenylpropiophenone or α-phenoxyacetophenone. However, the distance between the carbonyl oxygen and the aromatic ring in the β–position appears to be too long (even at the closest carbon) to permit an effective interaction that would make the triplet state undetectable (see Table 2.5). At the present time the most appealing explanation is simply that the triplet state is not detectable because it is formed very inefficiently or not at all. In other words, intersystem crossing must be very inefficient.

Table 2.5 Selected crystallographic parameters.

	dihedral angles[a]			distances[b] (Å)	
Substrate	A	B	C	D	E
α-GAV(1)	4.4	15.6	76.6	2.712	3.192
α-GAV(2)	-1.5	2.0	-85.7	2.743	3.251
α-GAV(3)	2.9	-0.3	-81.6	2.739	3.202
α-GAV(4)	4.9	12.7	-86.8	2.717	3.165

[a]Dihedral angles: A, C_{CO}-C_1-C_2-C_3; B, 0=C-C-O_{ether}; C, C_{CO}-C-O_{ether}-C_{aryl}. [b]Interatomic distances: D, O=C=CH_2-O; E, C_{CO}-C-O-C_{aryl}.

If the singlet state decays efficiently, at least there is no experimental evidence that such a decay yields free radicals. While it is conceivable that the free radicals from Scheme 2.3 would back-react efficiently to regenerate the starting material, it is surprising that no radicals would survive and that no ortho-ring coupling (which requires very limited motion) would take place. In the latter case we anticipate that the primary product, **XII**, would be readily detectable before its conversion to **XIII**.

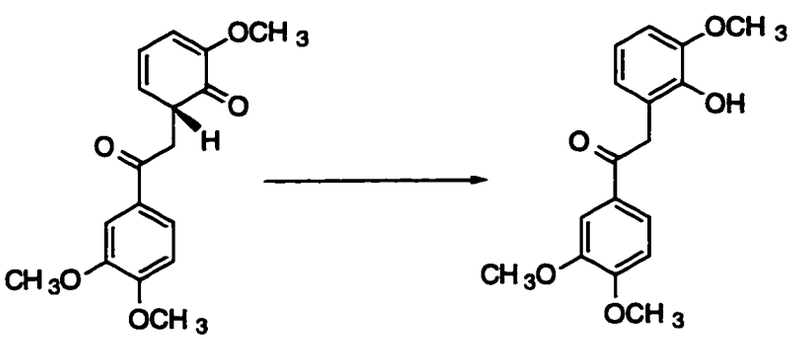

XII **XIII**

Scheme 2.24 Rearrangement of coupling products.

In fact, MM2 calculations for **XII** suggest that its lowest energy conformation is rather similar to that for α-GAV. Comparison of the MM2 optimized ring coupling product with the conformation of molecules of α-GAV based on the X-ray crystallographic data indicate that minimum motion would be required for this rearrangement. While explanations based on short lived transients (triplets and/or free radicals) that decay exclusively and rapidly to yield the starting material would be consistent with our results, the simplest explanation is clearly that such transients are not formed as a result of a competing efficient singlet deactivation.

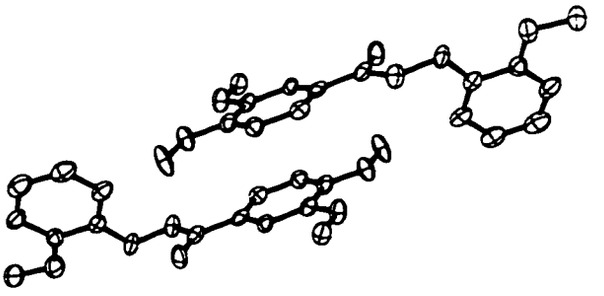

Figure 2.59 Side view of the central pair of α-GAV molecules in the unit cell. See Figure 2.24 for reference.

The crystal packing for α-GAV actually provides a clear indication of a possible singlet deactivation mechanism. The stacking of pairs of molecules, such as the one illustrated at the center of the unit cell in Figure 2.24, are ideally arranged for excimer-like interactions. These rings are perfectly parallel and located at a distance of 3.43 Å. Figure 2.59 shows a side view of this pair of molecules. We believe that the red shifted fluorescence emission of Figure 2.22 is due to this arrangement of chromophores. From the shift in the fluorescence maximum, we estimate the excited state stabilization energy at about 18 kcal/mol. Thus, the pre-formed dimers (or energy migration toward these sites) provide a mechanism for shifted fluorescence, as well as for efficient non-reactive decay from the singlet manifold. The two molecules involved are not perfectly overlapped, but rather somewhat shifted, as shown in Figure 2.59. Interestingly, pyrene crystals show very similar characteristics, with exclusively excimer emission from molecules in dimeric units separated by 3.53 Å.[86, 87] The molecules are partially overlapped, just as in the case of α-GAV, and it is believed that they may tend to move towards improved overlap once excited, even if these motions are resisted by the crystalline environment. Interestingly, these distances are not very different from the characteristic interlayer spacing in graphite (3.35 Å).[88]

Of particular interest in the solid-state NMR spectrum is the carbonyl region where three resonances of 2:1:1 intensity are present. Further, one of the oxygen bearing aromatic carbon atoms also appears as a group of three resonances in a 2:1:1 intensity ratio. Although one must be careful interpreting solid state ^{13}C NMR data quantitatively, the data suggest that the crystal structure contains four molecules in its asymmetric unit. The number of molecules in the unit cell must therefore be a multiple of four. Since in each group of resonances there are two of the same chemical shift one may speculate that two of the molecules in the asymmetric unit have similar conformation; however, similar crystal packing forces may also lead to the same effect. There are no ^{13}C resonances in the enol region indicating that this species is not present to any significant extent.

As indicated above, we assign the signals observed in the laser photolysis of crystalline **VII** to its triplet state. We interpret the second order decay of these signals as resulting from triplet-triplet annihilation following triplet energy migration through the crystal lattice. Further, the spectrum recorded in the crystals is virtually identical to that from triplet *p*-methoxyacetophenone, but significantly different (shifted) from that for radical **VIII**. The alternative interpretation that the signals are due to **VIII** is also inconsistent with several experimental facts: (a) If **VIII** was to decay by recombination with **IX** in a geminate fashion, their decay should follow first order kinetics; (b) If for any reasons the radical centers migrate, it is hard to imagine how they could fail to yield any new products and (c) if **IX** was formed, the absence of the 540 nm band would be surprising. The simplest explanation is that intersystem crossing into the triplet manifold is enhanced in crystalline media, and that the triplet, being in a conformation inadequate for β-aryl quenching lives long enough to be readily detectable.

2.3.7. Conclusions

The reasons underlying the detailed study of α-GAV in this study and in other studies result from its similarity to some of the structural units present in lignin which are believed to be responsible for light-induced yellowing of papers.[9, 10, 12, 13, 89, 90] In general, attempts at stabilizing the colour of these papers have been based on UV screens, excited state quenchers and/or free radical traps.

The results obtained in the α-GAV crystalline work show that α-GAV achieves excellent light stability spontaneously in the solid state by providing an energy sink for the excited singlet states via a preformed dimer that shows excimer emission and leads to little or no chemical change.

It is easy to see that an alternate way of stabilizing the colour of lignin-rich products may involve addition of a molecule capable of forming an excimer or an exciplex in a way similar to that illustrated in Figure 2.59. Clearly it would be preferable to utilize a molecule capable of ground-state association, so that stabilization does not rely on molecular mobility during the short singlet lifetime. It would be impractical to try to achieve this type of association for every aryl-carbonyl chromophore; to the extent that energy migration may take place, only a fraction of the chromophores would need to be stabilized. A further benefit of this approach may be that the blue fluorescence which can be expected through complexation (see Figure 2.22) may in fact improve the appearance of pulp and paper products. Putting these ideas to use will require considerable work in the area of energy migration and of ground- and excited-state complexation of methoxy-substituted benzoyl chromophores.

In the context of lignin photodegradation two of the processes studied in the pulse radiolysis studies are too fast for the species involved to be susceptible for scavenging. Specifically, the photofragmentation of **VII** and the cleavage of ketyl radicals (Scheme 2.5) are too fast to leave much room for effective trapping. Clearly if the discolouration of lignin rich products can be prevented by scavenging reaction intermediates, other long lived species (such as **VIII** and **IX**) will have to be targeted for scavenging.

The preliminary studies carried out with AET as a potential inhibitor for light-induced yellowing of mechanical pulps shows a slight stabilization effect, especially in the case of the unbleached samples. However, most of the effect seems to be due to the initial bleaching action the AET has on the paper samples in the 350 nm region, as can be best seen in Figure 2.44. Bleached TMP samples do not show any spectral features in the 350 nm range since AET would have less of a bleaching action on these samples. However, even the bleached samples show relative stabilization at longer wavelengths (500 nm and above) in the presence of AET, see Figure 2.49, page 125.

2.4.Experimental

2.4.1. Materials and general techniques

The solvents used in the photochemical studies were Omnisolv grade from BDH and used as received. SDS (BDH) was "specially pure" grade and used as received. The quenchers naphthalene (Aldrich), 1-methylnaphthalene (Aldrich, 98%), sorbic acid (Aldrich) and 2,5-dimethyl-2,4-hexadiene (Aldrich, 99%) were used as received. Di-*tert*-butyl peroxide (Aldrich) was passed through an alumina column immediately before use to eliminate traces of hydroperoxide. *p*-Methoxyphenol (Aldrich, 99%) was recrystallized before use. Guaiacol (Aldrich) was used as received. α-Bromo-*p*-methoxyacetophenone **(X)**, was purchased from Lancaster and recrystallized from hexane. 1,1-Diphenylethylene (Aldrich) was used as received.

α-Bromoacetoveratrone was prepared using the procedure of Landucci and coworkers.[91] Bromine was added to a solution of acetoveratrone in carbon tetrachloride under nitrogen. The solution was stirred for 20 minutes until the colour changed from a dark brown to an orange colour, at which point the solution was neutralized with a saturated solution of sodium bicarbonate. The organic phase was separated and dried with magnesium sulfate and recrystallized from methanol.

The ketones α-GAV, **IV**, and **VII** were synthesized by a method previously described by Adler and coworkers[92] by the condensation of the corresponding α-bromoacetophenone and phenol in dry acetone in the presence of base. The most favorable method of preparation involved stirring the phenol in the basic solution for 2 hours, followed by dropwise addition of an acetone solution of the ketone. The mixture was then refluxed until a GC trace showed > 95% conversion to the required

product. Work up involved removal of any excess phenol followed by purification of the ketone by recrystallisation from methanol or ethanol. The samples was >99.8% pure by gas chromatography.

Physical and spectroscopic data for **VII** is reported as follows. The melting point and ^{1}H NMR data recorded was in agreement with data in the literature[28]. **VII**: ^{13}C NMR ($CDCl_3$) δ 193.3 (C=O), 164.0 (-CH_2-O-C-), 154.3 (-$COCH_3$), 152.3 (-$COCH_3$), 130.4, 127.6, 115.9, 114.6, 113.9 (aromatic), 71.5 (-CH_2-), 55.6 (-OCH_3), 55.5 (-OCH_3); MS *m/z* (%) 272 (54.7), 136 (28.5), 135 (100), 121 (21.8), 107 (21.8), 92 (27), 77 (44.7), 28 (21); IR (CH_2Cl_2) 1695 cm^{-1} (ν_{CO}); UV-vis (MeOH, λ_{max} (nm), ε (M^{-1} cm^{-1})) 204 (19 800), 224 (17 100), 282 (17 700).

Steady-state irradiations of samples in solution were carried out in pyrex test tubes, sealed with rubber and parafilm under 350 nm lamps, and were continually rotated in the irradiation chamber to ensure homogeneous light exposure. Solutions were degassed by gently bubbling oxygen-free nitrogen for 10 minutes. Steady-state irradiations of solid samples were performed with 300 nm lamps in 3 mm x 7 mm cells made from Suprasil quartz tubing, and were continually rotated in the irradiation chamber to ensure homogeneous light exposure.

Product studies and quantum yield results were obtained through use of gas chromatography, using a Fisons Instruments GC 8000 series.

Laser dose dependence studies were carried out by using combinations of neutral density filters in the path of the laser beam in order to get a wide range of energies. Laser powers were measured at the sample, using a Molectron model JD2000 joulemeter ratiometer calibrated for 308 nm measurements. Traces were fit using Kaleidagraph software according to Equation 11, page 90.

TMP handsheets were treated by soaking tabs of TMP handsheets in aqueous solutions of the compounds shown in Scheme 2.15 and allowed to dry. Samples were irradiated under 300 nm lamps, with constant rotation to ensure homogeneous light intensity over all samples. Ground-state reflectance spectra were measured using a Varian Cary 1E spectrophotometer equipped with an attachment for solid samples, and corresponding software to run the instrument.

Fluorescence spectra were recorded, using front-face excitation, by a Perkin-Elmer LS-50 spectrofluorimeter equipped with an accessory for solid samples. Fluorescence lifetimes were measured with a PRA single-photon-counting instrument employing a hydrogen-filled lamp with a 1.5 ns pulse duration for excitation.

Laser flash photolysis techniques are be described in the first chapter of this thesis.

2.4.2.NMR Spectra

The ^{13}C CP/MAS NMR data were collected on a Bruker CXP-180 NMR spectrometer equipped with a double tuned Doty MAS probe using a 7 mm zirconia rotor. The duration of the ^{1}H 90° pulse was 3.4 seconds. A 3 ms contact time was used with a 4 second relaxation delay. The spinning rate was 5.6 kHz. 4 k data points were collected for each of the 548 transients using a sweep width of 20 kHz. The free induction decay was zero filled to 16 k points prior to Fourier transformation. No line broadening or resolution enhancement were applied to the data. The chemical shifts in the spectrum were referenced externally to the methyl resonance of solid hexamethylbenzene at 16.9 ppm. Partial assignment of the spectrum was made by acquiring a similar spectrum using the dipolar dephasing technique with a dephasing time of 40 μs. In this spectrum all resonances

due to proton bearing carbons, except those of the methoxy groups, were absent. The ^{13}C NMR spectrum in solution was recorded on a Varian Gemini 200 MHz spectrometer.

GC analysis was carried out on a PE Model 8320 capillary column chromatograph. IR spectra were recorded on a Bomem MB-100 FTIR and UV-vis spectra with a HP-8451A diode array spectrometer. Melting points were determined in a Mel-Temp apparatus and were not corrected.

2.4.3.Pulse Radiolysis

Pulse radiolysis experiments were carried out at the Notre Dame Radiation Laboratory. The solutions were irradiated with 5 ns pulses from an ARCO LP-7 linear accelerator. Computer control of the equipment has been described elsewhere.[46] Digitization of the transient signals was usually with a Biomation 8100. A Biomation 6500 was used for experiments below 1 ms full scale. Dosimetry experiments were carried out as previously reported.[93]

Solutions of ketones **VII**, **IV** and α-GAV in 70:30 methanol:water (containing 5-10 mM phosphate buffer) were flowed through the 10 mm pathlength irradiation cell under nitrogen. Solutions were prepared with water from a Millipore Milli-Q system and pH adjusted with reagent grade $HClO_4$. The spectrum of the *p*-methoxyphenoxy radical was recorded upon oxidation of *p*-methoxyphenoxide in basic aqueous solution by N_3 radicals.[46]

2.4.4.Molecular Modeling

Molecular modeling calculations were performed with the semi-empirical PM3 method implemented using the MOPAC package (Version 6.0) on a

Tektronix CAChe system run on a Macintosh IIvx. Geometries were optimized with the BFGS method as default.

Electronic absorption spectra were calculated at the ROHF level with the ZINDO package on the same system. The calculation was run with a configuration interaction setting of 9 and INDO/1 parameterization of the Hamiltonian.

Modeling calculations for the bond orders of the phenacyl radical were carried out on the same system, using the AM1 UHF semiempirical method, as part of the MOPAC program version 6.1.

2.4.5.X-ray crystallograpy of α-GAV

Data collection

A crystal of $O_5C_{17}H_{18}$ having approximate dimensions of 0.2, 0.2, 0.2 m m was mounted on a glass capillary. All the measurements were made on a Rigaku diffractometer with Mo Kα radiation. Crystal data are given in Table 2.6.

Cell constants and an orientation matrix for data collection, were obtained from least-squares refinements using the setting angles of 25 reflections in the range $40<2\Theta<45$ corresponded to a triclinic cell with dimensions: a = 17.314 (5); b = 25.127 (7); c = 7.251 (2); α = 90.73 (3); β = 93.55 (3); γ = 109.309 (23). For Z = 8 and FW = 302.32, the calculated density is 1.352 g/cm^3. Based on the systematic absences, the space group was determined to be P1. The data was collected at a temperature of -130 degrees using the omega-2Θ scan technique to a maximum 2Θ value of 45.

Data Reduction

A total of 7776 reflections was collected. The unique set contains only 7454 reflections. The standards were measured after every 150 reflections. No crystal decay was noticed. The data were collected for Lorentz and polarisation effects.[25] No absorption correction was made.

Solution and refinement

The structure was solved by direct methods. All the atoms were refined anisotropically except the hydrogen. The hydrogen atoms were calculated, assuming a distance C-H of 1.04Å. All the phenyl groups were refined as rigid groups to improve the ratio of reflections/parameters.

The final cycle of full matrix least-squares refinement was based on 5632 observed reflections ($I>2.5\ \sigma(I)$) and 698 variable parameters. Weights based on counting statistics were used. The maximum and minimum peaks on the final differences Fourier map corresponded to 0.340 and -0.310 e/a^3, respectively. All the calculations were performed using the NRCVAX crystallographic software package.[94]

2.4.6.X-ray crystallography of VII

Data collection:

A crystal of $O_4C_{16}H_{16}$ having approximate dimensions of 0.2 x 0.08 x 0.25 mm was mounted on a glass capillary. All the measurements were made on a Rigaku diffractometer with Mo Kα radiation. Crystal data are given in Table 2.6.

Cell constants and an orientation matrix for data collection were obtained from least-squares refinement using the setting angles of 25 reflections in the range $40° < 2\theta < 45°$; these corresponded to a monoclinic cell with

dimensions a = 10.683(2), b=9.268(3), c=13.534(3) Å, β=90.277(17)°. For z=4 and FW=272.20, the calculated density is 1.350 g/cm^3. On the basis of the systematic absences, the space group was determined to be P 21/c. The data were collected at -110°C using the ω-2θ scan technique to a maximum 2θ value of 46.9.

Data reduction:

A total of 2093 reflections were collected. The unique set contains only 1974 reflections. The standards were measured after every 150 reflections. No crystal decay was noticed. The data were corrected for Lorentz and polarisation effects.[95] No absorption correction was made.

Solution and refinement:

The structure was solved by direct methods. All the atoms were refined anisotropically except the hydrogen. The hydrogen atoms were found by differences Fourier map. The final cycle of full matrix least-squares refinement was based on 1469 observed reflections ($I > 2.5\ \sigma(I)$) and 246 variable parameters. Weights based on counting statistics were used. The maximum and minimum peaks on the final differences Fourier map corresponded to 0.220 and -0.230 e/a^3, respectively. All the calculations were performed using the NRCVAX crystallographic software package.[94]

Table 2.6 Crystal Data for α-GAV and VII

	α-GAV	VII
Empirical formula	$O_5C_{17}H_{18}$	$O_4C_{16}H_{16}$
Formula weight	302.32	272.20
Crystal shape	cube	needle
Crystal dimensions (mm)	0.2, 0.2, 0.2	0.2, 0.08, 0.25
Crystal system	triclinic	monoclinic
No. Reflection used for unit	25	25
Cell dimension (2Θ range)	40-45	40-47
Lattice parameters		
a, Å	17.314 (5)	10.683 (2)
b, Å	25.127 (7)	9.268 (3)
c, Å	7.251 (2)	13.534 (3)
α, deg	90.73 (3)	
β, deg	93.55 (3)	90.277 (17)
γ, deg	109.31 (23)	
Space group	P1	P21/c
Z value	8	4
Dcalc ($g.cm^{-3}$)	1.352	1.350
F (000)	1280.59	576.26
μ (mm^{-1})	0.05	0.09
No of reflections measured	7776	2093
No of reflections unique	7454	1974
No of reflections observed	5632	1469
No of atoms	160	36
No of variables	698	246
R_f (sign refl)	0.067	0.053
R_w (sign refl)	0.043	0.033
R_f (all refl)	0.096	0.079
R_w (all refl)	0.044	0.034
Goodness of fit	5.72	4.70
Last difference fourier map		
max peak	0.340	0.220
min peak	-0.310	-0.230

2.5.References

[1] E. Sjöström, *Wood Chemistry*. New York: Academic Press, **1981**.

[2] I. H. Isenberg, *Fibrous Raw Materials and Wood Structure*, vol. 1, 1 ed. New York: McGraw-Hill Book Company, **1962**.

[3] K. Freudenberg, "Lignin: Its Constitution and Formation from *p*-Hydroxycinnamyl Alcohols," *Science*, **148** (30 April) , 595, **1965**.

[4] B. Jordan and M. O'Neill, "The Case for Switching to CIE L*a*b* Color Description for Paper," *Pulp & Paper Canada*, **88** (10) , T382, **1987**.

[5] A. Castellan, H. Choudhury, R. S. Davidson, and S. Grelier, "Comparative Study of Stone-Ground Wood Pulp and Native Wood 3. Application of Fluorescence Spectroscopy to a Study of the Weathering of Stone-Ground Pulp and Native Wood," *J. Photochem. Photobiol. A: Chem.*, **81** (2) , 123, **1994**.

[6] C. Vanucci, P. Fornier de Violet, H. Bouas-Laurent, and A. Castellan, "Photodegradation of Lignin: A Photophysical and Photochemical Study of a Non-Phenolic α-Carbonyl β-O-4 Lignin Model Dimer, 3,4-Dimethoxy-α-(2'-methoxyphenoxy)acetophenone," *J. Photochem. Photobiol. A: Chem.*, **41** , 251, **1988**.

[7] J.-M. Rodier and A. Myers, "*cis*-Stilbene Photochemistry: Solvent Dependence of the Initial Dynamics and Quantum Yields," *J. Am. Chem. Soc.*, **115** (23) , 10791, **1993**.

[8] W. Eberbach and J. Hensle, "The Photorearrangement of o-Vinyl Diaryl Ethers into o-Hydroxy Stilbenes Evidence Against Dipolar Intermediates," *Tetrahedron Lett.*, **34** (30) , 4777, **1993**.

[9] G. J. Leary, "The Yellowing of Wood by Light: Part II," *Tappi*, **51** (6) , 257, **1968.**

[10] J. Grier and S. Y. Lin, "Photodegradation of Lignin: A Contribution to the Mechanism of Chromophore Formation," *Svensk Papperstidning*, **75** (7) , 233, **1972.**

[11] K. P. Kringstad and S. Y. Lin, "Mechanism in the Yellowing of High-Yield Pulps by Light: Structure and Reactivity of Free Radical Intermediates in the Photodegradation of Lignin," *Tappi*, **53** (12) , 2296, **1970.**

[12] A. Castellan, N. Colombo, C. Vanucci, P. Fornier de Violet, and H. Bouas-Laurent, "A Photochemical Study of an o-Methylated α-Carbonyl β-1 Lignin Model Dimer: 1,2-Di(3',4'-Dimethoxyphenyl)ethanone (Deoxyveratroin)," *J. Photochem. Photobiol. A: Chem.*, **51** , 451, **1990.**

[13] A. Castellan, J. H. Zhu, N. Colombo, A. Nourmamode, R. S. Davidson, and L. Dunn, "An Approach to Understanding the Mechanism of Protection of Bleached High-Yield Pulps Against Photoyellowing by Reducing Agents Using the Lignin Model Dimer: 3,4-Dimethoxy-a-(2'-methoxyphenoxy)-acetophenone," *J. Photochem. Photobiol. A: Chem.*, **58** , 263, **1991.**

[14] J. C. Netto-Ferreira, W. J. Leigh, and J. C. Scaiano, "Laser Flash Photolysis Study of the Photochemistry of Ring-Substituted β-Phenylpropiophenones," *J. Am. Chem. Soc.*, **107** , 2617, **1985.**

[15] R. Boch, C. Bohne, J. C. Netto-Ferreira, and J. C. Scaiano, "Effect of Methyl Substitution on the Photochemistry of *p*-Methoxy-β-phenylpropiophenone," *Can. J. Chem.*, **69** , 2053, **1991.**

[16] P. J. Wagner, P. A. Kelso, A. E. Kemppainen, A. Haug, and D. R. Graber, "Deactivation of Ketone Triplets by β-Phenyl Substitution," *Mol. Photochem.*, **2** (1) , 81, **1970.**

[17] M. V. Encina, E. A. Lissi, E. Lemp, A. Zanocco, and J. C. Scaiano, "Temperature Dependence of the Photochemistry of Aryl Alkyl Ketones," *J. Am. Chem. Soc.*, **105** , 1856, **1983.**

[18] J. C. Netto-Ferreira, I. G. J. Avellar, and J. C. Scaiano, "Effect of Ring Substitution on the Photochemistry of α-(Aryloxy)acetophenones," *J. Org. Chem.*, **55** , 89, **1990.**

[19] P. K. Das, M. V. Encinas, and J. C. Scaiano, "Laser Flash Photolysis of the Reactions of Carbonyl Triplets with Phenols and Photochemistry of *p*-Hydroxypropiophenone," *J. Am. Chem. Soc.*, **103** (14) , 4154, **1981.**

[20] C. Walling and P. J. Wagner, "Halogen Compounds. X. Solvent Effects on the Reactions of t-Butoxy Radicals," *J. Am. Chem. Soc.*, **86** , 3368, **1964.**

[21] P. J. Wagner and T. Nakahira, "Photochemistry of 1-Benzoyl-4-p-anisoylbutane. Reaction from Equilibrating Upper Triplets," *J. Am. Chem. Soc.*, **95** (25) , 8474, **1973.**

[22] J. C. Scaiano, "Review Paper: Intermolecular Photoreduction of Ketones," *J. Photochem.*, **2** , 81, **1973.**

[23] I. Carmichael and G. L. Hug, "Spectroscopy and Intramolecular Photophysics of Triplet States," in *Handbook of Organic Photochemistry*, vol. I, J. C. Scaiano, Ed. Boca Raton, Florida: CRC Press, **1989**, pp. 369.

[24] J. A. Schmidt, A. B. Berinstain, F. De Rege, C. Heitner, L. J. Johnston, and J. C. Scaiano, "Photodegradation of the Lignin Model α-

Guaiacoxyacetoveratrone, Unusual Effects of Solvent, Oxygen, and Singlet State Participation," *Can. J. Chem.*, **69** , 104, **1991.**

[25] J. C. Scaiano, C. Chen, and P. F. McGarry, "A Flash Photolysis and Optoacoustic Calorimetry Study of the cis-trans Isomerization of 1,2-diphenyltriazine," *J. Photochem. Photobiol. A: Chem*, **62** , 75, **1991.**

[26] N. J. Turro, *Modern Molecular Photochemistry*. Menlo Park: Benjamin/Cummings Publishing Co., **1978.**

[27] W. U. Palm and H. Dreeskamp, "Evidence for Singlet State β Cleavage in the Photoreaction of α-(2,6-Dimethoxyphenoxy)-acetophenone Inferred from the Time-resolved CIDNP Spectroscopy," *J. Photochem. Photobiol. A: Chem.*, **52** , 439, **1990.**

[28] W.-U. Palm, H. Dreeskamp, H. Bouas-Laurent, and A. Castellan, "The Photochemistry of α-Phenoxyacetophenones Investigated by Flash-CIDNP-spectroscopy," *Ber. Bunsenges. Phys. Chem.*, **96** (1) , 50, **1992.**

[29] D. S. Argyropoulos, C. Heitner, and F. G. Morin, "^{31}P NMR Spectroscopy in Wood Chemistry. Part III. Solid State ^{31}P NMR of Trimethyl Phosphite Derivative of Chromophores in Mechanical Pulp," , **46** , 211, **1992.**

[30] D. S. Argyropoulos, C. Heitner, and J. A. Schmidt, "Observation of Quinonoid Groups During the Light-Induced Yellowing of Softwood Mechanical Pulp," Pulp and Paper Research Institute of Canada PGRL-565, February **1994.**

[31] K. G. Kónya and J. C. Scaiano, "Development of Applications of Pyrene-Containing Fluorescent Probes for Monitoring the

Photodegradation of Lignin-Rich Products," *Chem. Mater.*, **6** (12) , 2369, **1994.**

[32] J. H. Zhu and D. G. Gray, "Fluorescence Emission from Mechanical Pulp Sheets II. Estimation of Quantum Yields," *J. Photochem. Photobiol. A: Chem.*, **73** , 67, **1993.**

[33] J. A. Olmstead and D. G. Gray, "Fluorescence Emission from Mechanical Pulp Sheets," *J. Photochem. Photobiol. A: Chem.*, **73** , 59, **1993.**

[34] J. A. Olmstead, J. H. Zhu, and D. G. Gray, "Fluorescence Spectroscopy of Mechanical Pulps III: Effect of Chlorite Delignification," *Can. J. Chem.*, **73** (11) , 1955, **1995.**

[35] J. H. Zhu and D. G. Gray, "Photoyellowing of Lignin-Rich Paper: Interaction of Excited States with Selected Additives," *J. Photochem. Photobiol. A: Chem.*, **87** , 267, **1995.**

[36] A. Castellan and R. S. Davidson, "Steady-State and Dynamic Fluorescence Emission from Abies Wood," *J. Photochem. Photobiol. A: Chem.*, **78** (3) , 275, **1994.**

[37] A. Castellan, H. Choudhury, R. S. Davidson, and S. Grelier, "Comparative Study of Stone-Ground Wood Pulp and Native Wood 2. Comparison of the Fluorescence of Stone-Ground Wood Pulp and Native Wood," *J. Photochem. Photobiol. A: Chem.*, **81** (2) , 117, **1994.**

[38] J. K. S. Wan, M. Y. Tse, and C. Heitner, "An ESR and Time-Resolved CIDEP Study of the Light-Induced Yellowing Processes of TMP Paper," *J. Wood Chem. Tech.*, **13** (3) , 327, **1993.**

[39] P. Fornier de Violet, A. Nourmamode, N. Colombo, J. Zhu, and A. Castellan, "Photochemical Brightness Reversion of Peroxide Bleached

Mechanical Pulps in the Presence of Various Additives," *Cellulose Chem. Technol.*, **24** , 225, **1990**.

[40] G. W. Kutney, "The Bleaching Action of Thiols on Mechanical Pulps," *J. Pulp Paper Sci.*, **12** (4) , J129, **1986**.

[41] B. J. W. Cole and K. V. Sarkanen, "Bleaching and Brightness Stabilization of High-Yield Pulps by Sulfur-Containing Compounds," *Tappi Journal* (November) , 117, **1987**.

[42] J. C. Scaiano, W. L. Leigh, M. A. Meador, and P. J. Wagner, "Sterically Hindered Triplet Energy Transfer," *J. Am. Chem. Soc.*, **107** , 5806, **1985**.

[43] P. J. Wagner and I. Kochevar, "How Efficient is Diffusion-Controlled Triplet Energy Transfer?," *J. Am. Chem. Soc.*, **90** , 2232, **1968**.

[44] E. Lissi, "Photolysis of Di-tert-butyl Peroxide in Solution," *Can. J. Chem.*, **52** , 2491, **1974**.

[45] T. J. Burkey, M. Majewski, and D. Griller, "Heats of Formation of Radicals and Molecules by a Photoacoustic Technique," *J. Am. Chem. Soc.*, **108** , 2218, **1986**.

[46] Z. B. Alfassi and R. H. Schuler, "Reaction of Azide Radicals with Aromatic Compounds. Azide as Selective Oxidant," *J. Phys. Chem.*, **89** (15) , 3359, **1985**.

[47] L. J. Johnston, N. Mathivanan, F. Negri, W. Siebrand, and F. Zerbetto, "Assignment and Vibrational Analysis of the 600 nm absorption Band in the Phenoxyl Radical and some of its Derivatives," *Can. J. Chem.*, **71** , 1655, **1993**.

[48] J. P. Fouassier and D. Burr, "Triplet-State Reactivity of α-Sulfonyloxy Ketones Used as Polymerization Initiators," *Macromolecules*, **23** , 3615, **1990**.

[49] I. Carmichael and G. L. Hug, "Triplet-Triplet Absorption Spectra of Organic Molecules in Condensed Phases," *J. Phys. Chem. Ref. Data*, **15** (1) , 1, **1986**.

[50] R. Korus and K. F. O'Driscoll, "Polymer Handbook," in *Polymer Handbook*, J. Brandrup, E. H. Immergut, and W. McDowell, Eds., 2nd ed. New York: Wiley Interscience, **1975**, pp. II.

[51] M. Tsunooka, S. Tanaka, and M. Tanaka, "Photocrosslinking of Poly(2,3-epoxypropyl methacrylate) Films with Organic Sulfur Compounds," *Makromol. Chem., Rapid Commun.*, **4** , 539, **1983**.

[52] E. A. Lissi and M. V. Encinas, "Representative Kinetic Behavior of Selected Reaction Intermediates: Triplet States," in *Handbook of Organic Photochemistry*, vol. II, J. C. Scaiano, Ed. Boca Raton, Florida: CRC Press, **1989**, pp. 111.

[53] R. V. Bensasson, E. J. Land, and T. G. Truscott, *Flash Photolysis and Pulse Radiolysis*: Pergamon Press, **1983**.

[54] A. B. Ross, W. G. Mallard, W. P. Helman, B. H. J. Bielski, G. V. Buxton, D. A. Cabelli, C. L. Greenstock, R. E. Huie, and P. Neta, *NDRL/NIST Solution Kinetics Database: Ver. 1*, 1.0 ed. Gaithersburg: NIST, U.S. Department of Commerce, **1992**.

[55] R. Boch, M. K. Whittlesey, and J. C. Scaiano, "Laser-induced Photoionization of Aromatic Ketones in Anionic Micellar Solution," *J. Phys. Chem.*, **98** (32) , 7854, **1994**.

[56] J. C. Scaiano, E. B. Abuin, and L. C. Stewart, "Photochemistry of Benzophenone in Micelles. Formation and Decay of Radical Pairs," *J. Am. Chem. Soc.*, **104** (21) , 5673, **1982.**

[57] C. Evans, K. U. Ingold, and J. C. Scaiano, "Magnetic Field Effects on the Decay of Ketyl-Aryloxy Radical Pairs in Micellar Solution," *J. Phys. Chem.*, **92** , 1257, **1988.**

[58] I. R. Gould, M. B. Zimmt, N. J. Turro, B. H. Baretz, and G. F. Lehr, "Dynamics of Radical Pair Reactions in Micelles," *J. Am. Chem. Soc.*, **107** , 4607, **1985.**

[59] F. L. Cozens and J. C. Scaiano, "A Comparative Study of Magnetic Field Effects on the Dynamics of Geminate and Random Radical Pair Processes in Micelles," *J. Am. Chem. Soc.*, **115** , 5204, **1993.**

[60] J. C. Scaiano, H. L. Casal, and J. C. Netto-Ferreira, "Intrazeolite Photochemistry. III. Use of β-Phenylpropiophenone and its Derivatives as Probes for Cavity Dimensions and Mobility," *ACS Symp. Ser.*, **278** , 211, **1985.**

[61] B. Maillard, K. U. Ingold, and J. C. Scaiano, "Rate Constants for the Reactions of Free Radicals with Oxygen in Solution," *J. Am. Chem. Soc.*, **105** (15) , 5095, **1983.**

[62] J. Chateauneuf, J. Lusztyk, and K. U. Ingold, "Absolute Rate Constants for the Reactions of some Carbon Centered Radicals with 2,2,6,6-Tetramethylpiperidine-N-oxyl," *J. Org. Chem.*, **53** , 1629, **1988.**

[63] A. Bromberg, K. H. Schmidt, and D. Meisel, "Photophysics and Photochemistry of Arylmethyl Radicals in Liquids," *J. Am. Chem. Soc.*, **107**, 83, **1985.**

[64] J. J. P. Stewart, "Optimization of Parameters for Semiempirical Methods I. Method," *J. Comput. Chem.*, **10** (2) , 209, **1989**.

[65] J. J. P. Stewart, "Optimization of Parameters for Semiempirical Methods II. Applications," *J. Comput. Chem.*, **10** (2) , 221, **1989**.

[66] G. Brunton, H. C. McBay, and K. U. Ingold, "Kinetic Applications of Electron Paramagnetic Resonance Spectroscopy. 30. Rearrangement of the Benzoylmethyl Radical," *J. Am. Chem. Soc.*, **77** (13) , 4447, **1977**.

[67] J. A. Schmidt, E. Goldszmidt, C. Heitner, J. C. Scaiano, A. B. Berinstain, and L. J. Johnston, "Photodegradation of α-Guaiacoxyacetoveratrone: Triplet-State Reactivity Induced by Protic Solvents," in *ACS Symposium Series: Photochemistry of Lignoncellulosic Materials*, vol. 531, C. Heitner and J. C. Scaiano, Eds. Washington, D. C.: American Chemical Society, **1993**, pp. 122.

[68] J. Renaud and J. C. Scaiano, "Hydrogen vs. Electron Transfer Mechanisms in the Chain Decomposition of Phenacyl Bromides. Use of Isotopic Labeling as a Mechanistic Probe," *Can. J. Chem.*, **74** , 1724, **1996**.

[69] J. Renaud and J. C. Scaiano, "Chain Mechanisms for the Dehydrobromination of Ring Substituted α-Bromoacetophenones in Alcohols," *Res. Chem. Intermed.*, **3-5** , 457, **1995**.

[70] J. K. S. Wan, M. Y. Tse, and M. C. Depew, "CIDEP Studies of the Photolysis of the Lignin Model Compound α-Guaiacoxyacetoveratrone: The Role of Triplet Reactions in Aqueous and Hydroxylic Solvents," *Res. Chem. Int.*, **17** , 59, **1992**.

[71] V. W. Bowry and R. Stocker, "Tocopherol-Mediated Peroxidation. The Prooxidant Effect of Vitamin E on the Radical-Initiated Oxidation of Human Low-Density Lipoprotein," *J. Am. Chem. Soc.*, **115** , 6029, **1993.**

[72] L. Hurrell, L. J. Johnston, N. Mathivanan, and D. Vong, "Photochemistry of Lignin Model Compounds on Solid Supports," *Can. J. Chem.*, **71** , 1340, **1993.**

[73] D. A. Plank, "The Photo-Fries Reaction of Aryl Esters: Effect of Solvent on Product Distribution," *Tet. Lett.*, **52** , 5423, **1968.**

[74] M. R. Sandner and D. J. Trecker, "On the Mechanism of the Photo-Fries Reaction," *J. Am. Chem. Soc.*, **89** (22) , 5725, **1967.**

[75] R. A. Finnegan and D. Knutson, "Photochemical Studies, VII. Solvent Effects on the Photolysis of Aryl Esters: Fries Rearrangement vs. Decarboxylation," *Tet. Lett.*, **30** , 3429, **1968.**

[76] Y. Ogata, K. Takagi, and I. Ishino, "Photochemical Rearrangement of Diaryl Ethers," *Tetrahedron*, **26** , 2703, **1970.**

[77] T. Arai, S. Tobita, and H. Shizuka, "Tunnelling Effects on the 1,3- and 1,5-Sigmatropic Hydrogen Shifts in the Ground State of Photo-Fries Rearranged Intermediates of Phenyl Acetate Studied by Laser Flash Photolysis," *J. Am. Chem. Soc.*, **117** (14) , 3968, **1995.**

[78] T. Shida, S. Iwata, and M. Imamura, "Electronic Absorption Spectra of Ion Radicals and Their Molecular Orbital Interpretation. IV. Anion Radicals of Aromatic and Unsaturated Aliphatic Carbonyl Compounds," *J. Phys. Chem.*, **78** (7) , 741, **1974.**

[79] D. V. Avila, J. Lusztyk, and K. U. Ingold, "Color Benzyloxyl, Cumyloxyl Orange, and 4-Methoxycumyloxyl Blue. Unexpected Discovery

that Arylcarbinyloxyl Radicals Have Strong Absorptions in the Visible," *J. Am. Chem. Soc.*, **114** (16) , 6576, **1992.**

[80] J. Bargon, F. Graf, W. Lau, and A. C. Ling, "Cross Conjugated Free Radicals. 1. An ESR and CNDO/INDO Study of the Geometry and Electronic Structure of Substituted Benzoylmethyl Radicals," *J. Phys. Chem.*, **83** , 269 , **1979.**

[81] D. M. Camaioni, H. F. Walter, J. E. Jordan, and D. W. Pratt, "ESR studies of 2-alkanonyl radicals," *J. Am. Chem. Soc.*, **95** , 7978, **1973.**

[82] G. A. Russell and S. V. Kulkarni, "Three-Component Radical Condensations Involving Benzoylmethyl Radicals, Alkenes, and Diphenyl Disulfide," *J. Org. Chem.*, **58** , 2678, **1993.**

[83] G. A. Russell, S. V. Kulkarni, and R. K. Khanna, "Radical and Ionic Reactions of (Benzoylmethyl)mercurials," *J. Org. Chem.*, **55** , 1080, **1990.**

[84] J. C. Scaiano, J. C. Netto-Ferreira, and V. Wintgens, "Fragmentation of Ketyl Radicals Derived from α-Phenoxyacetophenone: an Important Mode of Decay for Lignin-Related Radicals?," *J. Photochem. Photobiol. A: Chem.*, **59** , 265, **1991.**

[85] Y. Huang, D. Pagé, D. D. M. Wayner, and P. Mulder, "Radical-Induced Degradation of a Lignin Model Compound. Decomposition of 1-Phenyl-2-Phenoxyethanol," *Can. J. Chem.*, **73** (11) , 2079, **1995.**

[86] J. M. Robertson and J. G. White, "The Crystal Structure of Pyrene. A Quantitative X-ray Investigation," *J. Chem. Soc.* , 358, **1947.**

[87] A. Camerman and J. Trotter, "The Crystal and Molecular Structure of Pyrene," *Acta. Cryst.*, **18** , 636, **1965.**

[88] J. C. Kotz and K. F. Purcell, *Chemistry and Chemical Reactivity*, Second ed. Philadelphia: Saunders College Publ., **1990**.

[89] S. Y. Lin and K. P. Kringstad, "Photosensitive Groups in Lignin and Lignin Model Compounds," *Tappi*, **53** (4) , 658, **1970**.

[90] L. V. Forman, *Paper Trade J.*, **111** , 34, **1940**.

[91] L. L. Landucci, S. A. Geddes, and T. K. Kirk, "Synthesis of ^{14}C Labeled 3-Methoxy-4-Hydroxy-α-(2-Methoxy-phenoxy)- β-Hydroxypropiophenone, a Lignin Model Compound," *Holzforschung*, **35** , 66, **1981**.

[92] E. Adler, B. O. Lindgren, and U. Saedén, "The Beta-Guaiacyl Ether of Alpha-Veratryl-glycerol as a Lignin Model," *Svensk Papperstidning*, **55** (7) , 245, **1952**.

[93] L. K. Patterson and J. Lilie, "Pulse Radiolysis: Control of the NDRL system," *Int. J. Radiat. Phys. Chem.*, **6** , 129, **1974**.

[94] E. J. Gabe, F. L. Lee, and Y. Lepage, *J. Appl. Crystallogr.*, **22** , 384, **1989**.

[95] D. F. Grant and E. J. Gabe, "The Analysis of Single-Crystal Bragg Reflections from Profile Measurements," *J. Appl. Crystallogr.*, **11** , 114, **1978**.

3.Photochemical Probes in Biologically-Relevant Environments

3.1.Introduction

Nanosecond laser flash photolysis (LFP) is a powerful technique, giving the experimenter tremendous insight into the identity and behaviour of reaction intermediates involved in photo-induced reactions. The project described in this chapter explores the application of nanosecond laser flash photolysis techniques in biologically-relevant environments. We will describe the use of photoactive compounds as probes to characterize these environments and to study the photophysics and photochemistry of some of these probes under these conditions.

From our point of view, the most significant difference between a biological environment and a traditional solution-phase environment is that of restricted mobility. The most widely-studied simulated restricted mobility environment at room temperature is that created by detergent micelles.[1] Micelles offer great flexibility in that, depending on the micelle monomer molecule chosen, the micelle can take on different characteristics in size, reactivity, and ionic charge, and they are well characterized. In addition to these advantages, a micellar solution is most

often optically transparent at the wavelengths of interest, and the solutions are not turbid. This makes study by LFP techniques convenient.

Approaching the cellular environment even more are synthetic surfactant vesicles, formed from amphiphiles that form a bilayer in which the charged head groups are exposed to the internal entrapped water core and to the outer water phase.[2] Barra and coworkers[2] showed that the photodecomposition of 1,1,3,3-tetraphenylacetone and 1,1-diphenylacetone can be monitored in dioctadecyldimethylammonium chloride (DODAC) vesicles. In this study, they generated vesicles of two sizes; they produced 300 Å vesicles by sonication and 5000 Å vesicles by an injection method. The solutions of smaller vesicles were optically transparent but the larger vesicles were turbid suspensions and the traditional transmission-detection LFP techniques could not be used, due to the high light scattering of the suspensions. During the past 15 years, Wilkinson's group have pioneered the use of time-resolved diffuse reflectance detection laser flash photolysis in the study of transient phenomena in opaque systems.[3, 4] Barra and coworkers successfully used diffuse reflectance detection methods to study the turbid vesicle suspensions. In this study, they were able to study the magnetic field effects on the recombination of triplet radical pairs. Fox and coworkers have used diffuse reflectance LFP to study processes in TiO_2 suspensions.[5, 6]

The goals defined early in this project were to attempt to extend the work done by Barra and coworkers (also from the Scaiano group at the University of Ottawa) to the cellular environment. The present debate on the question of whether or not environmental magnetic fields are linked to health problems such as cancer has not produced any strong support for either side of the argument.[7-9] Knowing that magnetic fields do have an effect on the recombination of radical pairs in organized systems,[2, 10-12] it is

clear that the study of free radicals in biologically-relevant environments is of scientific importance.

In addition to studying free radical reactions in cells, recent advances in cancer treatment have developed the use of photoactive drugs, mostly from the porphyrin family of compounds, to treat localized tumours by photodynamic therapy.[13] Being able to study the reaction intermediates involved in this process in the cellular environment could lead to a better understanding of the mechanism of action of these drugs.

The goals defined, however, were very ambitious, as we quickly discovered when we approached the problem. Two main obstacles were encountered: incorporation of the photoactive compounds to be studied into the cellular environment and the optical characteristics of the cellular environment itself.

The first of these obstacles, incorporation, was the most challenging to deal with. Compounds such as tetraphenylacetone, which would be an excellent probe to use and could be a direct extension of the work started by Barra and coworkers, are not soluble in water and delivery into the cells was not straightforward. Biologists and biochemists have, of course, developed methods of incorporating foreign materials into cells, however many of the techniques are extremely sensitive, and, in most cases very little incorporation is necessary to detect an end point such as a genetic mutation. From a biological point of view, our method of detection, measuring optical absorbance changes following initial light absorption, is rather insensitive and requires relatively high amounts of probe molecules to be delivered to the cells. Since development of methods for incorporation of probes into the cellular environment was such a major part of the work carried out in this project, and many lessons were learned

from the experience, a major section of this chapter is dedicated to this subject alone.

The second major challenge, dealing with the optical characteristics of the cell suspensions, resulted in a greatly reduced number of candidates for photoactive compounds that could be used as probes. The cellular environment itself absorbs most light below 325 nm.

Even if we were able to incorporate tetraphenylacetone into the cells, the laser light used to excite the precursor would be predominantly absorbed by the cells themselves, preventing any probe photochemistry from occurring, due to the high absorption by the substrate. For this reason, all probes used in this project must absorb at longer wavelengths than 325 nm. In addition, LFP techniques rely on detection of light (by transmission or reflectance) at the monitoring wavelength. Since the cellular environment absorbs most light below 325 nm, any transients absorbing below these wavelengths are extremely difficult to monitor by our detection methods.

Bacteria can be divided into two broad classes - Gram-positive and Gram-negative - on the basis of their differential abilities to retain a crystal violet-iodine stain when treated with organic solvents such as alcohol or acetone.[14] Those bacteria that retain the stain are termed Gram-positive and those that lose it, Gram-negative. This staining property depends on the morphology and composition of the bacterial envelope.

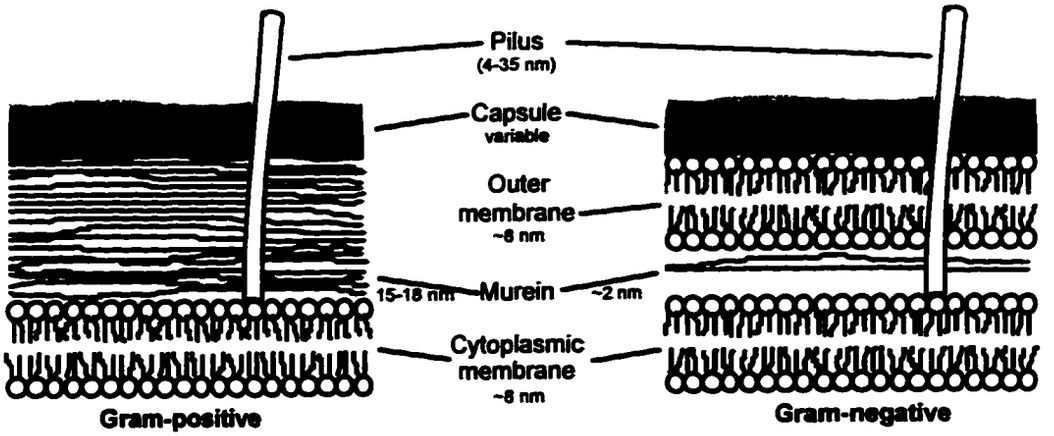

Figure 3.1 Comparison of the structure of the Gram-positive and Gram-negative envelopes.

The cell wall gives the cell its shape (whole cells of *B. subtilis* are rod-shaped), it protects the cell from external agents entering the cell, and it allows bacteria to survive in media that are typically hypotonic. The murein meshwork can be digested by the enzyme lysozyme, resulting in a cell with only the cytoplasmic membrane as its envelope, this form of the cell is called a protoplast. The cell can survive in a protoplast maintenance buffer (PMB, 0.5 M sucrose) but becomes spherical.

The cytoplasmic membrane controls substrate transport and electron transport; it is also the site of biosynthesis of extracellular macro-molecules. It is composed of a lipid component, a protein component, and lipotechoic acid. Lipids make up 30-50% (by weight) of the total membrane content. 20-40% of the total lipid is phosphatidyl ethanolamine; other components are cardiolipin and phosphatidyl glycerol.[14]

We concluded, in consultation with Dr. Dennis Sprott of the National Research Council's Division of Biological Sciences, that bacterial systems were the first to be used due to their ease of culture and their relatively robust nature. Our inexperience with cell culture and our traditional organic chemistry laboratory facilities lead us to try to find a relatively easy organism to culture. In addition, a Gram-positive cell was desired, due to

its simpler cell wall structure, since our goal was to incorporate probes into the cells. Taking all these factors into account, *Bacillus subtilis* became the cells of choice. Eventually protoplasts of *B. subtilis* were also used.

As we gained experience in cell culture and it became clear that a simpler cell wall structure was an advantage to incorporation of probes, mammalian cells were experimented with. In consultation with Dr. Jack McLean of the Health Protection Branch of Health Canada, mouse erythroleukemia (MEL) cells and U937 cells (a human leukemic cell line) were studied. This involved using much more stringent culture techniques and a small separate lab was transformed into a tissue culture area in order to carry out these studies.

In addition, we carried out experiments in cultured skin environments, which were purchased from a commercial supplier in their usable form. These cell culture samples are thin enough and transparent enough at some wavelengths to be studied by laser flash photolysis using transmission techniques for detection. While transmission techniques have been used before to study photochemistry in cell ghost suspensions,[15] this project deals with studying photochemical systems in a three-dimensional skin model on a collagen support or on a mesh support, as opposed to a free suspension. Also, these cultured skin samples are a coculture of different types of cells: human dermal fibroblasts and human keratinocytes that have formed a stratified and differentiated epidermis.[16-18] This is a rather different environment than a homogeneous suspension of one type of cell as in previous studies, and mimics better the properties of natural skin.

A major disadvantage to using the cultured skin samples is their prohibitive commercial cost to purchase, and we do not have the facilities

to culture the tissue ourselves. This limits the number of samples available to work with and the ability to try new approaches.

Over the past twelve years or so, there have been a few reports of detecting photochemical transients in biologically-relevant systems. Truscott and coworkers have detected transients by laser flash photolysis in liposomes and white blood cells,[15] and in other mammalian cells.[19] Firey and coworkers have detected transients in mammalian cells[20] and in erythrocyte ghosts.[21] More recently, Redmond and coworkers[22] and Roberts and coworkers[23] have detected transients by laser flash photolysis in mammalian systems and Oldham and coworkers have worked with bacterial suspensions.[24] In addition, Nakagawa[25] and Jurkiewicz[26] have reported directly detecting laser-generated free radicals in tissue by EPR. All of this work done by other groups (except the work by Nakagawa) have employed transmission detection laser flash photolysis and have used porphyrin-type sensitizers. The work presented in this thesis makes use of a combination of transmission and diffuse reflectance techniques, and it explores a wide variety of photochemical probes including thiophenes, porphyrins, benzophenones, anthraquinones, and thioxanthone.

3.2.Incorporation of probes being studied

In order to study the behaviour of selected photochemical probes in these biologically-relevant environments, methods had to be developed to incorporate them into the cellular structure. Optimal solutions to this problem are of course dependent on the probe and host characteristics, such as probe solubility in water, the overall charge (if any) of the probe, whether the host is the whole bacterial cell or in its protoplast form, etc. The results of the development of an incorporation strategy for this project are presented in chronological order, showing the refinement of the procedure from start to finish.

3.2.1.Direct injection of probe from organic solvent

In previous work from our laboratory[27] in micelle or vesicle systems, a direct injection method has been used. This is only necessary when the probe is insoluble in water. In this method, the host environment is prepared, and the probe is incorporated by separately preparing a small volume of a concentrated solution of the probe solution in an organic solvent and injecting this concentrated solution into the host solution or suspension. In many cases, this method works, with the probe redistributing itself in the host upon injection; although in exceptional cases this can take days, such as dodecylpyrene in micelles.[27]

This method seems simple and it was the first method attempted with the *B. subtilis* suspensions. Benzophenone or 4-benzoylbenzoic acid ethyl ester was dissolved in ethanol (0.2 M) in high concentration and 100 µL of this solution was quickly added to 300 mL of a cell suspension which was approximately 10^8 cells/mL. These suspensions were then allowed to incubate at 37°C for 1 hour. The cell suspensions were then washed twice with 0.1 M pH7 phosphate buffer and resuspended in a small volume of

buffer to give very thick cell suspensions (~10^{10} cells/mL), placed in 7x7 laser cells, and studied using diffuse reflectance laser flash photolysis techniques.

Although this method of preparation gave quite nice transient signals, a control experiment was run in which exactly the same procedure as described above was used, however no cells were present. Similar results were obtained. Microscopic analysis of the cell suspensions containing benzophenone incorporated with this method showed that crystals were present in the suspension.

It is clear that attempting to incorporate non-water soluble probes with this method yields a suspension containing some undissolved crystals of the probe, and these crystals can sometimes give rise to transient signals themselves. This method of incorporation was not used in any further studies.

3.2.2. Water soluble compounds with ionic charge in whole cells

To overcome the problems associated with incorporating non-water soluble probes, methods of incorporating water soluble probes were explored.

There exist a number of water soluble dyes that have interesting photochemistry, most of which have an overall cationic or anionic charge. Whole cells of *B. subtilis* have an overall negatively charged character to their cell wall.[14] This has important implications for the incorporation strategy. Suspension and incubation of whole cells of *B. subtilis* in probe-containing buffer was attempted.

Compounds such as methylene blue are used in stains in bacteriology and as anti-bacterial agents.[28] These cationic dyes easily attach themselves to

bacterial cell cultures due to the attraction to the negatively-charged cell wall, making this a seemingly easy way to incorporate probes for the purposes of our research. However, these compounds are toxic to the cells (probably since they disrupt the cell membranes), especially in the relatively high concentrations needed for our studies. This makes the study of these compounds by our methods irrelevant since we would no longer be studying living cells in their presence.

In the case of anionic dyes, the opposite effect occurs. Even after incubation for long periods of time (24 hours), compounds such as phthalocyanine tetrasulfonate do not incorporate into the membranes of the cells in any appreciable amount. The negative charge on the probe and the negative charge on the cell wall repel each other, preventing any incorporation.

This method was not pursued further for our studies. However, some success was achieved in protoplast systems, which will be described in section 3.2.6.

3.2.3.Electroporation

Electroporation is a method by which foreign materials can be incorporated into cells using high voltage pulses. It is used mostly for adding DNA strands to cells, causing mutations.[29] This method was explored for use in our studies.

A culture of *B. subtilis* was raised in Spizizen salts with casamino acids and tryptophan for 12 hours at 30°C, as previously reported.[29] The cells were harvested by centrifugation and rinsed once in HEPES buffer, then twice in cold electroporation buffer, and resuspended in 1/200th of the original culture volume in electroporation buffer.

A cell suspension (50 μL) was mixed with 2 μL of the probe solution (10 mg/mL of benzophenone ethyl ester in ethanol), chilled on ice for 1 minute, then transferred to a 0.2 cm electroporation cuvette.

The high voltage electric pulse was used with the following settings on the pulse controller: 25 μF capacitance, 1.5 to 2.5 kV set voltage, and 100-800 W resistance.

After administering the electric pulse, 1 mL of the original culture broth was added to the cell suspension and transferred to a tube for incubation at 30°C for 1 hour.

After washing the cells and resuspending them in phosphate buffer for laser experiments, no transient signals were obtained upon 355 nm excitation. The method of electroporation may be useful for incorporating small amounts of materials such as DNA fragments but the concentrations needed for our purposes are much higher, and we do not believe electroporation is a useful method to use for incorporation for our purposes.

3.2.4.Sonication of non-water soluble materials

In order to attempt to increase the amount of non-water soluble probes incorporated into the cells, sonication of probe suspensions in buffer was explored. A typical lab sonicating bath was used (Branson model 1210). In general, this method was not successful; in order to ensure that crystals were not present, the sonicated solutions were filtered with a 0.22 μm syringe filter. Upon filtering, most probes were not present in significant enough amounts to warrant attempted incorporation (determined by measuring the absorbance of the solution). If the solutions were not filtered, the final cell suspensions contained suspended crystals of probe

molecules and this situation is not acceptable since we would not know if any signals obtained by flash photolysis were from suspended particles or from incorporated probe.

In two cases, however, sonication was a useful aid in maximizing the amount of material dissolved in the buffer solution: α-terthienyl and isopropylthioxanthone, which are slightly soluble in water. However, as discussed below, an alternate method of incorporation was developed which made this method unnecessary.

3.2.5. Growth of cells in the presence of probes

In an attempt to increase the uptake of probe molecules into the bacterial cells, we added some of the probes directly to the growth medium. Positively-charged water-soluble compounds prevented growth, negatively-charged water-soluble compounds and non-water soluble probes were not incorporated in significant enough amounts for our purposes.

In one case, however, a different approach was taken which proved more successful. 5-Aminolevulinic acid (ALA) is a metabolic precursor to a naturally-occurring porphyrin in many biological systems.[30] When ALA is added to the growth medium, the concentration of this porphyrin is greatly increased in the cell. Details of these results will be shown in section 3.4.2.

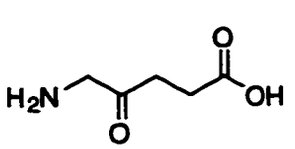

Figure 3.2 Structure of 5-aminolevulinic acid (ALA).

3.2.6. Negatively-charged water-soluble probes in protoplasts and in mammalian cells

When the cell wall of cells of *B. subtilis* is removed, the protoplast membrane is less negatively-charged than the original cell wall was.[14] This allows for incorporation of some negatively-charged, water-soluble probes into the cells. Phthalocyanine tetrasulfonate was the probe most successfully incorporated by this method. This method was also successful in studies with mammalian cells and phthalocyanine tetrasulfonate.

3.2.7. Encapsulation of photochemical probes in liposomes

Liposomes have often been used in recent years to model the cellular environment, especially for modeling membrane interactions, and liposomes have been used for the delivery of macromolecules into cells[31-35]. Hoekstra and coworkers[36-38] developed a method of monitoring liposome fusion with membranes using fluorescence methods. Salman and coworkers[39] used this method to show that liposomes fuse to *Mycoplasma capricolum* cells, Rose and coworkers[40] have shown that liposomes can be used to deliver viral DNA to animal cells for successful transfection of those cells, and Richter and coworkers[41] successfully delivered photosensitizers such as benzoporphyrin derivative monoacid to tumor tissue in a mouse tumor model.

Liposome delivery of photochemical probes to the cellular environment was used as the method of choice in this project for non-water soluble compounds, as it proved to be highly effective. Two methods of probe-containing liposome preparation were explored.

At first, the liposome solutions were prepared by a method similar to the modified injection method described by Kremer and coworkers.[42] 1 mL of a chloroform solution containing 15 mM dipalmitoyl phosphatidylcholine

(DPPC) and 7 mM probe was injected slowly into 10 mL of phosphate buffer at 70 °C over a period of 30 minutes. Nitrogen was bubbled through the buffer during injection and for 30 minutes following the end of the injection. The liposome solution was then allowed to cool to room temperature and passed through a Whatman #114 size filter to ensure the absence of any suspended crystals. This process was further improved by first centrifuging the liposome solution and then passing the supernatant through a 0.22 μm syringe filter. When liposomes were used to deliver the probe to protoplasts, the liposomes were prepared in protoplast maintenance buffer (PMB, 0.5 M sucrose).

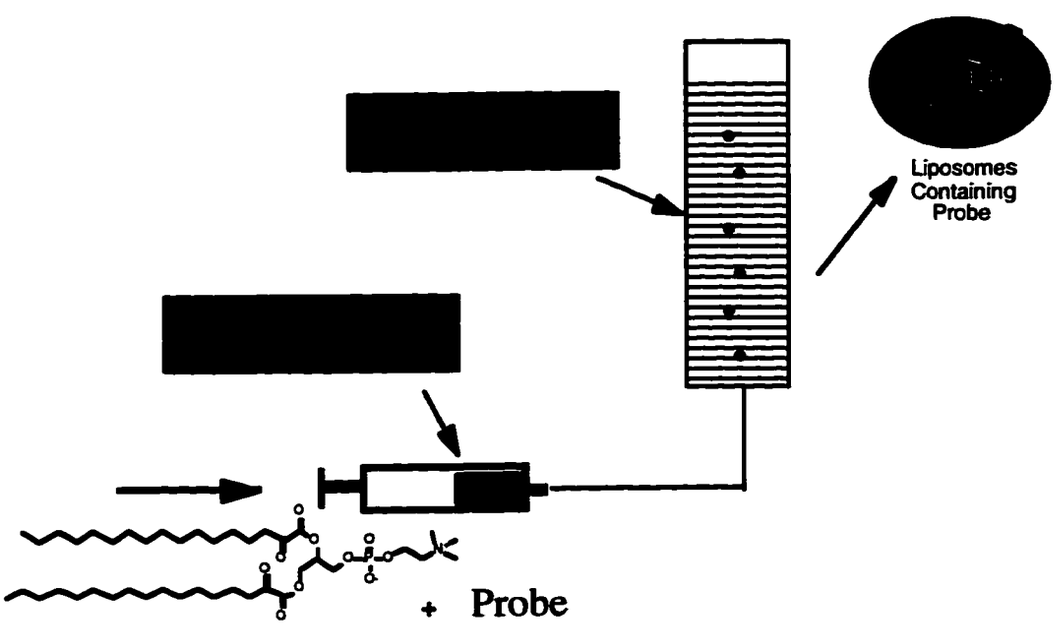

Figure 3.3 Illustration of modified injection method of making probe-containing liposomes.

The second method employed to prepare liposomes became the most convenient and reproducible method of preparation and was used exclusively for this project after its development. In this method, which is a modified version of the method used by Richter and coworkers,[41] up to 3 mL of 20-40 mg/mL each of probe and DPPC in the sterile buffer of choice

(0.1 M pH7 phosphate buffer or PMB) are sonicated for 3 to 4 hours in a laboratory sonicator (Branson model 1210) at room temperature. The resultant suspension is allowed to rest for 1 hour in the dark, then centrifuged for 10 minutes at 3500 rpm. The supernatant is then passed through a 0.22 μm syringe filter. This produces a concentrated solution of probe-containing liposomes less than 220 nm in size, free of any crystalline material. The suspension is stable for the duration of the preparation and delivery to the cells.

The liposome solution is then mixed and incubated with the receiving cells; these cells could be whole cells of *B. subtilis*, their protoplasts, or mammalian cells. They are typically incubated for 2 hours at the appropriate incubation temperature (30 °C for the bacterial systems and 37 °C for the mammalian systems). The cells are then washed three times to remove any remaining probe in the bulk solution and resuspended in the appropriate buffer for laser experiments.

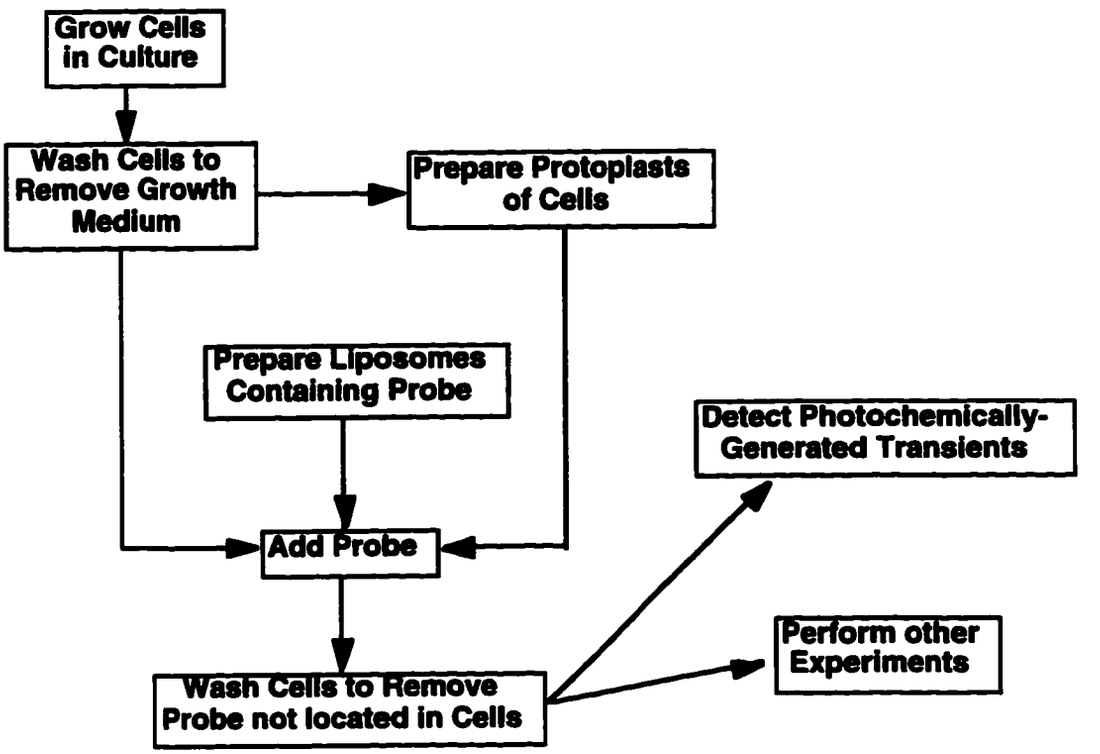

Scheme 3.1 Preparation of probe-containing cells.

3.2.8.Studies in cultured skin models

Incorporation of probe into the biological environment in the case of skin and skin models is relatively simple since the test compound can be dissolved in a known non-toxic solvent, applied to the surface of the skin, then the skin can be washed to remove any residual non-incorporated probe. The manufacturers of the commercially-available skin models have developed standard protocols for application of substances and for end-point testing.

The protocols suggested by the supplier companies were followed for application of test compounds to the tissue samples. Exact procedures are described as follows.

Living Skin Equivalent™ (LSE™)

For water-insoluble compounds such as α-terthienyl, dimethylsulfoxide (DMSO) was used as application solvent. Before application, the solutions were filtered (0.22 μm pore size) to sterilize the solution and to remove any undissolved material. A "well" of dissolved test compound on the skin surface was created using a specially-designed Teflon ring supplied with the kit. Probe solutions were typically 25 mg/mL in DMSO. The well was filled (~200 μL total volume applied to surface) and allowed to make contact with the skin overnight at 5% CO_2 and 37 °C.

After exposure, the assay medium below the skin sample was changed and the DMSO from the surface was aspirated. The surface of the skin was rinsed with DMSO followed by 0.1 M phosphate buffer (pH 7.0). The skin samples were then allowed to rest for 3 hours with fresh medium in the incubator. They were then carefully separated from their supports and placed between quartz plates for laser experiments.

For water-soluble compounds such as disodium anthraquinone 1,5-disulphonate, 25 mg/mL of the test compound were dissolved in the water-based assay medium provided with the kit. The balance of the sample preparation was identical.

Skin² Model ZK1300™ from Advanced Tissue Sciences (ATS)

For non-water-soluble compounds such as α-terthienyl, mineral oil was used as the solvent. In the case of water-soluble compounds, the assay medium provided with the kit was used as solvent. Solutions were filtered before use.

Solutions were applied (~200 μL) to pieces of filter paper cut to the same size as the culture samples following the protocol suggested by the manufacturer. These pieces of filter paper were then applied to the surface of the skin overnight (5% CO_2, 37 °C).

Since these culture samples cannot be separated from their mesh support without considerable damage to the three dimensional cellular structure, these samples were used "as is" and were placed between quartz plates for laser experiments.

Due to sample depletion and damage to the tissue during the pulsed laser experiments, the sample holder was attached to a sample mover which ensured a new area of irradiation for each laser shot. The laser beam was typically 5-7 mm in diameter. Laser power was kept to a minimum (~5mJ/pulse) to minimize physical damage to the cells by ablation or charring. The absorbance of the samples with the incorporated probe was typically 0.5 at 355 nm, ensuring that the laser light would penetrate all layers of cells.

3.3.α-Terthienyl as a probe

The purpose of the experiments carried out in this section is to explore how α-terthienyl (αT; 2,2':5',2"-terthiophene, Figure 3.4) can be used to probe biological environments. αT is a naturally-occurring compound from the plant family Asteraceae.[43] The plant uses the phototoxicity of these compounds as a defense against predators such as insects and fungi.[44] The triplet state of αT interacts readily with oxygen (at a rate of 2 x 10^9 M^{-1} s^{-1})[45], produces singlet oxygen with a quantum yield of 0.86,[46] and this singlet oxygen is thought to be responsible for its phototoxicity.[47] Photosensitization of yeast and *E. coli* occurs under aerobic but not anaerobic conditions.

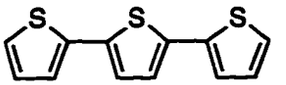

Figure 3.4 Structure of α-terthienyl.

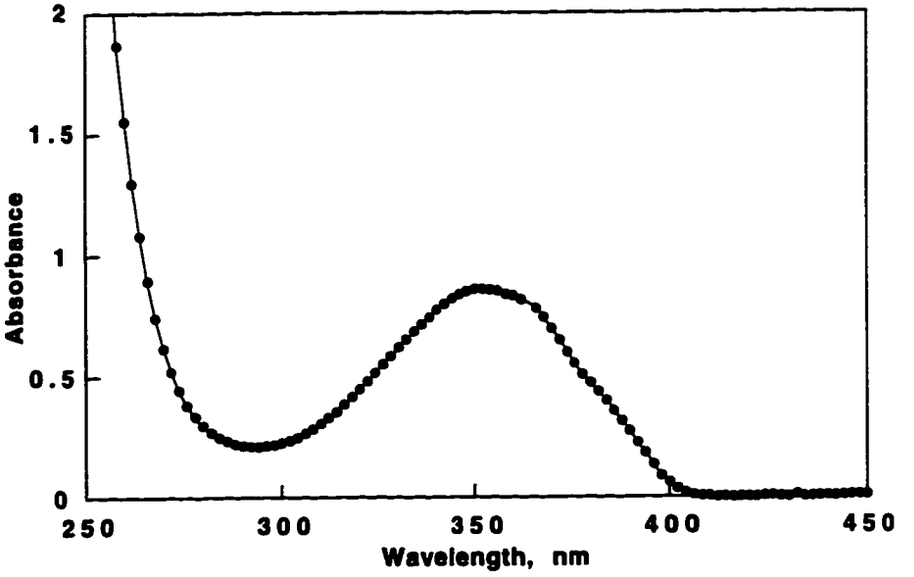

Figure 3.5 Ground state absorption spectrum of α-terthienyl in methanol.

The triplet state can be readily monitored by nanosecond laser flash photolysis techniques, with a λ_{max} at 470 nm.[48] The triplet energy is reported to be approximately 40 kcal/mol in energy and its intersystem crossing quantum yield from singlet to triplet is reported to be above 0.9.[47]

Methyl viologen has been shown to be a good αT triplet state quencher, quenching at a rate of 6.8×10^9 M^{-1} s^{-1} in methanol via an electron transfer mechanism, with methyl viologen being reduced in the process.[49] The αT radical cation can also readily be observed, with a λ_{max} at 530 nm.[49]

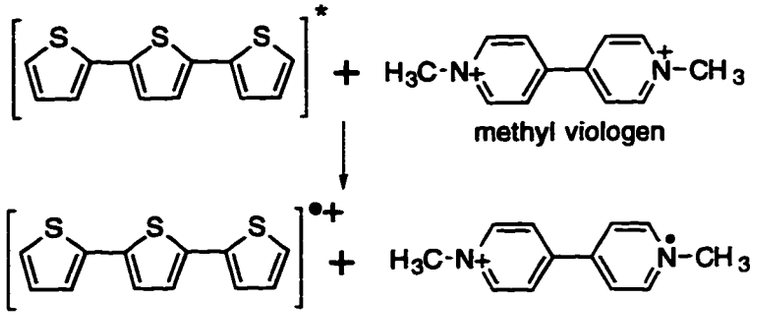

Scheme 3.2 Reaction of αT triplet with methyl viologen.

It has been reported that αT,[50] as with several other photosensitizers,[51] is located in the lysosomal membrane in mammalian cells, and causes damage to the lysosomal membrane as its phototoxic action.

3.3.1.Results and Discussion

α-Terthienyl is the only probe studied which lends itself to the direct injection method for incorporation into whole cells of *B. subtilis*. Careful microscopic examination of the cell suspensions after injection from methanol and washing the cells 3 times shows no evidence for suspended crystals of αT. With its large ground state absorption at 308 nm, early experiments with 308 nm laser excitation were successful. The spectrum

recorded following 308 nm laser excitation (using diffuse reflectance detection methods) of air saturated samples is shown in Figure 3.6. The spectrum obtained (λ_{max} 470 nm) is clearly that characteristic of the triplet state,[48] while the shoulder at ~530 nm suggests the presence of small concentrations of the radical cation.[45, 49] Control experiments using 308 nm and 355 nm excitation show that signals from cells without probe are much weaker.

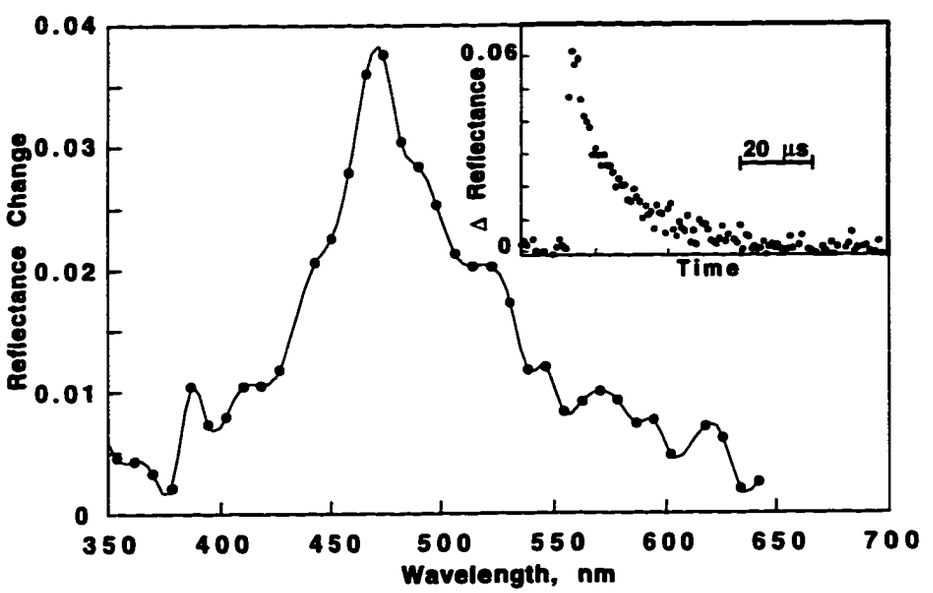

Figure 3.6 Transient spectrum recorded by 308 nm irradiation of *B. subtilis* with αT incorporated by the direct injection method. Inset: Diffuse-reflectance decay trace recorded at 465 nm.

Using liposomes to deliver probes to the host environments proved to be the most successful method of probe incorporation in this project. In the case of *B. subtilis*, αT was more successfully delivered if protoplasts of the cells were first prepared; the cell wall probably acting as a barrier for αT incorporation when liposomes are used.

Studying αT in the liposome environment as an analog to the cellular environment is an interesting case. Recording the αT characteristics in the

liposomes (before incorporation) also gives insight into the incorporation process itself, since changes to the αT transient signals before and after incorporation can be followed. Figure 3.7 shows transient spectra of αT triplet state in liposomes prepared by the sonication method. There may be a small amount of radical cation present, as can be seen in the spectrum recorded at 15.4 μs (note small signal at 530 nm in Figure 3.7).

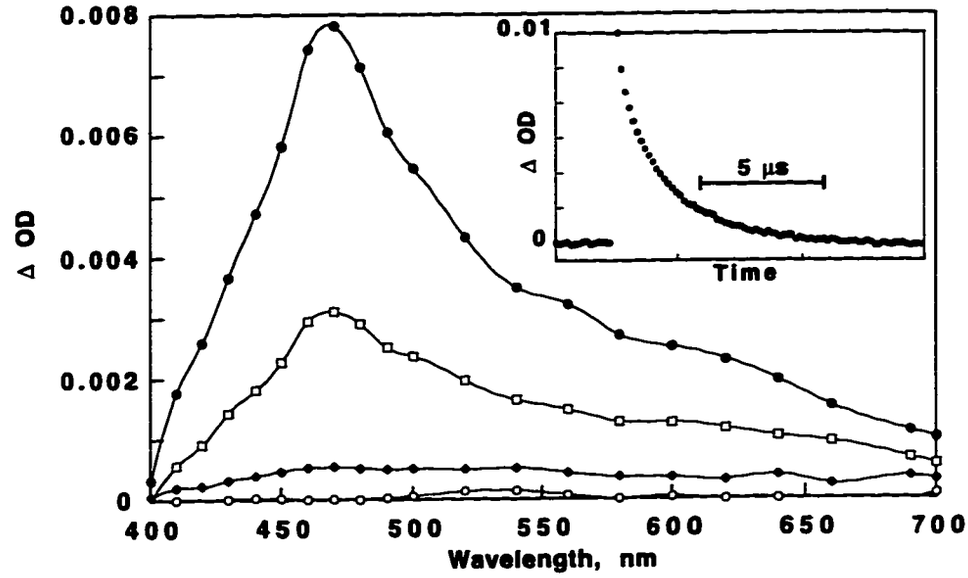

Figure 3.7 αT in liposomes (sonication method). Transient spectra recorded (by transmission detection) 480 ns, 2.32 μs, 7.44 μs, and 15.4 μs after 355 nm laser excitation. Inset: transient decay trace recorded at 470 nm. In 0.1 M pH7 phosphate buffer.

When these αT containing liposome are incubated with protoplasts, the αT is transferred to the cell and we can now probe the environment in the cell. The transient spectrum does not change, but the triplet decay kinetics do change. A comparison of the αT triplet decay traces is shown in Figure 3.8.

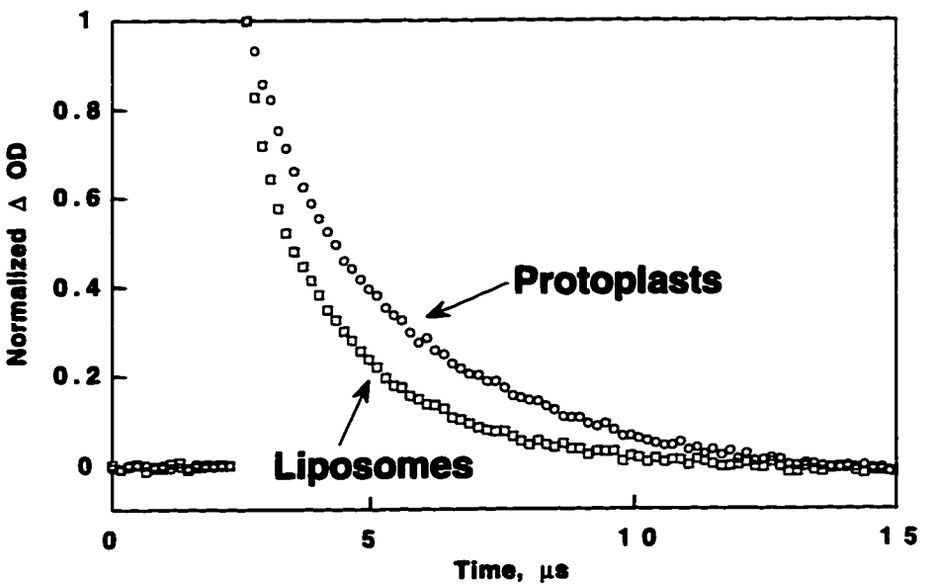

Figure 3.8 Decay of αT triplet in (□) liposomes and in (○) protoplasts of *B. subtilis*. Measured at 470 nm by transmission detection after 355 nm excitation. Triplet lifetimes are 2.1 μs in liposomes and 3.5 μs in protoplasts.

The fact that the triplet decay kinetics in liposomes and in protoplasts are different shows unequivocally that this method of incorporation successfully transfers the αT (and other probes using this method) from one environment to another. The protoplast suspension has been washed so the probe cannot be in the extracellular solution; the only possible location is within the *B. subtilis* cellular environment.

It is known that the αT triplet state is quenched by methyl viologen via an electron transfer mechanism, generating the radical cation of αT in the process.[45, 49] When αT is incorporated into protoplasts of *B. subtilis* by delivery of liposomes prepared by sonication, we can detect the αT triplet state readily (see Figure 3.8). As shown in Figure 3.9, when 20 mg/mL of methyl viologen is added to a protoplast suspension, the radical cation of αT can be detected. Interestingly, there was no effect of methyl viologen on the triplet state in the DPPC liposomes, which is more evidence for successful incorporation.

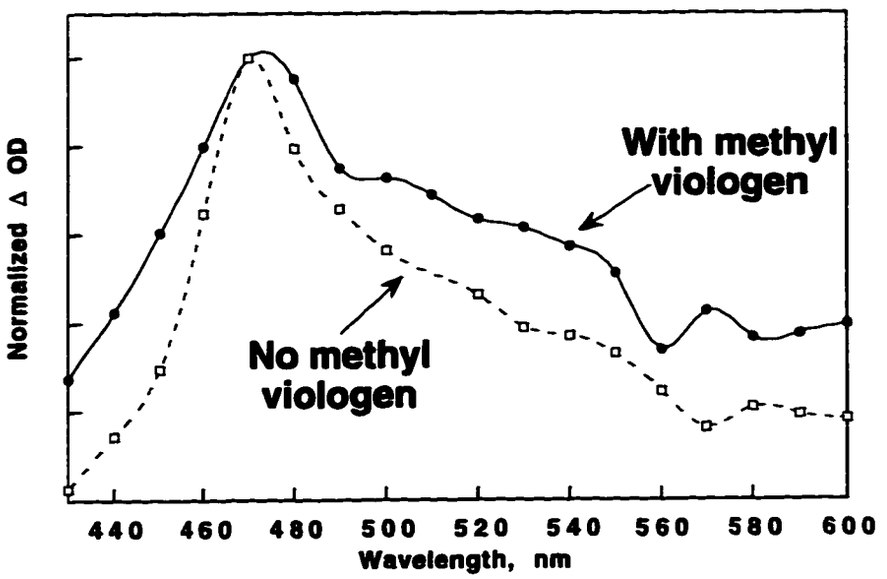

Figure 3.9 Transient spectra of αT in protoplasts of *B. subtilis* (by transmission detection) following 355 nm excitation; with and without methyl viologen present.

In order to probe the environment of mammalian cells, analogous experiments were carried out in U937 cells, a human leukemic cell line. Similar results (shown in Figure 3.10) were obtained to those in *B. subtilis* protoplasts, with an even more pronounced band for the radical cation.

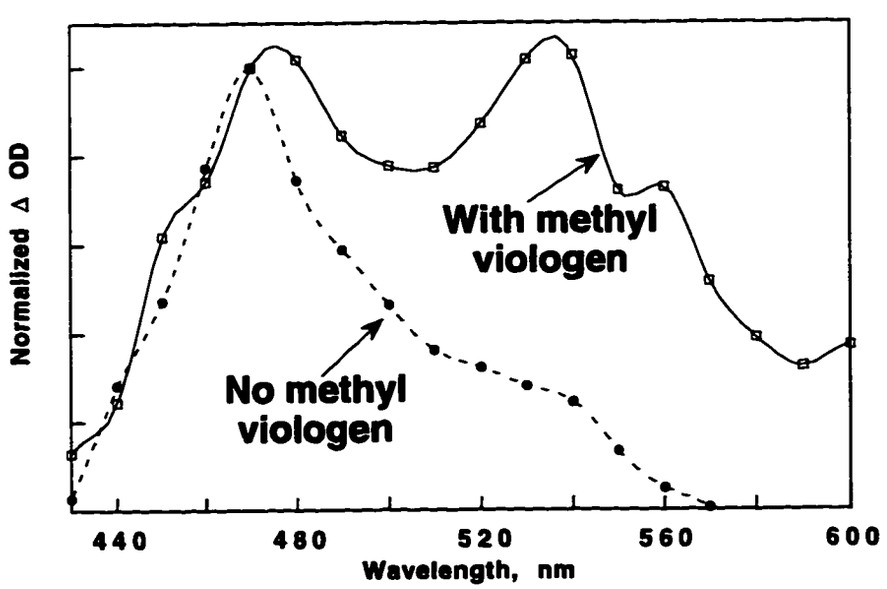

Figure 3.10 Transient spectra of αT in U937 cells (by transmission detection) following 355 nm excitation; with and without methyl viologen present.

In all the cases presented above, preparation of samples was done under ambient air conditions and no degassing of samples was carried out. It is known that the mode of action of αT as a phototoxin involves the formation of singlet oxygen.[48] Craw and coworkers[15] estimate the oxygen quenching rate constant of porphyrin triplets at 10^9 M^{-1} s^{-1} in a lipid environment. Firey and Rodgers[21] directly measured two oxygen quenching rate constants of porphyrin triplets in erythrocyte ghosts at 10^8 M^{-1} s^{-1} and 7×10^8 M^{-1} s^{-1}. Abuin and Lissi[52], Craw and coworkers[15], and Smotkin and coworkers[53] report that the oxygen concentration in liposomes is approximately the same as in the bulk water, which is 2.63×10^{-4} M under air-saturated conditions.[54] We have measured the triplet lifetime of αT in liposomes (under air) to be 2.1 μs. Using the Stern-Volmer quenching equation 13, a quenching rate constant of 5×10^8 M^{-1} s^{-1} (an approximation given the previous reports[15, 21]) and an oxygen concentration of 2.63×10^{-4} M, an estimated k_0 value (the triplet decay rate in the absence of oxygen) can be calculated at 29 μs (as an approximation). This is in good agreement with the reported triplet lifetime in organic environments (30 μs in methanol,[48] 57 μs in ethanol[55]). This is very different from the αT triplet lifetime in 0.1 M pH7 buffer, which has been measured at less than 100 ns.[56] Thus it seems that the main decay pathway for the αT triplet, in the environments studied in this project, is its reaction with oxygen.

Finally, the photochemistry of αT was studied in the cultured skin cell environment. Figure 3.11 shows the transient spectrum obtained after 355 nm excitation of αT in the LSE model. This spectrum shows the characteristic triplet-triplet absorption band for αT. In addition, it shows a shoulder at 520 nm which we assign to the radical cation. The lifetime of the triplet is relatively long with a half-life over 30 μs, indicating that the

detectable triplets are at a site which is remarkably well protected from oxygen. Figure 3.11 also shows the result of 355 nm excitation of αT in the ATS model. In this case, the radical cation shoulder is not present. The triplet lifetime is also long in this sample; a representative decay trace is shown in the inset. Both the ATS sample and the LSE sample gave very similar decay traces at 475 nm.

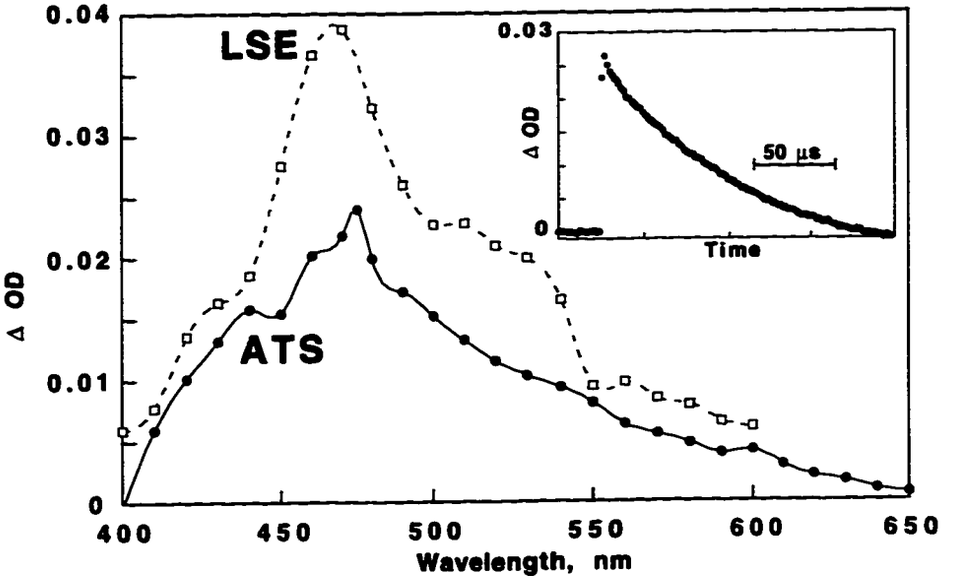

Figure 3.11 Transient spectra obtained following 355 nm laser excitation of skin samples containing α-terthienyl. (○) ATS sample, 6 μs after excitation, (□) LSE sample, 1 μs after excitation. Inset: Decay trace of ATS sample, monitored at 475 nm.

The main difference between the LSE model and the ATS model is that the ATS model lacks the top differentiated layer of the skin cells, the stratum corneum. These results may indicate that the stratum corneum may be a more oxidizing environment, or that it lacks antioxidants that may be present in the deeper layers of the skin.

3.4.Porphyrins

Porphyrins are important biomolecules, participating in heme-type structures in the bloodstream, for example, in myoglobin, hemoglobin, and cytochromes. Their efficient singlet oxygen sensitization from the porphyrin triplet state has been studied widely and its use in photodynamic therapy has been proven.[13] It has been shown that the location of porphyrin in the cell depends on its side chains.[57, 58]

The ground state of porphyrin molecules generally show an intense absorption band (called the B band or the Soret band) and less intense aborption bands (Q bands) in the 500 to 600 nm region.[59] See Figure 3.13, Figure 3.18, and Figure 3.24 as examples of ground state absorption spectra. The transient photochemistry of this class of compounds has been extensively studied; it can be solvent dependent and aggregation is a common phenomenon for these compounds in solution.[15, 19, 22, 59-70]

3.4.1.Mesoporphyrin IX

Mesoporphyrin IX is a suitable probe to use in this project, since it has relatively strong absorbance at 355 nm and its triplet state is readily detectable.

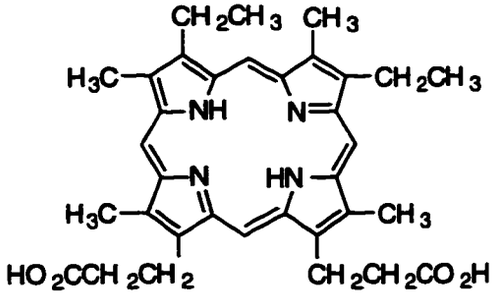

Figure 3.12 Structure of Mesoporphyrin IX (MPIX).

The ground state absorption spectrum in solution shows a λ_{max} at 400 nm.

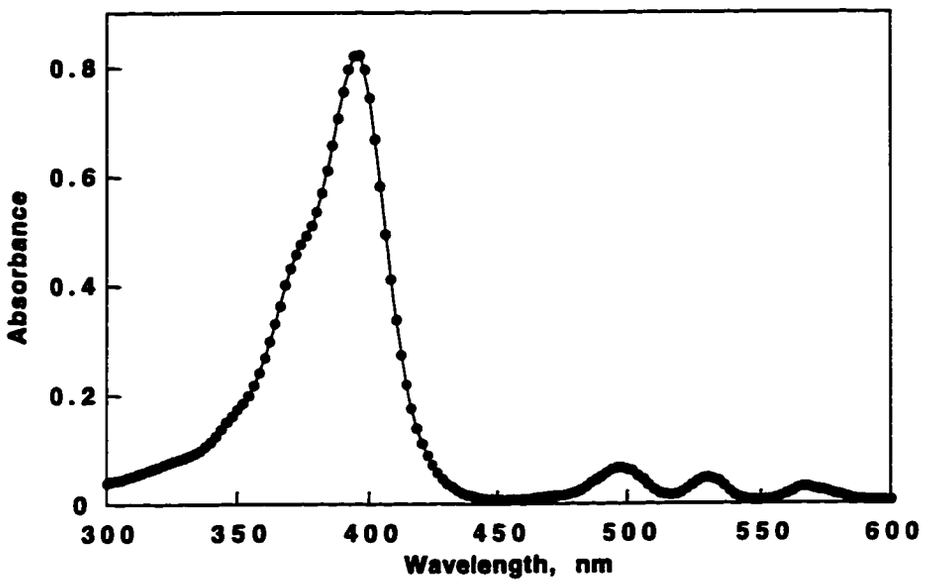

Figure 3.13 Ground state absorption spectrum of MPIX in ethanol.

The transient spectrum obtained following 355 nm excitation of MPIX in ethanol is shown in Figure 3.14. Note the bleaching of the ground state in the 400 nm region. All signals are readily quenched by oxygen.[61]

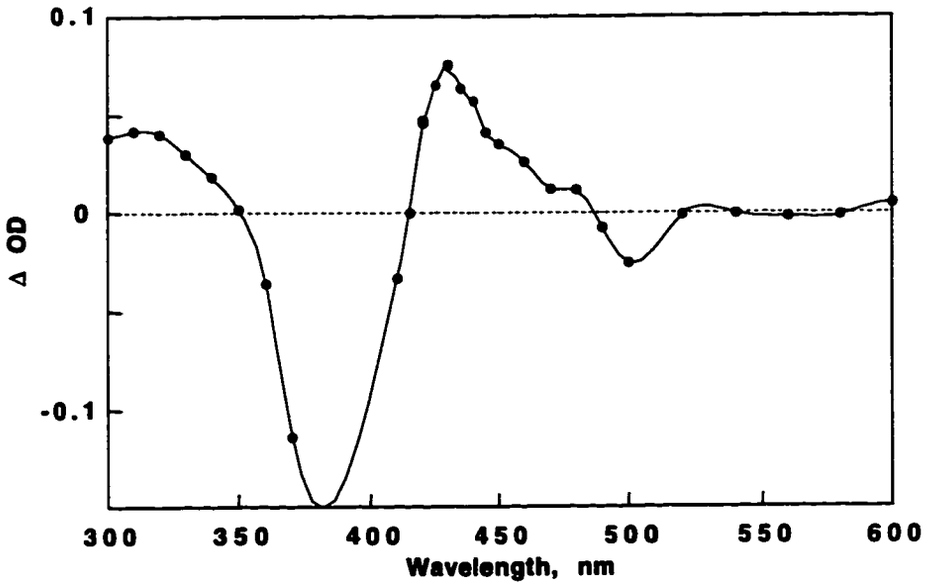

Figure 3.14 Transient spectrum of the triplet state formed and bleaching of the ground state following 355 nm laser excitation of MPIX dihydrochloride in ethanol, 5.6 μs after laser pulse.

MPIX was successfully incorporated into liposomes (by the sonication method), and it was delivered to the cellular environment after incubation of *B. subtilis* protoplasts. Collecting transient spectra in liposomes and in protoplasts is difficult since the volume of suspension needed for a flow system is difficult to obtain. For this reason, the bleaching at 400 nm was used to record the kinetics of the photochemistry of MPIX in these environments. In the absence of probe, no signals are obtained either in protoplasts or in liposomes.

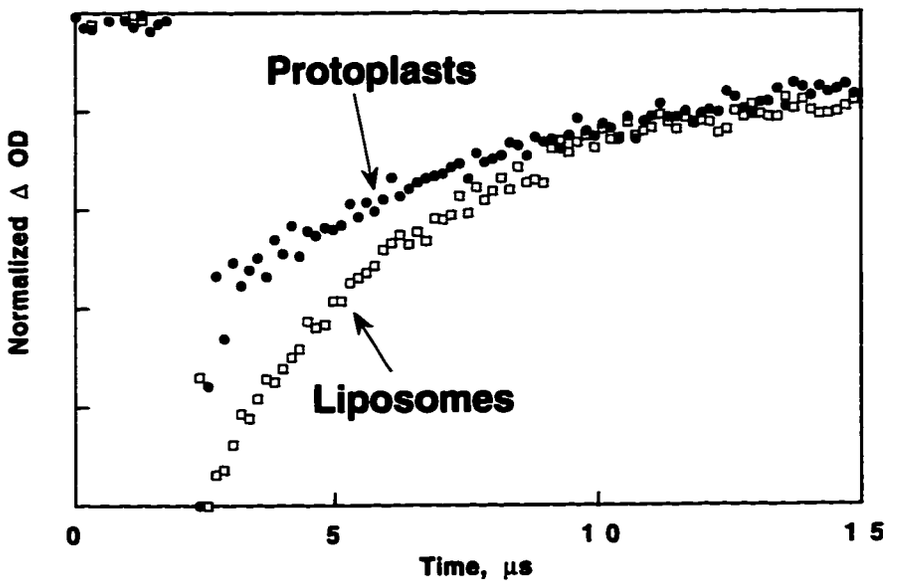

Figure 3.15 Bleaching and recovery of MPIX in (□) liposomes and in (○) protoplasts of *B. subtilis*. 355 nm laser excitation, measured at 400 nm.

The decay traces shown in Figure 3.15 show that porphyrin photochemistry can be followed in the cellular environment. These traces also show that there is a net photoreaction that occurs since the bleaching does not return to the pre-laser flash baseline level. The recovery kinetics occur with a half live of approximately 2.5 μs. Similar results were obtained in the case of MPIX in whole cells of *B. subtilis*, delivered using liposomes, although the recovery kinetics appear to occur faster in the

whole cells, with a half-life of approximately 1.5 μs. Figure 3.16 shows a trace of MPIX in whole cells of *B. subtilis*. When the same flash photolysis experiment is run with MPIX dissolved in ethanol or 0.1 M pH 7 phosphate buffer (with 1% v/v DMSO added to aid solubility), a similar net bleaching is obtained (non-return to baseline).

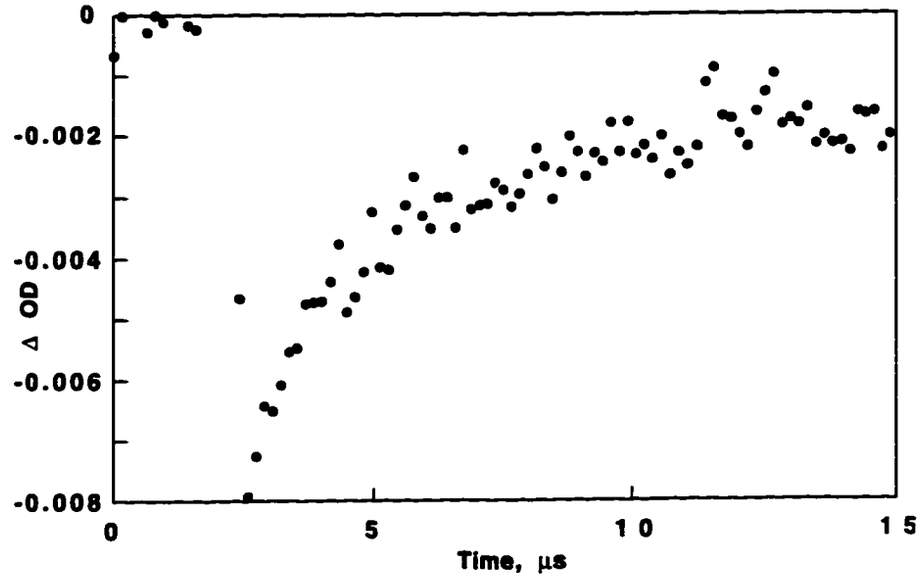

Figure 3.16 Kinetic trace obtained following 355 nm laser excitation of MPIX in whole cells of *B. subtilis*, measured at 400 nm.

3.4.2. Protoporphyrin IX and 5-Aminolevulinic Acid

Protoporphyrin IX (PPIX) is similar in structure and spectral characteristics to MPIX.

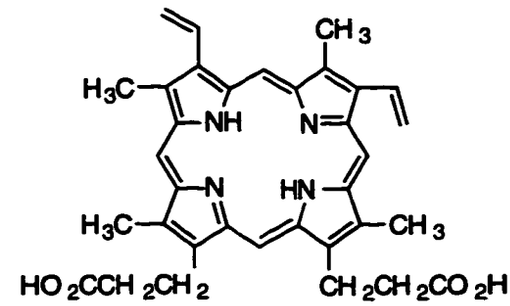

Figure 3.17 Structure of Protoporphyrin IX (PPIX).

PPIX is known to be a component of hematoporphyrin derivative, HpD, which is a mixture of various porphyrin monomers, dimers, and polymers with a characteristic bright red fluorescence and a tendency to accumulate preferentially in malignant tissues.[71] It can be used to visualize carcinomas, and has shown to be an efficient photochemotherapeutic agent.[72]

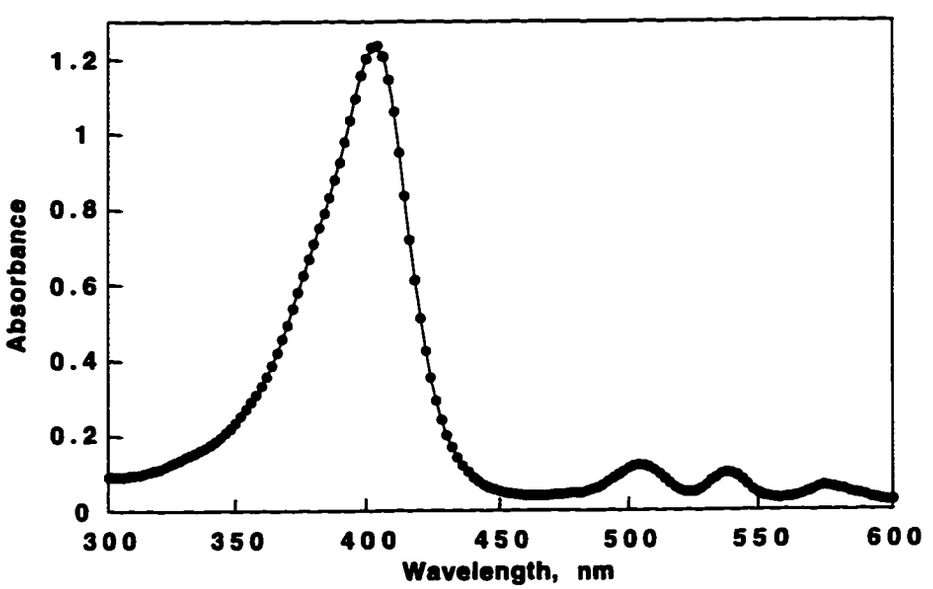

Figure 3.18 Ground state absorption spectrum of PPIX in ethanol.

In solution, PPIX demonstrates similar photochemistry on the nanosecond timescale as MPIX, with a bleaching feature in the 400 nm region. The PPIX triplet state is quenched by oxygen[61] at a rate of 1.5×10^9 M^{-1} s^{-1}. Figure 3.19 shows the transient spectrum obtained following 532 nm laser excitation.

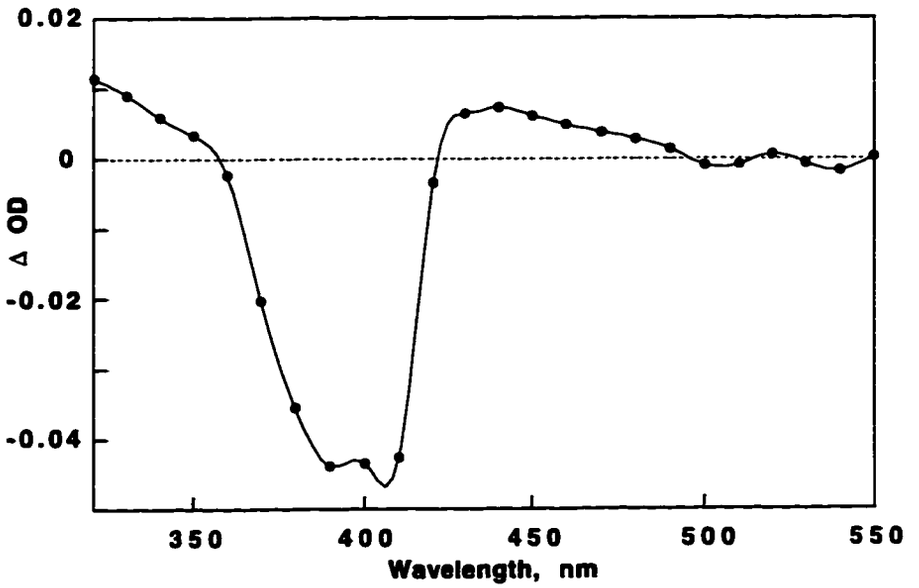

Figure 3.19 Transient spectrum of the triplet state formed and bleaching of the ground state following 532 nm laser excitation of PPIX dimethyl ester in ethanol, 550 ns after laser pulse.

It has been shown that 5-aminolevulinic acid (ALA, also called δ-aminolevulinic acid), when administered to a variety of organisms ranging from bacteria to plants to mice to humans, may induce the biosynthesis of an excess of PPIX in certain types of cells and tissues.[71]

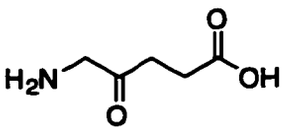

Figure 3.20 Structure of 5-aminolevulinic acid (ALA).

ALA is the primary building block of porphyrins, chlorophylls, and a wide range of tetrapyrroles.[73] This is an exciting prospect for the purposes of this project, since incorporation of the probe is done by the cells themselves and the product of metabolism of ALA, PPIX, is a suitable probe for our studies which, in addition, has interesting photodynamic properties.

A culture of *B. subtilis* was grown under usual conditions, except with 5 mg of ALA added per mL of growth medium. The most diagnostic test for the presence of PPIX is its strong red fluorescence. Figure 3.21 shows a fluorescence spectrum of a *B. subtilis* suspension that has been cultured in the presence of ALA, washed, and resuspended in 0.1 M pH7 phosphate buffer. The spectrum matches that found for PPIX in solution,[70] except that the maximum is shifted approximately 20 nm to the red. It does match, however, the fluorescence spectrum obtained in the skin of live mice when ALA is applied topically.[74]

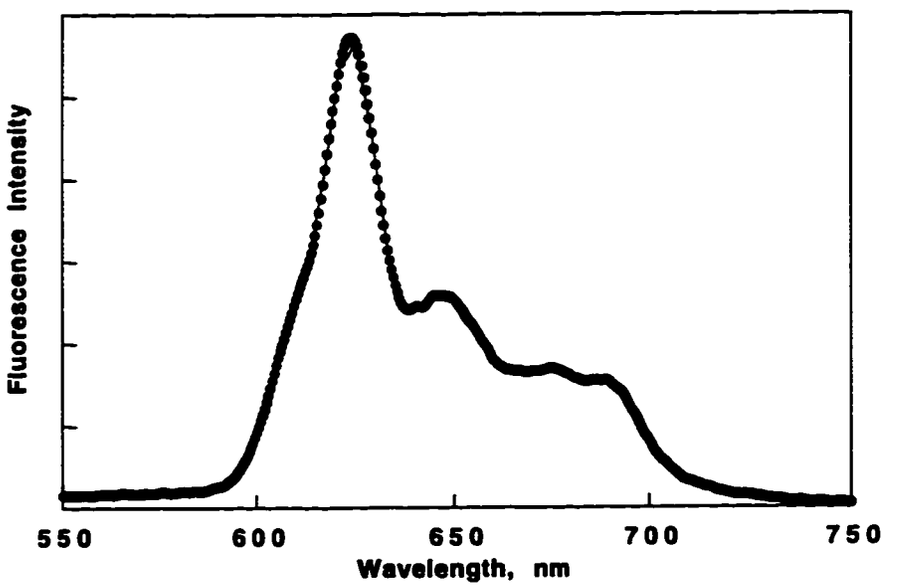

Figure 3.21 Fluorescence spectrum of *B. subtilis* cultured with ALA. Excitation at 400 nm.

Preliminary cell survival studies were carried out with this system to demonstrate the photodynamic action of PPIX delivered via ALA. To further confirm the presence of PPIX and to monitor the changes in the cell suspensions during irradiation, ground state diffuse reflectance absorption spectra were run, Figure 3.22. In the reference beam was placed a cell culture that was not grown in the presence of ALA. This gives us a sensitive method of detecting differences between ALA- and non-ALA fed

cultures. Irradiations were carried out under 350 nm lamps for 18 hours, 15 mL of culture in petri dishes, ~10^6 cells/mL in 0.1M pH7 phosphate buffer.

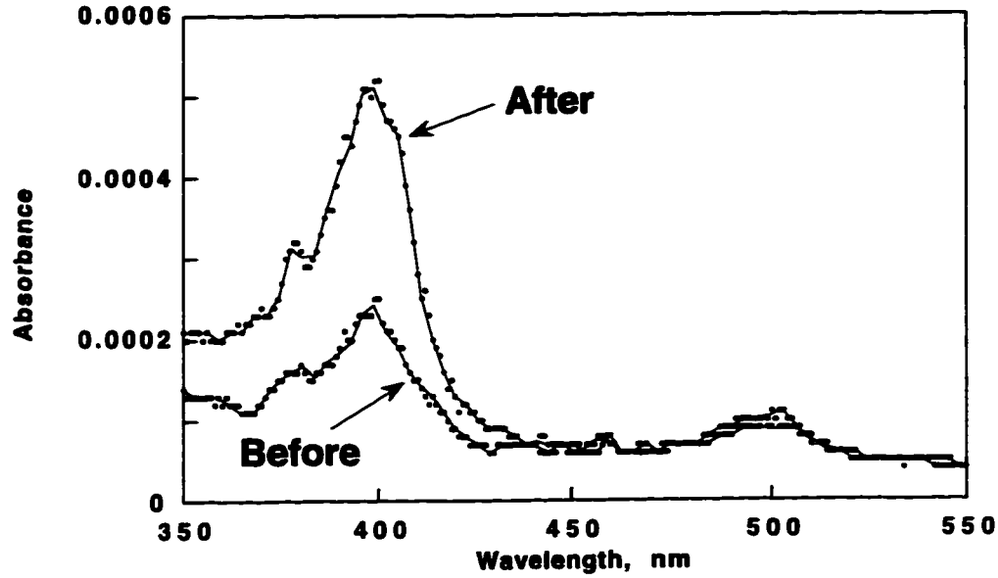

Figure 3.22 Ground state diffuse reflectance spectra of *B. subtilis* cultures grown in medium enriched with ALA, before and after irradiation with 350 nm lamps. Reference beam contains cell suspension unenriched with ALA.

These survival studies were carried out in triplicate and showed a small but reproducible decrease in cell density before and after irradiation of 8%, measured by transmission at 660 nm, vs. a sample which was ALA-enriched but not exposed to light. Exposure to light of an unenriched culture shows no decrease in cell density upon irradiation. Interestingly, irradiation causes an increase in the absorption at 400 nm over time. This remains unexplained.

3.4.3.Zinc phthalocyanine tetrasulfonate (ZPTS)

Zinc phthalocyanine tetrasulfonate, another compound from the porphyrin-type class of compounds, seemed, at first, to be a promising prospect for studies in cellular environments.

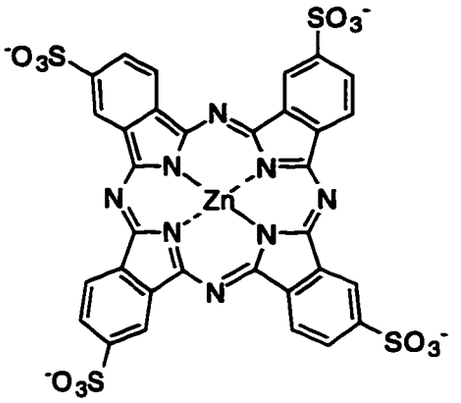

Figure 3.23 Structure of zinc phthalocyanine tetrasulfonate (ZPTS).

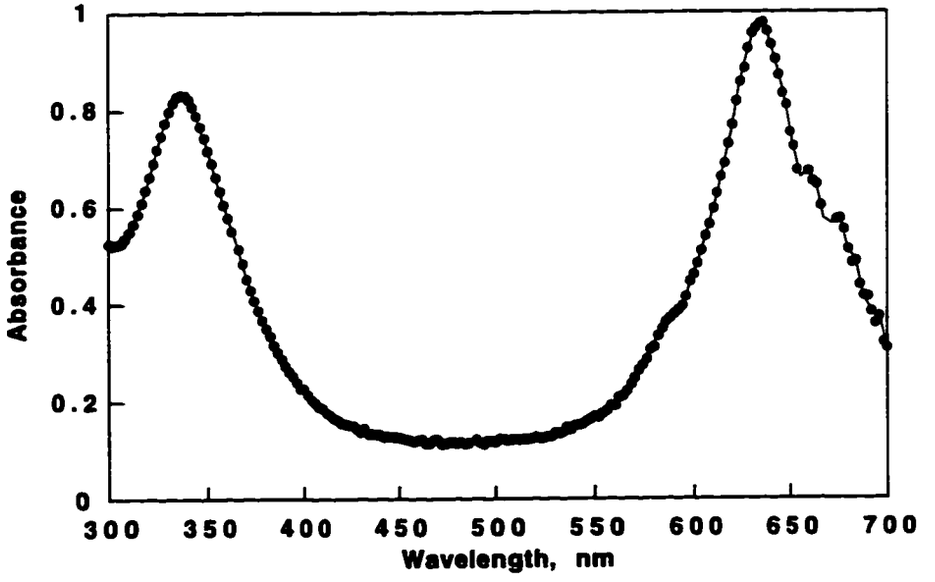

Figure 3.24 Ground state absorption spectrum of ZPTS in water.

The transient spectrum obtained when ZPTS is photolysed in buffer is shown in Figure 3.25. All signals are quenched by the presence of oxygen at a rate of 1.6×10^9 M^{-1} s^{-1}.[75]

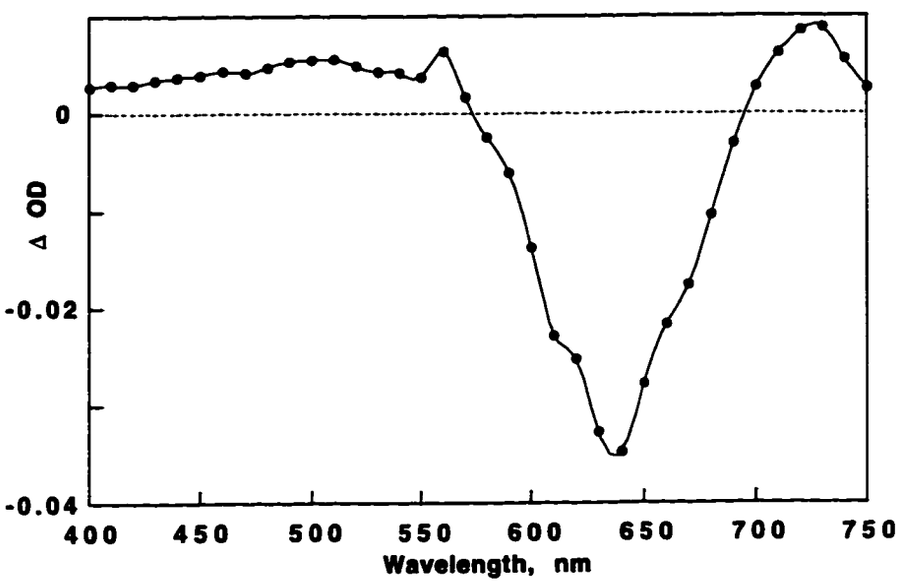

Figure 3.25 Transient spectrum obtained following 355 nm laser excitation of ZPTS in buffer, 1.1 μs after laser pulse.

ZPTS is water soluble and due to its anionic nature, it can be incorporated into protoplasts of *B. subtilis* and we have successfully incorporated ZPTS into U937 cells, simply by incubating the cells in buffer containing the probe and subsequently washing the cells by centrifugation. There is no doubt that incorporation occurs due to the fact that the cells take on the characteristic blue colour of the probe.

Unfortunately, upon incorporation, no transient signals can be obtained in the cellular environment. The size of the bleaching signal is quite small in solution, and this may contribute to the difficulty in detecting any bleaching in the cellular environment. ZPTS has been shown to deactivate Chinese hamster cells.[76, 77] The triplet state has been detected in

mouse myeloma cells, but singlet oxygen was not detected in these systems.[20]

3.5.Benzophenones

In a reducing environment, the triplet states of benzophenones and other carbonyl compounds will abstract hydrogen to form ketyl radicals.[12] It has been shown that when triplet radical pairs are formed in a restricted environment like micelles, the partition of this radical pair into products is strongly influenced by the micellar environment and by the application of magnetic fields.[12]

3.5.1.Benzoylbenzoic acid ethyl ester (BAEE)

Using benzophenone in this project is not straightforward. Its ground state does not have very high extinction coefficients at the excitation wavelengths optimal for cellular studies. Our success was therefore limited. A benzophenone derivative, benzoylbenzoic acid ethyl ester (BAEE, Figure 3.26) was successfully incorporated into whole cells of *B. subtilis* using liposomes for delivery.

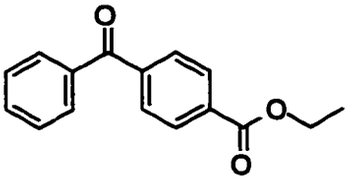

Figure 3.26 Structure of benzoylbenzoic acid ethyl ester (BAEE).

Figure 3.27 shows the BAEE triplet spectrum recorded in acetonitrile and the ketyl radical from BAEE recorded in isopropanol.

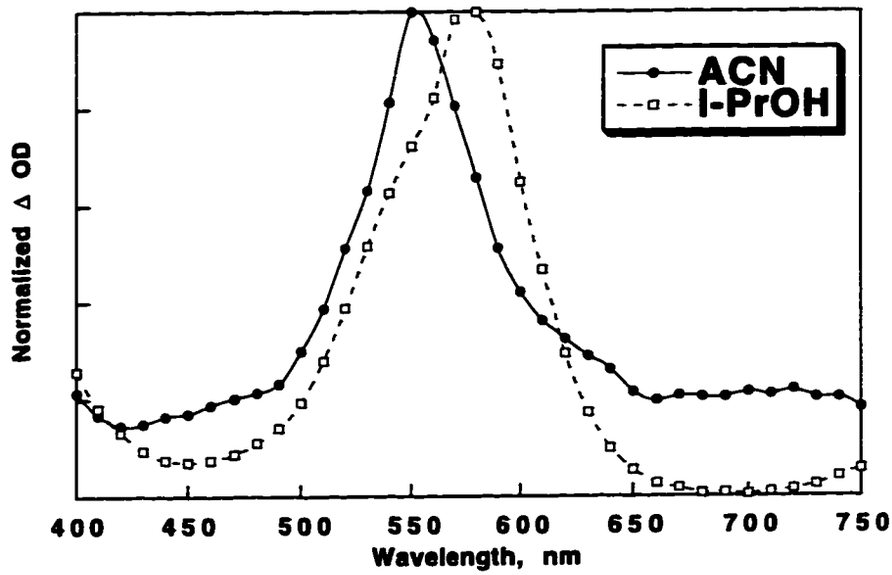

Figure 3.27 (○)Triplet BAEE in acetonitrile (lifetime 3 μs) and (❑) ketyl radical from BAEE in isopropanol (lifetime 12 μs). 308 nm excitation.

Figure 3.28 shows the transient spectrum obtained after 308 nm excitation of BAEE in whole cells of *B. subtilis*, using diffuse reflectance detection. The spectrum obtained is consistent with that of the ketyl radical shown in Figure 3.27, demonstrating that we can in fact generate and detect free radicals in living cells. In this case, the long lifetime of the transient measured is more diagnostic than the maximum absorption, though the longer wavelength absorption band in the cells is also consistent with the presence of ketyl radical and not triplet.

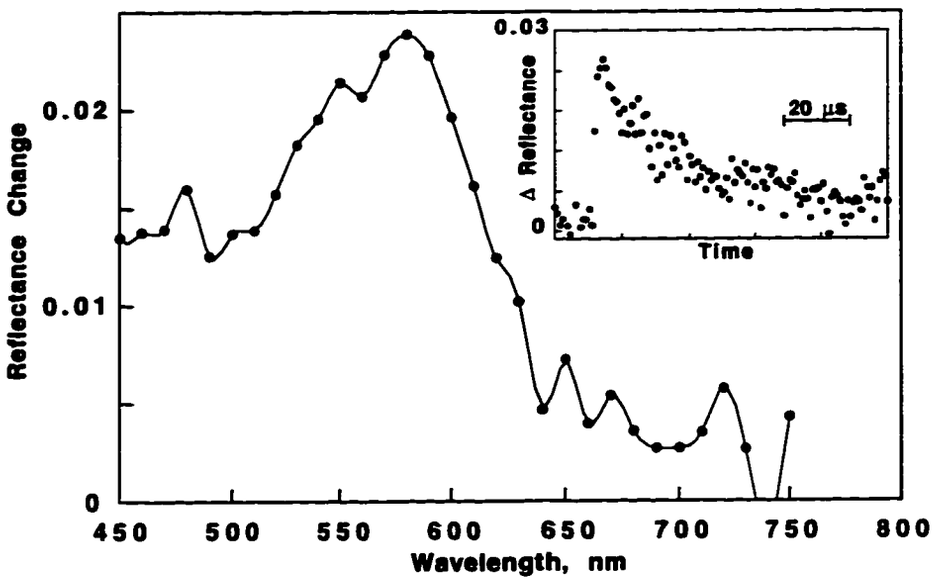

Figure 3.28 Transient spectrum recorded 1.6 μs after 355 nm laser excitation of BAEE in whole cells of *B. subtilis*.

3.5.2. Ketoprofen (KPF)

Ketoprofen (KPF) is a member of a group of drugs called non-steroidal anti-inflammatory drugs, or NSAIDs. Other drugs in this class are benoxaprofen, carpoprofen, ibuprofen, naproxen, and tiaprofenic acid.[78] KPF is used in the treatment of osteo-arthritis and other rheumatic diseases, usually applied topically as an ointment. There have been reports of dermatitis caused by KPF and others in this class, due to photosensitization.[79]

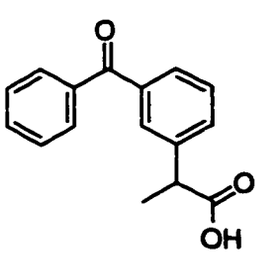

Figure 3.29 Structure of ketoprofen (KPF).

Costanzo and coworkers[78] showed that the photosensitization is most likely caused by a photohemolysis reaction involving free radicals, superoxide anion, and KPF photodegradation products. Chignell and coworkers[80] have recently shown that this photohemolysis is accelerated when a static external magnetic field is applied. A magnetic field does not accelerate the hemolysis caused by Protoporphyrin IX, which is believed to cause damage via singlet oxygen sensitization, as opposed to KPF which is believed to go through a free radical mechanism.[80]

In solution, the KPF triplet can be recorded by flash photolysis techniques. If the laser excitation is carried out in a reducing environment such as in isopropanol, the ketyl radical spectrum can be recorded, Figure 3.30. The triplet lifetime in acetonitrile was measured at 6 μs. In isopropanol, the ketyl radical lifetime is longer than can be measured by our system, i.e. >30 μs.

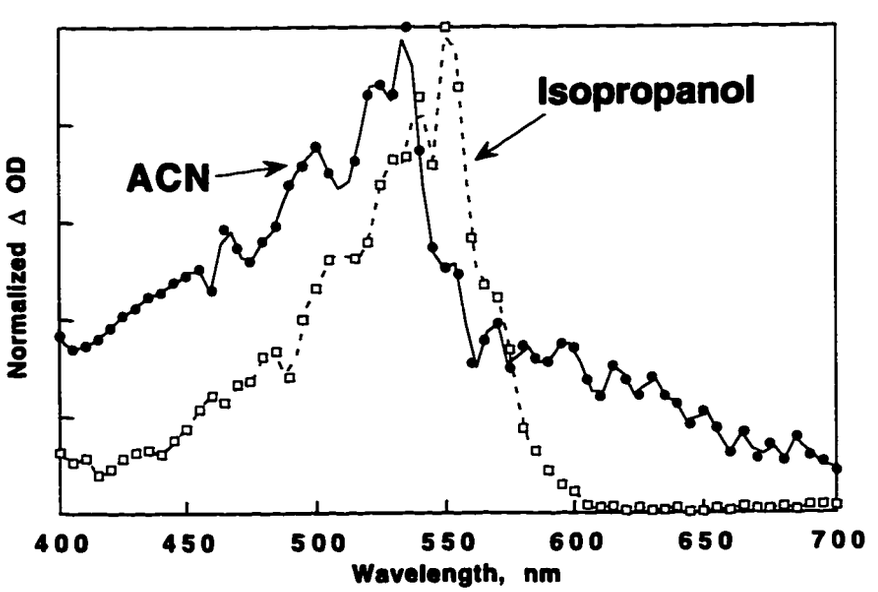

Figure 3.30 Transient spectra obtained following 337 nm laser excitation of KPF in (○)acetonitrile (2.4 μs after laser pulse) and (□)isopropanol (17.6 μs after laser pulse).

KPF was encapsulated into DPPC liposomes by the sonication method and studied by laser flash photolysis, using 337 nm excitation. The transient spectrum obtained is shown in Figure 3.31.

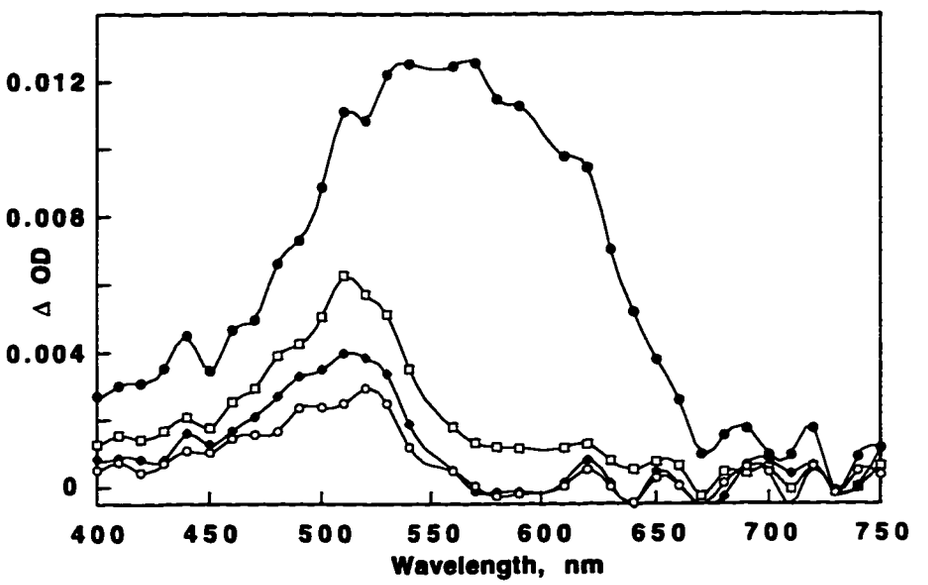

Figure 3.31 Transient spectra obtained following 337 nm laser excitation of KPF in DPPC liposomes. Spectra recorded 88 ns, 424 ns, 912 ns, and 1.48 μs after the laser pulse.

As can be seen in Figure 3.31, the transient spectra are not straightforward, and it is difficult to assign the transients. The kinetics at 520 nm and 600 nm are shown in Figure 3.32.

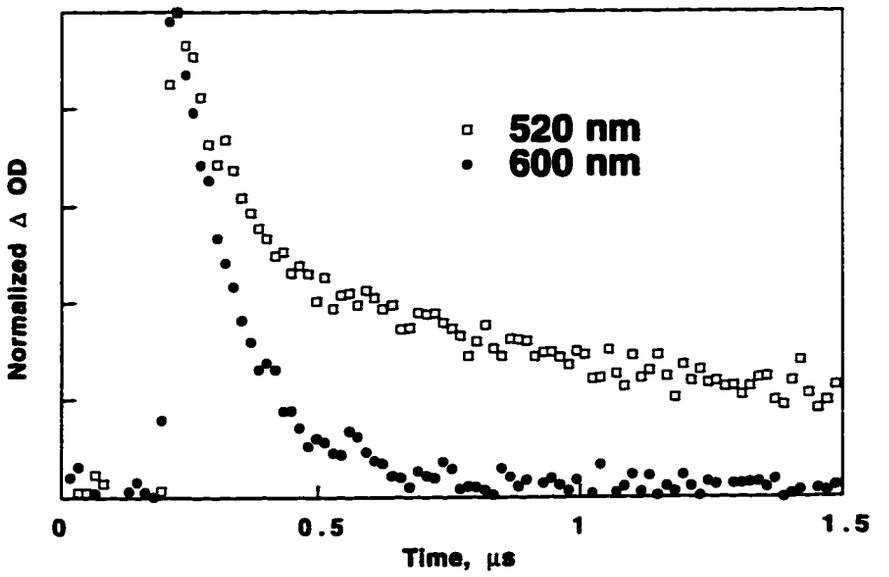

Figure 3.32 Decay traces at (□)520 nm and (○)600 nm following 337 nm laser excitation of KPF in DPPC liposomes.

The transient recorded at 600 nm decays by clean first-order kinetics with a lifetime of 125 ns. Although in solution the ketyl radical does not absorb at 600 nm, broadening of transient absorption bands can occur in organized systems.

We believe the long-lived signal with a maximum around 520 nm is a lipid-derived radical. This feature has been observed in systems using isopropylthioxanthone and perylene.

3.6.Anthraquinones

3.6.1.Anthraquinone-1,5-disulphonate in cultured skin (AQS)

Anthraquinone-1,5-disulphonate (AQS) is an anionic, water soluble, photoactive compound, whose ground state absorption tails out into the visible. These characteristics make it a suitable compound for study in this project.

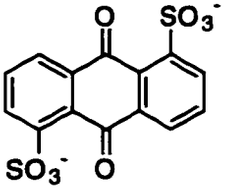

Figure 3.33 Structure of anthraquinone-1,5-disulphonate (AQS).

Figure 3.34 and Figure 3.35 show the transient spectra obtained after 355 nm excitation of AQS in the LSE model and the decay traces at 400 and 500 nm, respectively. The spectrum obtained in the LSE model shows two bands, with different decay kinetics, one centered at 400 nm and the other at 500 nm.

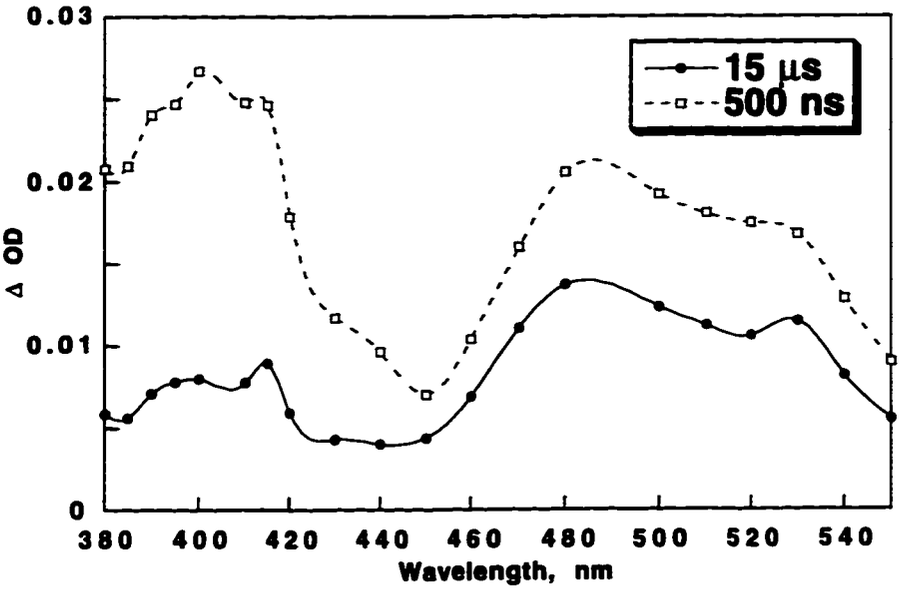

Figure 3.34 Transient spectra obtained following 355 nm laser excitation of AQS in LSE. (□)500 ns and (○)15 μs after laser pulse.

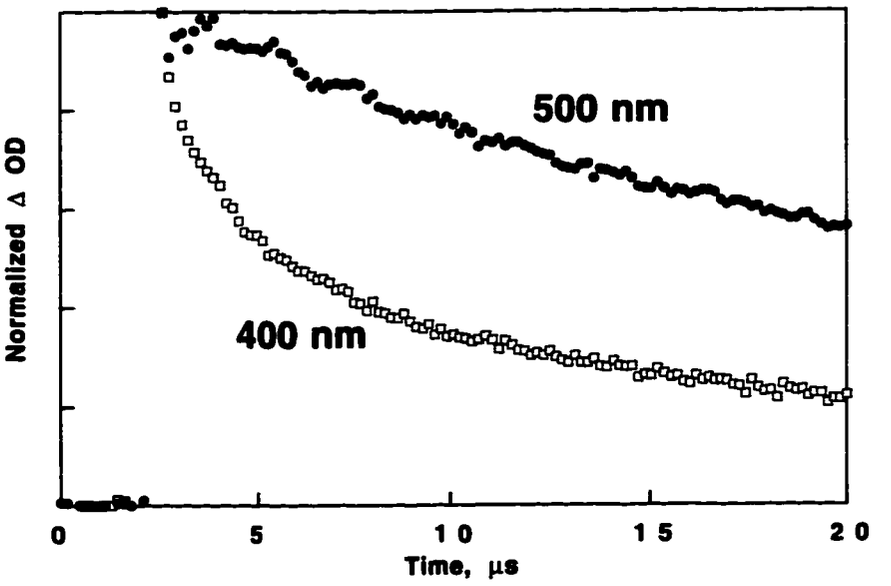

Figure 3.35 Decay traces recorded at (□)400 nm and (○)500 nm, following 355 nm laser excitation of AQS in LSE.

In the case of the ATS model, the long wavelength band is weaker and the short wavelength band has shifted to about 375 nm. The decay kinetics are similar to those found in the LSE model.

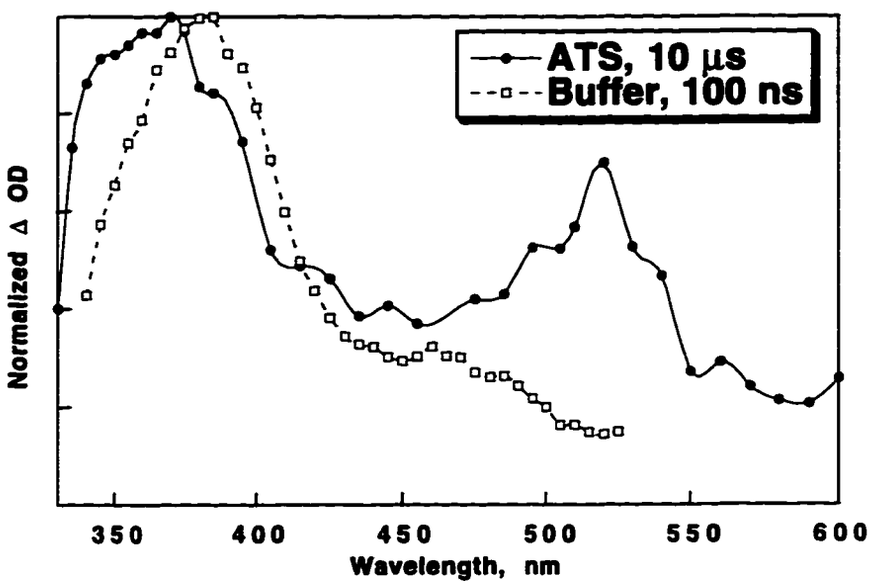

Figure 3.36 Comparison of transient spectra recorded following 355 nm laser excitation of AQS in (○)ATS skin model, 10 µs after laser pulse; and in (□)buffer, 100 ns after laser pulse.

In fact, the ATS model shows a spectrum much closer to that which is found in solution (pH 7 buffer), also shown in Figure 3.36. We note that the solution signal was 30-40 times stronger than those obtained in skin. None of these transients have been characterized in detail, although by analogy with several anthraquinones studied in solution[81, 82] it appears reasonable to assume that the band in the 360-400 nm region is due to the triplet state. The absorption in the 500 nm region most closely resembles the transient spectrum of the radical anion of the anthraquinone.[82]

To determine whether the mesh matrix contributed to the signals obtained in the ATS models, a control experiment was run with the blank mesh,

with no cultured cells attached. Treating the mesh the same way as the skin samples did not yield any significant transient signals.

3.6.2.Electron transfer reactions of AQS

Photophysics, photochemistry, and photo-induced electron transfer reactions of AQS and related compounds have been studied in detail.[82-90] Quinones play an important role in biological systems.[91-93]

In the case of AQS, the triplet state, the fluorescence from the singlet state, the semiquinone radical anion, and the semiquinone neutral radical have all been observed.[82] However, the radical cation, to the best of our knowledge, has never been observed for AQS or for any other related anthraquinone. We report the first observation of the AQS radical cation.

As reported by Moore and coworkers,[82] the AQS triplet state is short-lived and photostable in water. The triplet state spectrum shows maxima at 370 nm and 680 nm, which decay to baseline, with a lifetime of 140 ns. Nitrite ion, NO_2^-, quenches the triplet state of AQS with a rate constant of 2.6×10^8 M^{-1} s^{-1}, by an electron transfer mechanism to form the radical anion ($AQS^{\bullet -}$).[82] $AQS^{\bullet -}$ shows absorption maxima at 400 nm and 510 nm; it is a long-lived species which reacts with oxygen at a rate of 7×10^8 M^{-1} s^{-1}. On lowering the pH of the solution which generates the radical anion, Moore and coworkers were able to generate the neutral semiquinone radical, with an absorption maximum at 350 nm and a weak, broad absorption band centred at 660 nm. All of these results were reproduced in our study, and the transient spectra obtained are shown in Figure 3.37.

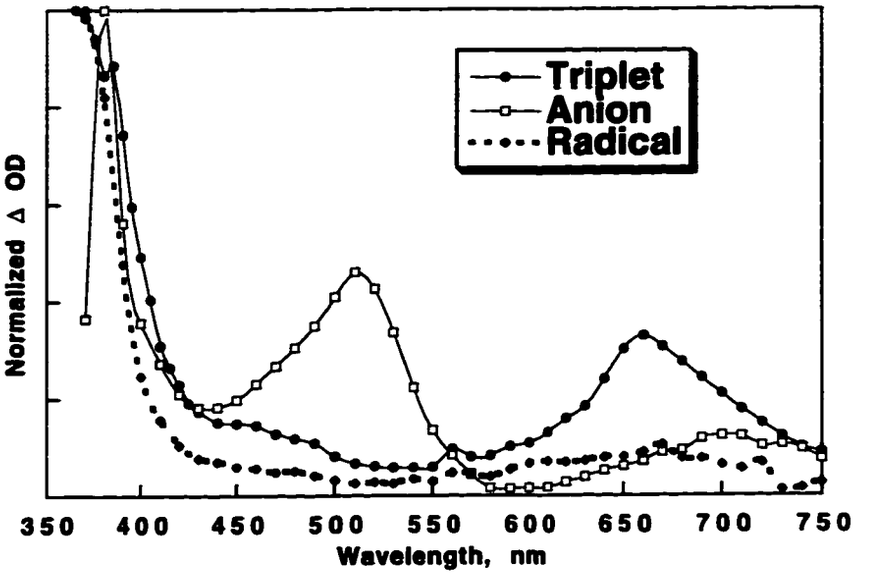

Figure 3.37 Transient spectra of AQS (○)triplet 48 ns after laser pulse, (□)radical anion 3.8 μs after laser pulse, and (◆)neutral radical, 40 ns after laser pulse. 355 nm laser excitation in water.

Methyl viologen is an efficient quencher of carbonyl triplets[94] through oxidation of the triplet being quenched.[95] Addition of 0.02 M methyl viologen (MV^{++}) to a solution of AQS in water quenches the triplet from a lifetime of 140 ns to 70 ns, but the characteristic absorption of the reduced methyl viologen is not detectable under nitrogen-saturated conditions. This may indicate that electron transfer may be occurring, but back-electron transfer may be following the quenching to give no net reaction, and no net formation of the oxidized and reduced species on the timescale of our experiment.

This behaviour has been observed for methyl viologen quenching of porphyrin triplets in aqueous solution.[63, 67, 94, 96-98] It was shown that if the electron donor and acceptor are of opposite charge, as in the case of AQS (-2) and methyl viologen (+2), "static" quenching can occur and back electron transfer occurs quickly, mainly due to the electrostatic attraction between the donor and the acceptor.

In order to disrupt this electrostatic attraction, the ionic strength of the aqueous solution was increased by adding 0.5 M NaCl. This resulted in the detection of long-lived signals which were not present in the absence of the salt, Figure 3.38.

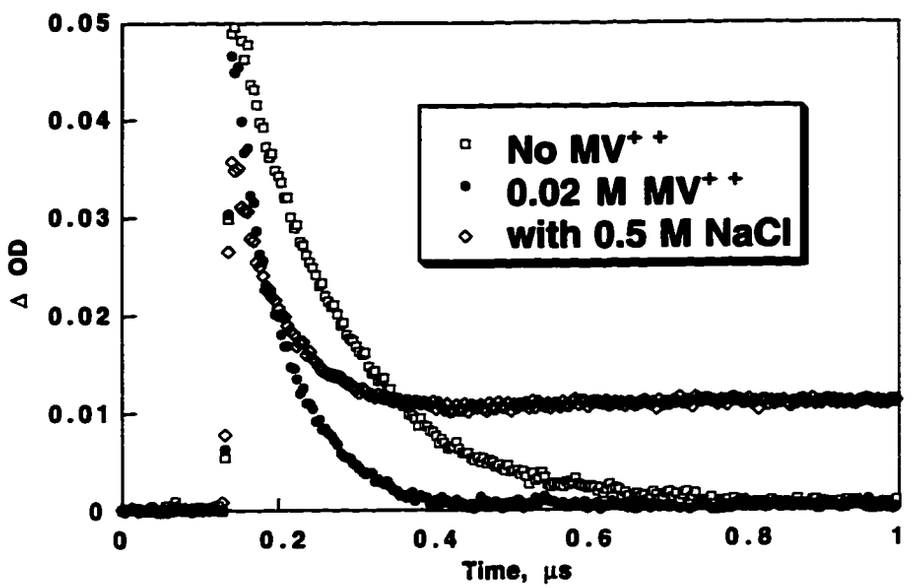

Figure 3.38 Decay traces obtained following 355 nm excitation of AQS in water, recorded at 370 nm. (□) AQS in water, (○) added 0.02 M MV^{++}, (◆) added 0.02 M MV^{++} and 0.5 M NaCl. Nitrogen-saturated solutions.

Thus it seems that the presence of NaCl prevents the back electron transfer from occurring as efficiently, and separation of the reduced methyl viologen and oxidized AQS may occur.

The transient spectrum obtained in the presence of NaCl contains more than one transient. It is known that the reduced methyl viologen species reacts very efficiently with oxygen[99] and the AQS triplet state has a short lifetime in the absence of any quenchers. Under air in aqueous solution (2.63×10^{-4} M O_2),[54] oxygen cannot compete with the quenching by 0.02 M methyl viologen. Therefore, in an air-saturated aqueous solution containing AQS, 0.02 M MV^{++}, and 0.5 M NaCl, the AQS triplet will be

quenched by MV^{++}, back-electron transfer will be retarded by the NaCl, the radical pair will separate, and the reduced methyl viologen species will quickly react with air. This will leave the oxidized AQS as the only species left in solution, since many radical cations do not react efficiently with oxygen.

Figure 3.39 shows the transient spectrum obtained under these conditions. The inset shows a decay trace recorded at 600 nm. What appears to be a fast decay at the beginning of the trace is the remaining triplet decay or possibly the reduced methyl viologen. The new transient, which we are tentatively assigning to the radical cation of AQS, has a lifetime of 8 μs in an air-saturated solution. It is possible that this is a hydrolysis product of the radical cation.

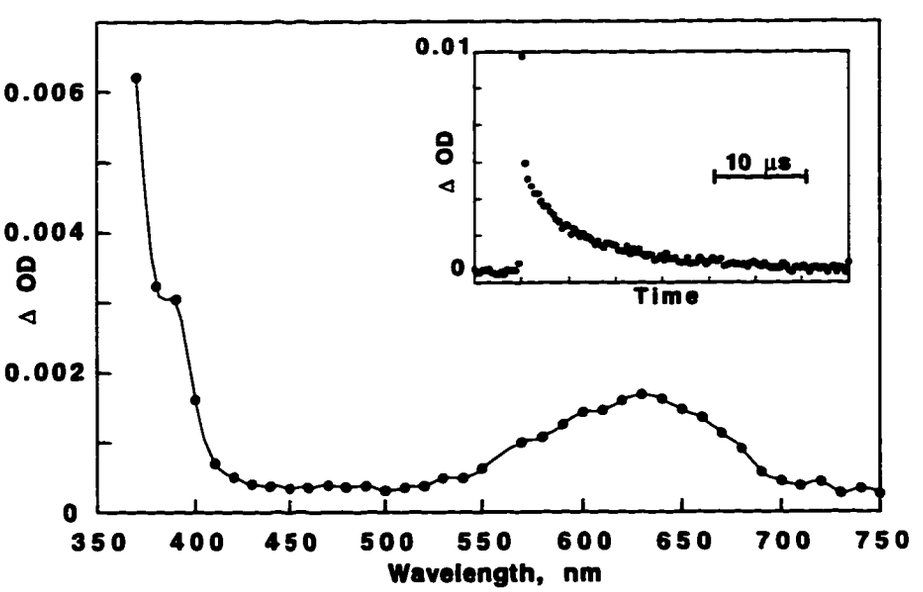

Figure 3.39 Transient spectrum of AQS•+ obtained by 355 nm laser excitation in an air-saturated aqueous solution with 0.02M MV^{++} and 0.5 M NaCl, recorded 3 μs after laser pulse. Inset: decay trace monitored at 600 nm.

3.7.Isopropylthioxanthone (ITX)

Xanthones and thioxanthones normally show triplet spectra that are very sensitive to the polarity of the media.[81]

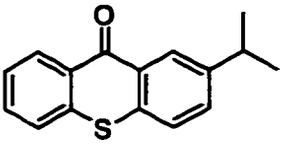

Figure 3.40 Structure of isopropylthioxanthone (ITX).

The position of the triplet absorption has frequently been employed as a polarity sensor; for example ITX show maxima at 610 and 655 nm in isopropanol and cyclohexane, respectively, shown in Figure 3.41.

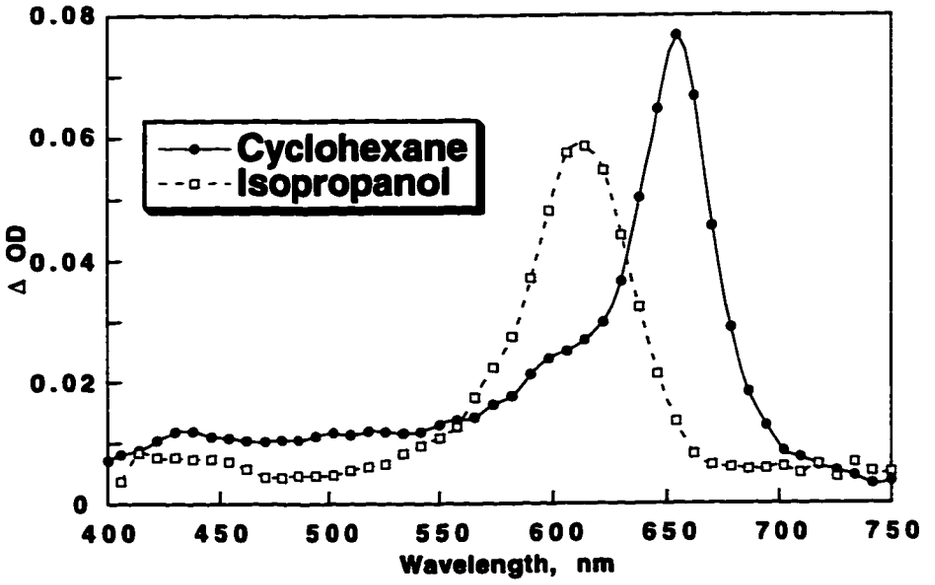

Figure 3.41 Transient spectra of the triplet state of isopropylthioxanthone recorded in (○)cyclohexane and in (□)isopropanol.

ITX was successfully incorporated into protoplasts and whole cells of *B. subtilis* using the liposome delivery method. The transient spectra

obtained following 355 nm excitation are shown in Figure 3.42, with a representative trace shown in the inset. In each of the environments, the triplet decay was very similar.

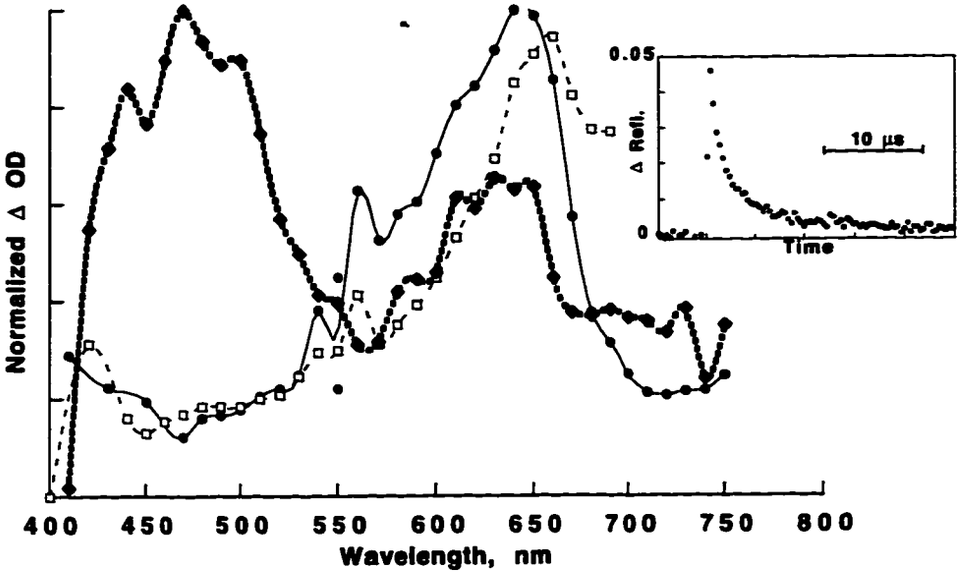

Figure 3.42 Transient spectra of ITX triplet state obtained following 355 nm excitation in (○)liposomes (transmission), (□)protoplasts (diffuse reflectance), and (◆)whole cells (diffuse reflectance), 1μs after laser pulse. Inset: typical decay trace monitored in protoplasts at 630 nm.

The spectra of Figure 3.42 suggest that the triplet is present predominantly in a rather hydrophobic environment, intermediate between the polarities of cyclohexane and isopropanol. The triplet half-lives were ~4 μs in all cases.

The signals at <520 nm in the case of whole cells may be due to radicals or to cell-derived transients. These signals are much longer lived and they resemble those obtained in two other cases. A similar band is observed in the case of ketoprofen (see Figure 3.31, page 207), and in the case of perylene in whole cells (see Figure 3.43). Perylene was incorporated using the liposome delivery method.

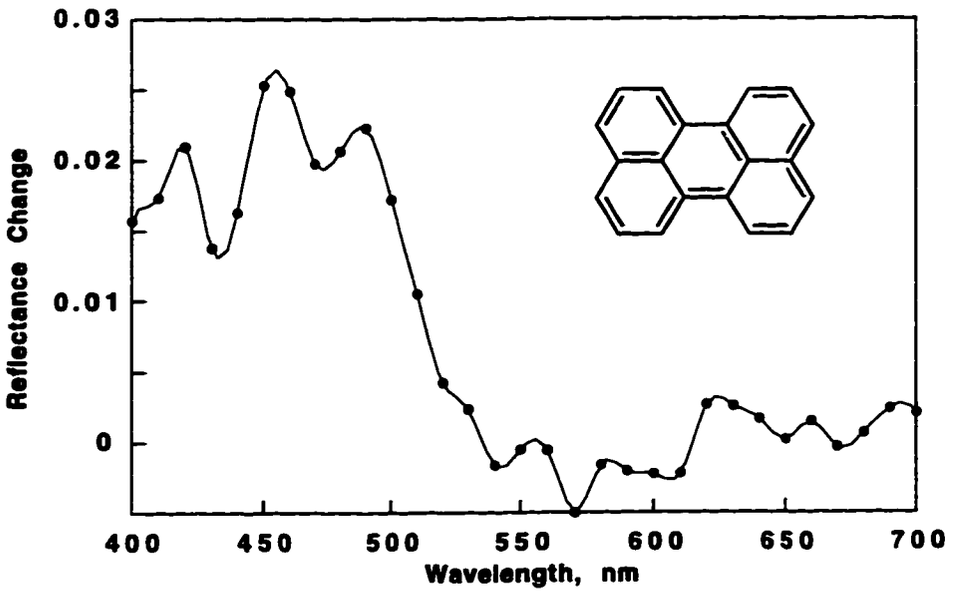

Figure 3.43 Transient spectrum obtained following 355 nm laser excitation of perylene in whole cells of *B. subtilis*. 16 μs after laser pulse. Inset: Structure of perylene.

This species is neither the triplet, nor one of the radical ions of perylene.[100] Conceivably it may be cell-derived and produced only in the presence of appropriate sensitizers.

3.8.Conclusions

Much of the lessons learned as a result of carrying out this project have been covered in the introduction and in the incorporation section of this chapter.

There is no doubt that this work shows great potential in studying the behaviour of photoactive compounds in microheterogeneous environments of biological relevance. Much has been learned in terms of handling the systems and delivering the probes to their target environments.

When studying model systems in photobiology, one must continuously evaluate the relevance of the system being studied to the native system being modeled. It is clear that transmission studies in skin samples as discussed in this chapter are interesting but any study in an *in vivo* skin system would necessitate diffuse reflectance detection, since the test subject would provide an optically opaque medium behind the skin at the time of the study. Also, one of the main reasons why transmission studies were possible in the case of the skin models was the fact that the samples were very thin. This means that the lengths of the optical paths for excitation and monitoring beams are short (on the order of less than 2 millimeters). These short pathlengths force us to use probes with relatively high extinction coefficients and high concentrations in order to obtain adequate absorbances in the precursor and in the transient. Again, this may force us to create systems which are not typical of the native environment being studied. The relationship of the optical properties of in vitro vs. *in vivo* studies of skin has been dealt with before[101] and these factors should of course be considered when attempting to extrapolate results from model systems to native systems.

We believe that the most promising work in terms of further study are the ketoprofen system and the ALA-PPIX system. The work by Chignell and coworkers[80] shows a direct link between benzophenone-type chemistry and magnetic field effects. Showing an effect in a time-resolved manner would be an important finding. Similarly, ALA proved to be a very elegant way to include a porphyrin molecule into a cell. The world of photodynamic therapy lacks good time-resolved data to really elucidate the mechanism of action of these photosensitizers, and ALA may be the first step to one approach of addressing this problem.

3.9.Experimental

Benzophenone, 4-benzylbenzoic acid ethyl ester, α-terthienyl, 5-amino-levulinic acid, methyl viologen, mesoporphyrin IX, protoporphyrin IX, ketoprofen, and anthraquinone-1,5-disulfonate were purchased from Aldrich Chemical Co. (Milwaukee, WI) and used as received.

Casamino acids, tryptophan, dipalmitoylphosphatidylcholine, and chicken egg white lysozyme were purchased from Sigma Chemical Co. (St. Louis, MO) and were used as received.

Phthalocyanine tetrasulfonate and zinc phthalocyanine tetrasulfonate were purchased from Porphyrin Products (Logan, Utah) and were used as received.

Isopropylthioxanthone was a generous gift from Shipley Co. (Marlboro, MA), and was used as received. It may contain more than one isomer, but substitution should be predominantly in the 2-position.

The Skin^2 ZK1300 skin model was purchased from Advanced Tissue Sciences (La Jolla, California) and was used as directed by the manufacturer. The Living Skin Equivalent skin model was purchased from Organogenesis, Inc. (Canton, Massachusetts) and was used as directed by the manufacturer.

Protoplast maintenance buffer (PMB) is 0.5 M sucrose containing 5 g/L K_2HPO_4, 4 g/L $MgCl_2$, and 10 mg/L bovine serum albumin.

B. subtilis cells were cultured in Bacto nutrient broth from Difco Labs (Detroit, MI). Mammalian cells were cultured in RPMI 1640 and 10% fetal calf serum from Gibco-BRL.

For electroporation, the *B. subtilis* culture was grown in Spizizen salts enriched with casamino acids and tryptophan for 12 hours. The cells were washed twice with cold 1 mM (240 mg/L) HEPES (N-2-hydroxyethyl-piperazine-N'-ethanesulfonic acid) buffer. Cells were electroporated with HG buffer (1 mM HEPES with 10 % glycerol).[29]

Protoplasts were prepared by incubating washed cells with 100 mg/L chicken egg white lysozyme in PMB for approximately 1 hour at 30 °C, or until cells appeared spherical by inspection with the microscope.

Frozen samples of *B. subtilis* were stored long term by first inducing sporylation in regular growth medium enriched with 5 g/L yeast extract, 100 mg/L $CaCl_2$, 200 mg/L $MgCl_2$, and 10 mg/L $MnCl_2$. Once sporylated, the cells were washed and resuspended in 15% glycerol/H_2O. These must be stored at -40 °C or lower. Short term storage (< 1 week) can be carried out by storing a grown culture in the refrigerator and using it to inoculate a fresh medium.

The laser flash photolysis equipment is described in a separate chapter in this thesis.

3.10.References

[1] J. K. Thomas, "Radiation-Induced Reactions in Organized Assemblies," *Chem. Rev.*, **80** (4) , 283, **1980.**

[2] M. Barra, C. Bohne, A. Zanocco, and J. C. Scaiano, "Exploratory Study of the Application of Transmission and Diffuse-Reflectance Laser Techniques in the Study of Free Radical Processes in Vesicles," *Photochem. Photobiol.*, **8** , 2390, **1992.**

[3] F. Wilkinson and G. Kelly, "Diffuse Reflectance Flash Photolysis," in *Handbook of Organic Photochemistry*, vol. I, J. C. Scaiano, Ed. Boca Raton, Florida: CRC Press, **1989**, pp. 293.

[4] R. W. Kessler and F. Wilkinson, "Diffuse Reflectance Triplet-Triplet Absorption Spectroscopy of Aromatic Hydrocarbons Chemisorbed on γ-Alumina," *J. Chem. Soc., Faraday Trans. 1*, **77** , 309, **1981.**

[5] R. B. Draper and M. A. Fox, "Titanium Dioxide Photosensitized Reactions Studied by Diffuse Reflectance Flash Photolysis in Aqueous Suspensions of TiO_2 Powder," *Langmuir*, **6** , 1396, **1990.**

[6] R. B. Draper and M. A. Fox, "Titanium Dioxide Photooxidation of Thiocyanate. $(SCN)_2^{\bullet-}$ Studied by Diffuse Reflectance Flash Photolysis," *J. Phys. Chem.*, **94** , 4628, **1990.**

[7] K. McLauchlan, "Are Environmental Magnetic Fields Dangerous?," *Physics World* (January) , 41, **1992.**

[8] B. Hileman, "Health Effects of Electromagnetic Fields Remain Unresolved," *C&EN* (November 8) , 15, **1993.**

[9] G. Taubes, "EMF-Cancer Links: Yes, No, and Maybe," *Science*, **262** (29 October) , 649, **1993.**

[10] J. C. Scaiano, N. Mohtat, F. L. Cozens, J. McLean, and A. Thansandote, "Application of the Radical Pair Mechanism to Free Radicals in Organized Systems: Can the Effects of 60 Hz Be Predicted From Studies Under Static Fields?," *Bioelectromagnetics*, **15** (6) , 549, **1994.**

[11] J. C. Scaiano, F. L. Cozens, and J. McLean, "Model for the Rationalization of Magnetic Field Effects *in vivo*. Application of the Radical-Pair Mechanism to Biological Systems," *Photochem. Photobiol.*, **59** (6) , 585, **1994.**

[12] J. C. Scaiano, E. B. Abuin, and L. C. Stewart, "Photochemistry of Benzophenone in Micelles. Formation and Decay of Radical Pairs," *J. Am. Chem. Soc.*, **104** (21) , 5673, **1982.**

[13] D. Dolphin, "1993 Syntex Award Lecture: Photomedicine and Photodynamic Therapy," *Can. J. Chem.*, **72** (4) , 1005, **1994.**

[14] F. C. Neidhardt, J. L. Ingraham, and M. Schaechter, *Physiology of the Bacterial Cell: A Molecular Approach*. Sunderland, Massachusetts: Sinauer Associates, Inc., **1990.**

[15] M. Craw, R. Redmond, and T. G. Truscott, "Laser Flash Photolysis of Haematoporphyrins in some Homogeneous and Heterogeneous Environments," *J. Chem. Soc., Faraday Trans. I*, **80** , 2293, **1984.**

[16] E. Bell, M. Rosenburg, P. Kemp, R. Gay, G. D. Green, N. Muthukumaran, and C. Nolte, "Recipes for Reconstituting Skin," *J. Biomech. Engineering*, **113** (May) , 113, **1991.**

[17] B. Coulomb, C. Lebreton, and L. Dubertret, "The Skin Equivalent: A Model for Skin and General Pharmacology," in *Models in Dermatology*, vol. 4, H. I. Maibach and N. J. Lowe, Eds. Basel: Karger, **1989**, pp. 20.

[18] P. Contard, R. L. Bartel, L. Jacobs II, J. S. Perlish, E. D. MacDonald II, L. Handler, D. Cone, and R. Fleischmajer, "Culturing Keratinocytes and Fibroblasts in a Three-Dimensional Mesh Results in Epidermal Differentiation and Formation of a Basal Lamina-Anchoring Zone," *J. Invest. Derm.*, **100** (1) , 35, **1993**.

[19] T. G. Truscott, A. J. McLean, A. M. R. Phillips, and W. S. Foulds, "Detection of Haematoporphyrin Derivative and Haematoporphyrin Excited States in Cell Environments," *Cancer Letters*, **41** , 31, **1988**.

[20] P. A. Firey, T. W. Jones, G. Jori, and M. A. J. Rodgers, "Photoexcitation of Zinc Phthalocyanine in Mouse Myeloma Cells: The Observation of Triplet States but not of Singlet Oxygen," *Photochem. Photobiol.*, **48** (3) , 357, **1988**.

[21] P. A. Firey and M. A. J. Rodgers, "Photochemical Properties of Erythrocyte Ghosts Containing Porphyrin," *Photochem. Photobiol.*, **47** (5) , 615, **1988**.

[22] B. M. Aveline, T. Hasan, and R. W. Redmond, "The Effects of Aggregation, Protein Binding, and Cellular Incorporation on the Photophysical Properties of Benzoporphyrin Derivative Monoacid Ring A (BPDMA)," *J. Photochem. Photobiol., B: Biology*, **30** (2-3) , 161, **1995**.

[23] J. E. Roberts, S. J. Atherton, and J. Dillon, "Detection of Porphyrin Excited States in the Intact Bovine Lens," *Photochem. Photobiol.*, **54** (5) , 855, **1991**.

[24] T. C. Oldham, I. V. Eigenbrot, B. Crystall, and D. Phillips, "Photophysics of Photosensitising Dyes in Living Cell Suspensions," *SPIE*, **2625** , 266, **1995.**

[25] K. Nakagawa, "Direct Observation of Laser Generated Free Radicals from a Myocardium Target Site," *Free Radical Biol. Med.*, **12** , 241, **1992.**

[26] B. A. Jurkiewicz and G. R. Buettner, "EPR Detection of Free Radicals in UV-Irradiated Skin: Mouse *Versus* Human," *Photochem. Photobiol.*, **64** (6) , 918, **1996.**

[27] C. Bohne, R. Konuk, and J. C. Scaiano, "Dynamics of the Redistribution of 1-Dodecylpyrene Aggregates in Micellar Solution," *Chem. Phys. Lett.*, **152** , 156, **1988.**

[28] T. D. Brock, D. W. Smith, and M. T. Madigan, *Biology of Microorganisms*, 4th ed. Englewood Cliffs, New Jersey: Prentice-Hall, Inc., **1984.**

[29] P. Brigidi, E. De Rossi, M. L. Bertarini, G. Riccardi, and D. Matteuzzi, "Genetic Transformation of Intact Cells of *Bacillus subtilis* by Electroporation," *FEMS Microbiol. Let.*, **67** , 135, **1990.**

[30] D. Voet and J. G. Voet, *Biochemistry*. New York: John Wiley & Sons, **1990.**

[31] L. T. Boni and S. W. Hui, in *Cell Fusion*, A. E. Sowers, Ed. New York: Plenum Press, **1987**, pp. 301.

[32] N. Düzgünes, J. A. Goldstein, D. S. Friend, and P. L. Felgner, "Fusion of Liposomes Containing a Novel Cationic Lipid, N-[2,3-(Dioleyloxy)propyl]-N, N,N-trimethylammonium: Induction by

Multivalent Anions and Asymmetric Fusion with Acidic Phospholipid Vesicles," *Biochemistry*, **28** , 9179, **1989**.

[33] T. D. Heath, in *Methods in Enzymology*, vol. 149, pt. B, R. Green and K. J. Widdler, Eds. New York: Academic Press, **1987**, pp. 135.

[34] S. Tomlinson, P. W. Taylor, and J. P. Luzio, "Transfer of Phospholipid and Protein into the Envelope of Gram-Negative Bacteria by Liposome Fusion," *Biochemistry*, **28** (21) , 8303, **1989**.

[35] J. Wilschut and D. Hoekstra, *Chem. Phys. Lipids*, **40** , 145, **1986**.

[36] R. S. Handley, A. J. Stern, and A. P. Schaap, "Effects of Heteroatom Substituents on the Properties of 1,2-Dioxetanes," *Tetrahedron Lett.*, **26** (27), 3183, **1985**.

[37] D. Hoekstra, T. deBoer, K. Klappe, and J. Wilschut, "Fluorescence Method for Measuring the Kinetics of Fusion Between Biological Membranes," *Biochemistry*, **23** (24) , 5675, **1984**.

[38] D. Hoekstra, K. Klappe, H. Hoff, and S. Nir, "Mechanism of Fusion of Sendai Virus: Role of Hydrophobic Interactions and Mobility Constraints of Viral Membrane Proteins," *J. Biol. Chem.*, **264** (12) , 6786, **1989**.

[39] M. Salman, M. Tarshis, and S. Rottem, "Small Unilamellar Vesicles are able to Fuse with *Mycoplasma capricolum* Cells," *Biochim. Biopys. Acta*, **1063** , 209, **1991**.

[40] J. K. Rose, L. Buonocore, and M. A. Whitt, "A New Cationic Liposome Reagent Mediating Nearly Quantitative Transfection of Animal Cells," *Biotechniques*, **10** (4) , 520, **1991**.

[41] A. M. Richter, E. Waterfield, A. K. Jain, A. J. Canaan, B. A. Allison, and J. G. Levy, "Liposomal Delivery of a Photosensitizer, Benzoporphyrin Derivative Monoacid Ring A (BPD), to Tumor Tissue in a Mouse Tumor Model," *Photochem. Photobiol.*, **57** (6) , 1000, **1993**.

[42] J. M. H. Kremer, M. W. J. v. d. Esker, C. Pathmamanoharan, and P. H. Wiersema, "Vesicles of Variable Diameter Prepared by a Modified Injection Method," *Biochemistry*, **16** (17) , 3932, **1977**.

[43] D. Weir, J. C. Scaiano, J. T. Arnason, and C. Evans, "Photochemistry of the Phototoxic Polyacetylene Phenylheptatriyne," *Photochem. Photobiol.*, **42** , 223, **1985**.

[44] J. T. Arnason, B. J. R. Philogène, P. Morand, K. Imrie, S. Iyengar, F. Duval, C. Soucy-Breau, J. C. Scaiano, N. H. Werstiuk, B. Hasspieler, and A. E. R. Downe, "Naturally Occurring and Synthetic Thiophenes as Photoactivated Insecticides," *ACS Symp. Ser.*, **387** , 164, **1989**.

[45] C. H. Evans and J. C. Scaiano, "Photochemical Generation of Radical Cations from α-Terthienyl and Related Thiophenes: Kinetic Behaviour and Magnetic Field Effects on Radical-Ion Pairs in Micellar Solution," *J. Am. Chem. Soc.*, **112** , 2694, **1990**.

[46] J. C. Scaiano, A. MacEachern, J. T. Arnason, P. Morand, and D. Weir, "Singlet Oxygen Generating Efficiency of α-Terthienyl and Some of its Synthetic Analogues," *Photochem. Photobiol.*, **46** (2) , 193, **1987**.

[47] J. C. Scaiano, R. W. Redmond, B. Mehta, and J. T. Arnason, "Efficiency of the Photoprocesses Leading To Singlet Oxygen ($^1\Delta_g$) Generation by α-Terthienyl: Optical Absorption, Optoacoustic Calorimetry and Infrared Luminescence Studies," *Photochem. Photobiol.*, **52** (4) , 655, **1990**.

[48] C. Evans, D. Weir, J. C. Scaiano, A. Mac Eachern, J. T. Arnason, P. Morand, B. Hollebone, L. C. Leitch, and B. J. R. Philogène, "Photochemistry of the Botanical Phototoxin, α-Terthienyl and some Related Compounds," *Photochem. Photobiol.*, **44** (4) , 441, **1986.**

[49] J. C. Scaiano, C. Evans, and J. T. Arnason, "Characterization of α–Terthienyl Radical Cation: Evidence Against Electron Transfer to Oxygen *In Vitro*," *J. Photochem. Photobiol. B: Biol.*, **3** , 411, **1989.**

[50] M. Sasaki, S. Koyama, K. Tokiwa, and H. Fujita, "Intracellular Target for α-Terthienyl Photosensitization: Involvement of Lysosomal Membrane Damage," *Photochem. Photobiol.*, **57** (5) , 796, **1993.**

[51] A. C. Allison, I. A. Magnus, and M. R. Young, "Role of Lysosomes and of Cell Membranes in Photosensitization," *Nature*, **209** , 874, **1966.**

[52] E. B. Abuin and E. A. Lissi, "Diffusion and Concentration of Oxygen in Microheterogeneous Systems. Evaluation from Luminescence Quenching Data," *Prog. Reaction Kinetics*, **16** , 1, **1991.**

[53] E. S. Smotkin, F. T. Moy, and W. Z. Plachy, "Dioxygen Solubility in Aqueous Phosphatidylcholine Dispersions," *Biochim. Biophys. Acta*, **1061** , 33, **1991.**

[54] A. J. Gordon and R. A. Ford, *The Chemist's Companion: a Handbook of Practical Data, Techniques, and References*. New York: John Wiley & Sons, **1972.**

[55] J. P. Reyftmann, J. Kagan, R. Santus, and P. Morliere, "Excited State Properties of α-Terthienyl and Related Molecules," *Photochem. Photobiol.*, **41** (1) , 1, **1985.**

[56] N. Mohtat, personal communication, **1996.**

[57] F. Ricchelli, G. Jori, G. Moreno, F. Vinzens, and C. Salet, "Factors Influencing the Distribution Pattern of Porphyrins in Cell Membranes," *J. Photochem. Photobiol. B: Biol*, **6** , 69, **1990**.

[58] K. W. Woodburn, N. J. Vardaxis, J. S. Hill, A. H. Kaye, and D. R. Phillips, "Subcellular Localization of Porphyrins using Confocal Laser Scanning Microscopy," *Photochem. Photobiol.*, **54** (5) , 725, **1991**.

[59] A. Harriman and A. O. Osborne, "Luminescence of Porphyrins and Metalloporphyrins. Part 6.-Luminescence of Aluminum(III) Tetraphenylporphine and its μ-Oxo Dimer," *J. Chem. Soc., Faraday Trans. 1*, **79** , 765, **1983**.

[60] G. J. Smith, "A Long-Lived Transient Resulting from Flash Photolysis of Hematoporphyrin in Aqueous Solution," *J. Photochem. Photobiol. B: Biol.*, **12** , 29, **1992**.

[61] R. S. Sinclair, D. Tait, and T. G. Truscott, "Triplet States of Protoporphyrin IX and Protoporphyrin IX Dimethyl Ester," *J. Chem. Soc., Faraday Trans. I*, **76** , 417, **1980**.

[62] E. Reddi, G. Jori, M. A. J. Rodgers, and J. D. Spikes, "Flash Photolysis Studies of Hemato- and Copro-Porphyrins in Homogeneous and Microheterogeneous Aqueous Dispersions," *Photochem. Photobiol.*, **38** (6), 639, **1983**.

[63] G. S. Nahor, J. Rabani, and F. Grieser, "Properties of Excited Tetrakis(sulfonatophenyl)porphyrin in Aqueous Solutions. Photoredox Reactions with Quenchers.," *J. Phys. Chem.*, **85** (6) , 697, **1981**.

[64] A. F. Mironov, A. N. Nizhnik, and A. Y. Nockel, "Hematoporphyrin Derivatives: An Oligomeric Composition Study," *J. Photochem. Photobiol. B: Biol*, **4** , 297, **1990**.

[65] C. R. Lambert, E. Reddi, J. D. Spikes, M. A. J. Rodgers, and G. Jori, "The Effects of Porphyrin Structure and Aggregation State on Photosensitized Processes in Aqueous and Micellar Media," *Photochem. Photobiol.*, **44** (5) , 595, **1986**.

[66] J. P. Keene, D. Kessel, E. J. Land, R. W. Redmond, and T. G. Truscott, "Direct Detection of Singlet Oxygen Sensitized by Haematoporphyrin and Related Compounds," *Photochem. Photobiol.*, **43** (2) , 117, **1986**.

[67] A. Harriman, G. Porter, and P. Walters, "Photo-oxidation of Metalloporphyrins in Aqueous Solution," *J. Chem. Soc., Faraday Trans. 1*, **79** , 1335, **1983**.

[68] E. Gross, B. Ehrenberg, and F. M. Johnson, "Singlet Oxygen Generation by Porphyrins and the Kinetics of 9,10-Dimethylanthracene Photosensitization in Liposomes," *Photochem. Photobiol.*, **57** (5) , 808, **1993**.

[69] G. Grabner, N. Getoff, T. Gantchev, D. Angelov, and M. Shopova, "Hydrated Electron Formation in Nanosecond and Picosecond Laser Flash Photolysis of Hematoporphyrin in Aqueous Solution," *Photochem. Photobiol.*, **54** (5) , 673, **1991**.

[70] J. Feitelson and N. Barboy, "Triplet-State Reactions of Zinc Protoporphyrins," *J. Phys. Chem.*, **90** (2) , 271, **1986**.

[71] D. X. G. Divaris, J. C. Kennedy, and R. H. Pottier, "Phototoxic Damage to Sebaceous Glands and Hair Follicles of Mice After Systemic

Administration of 5-Aminolevulinic Acid Correlates with Localized Protoporphyrin IX Fluorescence," *Am. J. Pathol.*, **136** (4) , 891, **1990**.

[72] P. J. Muller and B. C. Wilson, "Photodynamic Therapy of Malignant Primary Brain Tumours: Clinical Effects, Post-Operative ICP, and Light Penetration of the Brain.," *Photochem. Photobiol.*, **46** , 929, **1987**.

[73] A. R. Butler and S. George, "The Nonenzymatic Cyclic Dimerization of 5-Aminolevulinic Acid," *Photochem. Photobiol.*, **48** (37) , 7879, **1992**.

[74] R. H. Poittier, Y. F. A. Chow, J.-P. LaPlante, T. G. Truscott, J. C. Kennedy, and L. A. Beiner, "Non-Invasive Technique for Obtaining Fluorescence Excitation and Emission Spectra *in vivo*," *Photochem. Photobiol.*, **44** (5) , 679, **1986**.

[75] J. D. Spikes, "Phthalocyanines as Photosensitizers in Biological Systems and for the Photodynamic Therapy of Tumors," *Photochem. Photobiol.*, **43** (6) , 691, **1986**.

[76] E. Ben-Hur and I. Rosenthal, "Photosensitized Inactivation of Chinese Hamster Cells by Phthalocyanines," *Photochem. Photobiol.*, **42** (2), 129, **1985**.

[77] N. Brasseur, H. Ali, D. Autenrieth, R. Langlois, and J. E. van Lier, "Biological Activities of Phthalocyanines-III. Photoinactivation of V-79 Chinese Hamster Cells by Tetrasulfophthalocyanines," *Photochem. Photobiol.*, **42** (5) , 515, **1985**.

[78] L. L. Costanzo, G. De Guidi, G. Condorelli, A. Cambria, and M. Fama, "Molecular Mechanism of Drug Photosensitization - II. Photohemolysis Sensitized by Ketoprofen," *Photochem. Photobiol.*, **50** (3) , 359, **1989**.

[79] A. Alomar, "Ketoprofen Photodermatitis," *Contact Dermatitis*, **12** , 112, **1985.**

[80] C. F. Chignell and R. H. Sik, "Magnetic Field Effects on the Photohemolysis of Human Erythrocytes by Ketoprofen and Protoporphyrin IX," *Photochem. Photobiol.*, **62** (1) , 205, **1995.**

[81] I. Carmichael and G. L. Hug, "Triplet-Triplet Absorption Spectra of Organic Molecules in Condensed Phases," *J. Phys. Chem. Ref. Data*, **15** (1) , 1, **1986.**

[82] J. N. Moore, D. Phillips, N. Nakashima, and K. Yoshihara, "Photophysics and Photochemistry of Sulphonated Derivatives of 9,10-Anthraquinone. 'Strong' *versus* 'Weak' Sensitizers," *J. Chem. Soc., Faraday Trans. 2*, **83** (8) , 1487, **1987.**

[83] A. D. Broadbent, "Photochemical Reactions of 9,10-Anthraquinones in Water," *J. Chem. Soc., Chem. Comm.* , 382, **1967.**

[84] A. D. Broadbent and R. P. Newton, "Photolysis of Aqueous Solutions of 9,10-Anthraquinone-2-sulfonate. Part I. Dependence of Product Yields on Reaction Conditions," *Can. J. Chem.*, **50** , 381, **1972.**

[85] V. A. Kuzmin, A. K. Chibisov, and A. V. Karyakin, "Decay Kinetics of the Triplet and Anthrasemiquinone Radicals in Aqueous Organic Media," *Int. J. Chem. Kin.*, **4** , 639, **1972.**

[86] I. Loeff, A. Treinin, and H. Linschitz, "Photochemistry of 9,10-Anthraquinone-2-sulfonate in Solution. 1. Intermediates and Mechanism," *J. Phys. Chem.*, **87** (14) , 2536, **1983.**

[87] V. G. Chamupathi and G. Tollin, "Quinones as Mediators of Electron Transfer from Membrane-Bound Chlorophyll to Cytochrome *c* in

the Aqueous Phase in Lipid Bilayer Vesicles: Synergistic Enhancement of Cytochrome *c* Reduction by Lipophilic/Hydrophilic Quinone Pairs," *Photochem. Photobiol.*, **51** (5) , 611, **1990.**

[88] I. Loeff, S. Goldstein, A. Treinin, and H. Linschitz, "Interactions of Formate Ion with Triplets of Anthraquinone-2-sulfonate, 1,4-Naphthoquinone, Benzophenone-4-carboxylate and Benzophenone-4-sulfonate," *J. Phys. Chem.*, **95** (11) , 4423, **1991.**

[89] D. Beckert, M. Plüschau, and K. P. Dinse, "Study of Thermally Activated Radical Pair Separation in the Anthraquinone/Triethylamine Photoredox System by Fourier Transform EPR," *J. Phys. Chem.*, **96** , 3193, **1992.**

[90] R. S. Becker and L. V. Natarajan, "Comprehensive Absorption, Photophysical/Chemical, and Theoretical Study of 2-5-Ring Aromatic Hydrocarbon Diones," *J. Phys. Chem.*, **97** (2) , 344, **1993.**

[91] W. E. Ford and G. Tollin, "Chlorophyll Photosensitized Electron Transfer in Phospholipid Bilayer Vesicle Systems: Effects of Cholesterol on Radical Yields and Kinetic Parameters," *Photochem. Photobiol.*, **40** (2) , 249, **1984.**

[92] K. J. Reszka, P. Bilski, C. F. Chignell, J. A. Hartley, N. Khan, R. L. Souhami, A. J. Mendonca, and J. W. Lown, "Photosensitization by Anticancer Agents 11. Mechanisms of Photosensitization of Human Leukemic Cells by Diaminoanthroquinones: Singlet Oxygen and Radical Reactions," *J. Photochem. Photobiol. B: Biol.*, **15** , 317, **1992.**

[93] B. Armitage, C. Yu, C. Devadoss, and G. B. Schuster, "Cationic Anthraquinone Derivatives as Catalytic DNA Photonucleases:

Mechanisms for DNA Damage and Quinone Recycling," *J. Am. Chem. Soc.*, **116** (22) , 9847, **1994.**

[94] P. K. Das, "Triplet-mediated Photoreduction of Viologens by Aromatic Hydrocarbons. A Laser Flash-Photolysis Study," *J. Chem. Soc., Faraday Trans. 1*, **79** , 1135, **1983.**

[95] S. Baral-Tosh, S. K. Chattopadhyay, and P. K. Das, "A Laser Flash Photolysis Study of Paraquat Reduction by Photogenerated Aromatic Ketyl Radicals and Carbonyl Triplets," *J. Phys. Chem.*, **88** (7) , 1404, **1984.**

[96] G. S. Nahor and J. Rabani, "Charge Separation and Photoreduction of Zinc Tetrakis(sulfonatophenyl)porphyrin by Nitrobenzene and Methylviologen in Aqueous Solutions," *J. Phys. Chem.*, **89** (12) , 2468, **1985.**

[97] M. Woodle, J. W. Zhang, and D. Mauzerall, "Kinetics and Charge Transfer at the Lipid Bilayer-Water Interface on the Nanosecond Timescale," *Biophys. J.*, **52** , 577, **1987.**

[98] R. H. Schmehl and D. G. Whitten, "Photoinduced Redox Reactions in Aqueous Micelles. Quenching, Back-Reaction, and Competing Processes for Tetraanionic Porphyrins with Alkylviologens," *J. Phys. Chem.*, **85** (23) , 3473, **1981.**

[99] L. K. Patterson, R. D. Small, Jr., and J. C. Scaiano, "Reaction of Paraquat Radical Cations with Oxygen. A Pulse Radiolysis and Laser Photolysis Study," *Radiat. Res.*, **72** , 218, **1977.**

[100] T. Shida, S. Iwata, and M. Imamura, "Electronic Absorption Spectra of Ion Radicals and Their Molecular Orbital Interpretation. IV. Anion Radicals of Aromatic and Unsaturated Aliphatic Carbonyl Compounds," *J. Phys. Chem.*, **78** (7) , 741, **1974.**

[101] R. Marchesini, C. Clemente, E. Pignoli, and M. Brambilla, "Optical Properties of *in vitro* Epidermis and their Possible Relationship with Optical Properties of *in vivo* Skin," *J. Photochem. Photobiol. B: Biol.*, **16**, 127, **1992.**

4.Claims to Original Research

Increasing the stability of mechanical pulp products would have a significant effect on the Canadian pulp and paper industry. The research presented in this thesis contributes to the understanding of the photo-induced yellowing of mechanical pulps in the following ways:

i. We have established that the guaiacoxy radical is formed as a result of singlet state cleavage of α-GAV. We have demonstrated that, in solution, the main degradation pathway for α-GAV is from cleavage of the singlet state in protic and aprotic solvents.

ii. We have demonstrated that at high laser powers and excitation wavelengths of 308 nm and below, two transients are formed from laser excitation of α-GAV. The second transient is identified as the excited state of in-cage coupling product.

iii. We have established that the triplet lifetime of **VII** in solution is short, ~500 ps.

iv. We have demontrated that the ketyl radical of **VII** cleaves quickly (> 5 x 10^7 s^{-1}) to form the corresponding phenoxy radical.

v. We have demonstrated that the conformation of α-GAV in its crystal lattice provides for efficient deactivation of the excited state via an exciplex-type interaction.

We have developed methods for the study of reaction intermediates in living cell suspensions and in cultured skin samples, demonstrating the potential for application in studies involving photodynamic therapy and magnetic field effects in biologically-relevant environments.

i. We have developed new probe incorporation techniques suitable for use in laser flash photolysis studies.

ii. We present the first use of diffuse reflectance laser flash photolysis to directly monitor photochemically-generated transients in living cell suspensions and development of an integrated, user-oriented hardware and software design of a nanosecond laser flash photolysis system.

iii. We present the first direct detection of transients generated from α-terthienyl, PPIX biosynthesized from ALA, BAEE, KPF, AQS, and ITX in living cell suspensions and liposomal systems.

iv. We present the first study of photoactive compounds in cultured skin models by laser flash photolysis.

v. We present the first detection of a radical cation from an anthraquinone in solution.

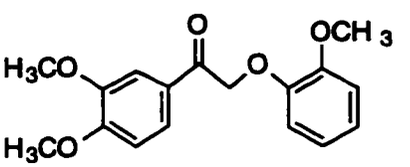

α-GAV

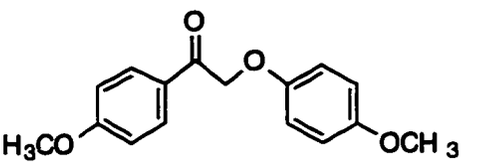

VII

Publications resulting from the work presented in this thesis

[1] A. B. Berinstain, J. C. Scaiano, and J. R. N. McLean, "Applications of Laser Flash Photolysis in Living Cell Suspensions and in Cultured Skin Models. α-Terthienyl and Anthraquinone-1,5-disulphonate.," *manuscript in preparation* , , **1997**.

[2] A. B. Berinstain and J. C. Scaiano, "Direct Detection of the Radical Cation of Anthraquinone-1,5-Disulphonate in Solution," *manuscript in preparation* , , **1997**.

[3] S. V. Jovanovic, J. Renaud, A. B. Berinstain, and J. C. Scaiano, "Kinetic Study of the Reactions of Methoxy-Substituted Phenacyl Radicals," *Can. J. Chem.*, **73** (2) , 223, **1995**.

[4] J. C. Scaiano, M. K. Whittlesey, A. B. Berinstain, P. R. L. Malenfant, and R. H. Schuler, "Pulse Radiolysis and Laser Flash Photolysis Studies of the Lignin Model α-(p-methoxyphenoxy)-p-Methoxyacteophenone and Related Compounds," *Chem. Mater.*, **6** (6) , 836, **1994**.

[5] J. A. Schmidt, E. Goldszmidt, C. Heitner, J. C. Scaiano, A. B. Berinstain, and L. J. Johnston, "Photodegradation of α-Guaiacoxyacetoveratrone: Triplet-State Reactivity Induced by Protic Solvents," in *ACS Symposium Series: Photochemistry of Lignoncellulosic Materials*, vol. 531, C. Heitner and J. C. Scaiano, Eds. Washington, D. C.: American Chemical Society, **1993**, pp. 122.

[6] J. C. Scaiano, A. B. Berinstain, M. K. Whittlesey, P. R. L. Malenfant, and C. Bensimon, "Lignin-Like Molecules: Structure and Photophysics of Crystalline α-Guaiacoxyacetoveratrone," *Chem. Mater.*, **5** (5) , 700, **1993**.

[7] A. B. Berinstain, M. K. Whittlesey, and J. C. Scaiano, "Laser Techniques in the Study of the Photochemistry of Carbonyl Compounds Containing Ligninlike Moieties," in *ACS Symposium Series: Photochemistry of Lignocellulosic Materials*, vol. 531, C. Heitner and J. C. Scaiano, Eds. Washington, D. C.: American Chemical Society, **1993**, pp. 111.

[8] A. B. Berinstain, J. C. Scaiano, C. Bohne, P. R. L. Malenfant, and G. D. Sprott, "Application of Time-Resolved Diffuse Reflectance Techniques in Studies of Reaction Intermediates in Suspensions of *Bacillus subtilis*," *Photochem. Photobiol.*, **56** (4) , 423, **1992**.

Other publications

[9] L. C. Bush, R. B. Heath, X. W. Feng, P. A. Wang, L. Maksimovic, A. I. Song, W. S. Chung, A. B. Berinstain, J. C. Scaiano, and J. A. Berson, "Tuning the Singlet-Triplet Energy Gap in a Non-Kekulé Series by Designed Structural Variation. The Singlet States of N-Substituted 3,4-Dimethylenepyrrole Biradicals," *J. Am. Chem. Soc.*, **119** (6) , 1406, **1997**.

[10] A. B. Berinstain, N. Mohtat, and J. C. Scaiano, "The Singlet State of α-Terthienyl," *manuscript in preparation* , , **1997**.

[11] R. B. Heath, L. C. Bush, X.-W. Feng, J. A. Berson, J. C. Scaiano, and A. B. Berinstain, "Absolute Rates of Heterocyclic Singlet Biradical Reactions Determined by Nanosecond Time-Resolved Absorption Spectroscopy. Dimerizations and Cycloadditions to Alkenes and to Dioxygen," *J. Phys. Chem.*, **97** , 13355, **1993**.

[12] J. H. Reynolds, J. A. Berson, K. K. Kumashiro, J. C. Duchamp, K. W. Zilm, J. C. Scaiano, A. B. Berinstain, R. Rubello, and P. Vogel, "2,3,5,6-Tetrakis(methylene)-1,4-cyclohexanediyl(1,2,4,5-Tetramethylenebenzene), a Disjoint Non-Kekulé Singlet Hydrocarbon Biradical," *J. Am. Chem. Soc.*, **115** (18) , 8073, **1993**.

[13] C. Marton, A. B. Berinstain, and J. Criswick, "An Innovative Approach to Space Education," presented at Second Annual International Space University Alumni Conference, Huntsville, Alabama, **1993**.

[14] J. H. Reynolds, J. A. Berson, J. C. Scaiano, and A. B. Berinstain, "Photochemical Generation and Preparative Capture of 1,2,4,5-Tetramethylenebenzene in Fluid Solution. Nanosecond Time-Resolved Spectroscopic Determination of Absolute Rates of Dimerization and

Oxygen Trapping of a Disjoint Singlet Hydrocarbon Biradical," *J. Am. Chem. Soc.*, **114** , 5866, **1992.**

[15] J. A. Schmidt, A. B. Berinstain, F. de Rege, C. Heitner, L. J. Johnston, and J. C. Scaiano, "Effect of Solvent on the Photodegradation of α-Guaiacoxylacetoveratrone, a Phenacyl-α-aryl Ether Lignin Model," *Ligno-Cellul. [Cellucon 90]* , 587, **1992.**

[16] J. A. Schmidt, A. B. Berinstain, F. De Rege, C. Heitner, L. J. Johnston, and J. C. Scaiano, "Photodegradation of the Lignin Model α-Guaiacoxyacetoveratrone, unusual effects of Solvent, Oxygen, and Singlet State Participation," *Can. J. Chem.*, **69** , 104, **1991.**

[17] A. Azarani, A. B. Berinstain, L. J. Johnston, and S. Kazanis, "Electron Transfer Reactions Between Excited Diarylmethyl and Triarylmethyl Carbocations and Aromatic Donors," *J. Photochem. Photobiol. A: Chem.*, **57** , 179, **1991.**

[18] T. Nagaoka, A. B. Berinstain, D. Griller, and D. D. M. Wayner, "Acidities of Arenium Ions in Acetonitrile," *J. Org. Chem.*, **55** , 3707, **1990.**

[19] A. B. Berinstain, A. M. English, B. C. Hill, and D. Sharma, "Picosecond Flash Photolysis of Carboxy Horseradish Peroxidase: Rapid Geminate Recombination in the Presence of Benzohydroxamic Acid," *J. Am. Chem. Soc.*, **112** (26) , 9649, **1990.**